UiT
THE ARCTIC
UNIVERSITY
OF NORWAY

Department of Chemistry, Faculty of Science and Technology

Rhenium- and technetium-oxo corroles:

Toward corrole-based drugs and radiopharmaceuticals

Rune Finsås Einrem

KJE-3900 Master's thesis in Chemistry, November 2017

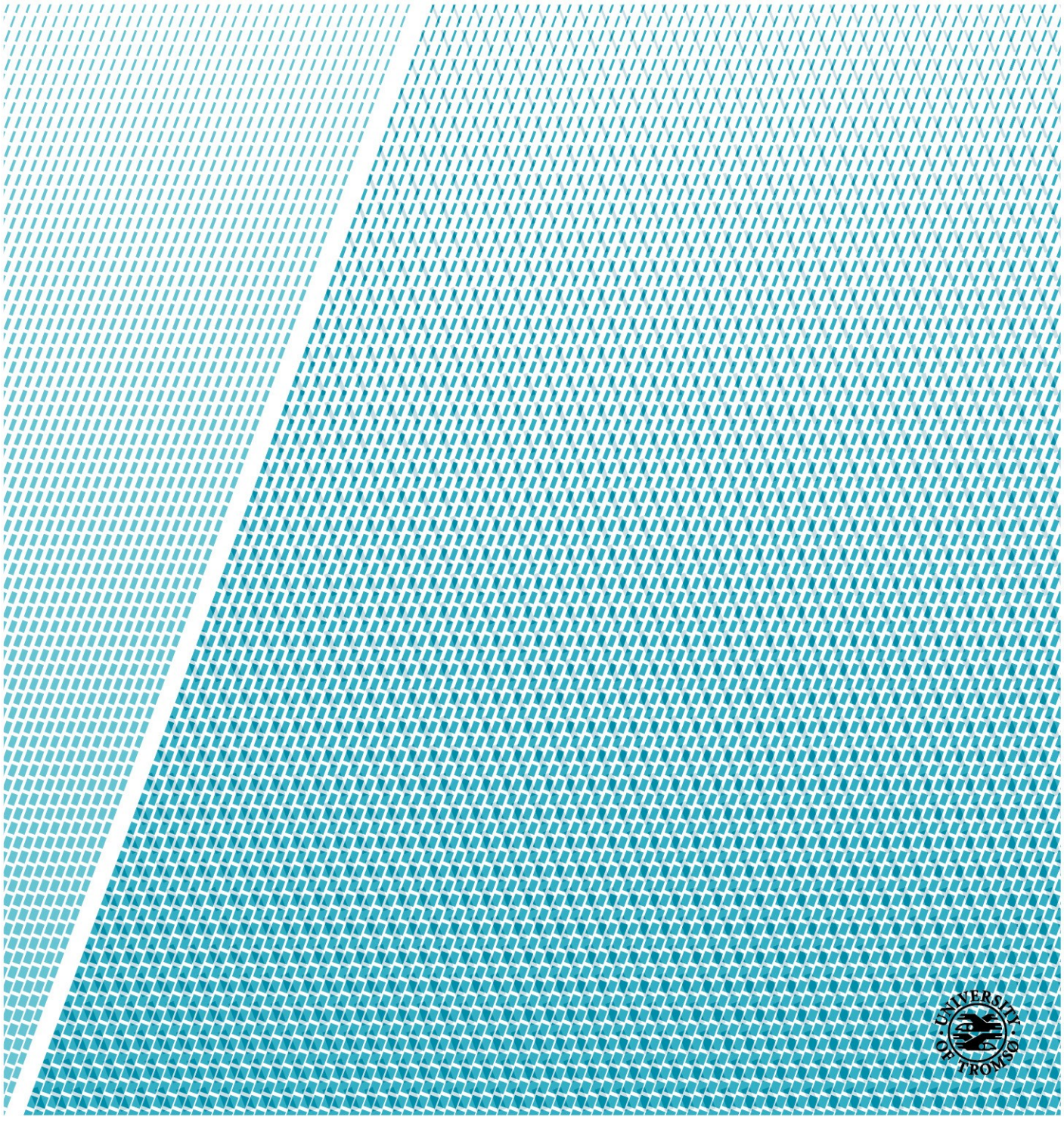

ABSTRACT

Corroles are an important class of contracted porphyrin analogues. Since quasi-one-pot syntheses of corroles were first reported in 1999, their coordination chemistry has been extensively studied.

In the course of this thesis, the "periodic table of corroles" has been extended by two new elements, rhenium and technetium. Except from an accidental synthesis of an $Re^{V}O$ corrole via ring contraction of a porphyrin, no Re corroles were known prior to this work. As part of this thesis, I have developed the first rational synthesis of Re corroles, based on oxidative metalation of *meso*-triarylcorroles with $Re_2(CO)_{10}$ in refluxing decalin. A total of 9 $Re^{V}O$ complexes, have been made, including 5 that were structurally characterised. I also prepared the first 99-technetium corroles using $[NEt_4]_2[^{99}TcCl_3(CO)_3]$ as the ^{99}Tc source; one of these complexes was structurally characterized.

The $Re^{V}O$ corroles were found to exhibit near-IR phosphorescence at room temperature, with long triplet lifetimes ~60 μs, but low quantum yields ~2.9%. Furthermore, two amphiphilic $Re^{V}O$ corroles exhibited strong cytotoxicity against AY27 rat bladder cancer cells and WiDr human colon cancer cells under blue light illumination.

My hope is that the work presented here will pave the way toward ^{99m}Tc corroles and other metallocorroles as new metallodrugs and radiopharmaceuticals.

ACKNOWLEDGEMENTS

I would like to thank my supervisors – Prof. Abhik Ghosh for the many opportunities that made this work possible; Dr. Odrun A. Gederaas for introducing me to a completely new area of research and for making my trips to her laboratory in Trondheim both educational and fun; and Dr. Abraham Alemayehu for day-to-day supervision and never-failing humour. I am grateful for your guidance, help, and inspiration. Without you, I would never come this far.

I am deeply grateful to Prof. Roger Alberto for hosting me in his laboratory at the University of Zürich and to Dr. Henrik Braband for giving me hands-on training in handling low-level radioactive materials, in particular ^{99}Tc and ^{99m}Tc. Their hospitality made for unforgettable stays in Switzerland.

My gratitude goes to all group members including Ivar Thomassen, Hans-Kristian Norheim, Simon Larsen, Sumit Ganguly, Dr. Hugo Vazques-Lima, and especially Dr. Kolle E. Thomas for all help.

My thanks also go to the engineers Jostein Johansen, Frederick Leeson, and Arnfinn Kvarsnes, and Dr. Truls Ingebrigtsen for assistance with NMR and mass spectroscopy and much more.

I would like to thank Renate Lie Larsen and Valentina Burkow Vollan for assistance with administrative matters.

I would like to thank my fellow master students Tone Kristoffersen, Philip Rainsford and Gulbrand Nilsen, as well as Magnus Engqvist, Marc Boomgaren, and the rest of the organics for a good learning environment and pleasant social atmosphere.

I thank Prof. Tore Lejon for having me as a student in many of his excellent courses as well as for nice discussions and stories.

Finally, I thank my family and friends for believing in me and always being supportive. A huge thank-you to Ane Finstad for coping with me through all the ups and downs during this time!

Rune F. Einrem

Tromsø, November 2017

TABLE OF CONTENTS

ABBREVIATIONS

AcOH	Acetic acid
CV	Cyclic voltammetry
DCM	Dichloromethane
DDQ	2,3-dichloro-5,6-dicyano-1,4-benzquinone
DFT	Density functional theory
DMF	Dimethylformamide
DMSO	Dimethyl sulfoxide
HOMO	Highest occupied molecular orbital
IC	Internal conversion
IR	Infrared spectroscopy
ISC	Intersystem crossing
LSC	Liquid scintillation counting
LUMO	Lowest unoccupied molecular orbital
MTT	3-(4,5-dimethylthiazol-2-yl)-2,5diphenyl tetrazolium bromide
NMR	Nuclear magnetic resonance
OAT	Oxygen atom transfer
PBS	Phosphate buffer saline
PDT	Photodynamic therapy
ROS	Reactive oxygen species
TBAP	Tetra(*n*-butyl)ammonium perchlorate
TPC	Triphenylcorrole
UV	Ultraviolet-visible spectroscopy

1 INTRODUCTION TO INORGANIC DRUGS AND PHOTODYNAMIC THERAPY

1.1 HISTORICAL INTRODUCTION

Cancer affects almost everyone either directly or indirectly and records show that it has been the case throughout human history. The first documentation of the disease is from an Egyptian scripts dated to about 3000 BC where they referred to a sickness where "there is no treatment".[1] At the end of 2014 more than 252 000 Norwegians had had at least one cancer diagnosis at an earlier point of life. A total of 10 971 people died from cancer in 2014 in Norway alone. In 2015, 32 592 new cases of cancer were recorded in Norway. For men, the most common cancers involved the prostate, lung, colon, bladder, and the urinary tract, while for women they were breast, colon, and lung cancer.[2]

Fortunately, unlike 5000 years ago, the survival ratio today is relatively high, ranging from 91-93% for prostate cancer to 66-68% for rectal cancer.[3] If cancer on its own was not bad enough, will treatment in many cases cause severe physical damages. Radiotherapy kills not only the cancer cells but also other tissues. Chemotherapy, the most commonly used treatment for cancer, like radiotherapy, is not selective enough against cancer cells and also kills healthy cells as well. Surgery is effective but is mostly limited to solid, accessible tumours. Surgery on its own is dangerous by its use of anaesthesia and may cause scars and infections.

The disadvantages related to the above classic approaches have led to new modalities for cancer treatment. Among these are photodynamic therapy (PDT), a technique that uses light sensitive chemical compounds (photosensitiser) to kill cells by activating molecular oxygen (O_2).

Another approach were development of new cytotoxic and cytostatic drugs, among them inorganic compounds. The use of inorganic compounds for the treatment of a variety of afflictions is not new, but are documented in Egyptian texts dating back to 1550 BC. There they described the use of garlic containing selenium as a treatment for illness.[4-5] One of the first inorganic complexes used in medicine was salvarsan (Figure 1), an arsenic-based agent developed by Paul Ehrlich in 1910, and in 1912 he published his results of salvarsan as treatment against syphilis.[6-7]

In 1979 the U.S Food and Drug Administration approved an anticancer drug called *cis*-dichlorodiamineplatinum(II) or cisplatin, as shown in Figure 1. Cisplatin became known as the penicillin among anticancer drugs and the discovery greatly energized the investigation of other metal-containing drugs with cytotoxic and/or cytostatic effect that specifically inhibit tumour cells.[8]

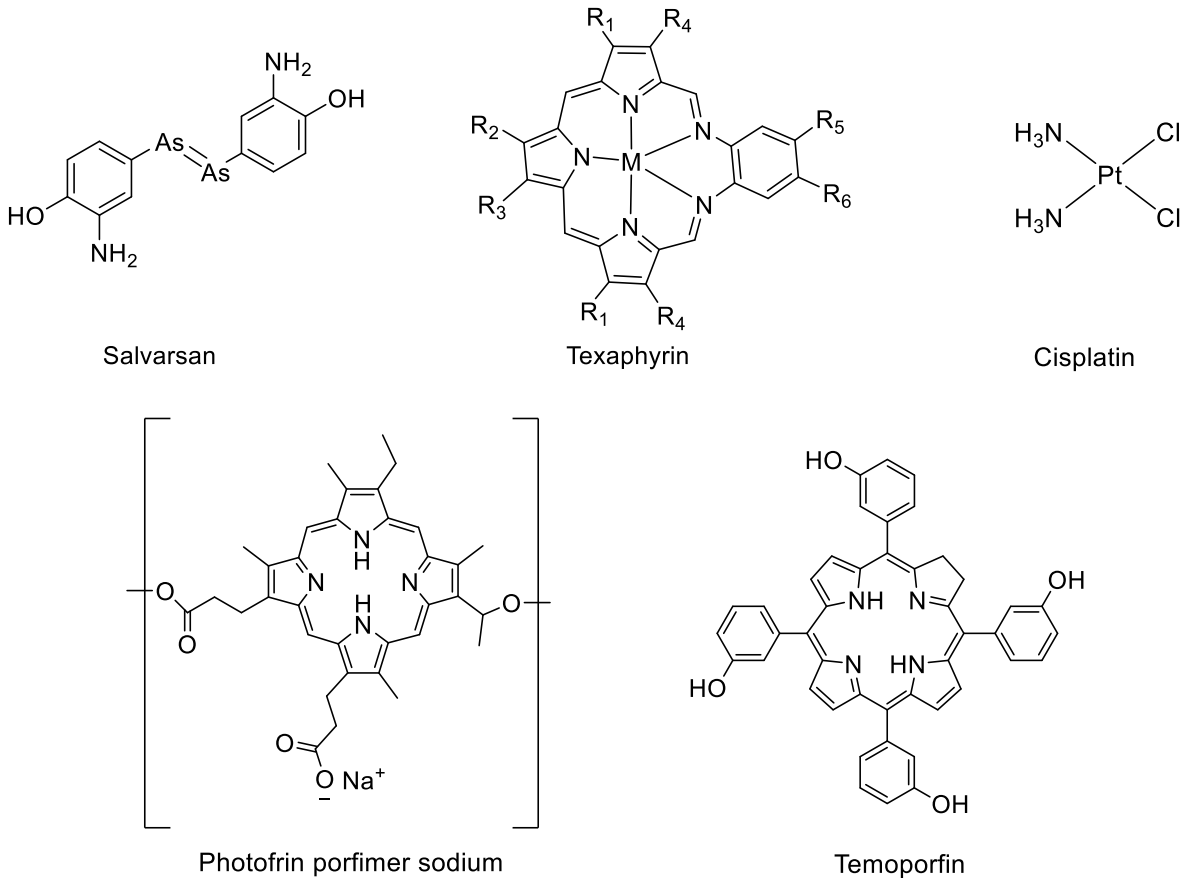

Figure 1. Some pioneering metallo- and PDT drugs.

A different use of inorganic compounds for medicinal applications that also got a boost simultaneously, consisted of small molecules working as photosensitisers for generating reactive oxygen for photodynamic therapy. The most promising drugs were found to be those that produce ROS upon irradiation of tissue-penetrating light.[9] The best PDT agents to date have proved to be porphyrin and related macrocycles.[10] Among the most promising compounds is an expanded porphyrin called texaphyrin (Figure 1), which has reached advanced stages of clinical testing.[11] During the last 20 years corroles, a class of contracted porphyrins, have also been investigated as possible agents in PDT.[5]

1.2 NUCLEAR MEDICINE AND RADIOPHARMACEUTICALS

Nuclear medicine involves both treatment and imaging by the use of radioactive isotopes. Commonly used isotopes for nuclear imaging include ^{99m}Tc, ^{123}I, ^{67}Ga, and ^{125}I, of which ^{99m}Tc (where the superscript "m" refers to a metastable nuclear excited state) is the working horse. A key consideration for the use of a given isotope is the half-life. An excessively long half-life will result in radiation damages to our body while an unduly short half-life will lead to insufficient imaging.

Technetium is the first and lightest element in the periodic table without any stable isotopes.[12] Today, 22 isotopes and 9 isomers (i.e., nuclear excited states) of technetium are known. The longest-living isotopes of technetium is ^{98}Tc with a $t_{1/2}$ of 4.2 million years, followed by ^{97}Tc with a $t_{1/2}$ of 2.6 million years, and ^{99}Tc with a $t_{1/2}$ of 211,100 years. The ^{99}Tc isotope is such a weak β^--emitter that ordinary laboratory glassware provide adequate protection against the radiation, making it suitable for synthetic studies. In addition, technetium has several metastable isomers, of which the most stable is ^{97m}Tc with $t_{1/2}$ of 90.1 days, followed by ^{95m}Tc with $t_{1/2}$ of 61 days, and ^{99m}Tc with half-life of 6.01 hours. Because of ^{99m}Tc's short half-life and the fact that it is a γ-emitter makes it ideally suited for nuclear medicine applications. The ^{99m}Tc was first isolated in the 1940s and is today used in some ten million medical diagnostic procedures annually, making up ~85% of radio medicinal diagnosis.[12-13]

Rhenium has two radioactive isotopes - ^{186}Re and ^{188}Re, both β-emitters – which are also used in nuclear medicine, albeit far less frequently than ^{99m}Tc. The range of ^{186}Re and ^{188}Re's β-particles in tissue is about 50 – 1000 cell diameters, making them suitable for treating larger or poorly vascularized tumours. The two Re radioisotopes have been used for bone cancer and certain other late stage cancers.[14]

Radiopharmaceuticals incorporate a radioactive isotope within a drug or chemical agent. They are generally categorized as 1st, 2nd and 3rd generations.

First-generation radiopharmaceuticals consist of common complexes such as $^{99m}TcO_4^-$ and ^{99m}Tc-phosphonates whose action depends on their simple absorption, distribution, and excretion properties. They have been around the longest and are today in use for brain, heart, kidney, and liver imaging.

Second-generation radiopharmaceuticals involve carefully tailored ligands. The *in vivo* performance of the complexes have generally been carefully analysed in terms of their

molecular size, charge and lipophilicity. Examples include the cardiac imaging agent ^{99m}Tc-MIBI (sestamibi, Cardiolite®) and ^{99m}Tc-tetrofosmin (Myoview®) and the brain imaging agent ^{99m}Tc-HMPAO (examentazime, Ceretec®) and ^{99m}Tc-ECD (bicisate, Neurolite®). Newer products under this category include the renal imaging agent ^{99m}Tc-MAG3 (Mertiatide) and the hepatobiliary agent ^{99m}Tc-mebrofenin.

Third-generation radiopharmaceuticals couple a radioisotope with a biological targeting agent such as a peptide or sugar to reach specific biomolecular targets such as receptors and transporters. The development of such reagents has required the development of sophisticated labelling methods, such as those for incorporating $Tc^{I}(CO)_3$ and $Tc^{V}N$ groups.

The most commonly used technique for nuclear imaging is called single-photon emission computed tomography (SPECT), which involves a γ-emitter such as ^{99m}Tc. The method typically involves the injection of a γ-emitting radiopharmaceutical into the blood stream. A γ-ray camera then acquires 2D images from a variety of angles which are then computationally processed to generate 3D image of the distribution of the radioisotope in the bloodstream in a process similar to magnetic resonance imaging (MRI) or positron emission tomography (PET).

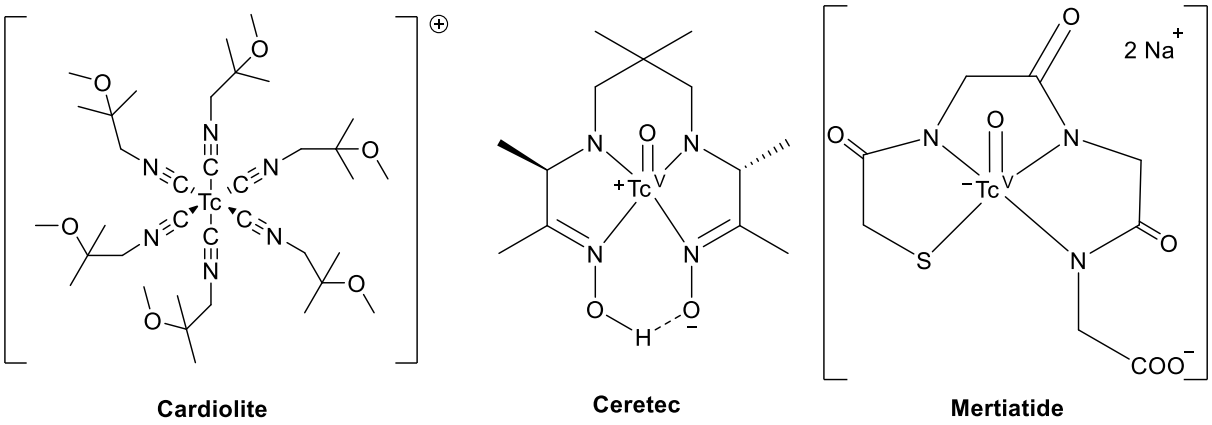

Figure 2. Examples of ^{99m}Tc complexes in clinical use.

1.3 PHOTODYNAMIC THERAPY

Use of light in therapeutic settings is not a new development. Indeed the first recorded use of light for medicinal purposes dates back to 1400 BC, when sunlight was used in conjunction with extracts from plants growing along the Nile in Egypt for the treatment of skin diseases. The birth of modern phototherapy, however, began with Niels Ryberg Finsen, a Danish physician, and his discovery of the bacteria-destroying effect of sunlight and ultraviolet light. Finsen received the Nobel Prize in Medicine in 1903 for this work.[15] Until the 20th century, phototherapy was widely used largely for dermatological applications.[16] With the invention of medical lasers and fiber optic cables, modern photodynamic therapy enjoys far wider application, including the treatment of organs deeper inside the human body.[17]

Photodynamic therapy combines the use of light, a photosensitive chemical compound (photosensitiser), and molecular oxygen. Individually, each component is nontoxic but, under the right conditions on exposure to light of a specific wavelenght, the sensitiser may be excited to a higher energy state. The excited state may then transfer its excess energy to molecular oxygen to produce singlet oxygen ($^1O_2$), a highly reactive exited state of oxygen, or may transfer an electron to generate another reactive oxygen species (ROS).

In 1995, Porfimer sodium (Figure 1) became the first drug to be approved for photodynamic therapy. It is a porphyrin oligomer and is now approved for use in more than 40 countries for lung cancer. Temoporfin is another PDT drug used for head and neck cancer which was approved in 2001 in the European Union including Norway and Iceland. It is based on the chlorin skeleton depicted in Figure 3, which also shows some other macrocycles that are under investigation as potential PDT drugs.

Photochemical internalization, a Norwegian discovery,[18] is a variety of PDT where a drug is internalized via the process of endocytosis and the endocytic vesicles are subsequently ruptured by light to release the drug inside the cell.[19]

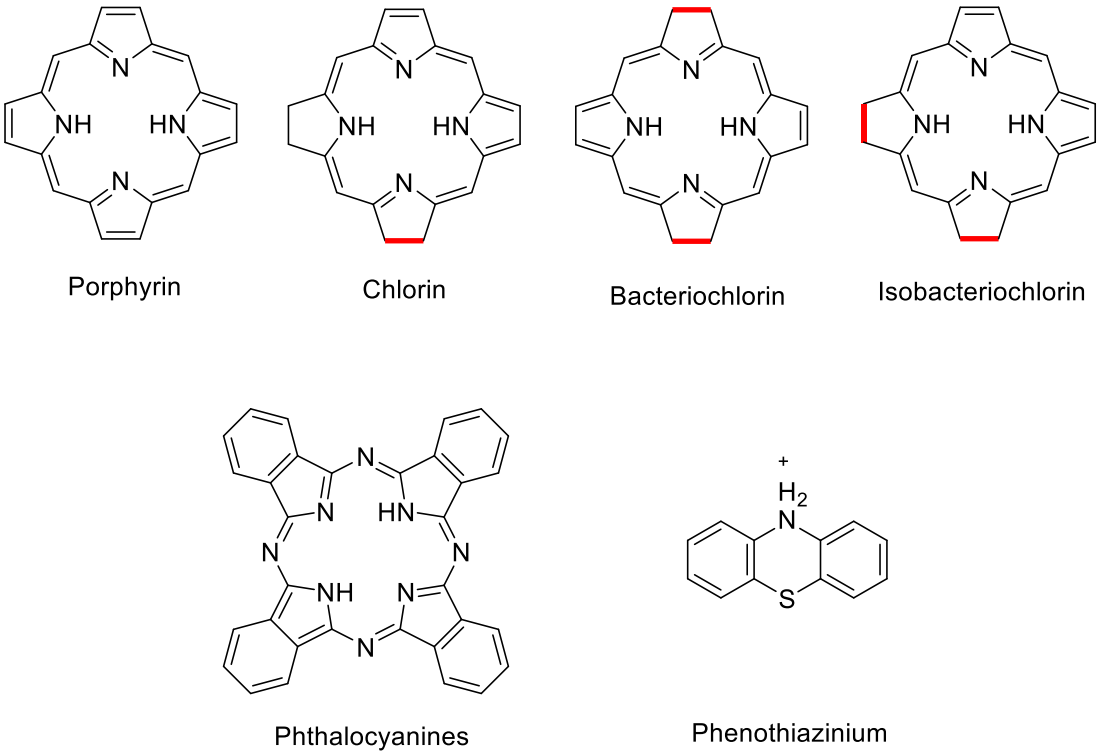

Figure 3. Parent heterocycles of some common photosensitisers used in photodynamic therapy.

1.4 REACTIVE OXYGEN SPECIES

Reactive oxygen species (ROS) in biological systems derive largely from atmospheric oxygen and to some extent also from water. They commonly arise via "leakage" from oxygenated forms of heme proteins and other metalloproteins, including globins, peroxidases, and superoxide dismutases. Common ROS includes hydrogen peroxide (H_2O_2), the superoxide radical anion ($O_2^{\bullet-}$), hydroxyl radicals ($OH^{\bullet}$), ozone (O_3), and singlet oxygen ($^1O_2$). Less common ROS include alkoxyl ($RO^{\bullet}$) and peroxy ($ROO^{\bullet}$) radicals. ROS are of great biological importance in that they can inflict damage DNA, proteins, and other cellular components. Aerobic organisms have evolved a variety of defensive mechanisms to deal with ROS that arise naturally in their bodies. A number of reactive nitrogen species (RNS), including nitrogen dioxide radicals ($NO_2^{\bullet}$), and peroxynitrite ($ONOO^-$), also play similar role as ROS.

Photodynamic therapy results in the localized production of ROS in the neighbourhood of the photosensitiser. By far the greatest proportion of these ROS is singlet oxygen, which arises via energy transfer from a triplet exited state of the sensitiser to ground, triplet state of molecular oxygen. The electronic configuration of these two forms of oxygen are depicted schematically

in Figure 4. The superoxide anion can also arise under PDT, by electron transfer from the excited photosensitiser to molecular oxygen.

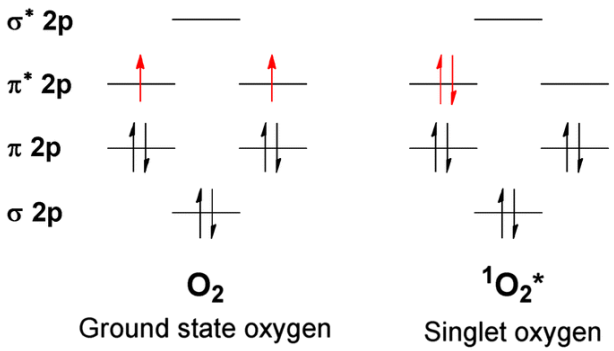

Figure 4. Molecular orbital diagram of ground state triplet oxygen and excited singlet oxygen.

1.5 PHOTOCHEMISTRY AND PHOTOCHEMICAL REACTIONS WITH OXYGEN

Here I summarize some elementary photochemical concepts relevant to my findings in the are of photodynamic therapy described in this thesis.

A photochemical reaction occur when a molecule absorbs light. A photochemical reaction is a chemical reaction that is caused by absorption of light, typically in the ultraviolet (100-400 nm), visible (400-750 nm), and infrared (750 -2500) ranges. This definition, i.e., the fact that light absorption is a necessary condition of a photochemical reaction, is sometimes called the first law of photochemistry or the Stark-Einstein law, which state that each molecule absorbed by a chemical system excites only a single molecule.

When a molecule in its (singlet) ground electronic state (S_0) absorbs a photon, it gets excited to higher-energy singlet state, S_1, S_2, S_3, S_4, etc., depending on the energy of the photon. The excitation process maintains the total spin of the system, i.e., the excited electron does not undergo a spin flip. The higher excited states S_2, S_3, S_4, etc., as a rule (the so-called Kasha's rule), quickly relax via radiation decay (internal conversion, IC) to S_1, which is generally the only relevant singlet excited state. A number of possible paths are generally available for decay of the S_1 state to S_0.

Deexitation may happen in a radiationless manner, i.e., IC.

Deexcitation may happen via spin-allowed radiation, a process called fluorescence.

Finally, the S_1 state might undergo so-called intersystem crossing (ISC) to the lowest triplet state T_1, which as a rule (Hund's rule) has a slightly lower energy than S_1. The T_1 state may then decay to S_0 via either IC or radiatively, by a process called phosphorescence. Because the T_1 to S_0 transition is spin-forbidden, the T_1 state has a much longer lifetime than S_1; i.e., phosphorescence is a much slower process than fluorescence. Some phosphorescence processes are so slow that the corresponding materials, called phosphors, are used for glow-in-the-dark applications, such as emergency signs.[20]

The presence of a heavy atom in a molecule promote phosphorescence by facilitating intersystem crossing from S_1 to T_1 due to a phenomenon called spin-orbit coupling.[21] This is the reason behind the efficacy of 5d metalloporphyrins and metallocorroles, including the Re corroles in this thesis, as phosphors. The phosphorescence of these molecules, however, is not visible to the naked eye, since it occurs in the near-infrared.

A schematic depiction of the above processes is called a Jablonski diagram and is presented in Figure 5.

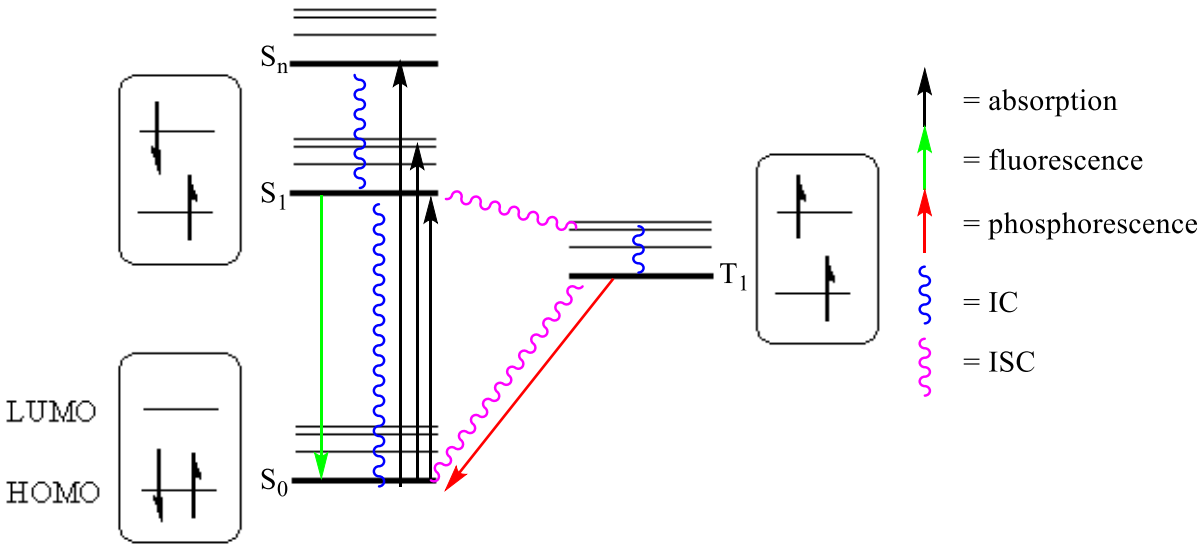

Figure 5. Jablonski diagram illustrating the different excited states and the various radiative (indicated by arrows) and nonradiative paths (indicated by wavy lines) connecting them.

There are three potential reaction paths, divided into two categories, between a molecule in an excited triplet state and oxygen. Category 1 may be subdivided into mechanism I and II, where mechanism I proceeds via reduction of the photosensitiser and II via oxidation. In more detail, mechanism I involves transfer of an electron from a substrate molecule to the excited photosensitiser, which results in a photosensitiser radical anion and a substrate radical cation (Figure 6), where type II involves reduction of the substrate through transfer of a hydrogen atom to the excited photosensitiser.

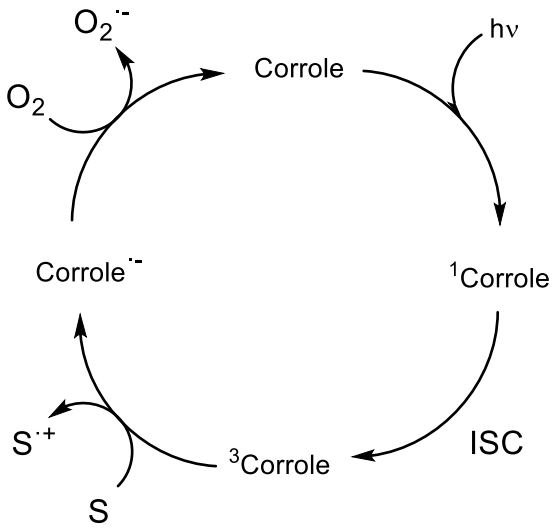

Figure 6. Reaction scheme of category 1, type I reaction of a photosensitiser, in this case a corrole.

Category 2 involves direct reaction of the excited triplet state of the photosensitiser and ground triplet state oxygen to generate excited, singlet oxygen and ground-state photosensitiser, as illustrated in Figure 7. The process is sometimes called triplet-triplet annihilation, since two triplets are mutually quenched to generate two singlets, one in the ground state and one in the excited state.

As mentioned above, it is singlet oxygen that is the key cytotoxic agent in photodynamic therapy. Singlet oxygen, $^1O_2$, has a short lifetime of less than 50 ns. Accordingly, it only has a limited radius of cellular action, which is approximately 20 nm. In other words, cell damage will occur only within the immediate proximity of the photosensitiser.

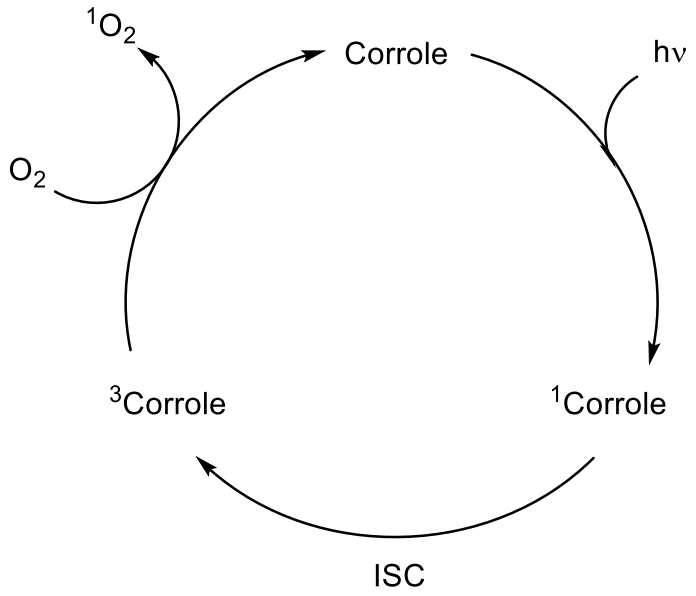

Figure 7. Reaction scheme of a category 2 reaction between a corrole and oxygen.

A key prerequisite of photodynamic therapy is that the light penetrates the tissue and reaches the photosensitiser. In general, light can penetrate only through a limited depth of soft tissue. In biology and medicine, one often talks about the optical window, therapeutic window or near-infrared window, which refers to a wavelength range from 600 to 1200 nm, for which electromagnetic radiation has the greatest depth of penetration in tissue. Yet, wavelengths longer than 800 nm are not used in standard PDT, since such radiation does not have enough energy to convert $^3O_2$ to $^1O_2$. For wavelengths in the 600-800 nm range, light penetrate only a few millimeters to about 1 cm in soft tissue. Yet another consideration is that the photosensitiser must have high absorbance at the wavelength of light employed. [9, 23]

2 INTRODUCTION TO PORPHYRINOIDS

2.1 INTRODUCTORY REMARKS

Porphyrinoids or porphyrin-type molecules are ubiquitous in nature and many of them, especially the chlorophylls (Figure 8), exhibit superior light absorption and harvesting properties. They are found in *Archaea, Bacteria* and in *Eukarya*, including in our own bodies. True porphyrins are aromatic macrocycles with a total of 22 conjugated π-electrons.[24] One of the best-known porphyrin cofactors is heme b, the pigment that gives haemoglobin in the blood its red colour. Porphyrinoid cofactors play many important biochemical roles. Thus, haemoglobin and myoglobin act as oxygen carriers in mammals and certain other vertebrates. The heme protein cytochrome P450 catalyse oxygen atom transfer (OAT) to organic compounds, especially toxins, and help destroy them in the liver.[25] The cobalt-containing porphyrinoid B_{12} is an essential nutrient and acts as a cofactor in many biochemical reactions, whereas the nickel porphyrinoid F430 is the cofactor of methylcoenzyme M reductase, which catalyses the last step of biological methane production. Many porphyrinoids, especially those with aryl groups at the *meso* positions, Figure 9, can be readily synthesized in the laboratory. Figure 10 depicts elementary aspects of porphyrinoid nomenclature, including skeletal atom numbering according to IUPAC nomenclature and the definition of a α, β, and *meso* carbons.

The wide availability of synthetic porphyrinoids has led to a deep appreciation of their diverse chemistry, including their fundamental coordination chemistry and applications such as catalysis, photodynamic therapy, and dye-sensitised solar cells.[5, 26-29] Indeed, the "periodic table of porphyrins" is nearly complete and the vast majority of transition metals and many non-metals have also been coordinated to corroles.[30]

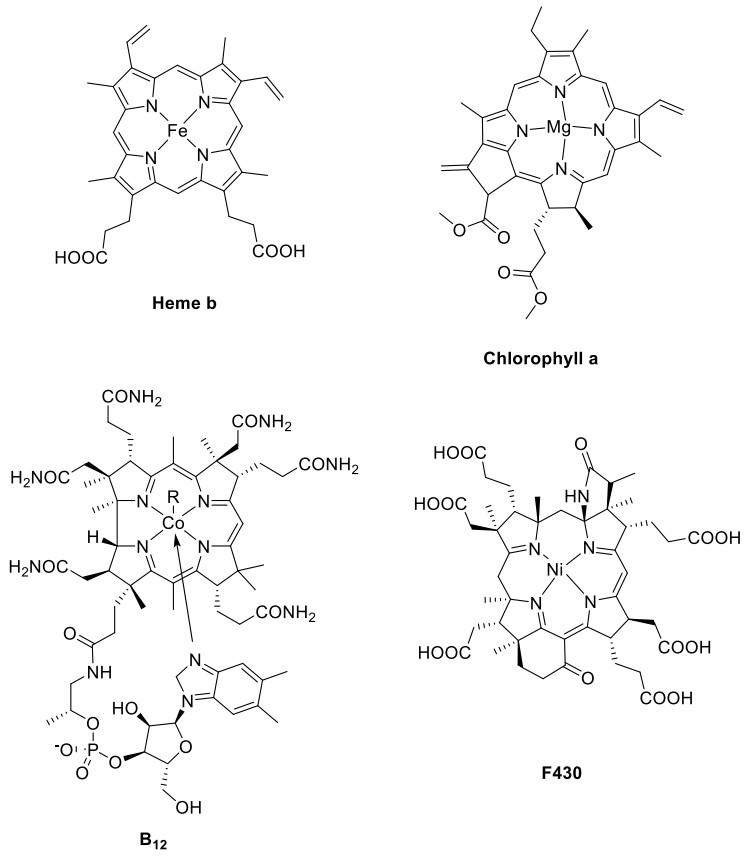

Figure 8. Four porphyrinoid cofactors.

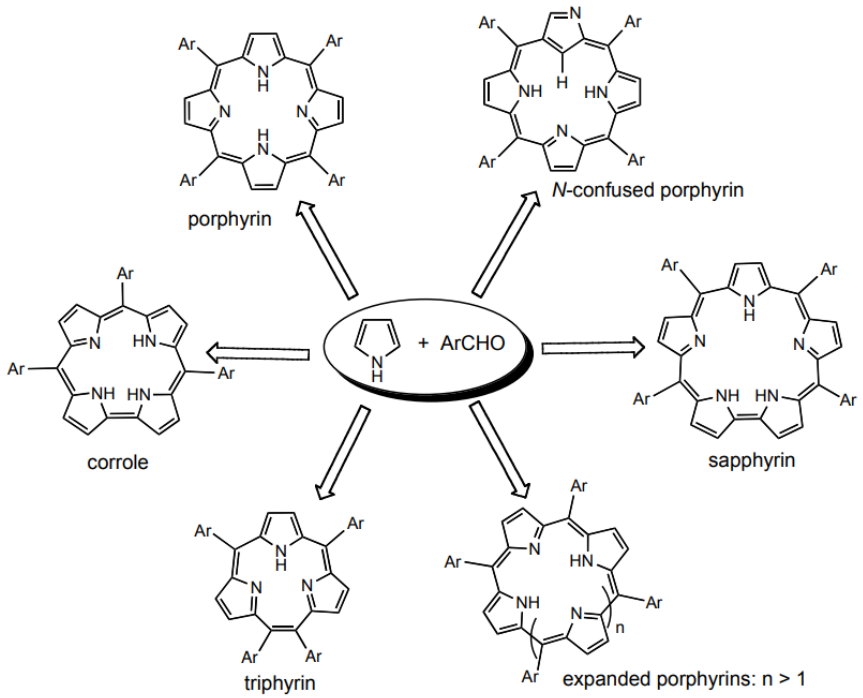

Figure 9. Porphyrinoid macrocycles obtained via pyrrole-aldehyde condensations. Reused with permission from "Letters to a Young Chemist", Copyright © 2011, John Wiley & Sons.

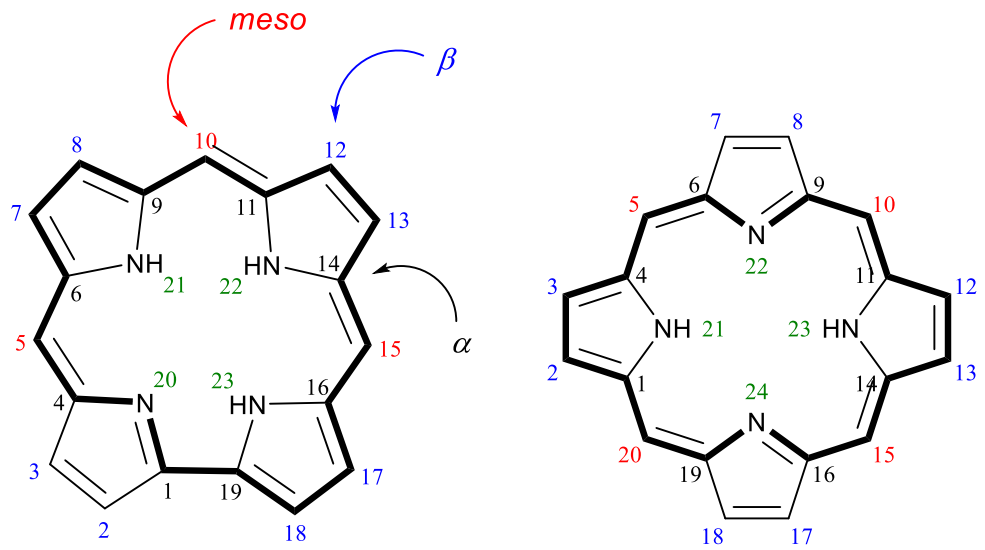

Figure 10. IUPAC numbering of skeletal atoms for free-base corrole (left) and porphyrin (right) and definition of *α*, *β*, and *meso* positions.

Porphyrins and corroles have characteristic absorption in the near-ultraviolet and visible region of the electromagnetic spectrum, the latter being the reason for their strong colours. Both porphyrins and corroles have a distinct strong Soret (or B) band, usually between 390-450 nm, and two to four weaker Q bands in the 480 – 700 nm region, as shown in Figure 11 for free-base triphenylcorrole. For free-base and nontransition metal porphyrins, the absorptions are generally well described in terms of a Martin Gouterman's four-orbital model, i.e., transitions between the two HOMOs and the two LUMOs of the molecules.[31]

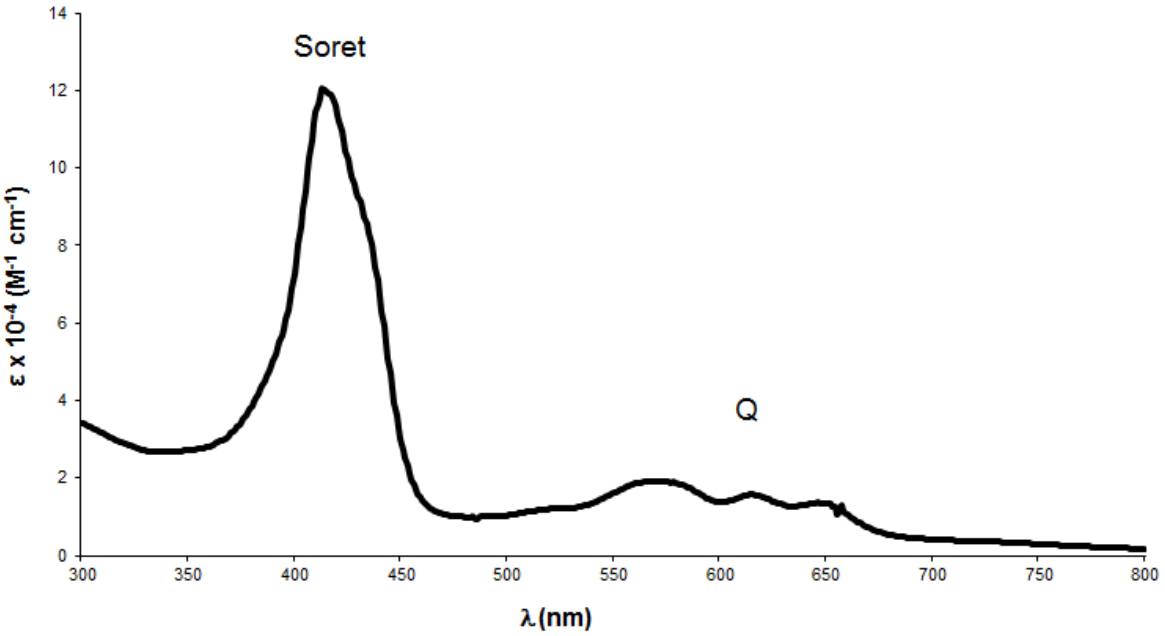

Figure 11. Electronic absorption spectrum of free-base *meso*-triphenylcorrole, H_3[TPC].

Free-base porphyrinoids and many nontransition element complexes are generally also strongly fluorescent,[31] with the exception of *meso*-aryl compounds with halogens at the phenyl *ortho*-position.[32] Transition metal complexes typically quench the fluorescence.[33] Heavy element porphyrins, however, exhibit phosphorescence,[34] i.e., emission from long-lived triplet states, a property that also have been characterized and exploited for $Re^{V}O$ corroles.

2.2 THE SYNTHESIS OF PORPHYRINS

One-pot syntheses provide the most convenient methods for porphyrin preparation. In 1935, Rothemund published the first one-pot synthesis for free-base porphyrins by condensation of pyrrole and aldehydes in a sealed vessel at high temperature.[35] This procedure was later modified to synthesise tetraphenylporphyrin by refluxing equimolar amounts of pyrrole and benzaldehyde in propionic acid.[36]

The search for gentler methods of porphyrin resulted in one by Lindsey, where equimolar amounts of aldehyde and pyrrole were condensed in DCM catalysed by either trifluoroacetic acid or boron trifuoride-etherate under inert atmosphere, followed by oxidation by DDQ or *p*-chloranil, as shown in Figure 12.[37]

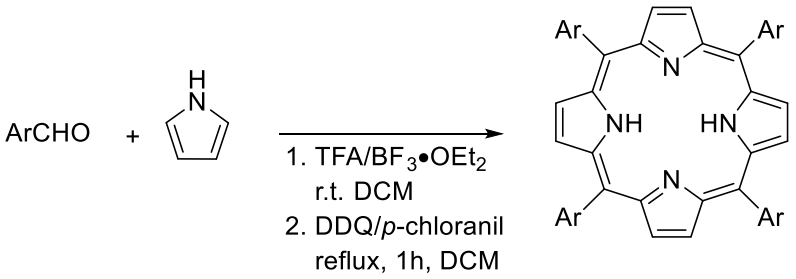

Figure 12. One-pot porphyrin synthesis through the condensation of pyrrole and an aromatic aldehyde.

A variety of multistep approaches have been developed for the synthesis of unsymmetrical porphyrins. While these are largely outside the scope of this thesis, it is worth mentioning the most commonly used [2 + 2] addition of dipyrromethanes or dipyrromethenes. As shown in Figure 13, careful attention to symmetry considerations is required in this method.

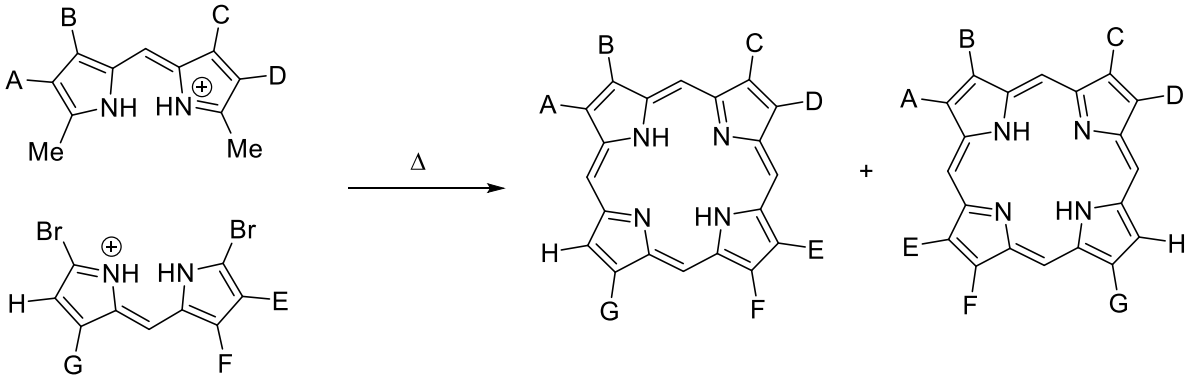

Figure 13. Symmetry problems for porphyrin synthesis through [2 + 2] addition.

Due to dipyrromethanes' sensitivity to acids, most of the early work was done on dipyrromethenes. A breakthrough in porphyrin synthesis came in 1960 with the MacDonald synthesis which used dipyrromethanes, as shown in Figure 14, yielding porphyrins in up to 60% yield. The author showed that a 1,9-diformyldipyrromethane could be condensed with either a 1,9-di-unsubstituted dipyrromethane or its 1,9-dicarboxylic acid in the presence of an acid.[38] A variant of the MacDonald synthesis played a significant role in Woodward's chlorophyll a synthesis,[39] which contributed to his winning of the Nobel Prize in chemistry in 1965.

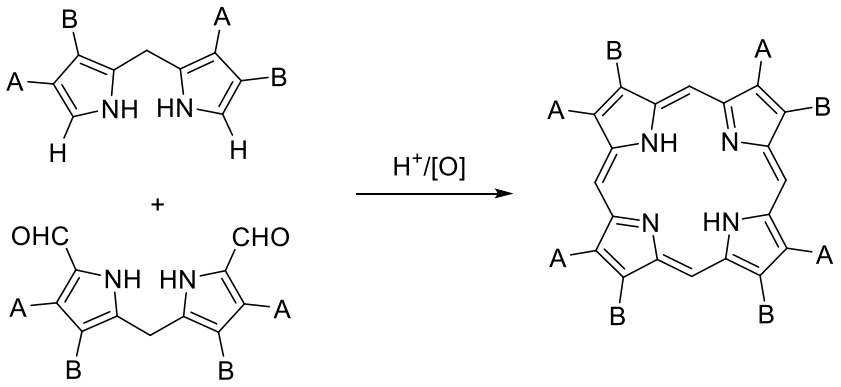

Figure 14. MacDonald's [2 + 2] porphyrin synthesis.

To avoid the use of large quantities of chlorinated solvents, porphyrin chemists have searched for "greener" methods of porphyrin synthesis. One of the most promising approaches so far has involved ionic liquids, which may act as both solvents and catalysts, besides the fact that they are also reusable. Certain of the syntheses resulted in yields ~40%, thus rivalling Lindsey's conditions.[40,41]

2.3 SUBPORPHYRINS

Subporphyrins are a class of contracted porphyrins containing three pyrroles linked by methine bridges from an aldehyde. In 2007, Kobayashi *et al*. published a procedure for preparation of *meso*-aryl-substituted subporphyrins, as shown in Figure 15.[42] Their synthesis, however, has so far only yielded the boron complex and removal of the central boron has proven difficult.

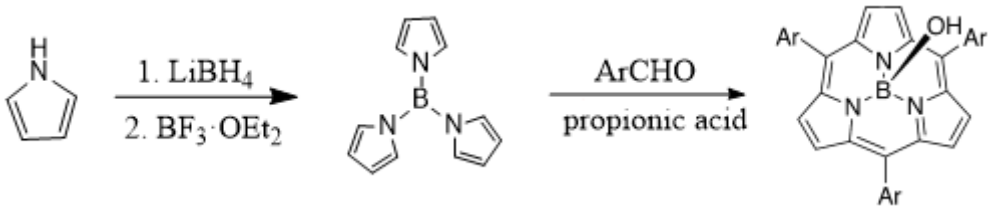

Figure 15. Synthetic route to boron-containing subporphyrins. Reused with permission from ref. 42. Copyright © 2007, WILEY-VCH Verlag GmbH & Co.

One year later the same group also published a synthesis for preparation of free-base triphyrins, with a two-carbon bridge between two of the pyrrole rings, via a modified Lindsey

condensation, as shown in Figure 16.[43] Two groups subsequently published protocols for the synthesis of *meso*-unsubstituted and *β*-unsubstituted triphyrins through McMurry coupling.[44,45]

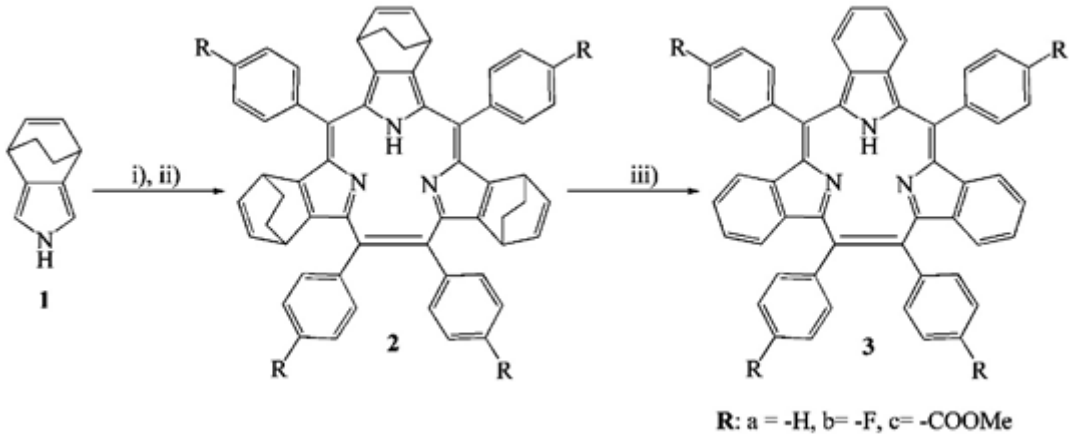

Figure 16. Synthesis of *meso*-aryl-substituted [14]triphyrin(2.1.1), (i) *p*-RC_6H_4CHO, BF_3•Et_2O, DCM, r.t., 12 h; (ii) *p*-chloranil, 2 h; (iii) 220˚C, 2 mmHg, 20 min. Reused with permission from ref. 43. Copyright © 2008, American Chemical Society.

The preparation of free-base triphyrins led to the investigation of new metal complexes.[44,46] Triphyrin complexes are thus known for Mn(I), Re(I), Ru(II), and Pt(II), and Pt(IV). In Figure 17, whereas d^8 Pt(II) leads to a square-planar complex involving only two of the triphyrin nitrogens, d^6 Pt(IV) affords an octahedral complex with full coordination by the triphyrin.[43-46]

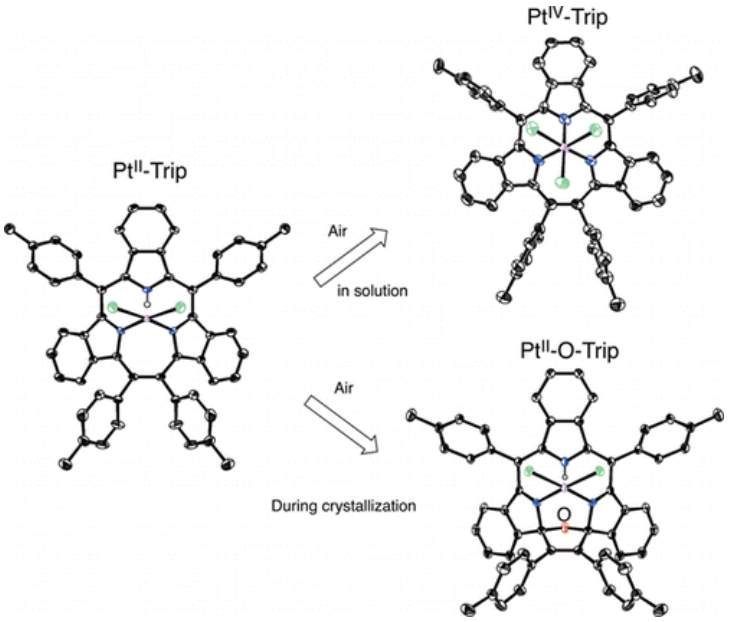

Figure 17. Pt(IV) and Pt(II) triphyrin complexes. Reproduced with permission ref. 46. Copyright © 2013, American Chemical Society.

2.4 *N*-CONFUSED PORPHYRINS

Whereas porphyrins contain pyrroles linked via α-carbons, an *N*-confused porphyrin has one or more pyrroles links via an α–carbon and a β–carbon with the rest of the molecule, as shown in Figure 18.

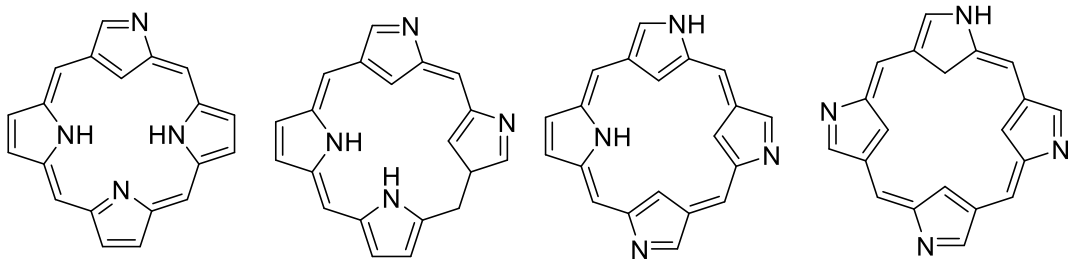

Figure 18. From left to right: singly, doubly, triply, and fully *N*-confused porphyrins.

N-confused porphyrins are generally obtained as by-products of one-pot syntheses, as illustrated in Figure 19.[47] The best yields, however, have been obtained by using a modified MacDonald synthesis using a dialdehyde and a tripyrrane via a [3 + 1] addition.[48]

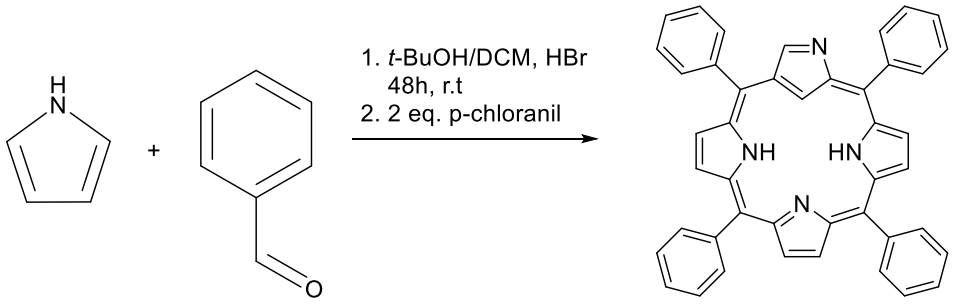

Figure 19. Synthesis of singly *N*-confused porphyrin via condensation of an aromatic aldehyde and pyrrole in 5-7% yield, which also yielded the porphyrin (~20%).

The first doubly *N*-confused porphyrin was synthesized in low yield in 2001 via the [2 + 2] coupling of an *N*-confused dipyrromethane under Lewis acid catalysis, as shown in Figure 20.[49]

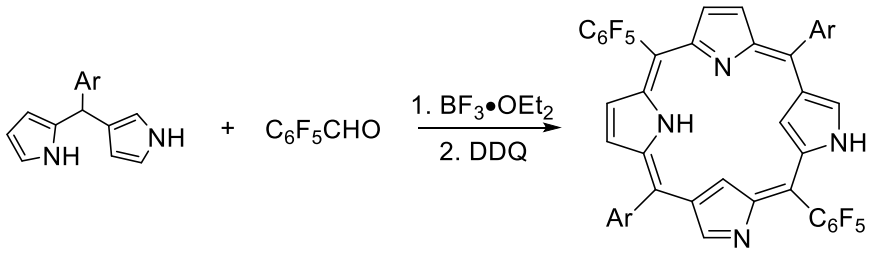

Figure 20. Synthesis of a doubly *N*-confused porphyrin from an *N*-confused dipyrromethane.

N-confused porphyrins generally yield square-planar or square-pyramidal complexes. For singly *N*-confused porphyrins Ni, Pd, Pt, Cu, Ag, Au, Rh, and Cu complexes are known, while for doubly confused porphyrins Cu, Ag, Pd, and Rh complexes have been reported.[50]

2.5 EXPANDED PORPHYRINS

Sapphyrins and other expanded porphyrins exhibit significant absorption in red and near-infrared and are therefore of interest from the point of view of photodynamic therapy.[51] By a modified Lindsey condensation with high concentrations pyrrole and aldehyde (67 mM each) and 4.2 mM boron trifluoride diethyl etherate, a mixture with nine different expanded so-called [n]phyrins were obtained, as shown in Figure 21. The compounds could all be separated with column chromatography.[52]

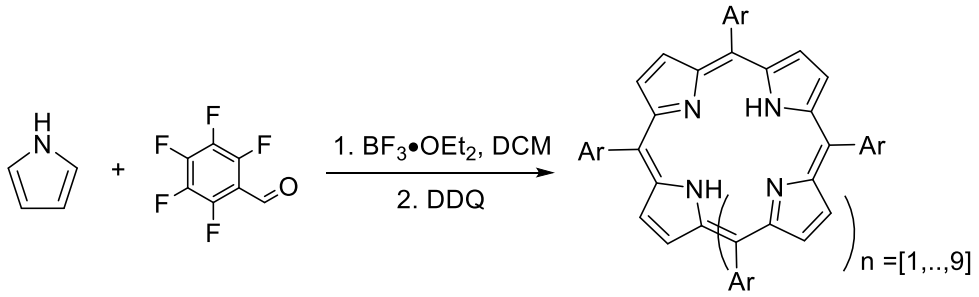

Figure 21. Synthesis of the [n]phyrins.

Among the [n]phyrins, hexaphyrin has exhibited quite remarkable, new coordination chemistry. Thus, hexaphyrin can act as a binucleating ligand, coordinating either one or two gold atoms (Figure 22). Compared to the free base (~550 nm), the digold(III) complex exhibits a dramatically redshifted Soret maxima at ~680 nm.[51]

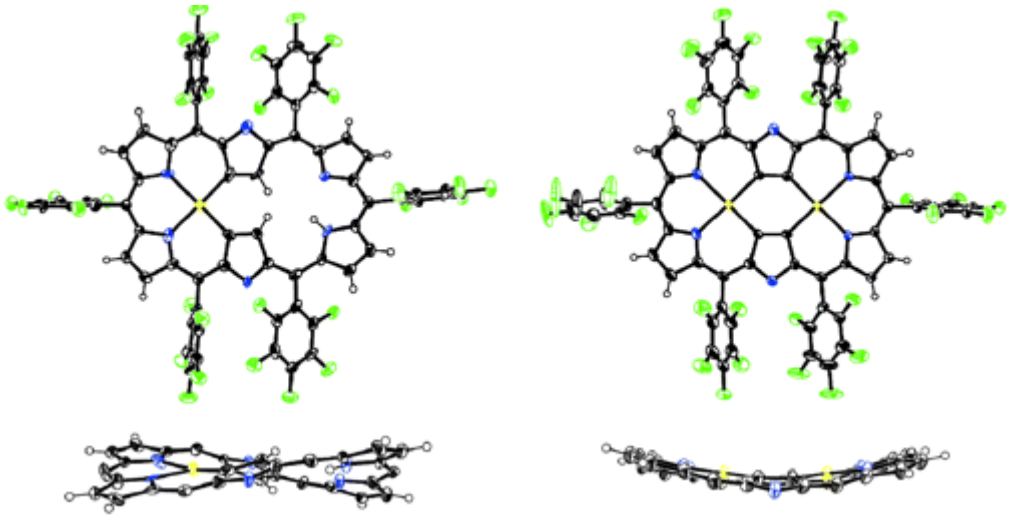

Figure 22. X-ray structure of mono- and digold hexaphyrin. Reused with permission from ref. 51. Copyright © 2005, American Chemical Society.

2.6 SAPPHYRINS

Sapphyrins, which got their name from their blue colour, have not been very extensively studied. They were first reported in 1973 during Woodward's total synthesis of vitamin B_{12}.[53] A second, multistem synthesis was published in 1982 but it resulted in a poor final yield.[54] Because of their poor availability,[55] the coordination chemistry of sapphyrins has not been studied in depth. However, they have been shown to coordinate the uranyl cation and the resulting complex has been found to exhibit interesting peripheral reactivity, as shown in Figure 23.[56]

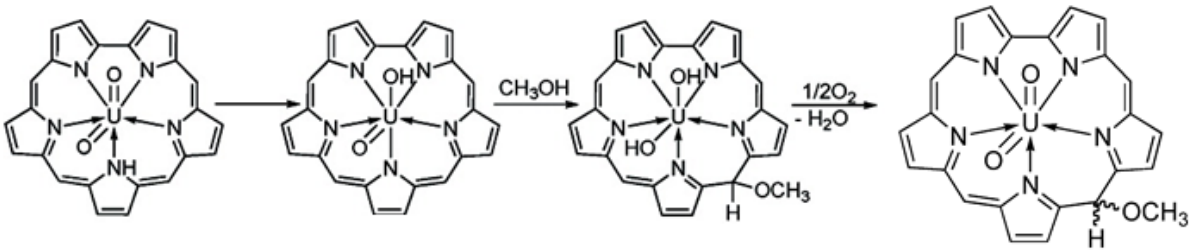

Figure 23. Reactivity of a uranyl sapphyrin. Reused with permission from ref. 56. Copyright © 2011, American Chemical Society.

2.7 PORPHYRAZINES AND PHTHALOCYANINES

Porphyrazines and phthalocyanines are porphyrin analogues where the *meso* carbon have been substituted by nitrogens. They are purely synthetic compounds and have been widely used in numerous applications due to their high thermal, chemical, and photochemical stability.[57,58] Their synthesis generally involve cyclopolymerization reactions that proceed in moderate to quite good yields (45 – 80%), as shown in Figure 24.[59,60]

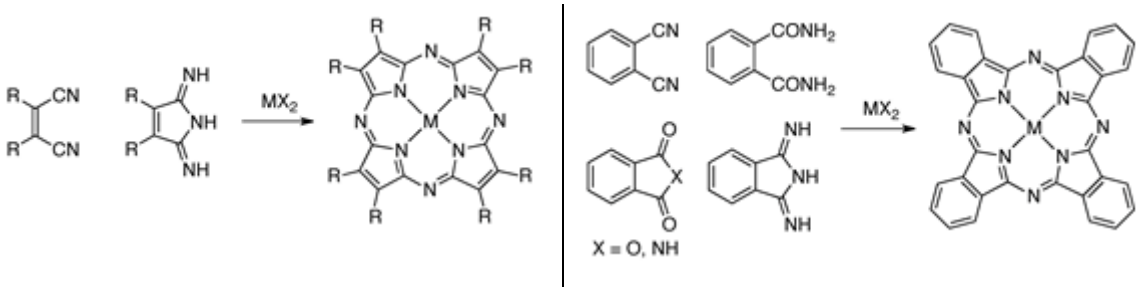

Figure 24. Syntheses of the porphyrazine and phthalocyanine ring systems. Reused with permission from ref. 60. Copyright © 2017, American Chemical Society.

Because C-N bonds are shorter than C-C bonds with the same bond order, porphyrazines and phthalocyanines have smaller N_4 cores than porphyrins, which leads to distinctive properties as ligands. Thus, the smaller N_4 core of octaethylporphyrazine leads to an $S = 3/2$ ground state for Fe[OEPz]Cl, compared to an $S = 5/2$ ground state for Fe[OEP]Cl and most other FeCl porphyrins.[61]

2.8 CORROLAZINE

The interaction of a porphyrazine with a phosphorus electrophile such as PBr_3 results in low yields of ring-contracted product – a phosphorus corrolazine.[62] The phosphorus proved difficult to remove but the free ligand was finally obtained under reductive conditions with an excess of Na/NH_3, as shown in Figure 25. The tetrabenzo analogue – tetrabenzocorrolazine – has also been synthesized in an analogous manner.[63]

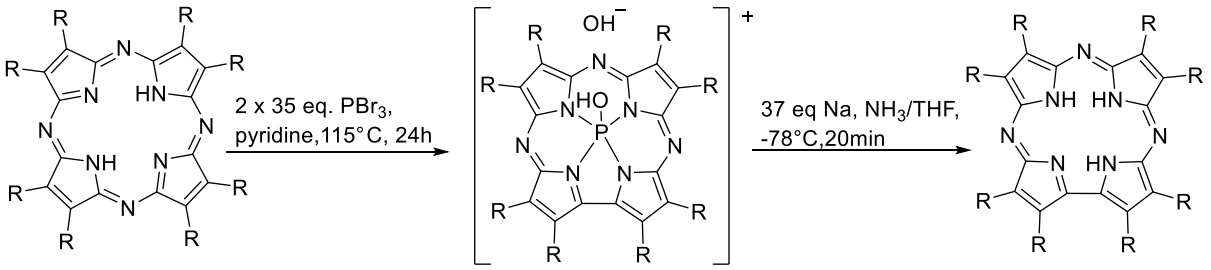

Figure 25. Preparation of corrolazine through ring contraction of a porphyrazine and demetalation.

Like corroles, corrolazines have been found to yield high-oxidation-state complexes as well as catalysts. However, because of their inaccessibility, corrolazines never reached the popularity that corroles enjoy.[64]

2.9 HYDROPORPHYRINS

Hydroporphyrins, or reduced porphyrins, include chlorin, bacterochlorin, and isobacterichlorin (Figure 3), which occur naturally in various chlorophylls.[65] A variety of synthetic approaches have been developed for these ring systems, including several [2 + 2] strategies such as the MacDonald synthesis, as shown in Figure 26.[66,67] Chlorins, bacteriochlorins, and isobacteriochlorins exhibit strong Q bands in the red or near-infrared,[68] these can be redshifted even further with appropriate conjugated substituents. Hydroporphyrins therefore are of great importance as sensitisers in photodynamic therapy.[69,70]

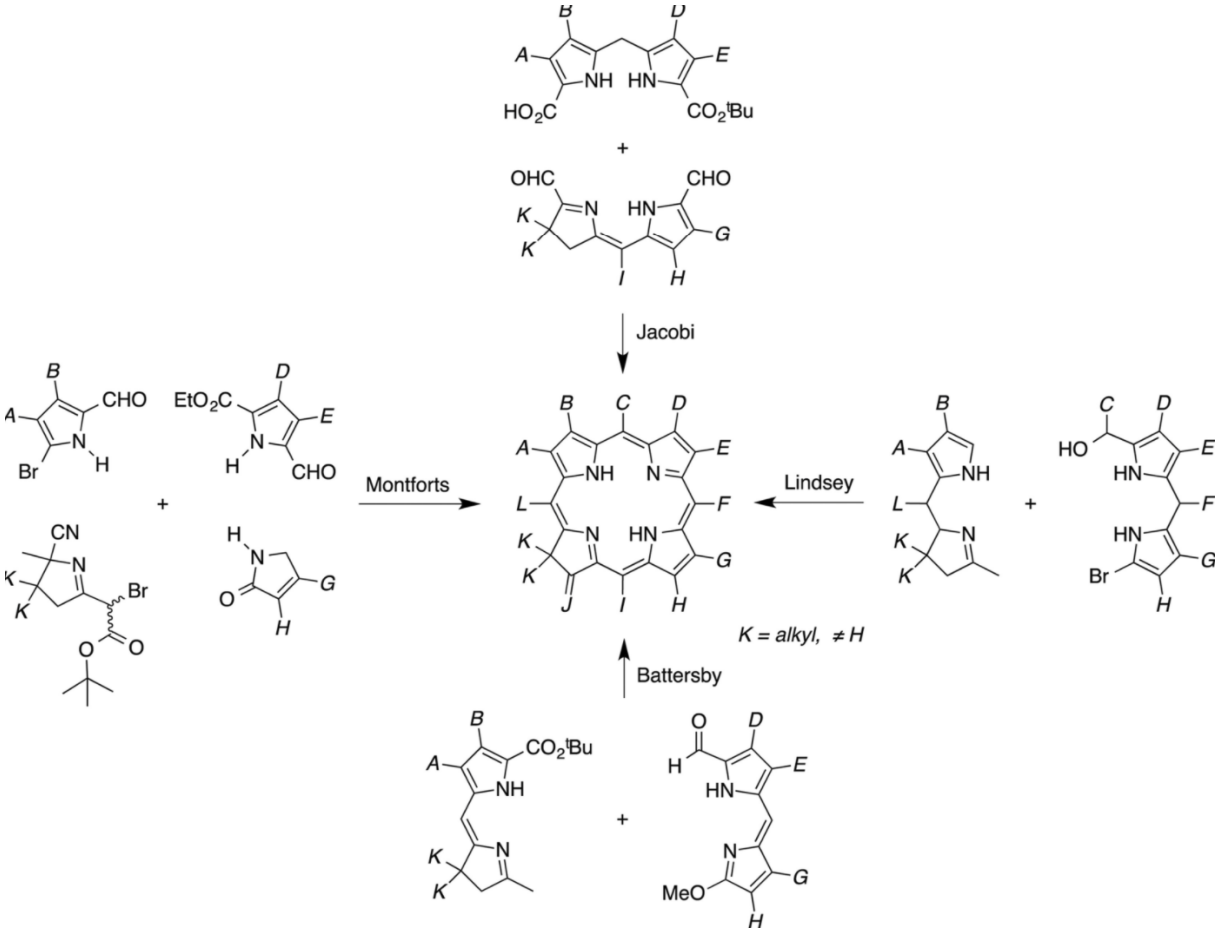

Figure 26. Four syntheses of the free-base chlorin. Adapted with permission from ref. 68b. Copyright © 2017, American Chemical Society.

2.10 CORROLES

The first synthesis of a corrole was reported by Johnson and Kay in 1964 in the course of their unsuccessful attempt to synthesize corrin, the macrocyclic ring system of Vitamin B_{12}.[71] Progress from that point on was slow, until 1999, when two groups led by Gross[72] and Paolesse[73] independently reported one-pot syntheses of *meso*-triarylcorroles. Gross's "solvent-free" method employed pyrrole and pentafluorobenzaldehyde in the presence of a solid support (silica or alumina) at 100˚C for 4 hours, followed by DDQ oxidation (Figure 27).

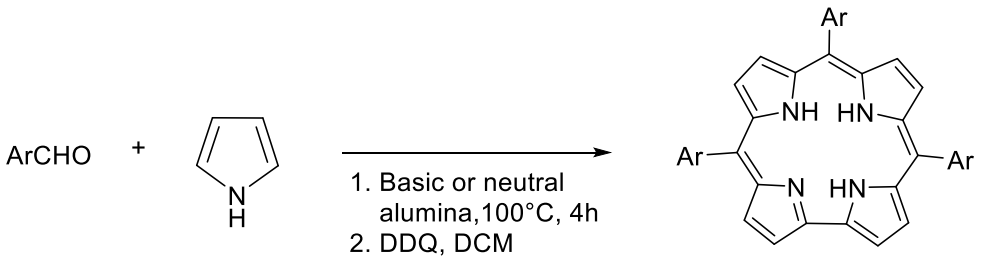

Figure 27. Gross's solvent-free corrole synthesis on a solid support.

Paolesse employed a Rothemund-like procedure, employing a 3:1 mixture of pyrrole and benzaldehyde in refluxing acetic acid for 4 hours (Figure 28).

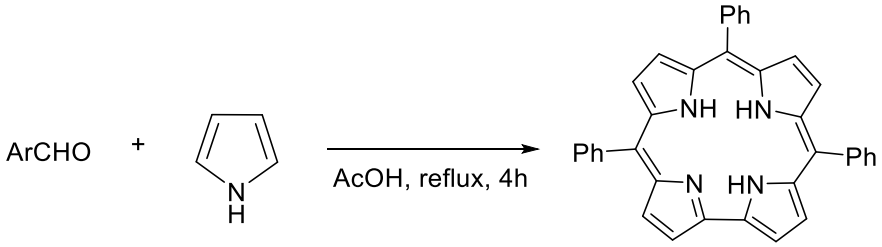

Figure 28. Paolesse's synthesis of *meso*-triphenylcorrole.

Ghosh *et al.*[74] extended Gross's method to aromatic aldehydes other than benzaldehyde as well as 3,4-difluoropyrrole (Figure 29).

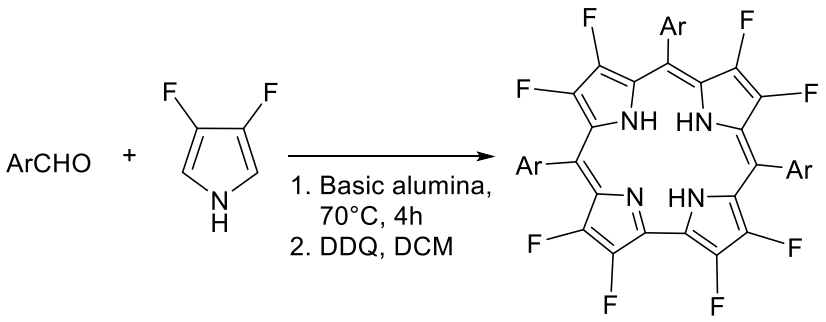

Figure 29. Ghosh's synthesis of free-base octafluorocorroles.

All of the above syntheses proceeded in poor yields, ranging from 5-20%. The syntheses proved practical only because of their simple, one-pot procedure.

In 2006, Gryko and co-workers reported a substantially improved synthesis for corroles.[75] Their protocol involved two steps: the interaction of an aldehyde and pyrrole (2:1 molar ratio) in an acidified water-methanol (1:1) mixture, followed by extraction and oxidation of the resulting bilane with *p*-chloranil or DDQ (Figure 30). The method routinely led to yields above 20%.

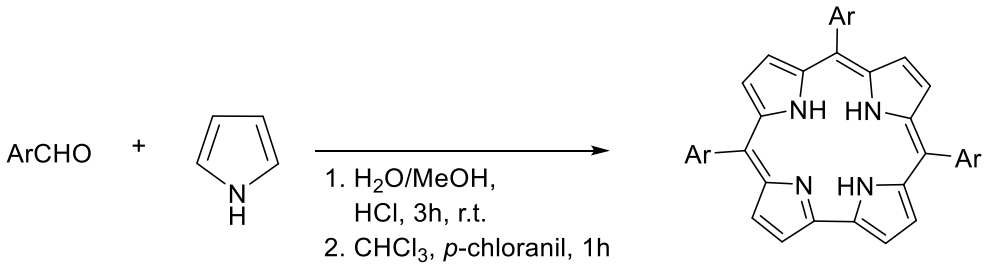

Figure 30. One-pot synthesis of corrole through Gryko's water-methanol method.

In the same publication, the authors also reported a procedure for the preparation of *trans*-A_2B triarlycorroles. The synthesis required an additional step, namely the synthesis of an arlydipyrromethane (Figure 31).

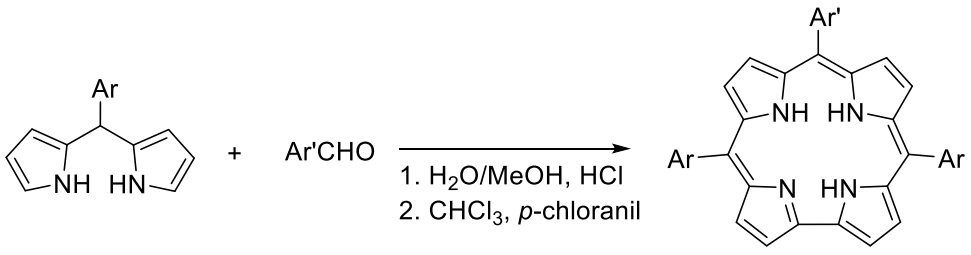

Figure 31. Synthesis of A_2B corroles.

Soon thereafter, the Gryko group reported an optimized procedure for the synthesis of 5-aryldipyrromethanes (Figure 32).[76] The method, which involves the interaction of an aromatic aldehyde and pyrrole (1:3) in water acidified with HCl, yieldeds 5-aryldipyrromethane in excellent yields (80-97%).

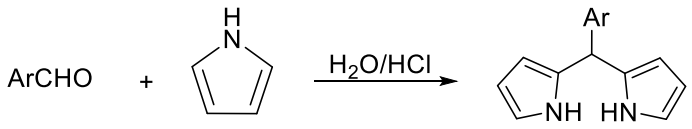

Figure 32. Gryko's synthesis of 5-aryldipyrromethanes.

Like porphyrins, corroles are aromatic molecules with rich spectroscopic properties. Free-base and nontransition metal corroles are generally fluorescent. First-row transition metal corroles, like their porphyrin analogue, are generally nonluminescent. On the other hand, many 5d metallocorroles, including ReO corroles reported in this thesis, exhibit near-IR phosphorescence.[77] Corrole derivatives, however, have only been applied to a limited extent in photodynamic therapy – a state of affairs that the present work will hopefully change in the near future.

2.11 METALLOCORROLE COMPLEXES

The coordination chemistry of corroles has grown vigorously over the last two decades and the "periodic table of corroles" (Figure 33) is today almost as extensive as "the periodic table of porphyrins". Thus, nearly all transition metals and many main-group and f-elements have been complexed to corroles. Despite their superficial similarity to porphyrins, corroles exhibit substantially different coordination chemistry, including a variety of high-valent complexes. This difference reflects primarily two factors, a contracted N_4 core relative to porphyrins and a 3- rather than 2- charge as ligands.

1																	18
H	2											13	14	15	16	17	He
Li	Be											B	C	N	O	F	Ne
Na	Mg	3	4	5	6	7	8	9	10	11	12	Al	Si	P	S	Cl	Ar
K	Ca	Sc	Ti	V	Cr	Mn	Fe	Co	Ni	Cu	Zn	Ga	Ge	As	Se	Br	Kr
Rb	Sr	Y	Zr	Nb	Mo	Tc	Ru	Rh	Pd	Ag	Cd	In	Sn	Sb	Te	I	Xe
Cs	Ba	*	Hf	Ta	W	Re	Os	Ir	Pt	Au	Hg	Tl	Pb	Bi	Po	At	Rn
Fr	Ra	**	Rf	Db	Sg	Bh	Hs	Mt	Ds	Rg	Cn	Nh	Fl	Mo	Lv	Ts	Og
*Lanthanoids			La	Ce	Pr	Nd	Pm	Sm	Eu	Gd	Tb	Dy	Ho	Er	Tm	Yb	Lu
** Actinoids			Ac	Th	Pa	U	Np	Pu	Am	Cm	Bk	Cf	Es	Fm	Md	No	Lr

Figure 33. The periodic table of corroles. The blue shaded elements are those known to be coordinated to a corrole up to November 2017. The red-framed are those included in this thesis. Adapted with permission from ref. 27. Copyright © 2017, American Chemical Society.

The following section briefly summarizes our current knowledge about the major classes of corrole complexes.

2.11.1 The s- and p-block complexes

Among s-block elements, only lithium has been coordinated to corroles and a dilithium-corrole-anion, has been structurally characterised, as shown in Figure 34.[78] In the hands of Arnold and co-workers, lithiated corroles proved to be important starting materials for the synthesis of early transition metal and f-block metal corrole derivatives, as depicted for Group IV metallocorroles in Figure 35.[79]

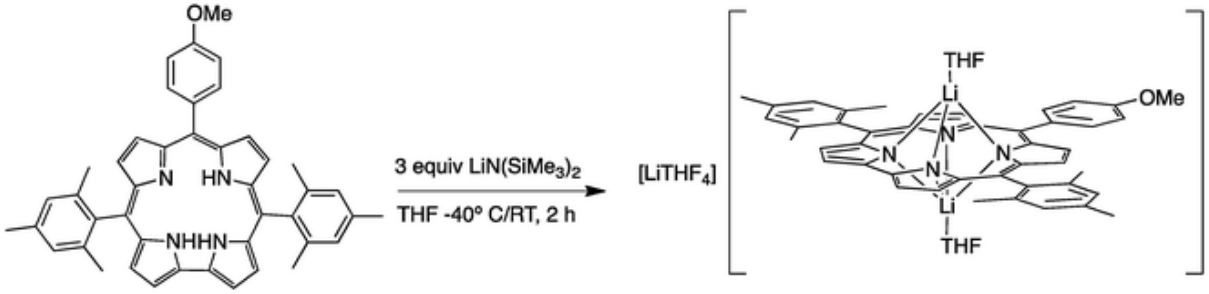

Figure 34. Synthesis of lithium corrole complexes. Reproduced with permission from ref. 78. Copyright © 2012, Royal Society of Chemistry.

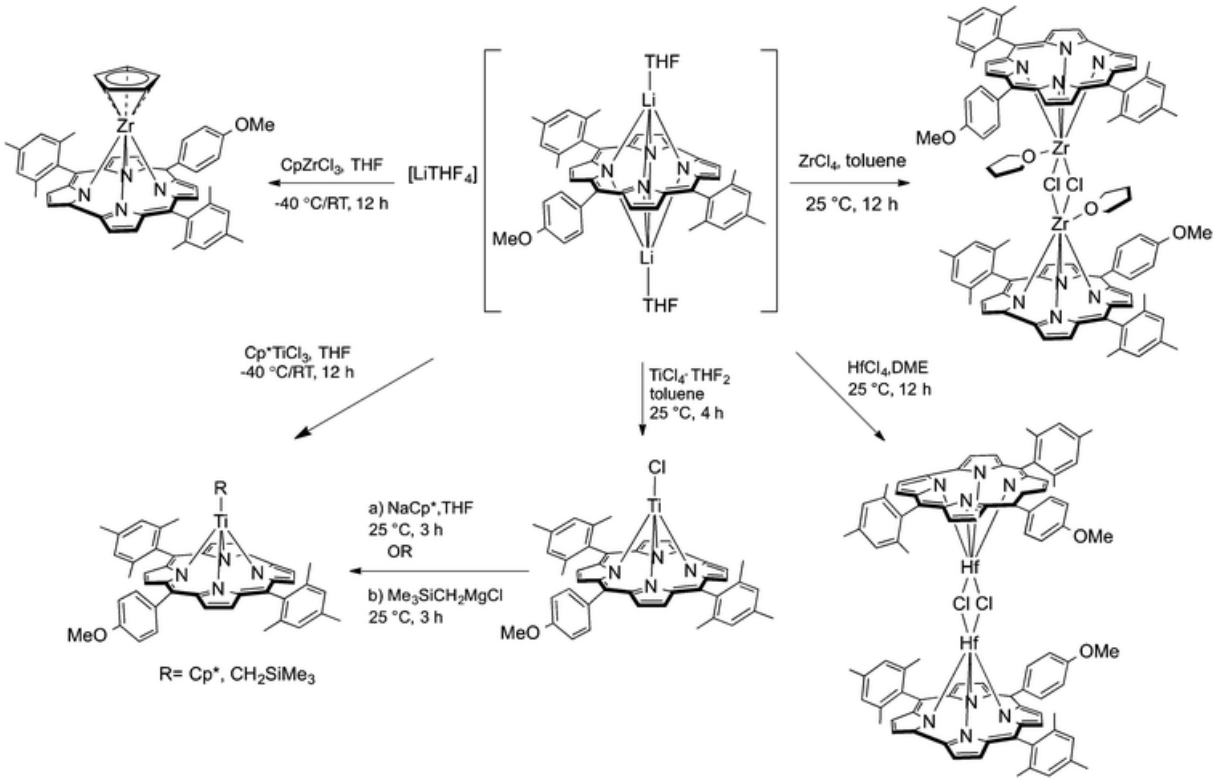

Figure 35. Syntheses of Group IV metallocorroles from lithiated corrole. Reused with permission from ref. 79. Copyright © 2014, Royal Society of Chemistry.

Several *meso*-triarylcorrole derivatives of the p-block elements have been synthesized, including those of Ge,[80] Sn,[80,81] Pb,[82] P,[80,83,84] Sb,[85] and Bi,[86] as shown in Figure 36. Among the most interesting of these complexes are the boron corroles, in which boron acts as a binucleating ligand.[87] Like free-base corroles, many of the complexes involving lighter p-block elements such as Al, P, and Ga are strongly fluorescent, with great potential in the area of medical imaging.[88,90]

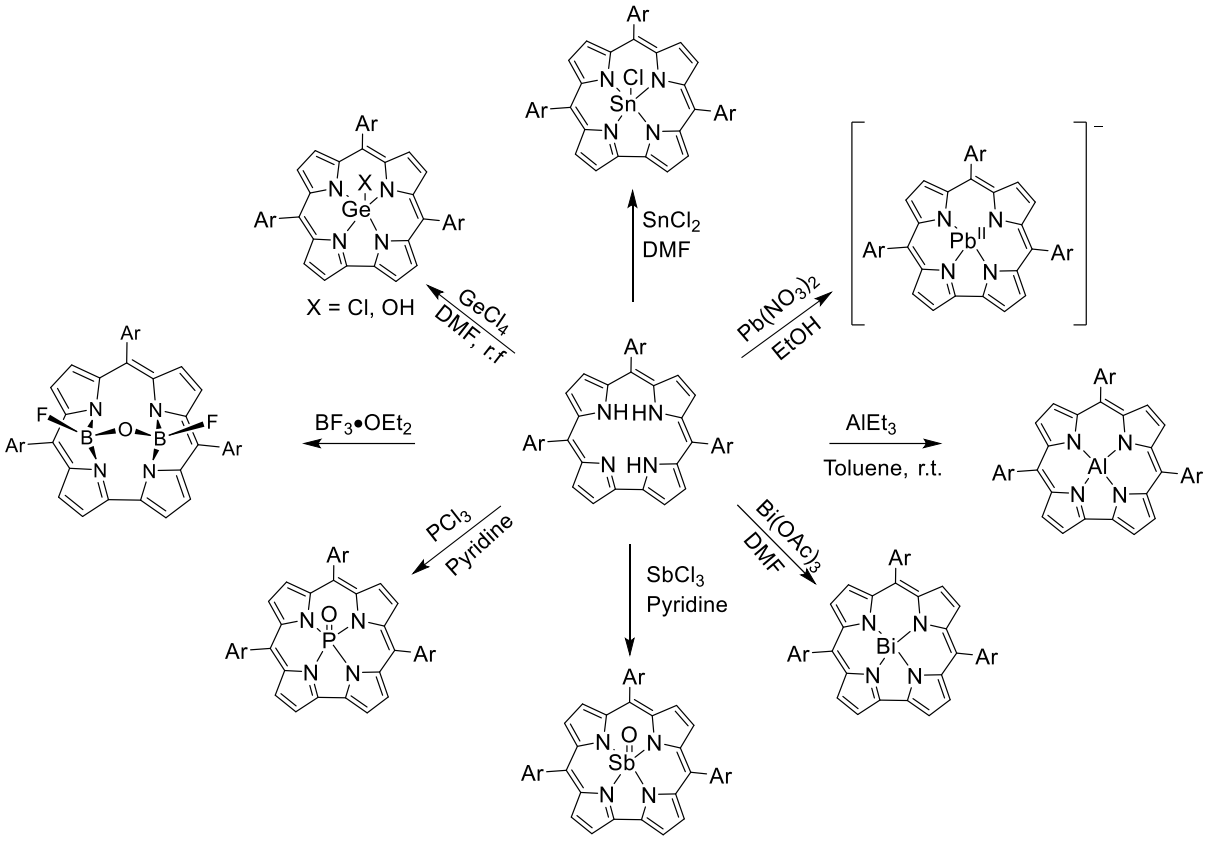

Figure 36. Syntheses of Group 13, 14, and 15 *meso*-triarylcorrole complexes.

2.11.2 The d-block elements

The 3d metallocorroles have been intensively studied, especially those involving the elements Cr, Mn, Fe, Co, and Cu. The complexes are generally easily synthesized and many exhibit novel reactivity and catalytic activity, for instance activation of O_2.[91]

The first chromium corroles were prepared from 7,8,12,13-tetraethyl-2,3,17,18-tetramethylcorrole and $CrCl_2$ in refluxing DMF.[92] Subsequently $Cr^{V}O$ corroles have been more conveniently prepared from *meso*-triarylcorroles and $Cr(CO)_6$ in refluxing toluene.[93]

Manganese complexes can be prepared by direct metalation of octaalkylcorroles using $Mn_2(CO)_{10}$ in refluxing toluene or $Mn(OAc)_3$ in refluxing DMF.[94,95] Preparation of manganese *meso*-triarylcorroles can be made by refluxing the free-base with $Mn(OAc)_3$ in either DMF, MeOH or pyridine.[96-99] Using Mn(III)-*meso*-triarylcorrole it has been possible to further oxidise manganese to higher states[100]. Some of these routes are shown in Figure 37. Among these the $Mn^{V}O$ has been investigated as possible electron-, oxygen-, and hydrogen atom transfer agents.[101-102]

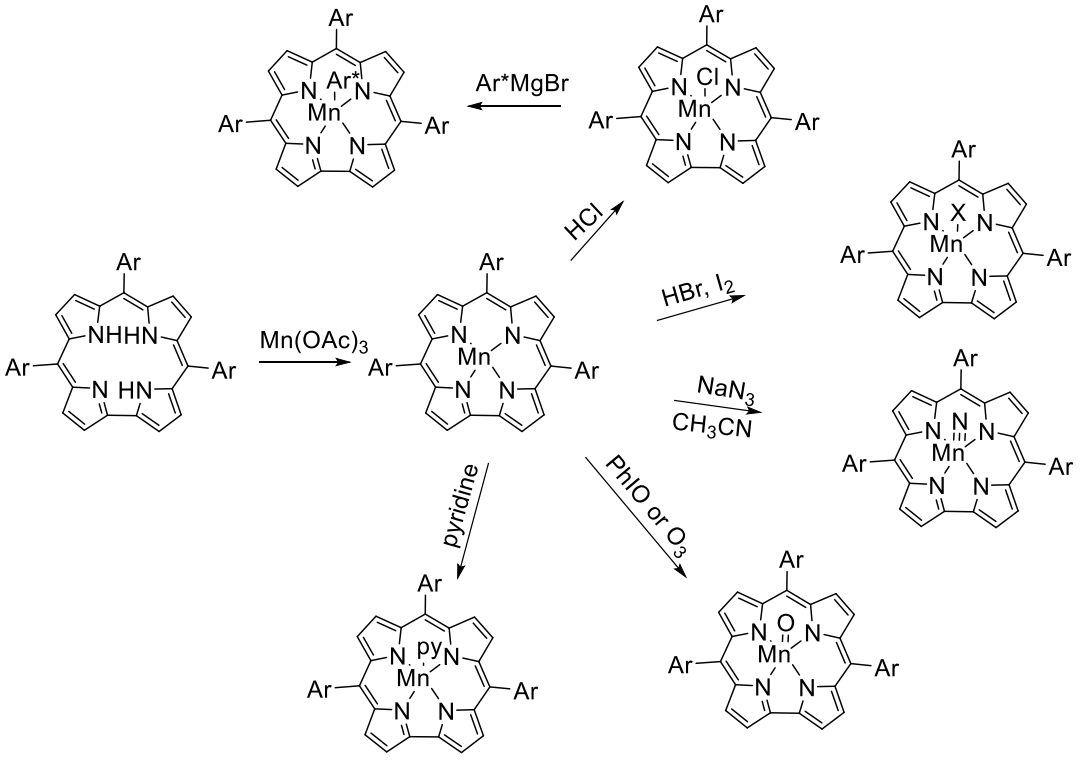

Figure 37. Syntheses and key transformations of Mn corroles.

Iron corroles can be prepared by several procedures. The first one reported used octamethylcorrole and $FeCl_3$ in DMF at reflux.[94] It was also possible to prepare using $Fe(CO)_5$ in toluene at reflux.[94] Preparation of Iron(III) *meso*-triarylcorroles can also be done by almost identical methods.[103] As with manganese corroles, a wide range of axially ligated iron corroles have been reported in recent years. Figure 38 shows some of the major synthetic transformations involving iron corroles. Iron corroles have been under extensive investigation on whether the corrole acts as an innocent 3- ligand or a noninnocent •2-, as described later.[104-107]

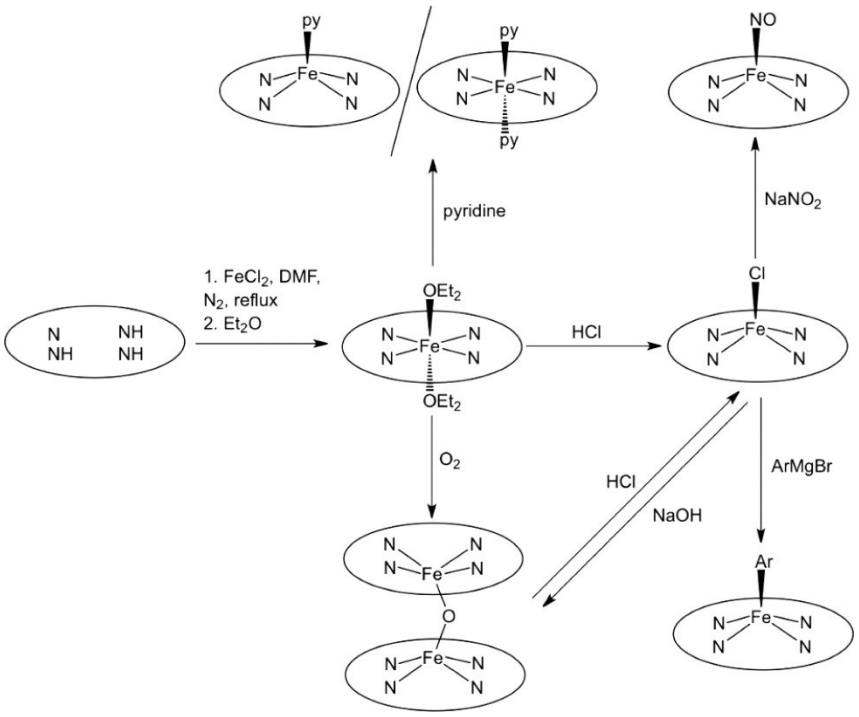

Figure 38. Schematic diagram of the major synthetic transformations involving Fe corroles. Reused with permission from ref. 106b. Copyright © 2017, American Chemical Society.

Cobalt corroles are easily made by reacting a free-base corrole with Co(II)$(OAc)_2$ in either refluxing pyridine or in MeOH and in presence of PPh_3,[108,109] conditions that yield Co^{III}-corrole with either two pyridines or one PPh_3 as axial ligand.

Nickel corroles have been made from *β*-octaalkylcorrole and either $NiCl_2$ in CH_2Cl_2/MeOH or $Ni(OAc)_2$ in DMF. EPR studies have indicated that nickel does not exist as Ni(III) but rather as Ni(II) in conjunction with a corrole radical.[110]

Copper is easily inserted into corroles using Cu(II) salt such as $Cu(OAc)_2$. The resulting formally Cu(III) salts are actually better viewed as Cu^{II}-corrole$^{\bullet 2-}$ metalloradicals, where antiferromagnetic coupling between the Cu(d_{x2-y2}) electron and the corrole radical leads to significant saddling of the corrole macrocycle. Copper corroles are also readily *β*-octabrominated and the resulting Cu *β*-octabromocorrole serve as starting material for other transformations such as Suzuki-Miaryura coupling. A very useful property of Cu corroles is that they can be demetallated under reductive conditions (e.g., 5-200 eq. of $FeCl_2$ or $SnCl_2$ and concentrated H_2SO_4), serving as a path for *β*-octabromo free-base corroles.[71,74,110,111]

2.11.3 The 4d metallocorroles

As of today, Zr, Mo, Tc (this work), Ru, Rh, and Ag of the 4d transition series have been coordinated to a corrole and the products structurally characterized. The syntheses generally involve a high-boiling solvent and are carried out under more forcing conditions compared with 3d metallocorroles.

As shown in Figure 35, Arnold and co-workers have prepared Zr corroles via the interaction of a lithiated corrole with $CpZrCl_3$ or $ZrCl_4$ at a low temperature in an aprotic solvent.[78]

Molybdenum corroles have been prepared by refluxing a free-base corrole with $Mo(CO)_6$, in decalin.[112] The product is either a molybdenum(V)-oxo-corrole or a molybdenum(VI) biscorrole, depending on whether oxygen is strictly excluded or not. Molybdenum(V)-oxo corroles undergo one-electron metal-center reduction; thus, addition of trimesitylvanadium(III) or bromo(mesityl)magnesium bromide to a Mo(V)-oxo corrole in THF resulted in the immediate formation of the binuclear molybdenum(IV)-oxo corrole complex depicted in Figure 39.

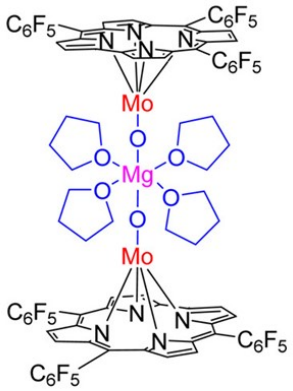

Figure 39. A binuclear molybdenum(IV) corrole. Reused with permission from ref. 27. Copyright © 2017, American Chemical Society

Early attempts at synthesizing ruthenium corroles via the reaction of a free-base corrole with $Ru_3(CO)_{12}$ or $RuCl_3$ failed and led instead to the corresponding porphyrin.[94] Subsequently Ru corroles were prepared by several groups, from a free-base corrole and $[Ru(cod)Cl_2]_2$ in refluxing 2-methoxyethanol in the presence of trimethylamine (Figure 40).[113,114] In the absence of other additives, the product is a chemically inert metal-metal-bonded Ru corrole dimer. Later it was found that the initially formed mononuclear Ru-corrole intermediates could be trapped

by $NaNO_2$, affording RuNO corroles. Prolonged heating resulted in deoxygenation of the RuNO corrole, leading to ruthenium(VI)-nitrido corroles, which have been structurally characterized.

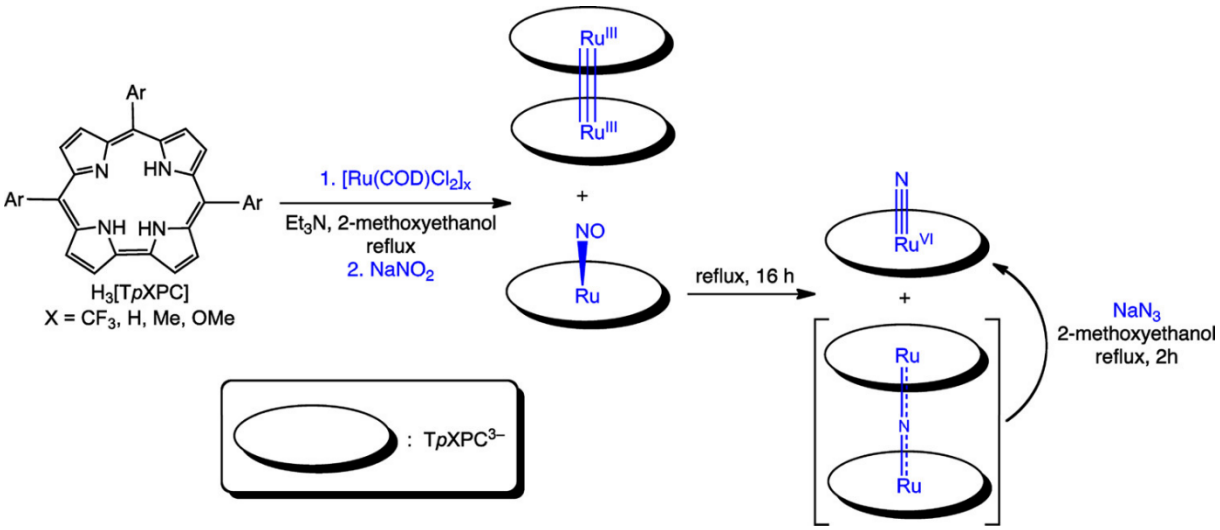

Figure 40. Synthetic routes to Ru *meso*-triarylcorroles. Reused with permission from ref. 114b. Copyright © 2017, American Chemical Society.

By comparison, rhodium is rather simply inserted into corroles. The interaction of free-base corroles with $[Rh(CO)_2Cl]_2$ in the presence of PPh_3 and K_2CO_3 in an aprotic solvent affords rhodium(III) corroles axially coordinated to a PPh_3 ligand.[103] Electrochemical analyses of Rh(III)-PPh_3-β-octamethylcorrole showed that the π-system was oxidised while the reduction was at the Rh-metal center.[115]

Silver(III) corroles are also easily prepared by stirring free-base corroles in hot pyridine with an excess of silver(I) acetate.[116] Interestingly, silver(III) corroles undergoes facile reductive demetalation, indeed much more readily than Cu corroles.

2.11.4 The 5d Metallocorroles

The 5d metallocorroles have only been synthesized recently.

The first metallocorrole was obtained accidentally in 1998 via ring contraction of *meso*-tetrakis(trifluoromethyl)porphyrin upon reflux with $Re_2(CO)_{10}$ in with benzonitrile, as shown in Figure 41.[117] Under these conditions, the rhenium(V)-oxo-corrole complex was obtained in ~9% yield.

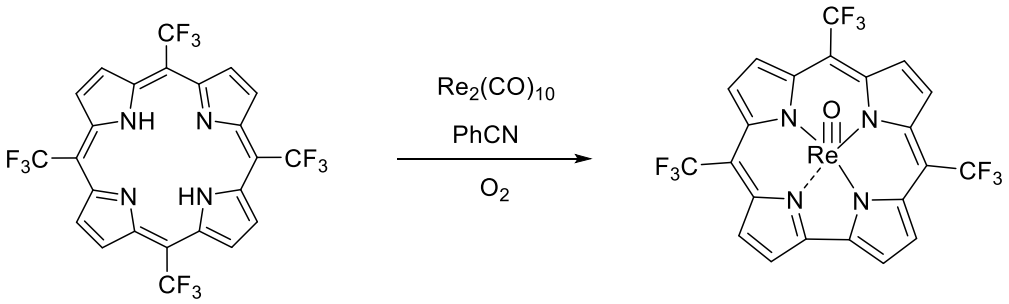

Figure 41. Accidental synthesis of an $Re^{V}O$ corrole via ring contraction of *meso*-tetrakis(trifluoromethyl)porphyrin.

Subsequently, in 2008, Gray and co-workers reported iridium(III) corroles, which marked the serious beginning of the 5d metallocorrole field. The complexes were all prepared by refluxing a free-base corrole with $[Ir(cod)Cl]_2$ and K_2CO_3 in THF under argon. The initially obtained iridium(I)-corrole-cod product was converted to iridium(III) corroles upon exposure to air or to another oxidant. In the presence of a ligand such as ammonia or pyridine, the product is obtained in axially bis-ligated form.[118-120] Iridium corroles are electron-rich and readily undergo octabromination upon exposure to elemental bromine.[119]

Gold corroles were next in line and was reported nearly simultaneously by the Ghosh[121] and Gross[122] groups. Both groups used *β*-octabromo-*meso*-triarylcorroles as substrates, with $HAuCl_4$ leading directly to the Au(III) complexes. This method, however, could not be applied to simple triarylcorroles. Subsequently, a general method for Au(III) corroles were reported, consisting of the interaction of a free-base corrole with gold(III) acetate in pyridine at room temperature, as shown in Figure 42.[121]

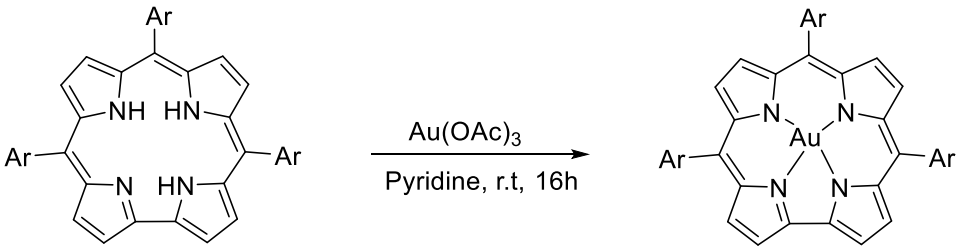

Figure 42. Synthesis of Au(III) corroles.

The synthesis of Pt corroles proved considerably more troublesome. They were finally accessed in low yield via a microwave synthesis involving the tetranuclear salt $[Pt(OAc)_2]_4$•2AcOH, a free-base corrole in benzonitrile, and microwave irradiation at 140-150˚C for 2 hours.[123]

By comparison, osmium(VI)-nitrido corroles were synthesized in reasonably good yields via the interaction of a *meso*-triarylcorrole with $Os_3(CO)_{12}$ and NaN_3 in refluxing diethylene glycol monomethyl ether/glycol (1:2 ratio) for 16 hours.[124]

The early transition metal Hf on the other hand was inserted via the reaction of a lithiated corrole with $HfCl_4$ in dimethoxyethane.[125] The other early 5d metal Ta was similarly inserted using a lithiated corrole and $TaMe_3Cl_2$ via prolonged heating in toluene at 100˚C (Figure 43). The resulting Ta^VCl_2 corrole could be derivatized to other complexes by displacing the chlorides with other nucleophiles. An alternative strategy for Ta insertion consisted of prolonged heating of a free-base corrole with $TaBn_3N^tBu$ in toluene, as shown in Figure 44.[126]

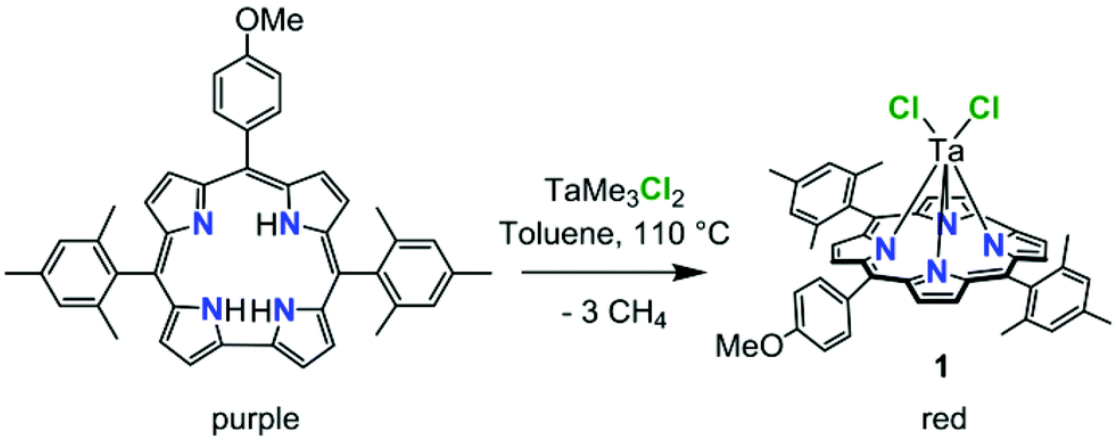

Figure 43. Synthesis of a dichlorotantalum corrole. Reused with permission from ref. 126. Copyright © 2016, Royal Society of chemistry.

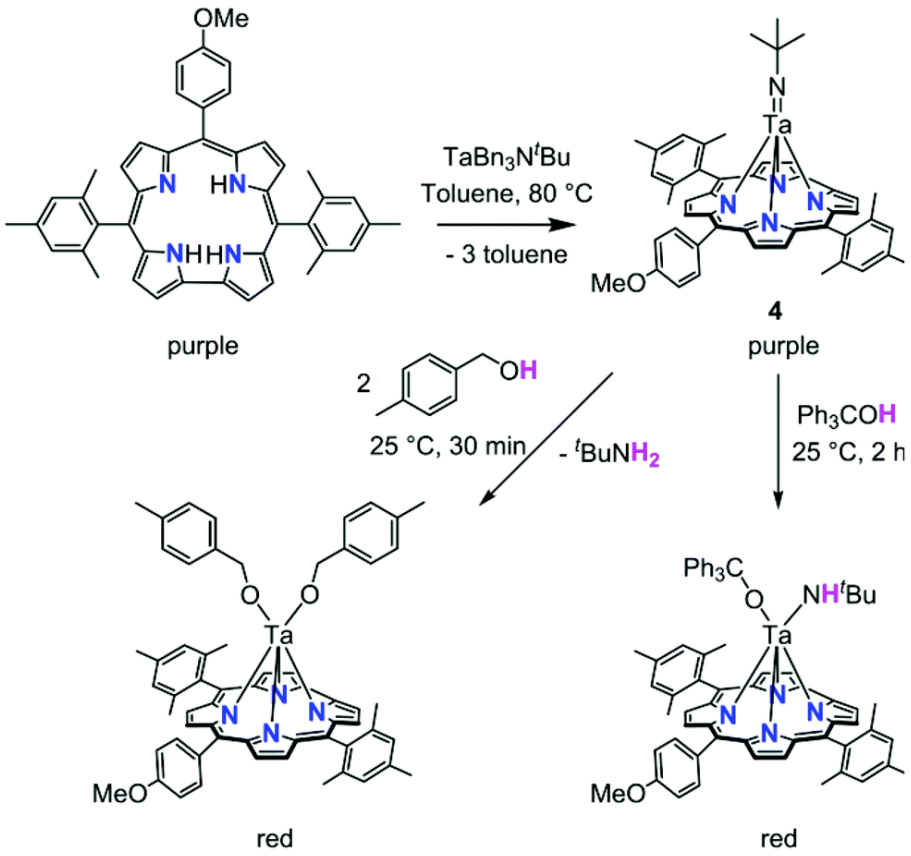

Figure 44. Synthesis of an imidotantalum corrole and its subsequent protonolysis with alcohols. Reproduced with permission from ref. 126. Copyright © 2016, Royal Society of Chemistry.

Tungsten corroles are known in two oxidation states, tungsten(V) and tungsten(VI). The first tungsten corrole was prepared via the reaction of tris(pentafluorophenyl)corrole and WCl_6 in decalin at 180˚C, which resulted in a binuclear complex in which two tungsten(VI) corrole moieties were bridged by three oxygens. The interaction of a lithiated corrole with WCl_6 in toluene at -40˚C on the other hand led to $W^{V}Cl_2$ corrole.[127] The latest contribution to tungsten corroles has come from our group in Tromsø in the form of a series of tungsten(VI) biscorroles, which were prepared by reacting free-base corroles with $W(CO)_6$ under anaerobic conditions in decalin at 180˚C.[128] These sandwich compounds are chiral and their stereochemically stable enantiomers have been resolved with chiral HPLC.

2.11.5 The f-block metallocorroles

A total of six metallocorroles containing f-block elements have been synthesized to date. Of these, four belongs to the lanthanide series; lanthanum, europium, gadolinium, and terbium, and despite of their radioactive nature, thorium and uranium from the actinide series. A couple of points are worth noting: the synthetic strategies are similar to those used for early transition metal corroles, and, the large metal ions are displaced far above the corrole macrocycle (Figure 45)

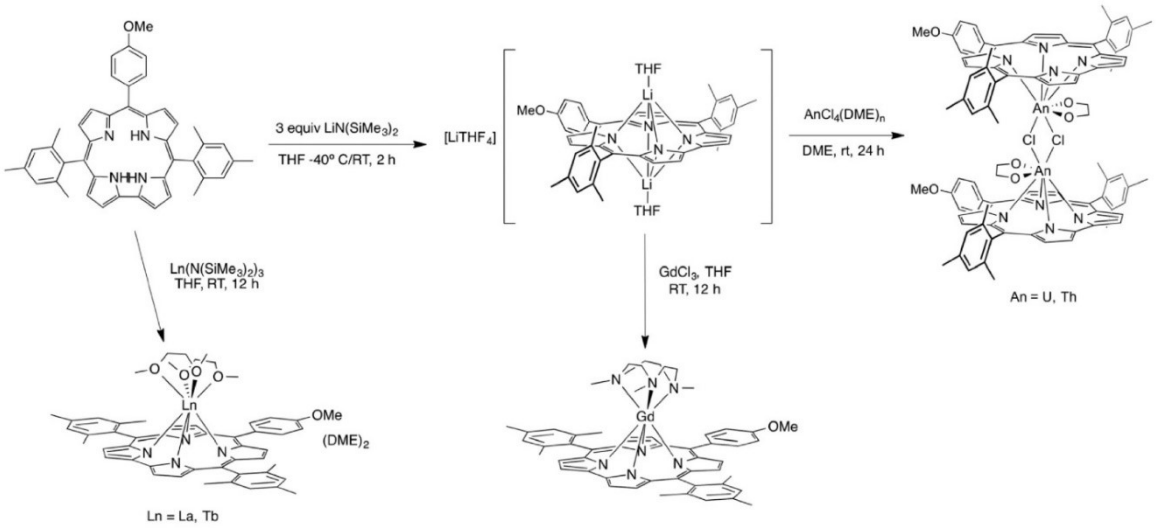

Figure 45. Synthetic approaches to f-block metallocorroles. Adapted with permission from ref. 129. Copyright © 2013, Royal Society of Chemistry.

Lanthanum, gadolinium and terbium were presented in the same publication. Lanthanum and terbium were prepared by mixing free-base corrole and $M[N(SiMe_3)_2]_3$ (M = La or Tb), respectively, in THF at room temperature and stirred for 12 hours. Gadolinium corrole complex were made starting with $GdCl_3$ and the lithiated free-base corrole in THF at room temperature for 12 hours.[129]

The europium corrole has only been reported as a triple-decker compound made by reaction of free-base corrole with the phthalocyanine complex in octanol.[130-132]

Both the thorium and uranium corroles were made in high yields 93% and 83% respectively starting with $ThCl_4(DME)_2$ or UCl_4 and lithiated free-base corrole in 1,2-dimethoxyethane at room temperature for 24 hours.[133]

2.11.6 Water-soluble corroles

To develop corroles as medical agents, water-soluble analogues were needed. Towards that end, several approaches were attempted. One obvious approach, based on the ready availability of cationic peripherally *N*-alkylated *meso*-tetrapyridylporphyrin,[135] involves analogous *meso*-tripyridylcorroles (Figure 46).[134] The first such corrole that has been tried in PDT experiments is P1021, which is similar to the molecules depicted in Figure 46. Published protocols for the synthesis of *meso*-tris(4-pyridyl)corrole, however, result in miserable yields of 2% or so.[136,137] Accordingly, PDT researchers have sought additional types of water-soluble corroles.

In a different approch to amphiphilic corroles, Gross *et al*., selectively obtained the corrole disulfonic acid shown in Figure 47 via brief interaction (5 minutes) of tris(pentafluorophenyl)corrole with chlorosulfonic acid.[138] The speed, simplicity, and high-yielding nature of the synthesis led to the synthesis of the corresponding Ga(III) complex and its exploration as a promising *in vivo* imaging agent.[139]

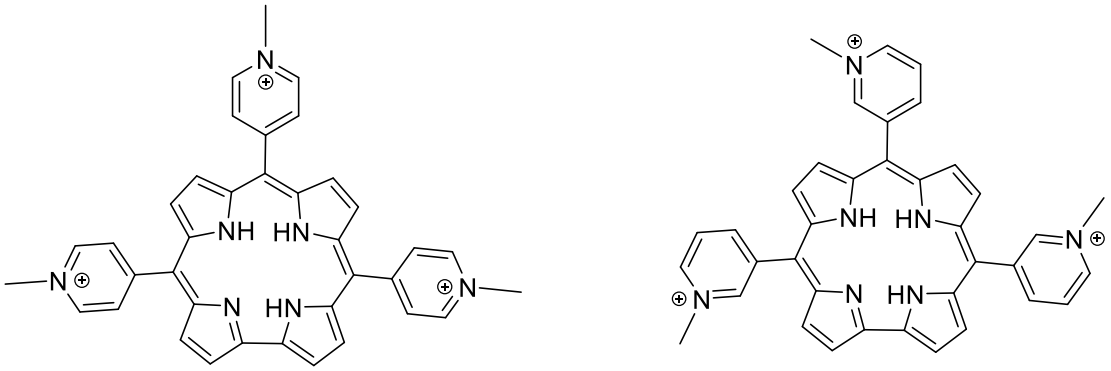

Figure 46. Cationic *meso*-pyridyl corroles.

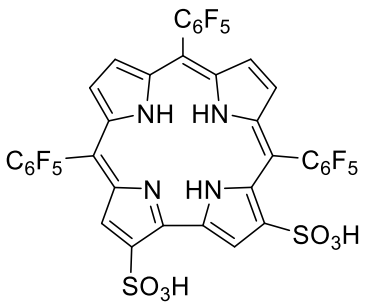

Figure 47. A corrole disulfonic acid synthesized by Gross and coworkers.

Ghosh *et al*. published yet a third route to amphiphilic corroles via alkaline hydrolysis of Au *meso*-triarylcorroles with carboxylate ester functionalities (Figure 48).[22] The corresponding Au corrole-acids have been found to exhibit excellent cytotoxicity against AY27 rat bladder cancer cells under blue light illumination.

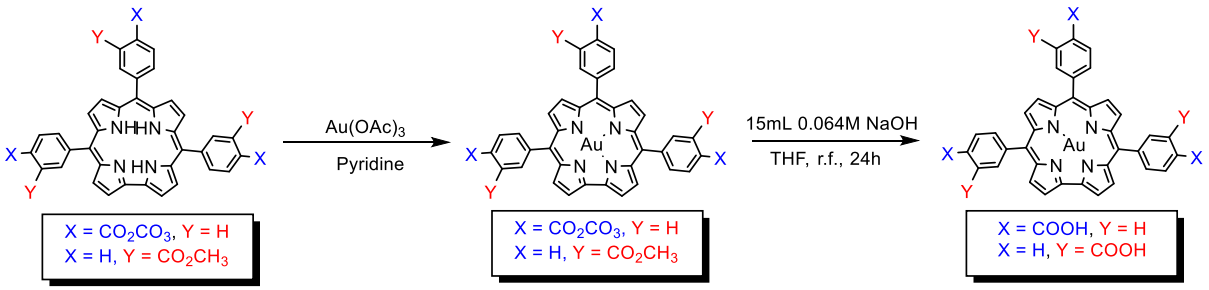

Figure 48. Synthesis of water-soluble Au(III) corroles through ester hydrolysis.

2.11.7 Innocent and noninnocent corroles

For many metallocorroles, the question arises as to whether the corrole is innocent or noninnocent. A ligand is said to be noninnocent when the oxidation state of the coordinated metal is uncertain or ambiguous from a casual inspection of the molecular or structural formula. First-row transition metal corroles provide many instances of noninnocent corrole ligands. Although fully coordinated corrole ligands are formally 3-, noninnocent corrole ligands have varying degrees of •2- character.

Although, noninnocent character have been determined by several spectroscopy techniques, have the most convenient probe come from UV-vis spectra. A large number of studies have shown that for noninnocent metallocorroles, the Soret maximum redshifts markedly with increasing electron-donation *para* substituents. Thus, as shown in Table 1, two different classes of corroles has emerged. According to this the $Re^{V}O$ and $^{99}Tc^{V}O$ triarylcorroles included in this thesis are innocent and do not show redshift in UV-vis depending on substituents.

Electrochemical redox potentials provide another simple clue to ligand noninnocence. For redox-inactive coordinated atom, the electrochemical HOMO-LUMO gap is approximately 2.1 V for both porphyrin and corrole derivatives. This is simply the π-π* energy gap of the macrocycle. For noninnocent metallocorroles and even innocent metallocorroles with redox-active coordinated metals, the electrochemical HOMO-LUMO gap is typically substantially smaller. Again, for the $Re^{V}O$ and $^{99}Tc^{V}O$ the electrochemical HOMO-LUMO gap is 2.1-2.2 V.

Two of the best classes of noninnocent metallocorroles are FeCl and Cu corroles. For both metals, evidence of ligand noninnocent has come from a variety of analytical sources including the two discussed above. The findings have been strongly supported by DTF calculations.

Table 1. Soret maxima (nm) of metal-tris(*p*-X-phenyl)corrole complexes classified according to their innocent and noninnocent character.

	para-substituent				
Series	CF_3	H	CH_3	OCH_3	Reference
Noninnocent					
Cu(T*p*XPC)	407	413	418	433	74
Fe(T*p*XPC)(Cl)	402	411	421	426	106, 107
Mn(T*p*XPC)(Cl)	423	433	441	-	140
Fe(T*p*XPC)(NO)	385	390	400	416	104, 105
Innocent					
H_3(T*p*XPC)	417	417	417	421	74
Ag(T*p*XPC)	423	423	423	423	141
Au(T*p*XPC)	418	419	420	420	22, 121
Pt(T*p*XPC)(PhCN)(Ar)	430	426	427	427	123
Os(T*p*XPC)(N)	441	442	443	445	124

3 RESULTS AND DISCUSSION: COORDINATION CHEMISTRY

3.1 RHENIUM(V)-OXO-COMPLEXES

A major aim of this project was to synthesise phosphorescent 5d metallocorroles that could potentially act as sensitisers in photodynamic therapy experiments. Hence, I turned my focus to develop a general synthetic route for rhenium corrole complexes, to which little was known prior to my work. The only known Re corrole was synthesized accidentally via ring contraction of *meso*-tetrakis(trifluoromethyl)porphyrin in the presence of dirhenium decacarbonyl, Re_2CO_{10}, as described in Chapter 2. The synthetic route that I developed is shown in Figure 49. The *meso*-aryl substituent can be varied considerably, affording a wide range of electronically tuned $Re^{V}O$ corroles.

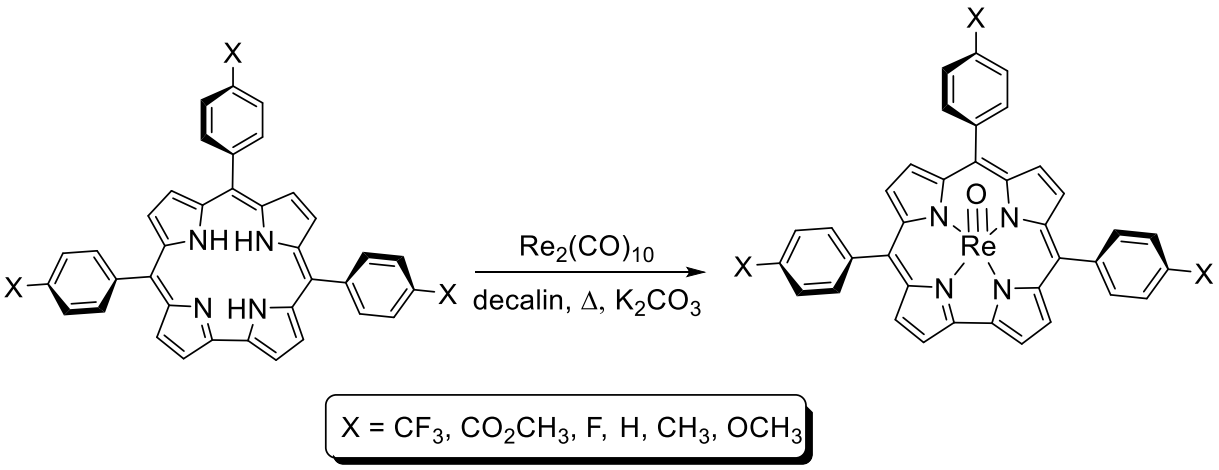

Figure 49. General synthetic method for synthesis of $Re^{V}O$ corroles.

When a free-base corrole (1 eq), $Re_2(CO)_{10}$ (4 eq), and K_2CO_3 were dissolved in decalin (15 mL) and heated to ~180˚C with constant stirring in an inert argon atmosphere, a color change occurred from dark green to red/brown after 40 minutes. The Soret maximum was seen to redshift by about 25 nm relative to the free base's (~415 nm), as shown in Figure 50.

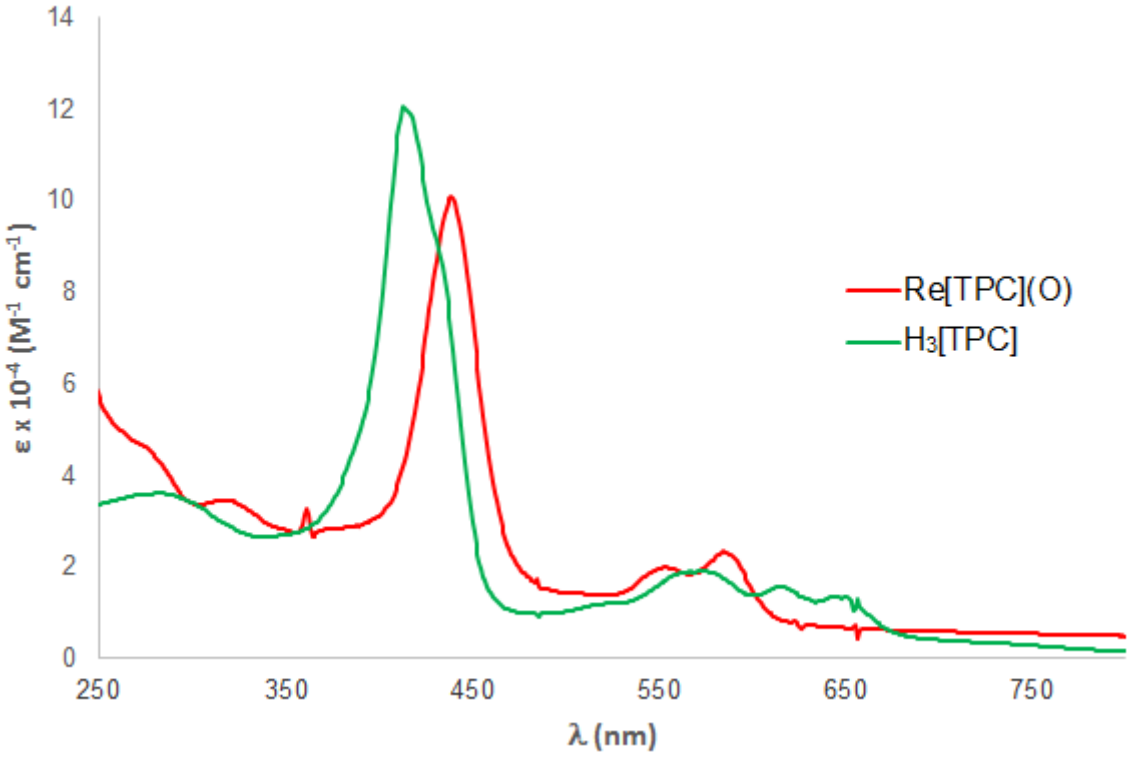

Figure 50. Electronic absorption spectrum of free-base H_3[TPC] and Re[TPC](O).

The reaction was essentially complete after 3 hours, whereupon the reaction mixture was cooled to room temperature and processed via silica gel chromatography, as described in Chapter 8. The yields were slightly improved upon increasing the reaction time from 3 hours to overnight. Table 2 shows the Soret and Q band maxima of the rhenium corrole complexes.

Table 2. UV-vis absorption maxima (λ_{max}, nm) of $Re^{V}O$ complexes.

Complex	λ_{max} (nm)		
	Soret	Q	Q
Re[T*p*CF_3PC](O)	440	553	586
Re[T*p*CO_2CH_3PC](O)	441	555	587
Re[T*p*CO_2HPC](O)	439	553	585
Re[T*m*CO_2CH_3PC](O)	439	553	586
Re[T*m*CO_2HPC](O)	438	553	586
Re[T*p*FPC](O)	440	554	586
Re[TPC](O)	440	554	586
Re[T*p*CH_3PC](O)	442	556	588
Re[T*p*OCH_3PC](O)	443	557	590
PtTPTBP	430	564	614

As shown in in Table 3, electronspray ionization mass spectra indicated a molecular formula consisting of 'Re + corrolate + O', consistent with a $Re^{V}O$ corrole.

Table 3. ESI-MS analyses for ReO complexes.

Complex	Formula	Expected	Calculated
Re[T*p*CF_3PC](O)	$C_{40}H_{20}N_4F_9ORe$	930.10	929.81
Re[T*p*CO_2CH_3PC](O)	$C_{43}H_{297}N_4O_7Re$	900.16	900.15
Re[T*m*CO_2CH_3PC](O)	$C_{43}H_{297}N_4O_7Re$	900.16	900.16
Re[T*p*FPC](O)	$C_{37}H_{20}F_3N_4ORe$	780.11	779.84
Re[TPC](O)	$C_{37}H_{23}N_4ORe$	726.14	725.81
Re[T*p*CH_3PC](O)	$C_{40}H_{29}N_4ORe$	768.18	767.89
Re[T*p*OCH_3PC](O)	$C_{40}H_{29}N_4O_4Re$	816.17	815.89

From the ^{1}H NMR spectra, it was clear that the compounds were diamagnetic. The temperature-dependent behaviour and non-equivalence of the *ortho* and *meta* protons for a given aryl substituent were consistent with a square-pyramidal complex, in which the two faces of the corrole are different. Comparison of room-temperature and cold-temperature, -20˚C, ^{1}H NMR for Re[T*p*OCH_3PC](O) is shown in Figure 51. As shown in Figure 53, COSY analyses led to full assignment of all the protons in the various complexes; the assignments were also in agreement with the integrals, as shown in Figure 54.

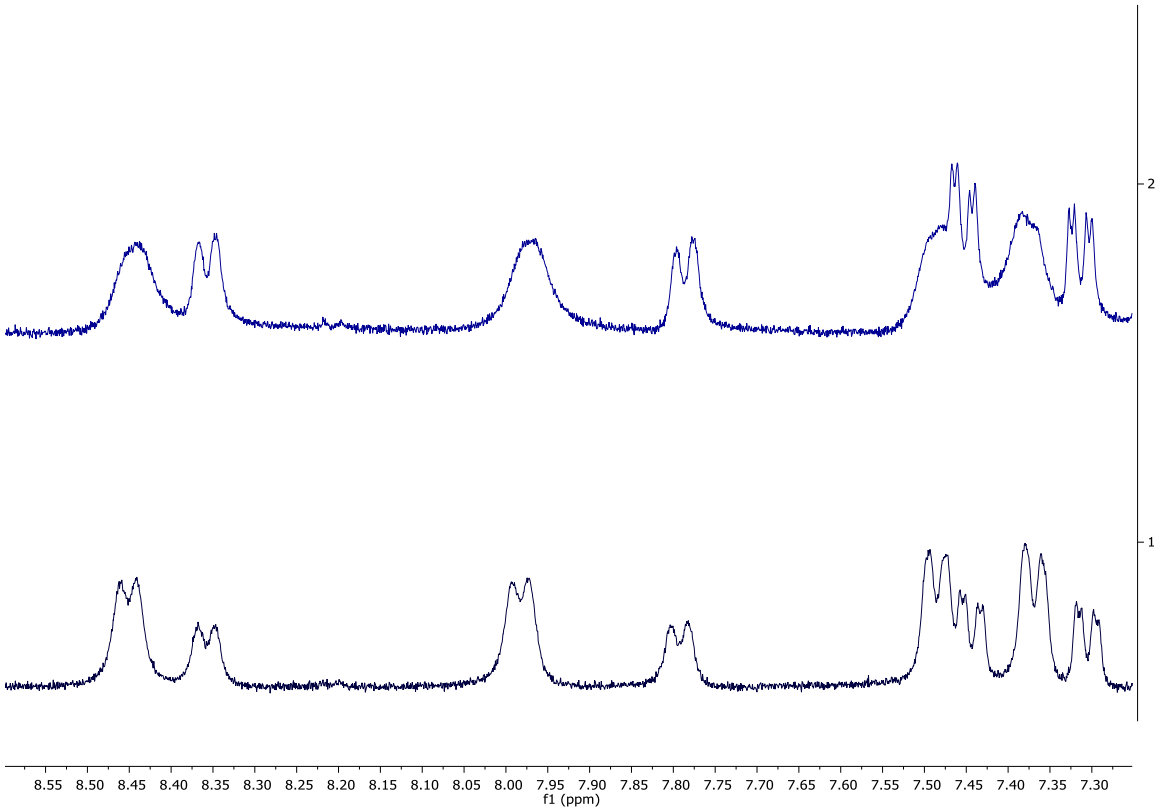

Figure 51. Temperature-dependent ^{1}H NMR spectra of Re[T*p*OCH$_3$PC](O) corrole, 20˚C (top) and -20˚C (bottom).

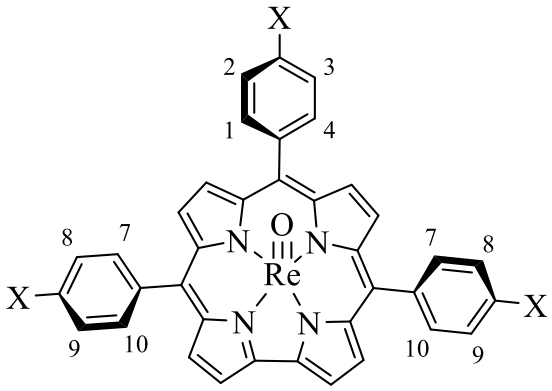

Figure 52. Molecular structure of Re^{V}O corroles. The proton numbering refers to the NMR spectra shown in Figure 53 and Figure 54.

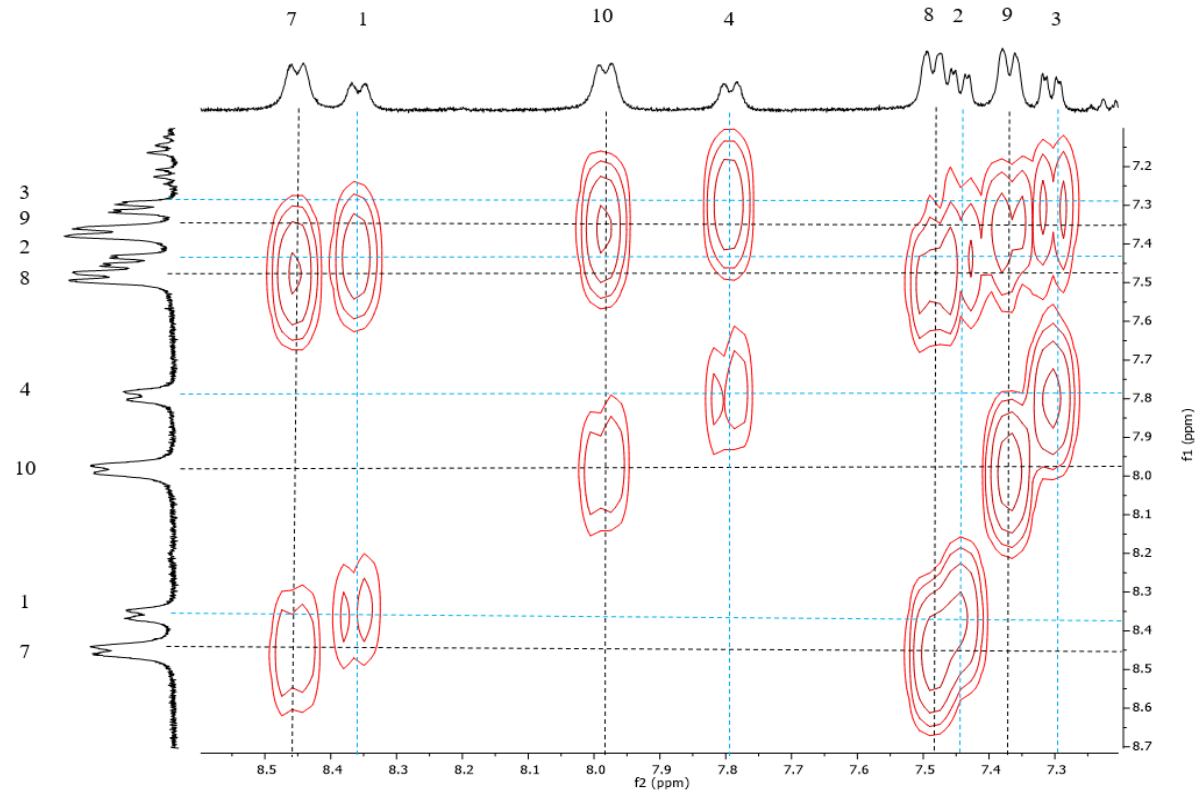

Figure 53. ^{1}H COSY of Re[T*p*OCH$_3$PC](O) showing phenyl proton pattern. Numbering refers to proton numbering in Figure 52.

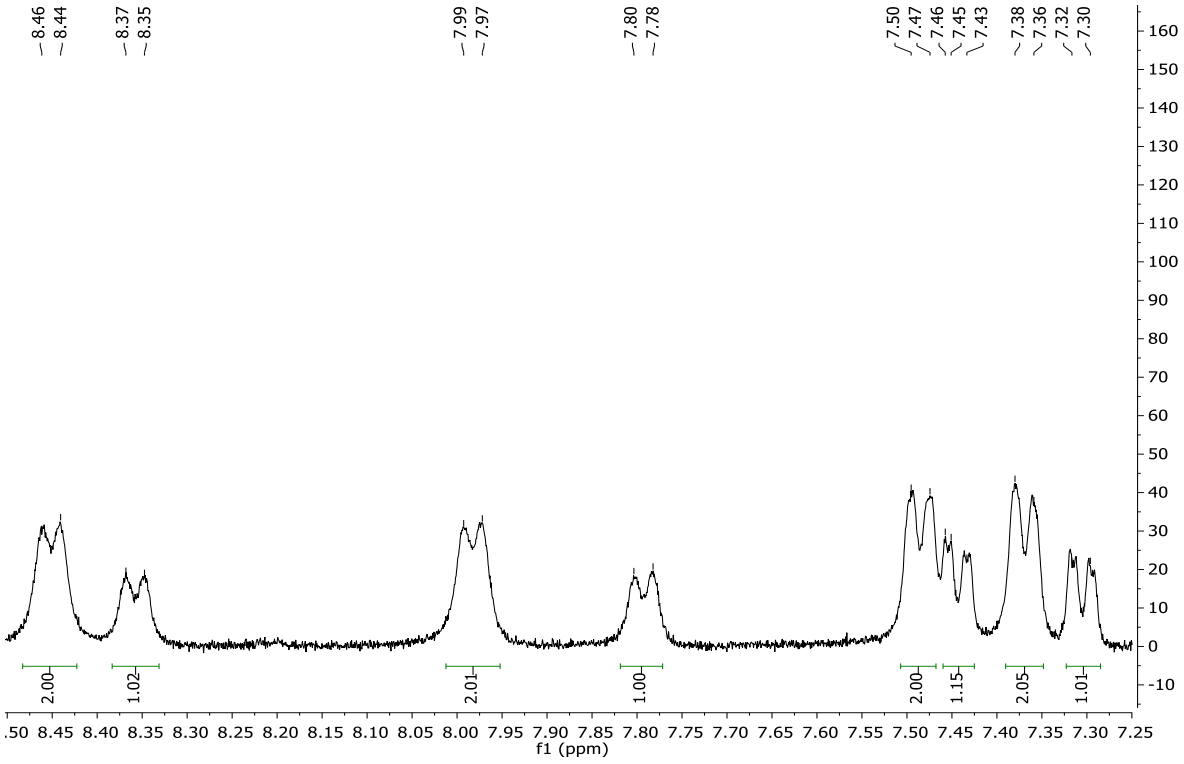

Figure 54. ^{1}H NMR of Re[T*p*OCH$_3$PC](O) with integrations for Figure 53.

For all the Re complexes, IR spectra revealed a band at 984± 6 cm^{-1} (Table 4) consistent with a Re-O triple bond, as expected for a $Re^{V}O$ corrole.[142] The existence of a ReO triple bond follows from ligand field theory, whereby the two d electrons of Re(V) occupy the $5d_{xy}$ orbital, whereas the $5d_{xz}$ and $5d_{yz}$ accept the oxygen's $2p_x$ and $2p_y$ lone pairs, respectively, via π-bonds, as depicted in Figure 55. The strong metal-oxygen triple bond in $Re^{V}O$ and $^{99}Tc^{V}O$ corroles accounts for the great stability of these complexes.

Table 4. Redox potentials and Re-O stretching frequencies for ReO complexes.

Complex	$E_{1/2ox}$ (V)	$E_{1/2red}$ (V)	ΔE (V)	ν_{ReO} (cm^{-1})
Re[T*p*CF_3PC](O)	1.10	-1.16	2.26	990
Re[T*p*CO_2CH_3PC](O)	1.06	-1.15	2.21	989
Re[T*m*CO_2CH_3PC](O)	1.05	-1.21	2.25	985
Re[T*p*FPC](O)	1.01	-1.23	2.24	992
Re[TPC](O)	0.98	-1.26	2.24	992
Re[T*p*CH_3PC](O)	0.94	-1.29	2.23	984
Re[T*p*OCH_3PC](O)	0.93	-1.29	2.22	978

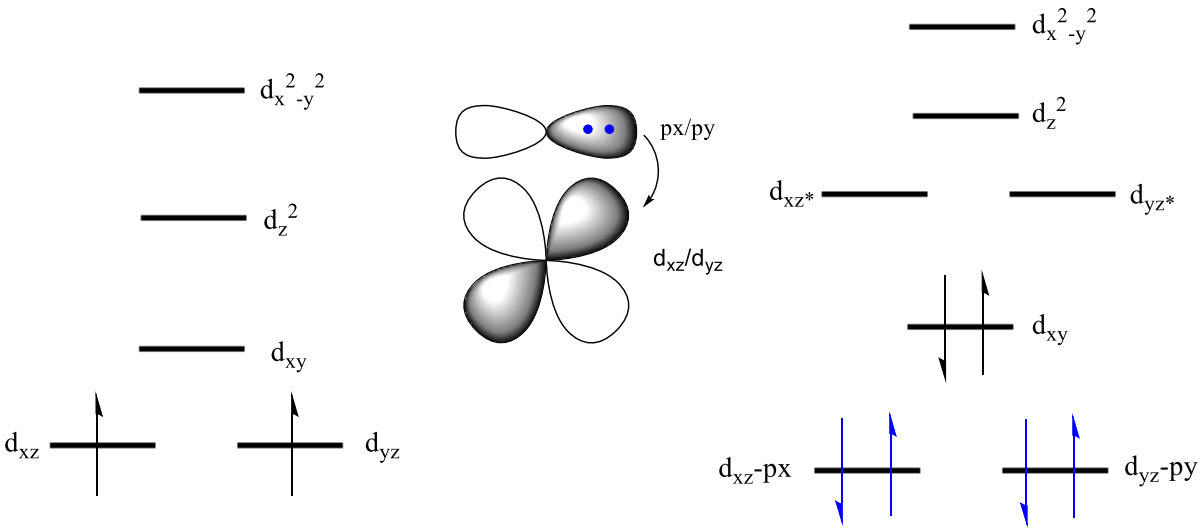

Figure 55. Electronic configuration of ReO corroles according to crystal field(left) and ligand field theory(right).

The above spectroscopic analyses were borne out by single-crystal X-ray crystallography. All crystals were obtained by carefully layering concentrated DCM solutions with *n*-hexane. A total of five structures were all solved at the Advanced Light Source, Berkeley, California, by staff scientist Dr. Kevin Gagnon. An example of an X-ray structure obtained is shown in Figure 56. Table 5 lists key metrical parameters of the complexes. Although the metal-nitrogen bond distance are not too different from those in 3d metallocorroles, the corrole in each molecule is strongly domed and the Re is sharply displaced from the corrole N_4 plane by ~0.7 Å, illustrating the steric demands of the Re atom.

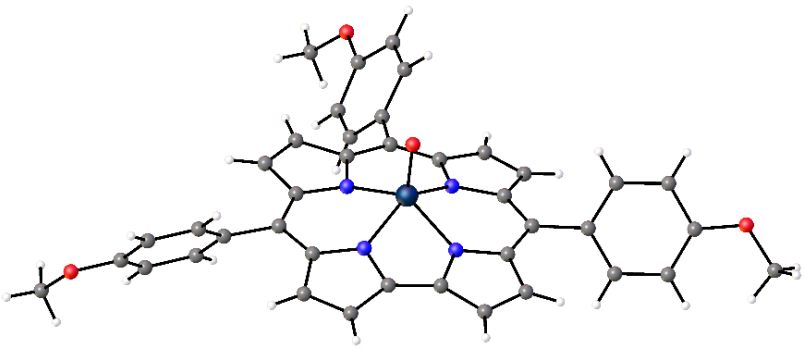

Figure 56. X-ray structure of Re[T*p*OCH$_3$PC](O).

Table 5. Selected crystallographic geometry parameters for Re^{V}O triarylcorroles.

Distance [Å]	Re[T*p*CF$_3$PC](O)	Re[T*p*FPC](O)	Re[TPC](O)	Re[T*p*CH$_3$PC](O)	Re[T*p*OCH$_3$PC](O)
Re-N1	1.986	1.987	1.986	1.977	1.989
Re-N2	2.000	2.012	2.2005	2.006	2.007
Re-N3	2.014	2.006	2.004	2.004	2.007
Re-N4	1.988	1.995	1.990	1.981	1.985
Re-O	1.677	1.668	1.677	1.681	1.685
ΔRe-N$_4$	0.694	0.704	0.704	0.0694	0.689

As shown in Table 2, the Soret maxima are near constant, shifting by only ~3 nm across the various Re^{V}O triarylcorroles studied. This consistency is indicative of an innocent corrole, as discussed in Chapter 2. An innocent corrole was also indicated by cyclic voltammetry, which revealed a large HOMO-LUMO gap of ~2.24 eV, as shown in Table 4, indicating that one-electron oxidation and reduction involve the corrole π-system.

The $Re^{V}O$ triarylcorroles were found to exhibit room temperature phosphorescence in anoxic toluene. The phosphorescence analysis were provided by Dr. Sergey Borisov of the Technical University of Graz, Austria. The observed emission was completely quenched upon exposure to oxygen, as expected for phosphorescence. Platinum(II) tetraphenylbenzoporphyrin (PtTPTBP) was used as the standard for these measurements. As shown in Table 6, the compounds exhibit relatively long phosphorescence lifetimes of 55-66 μs, but low luminescence quantum yields of 2.6-3.7%. The long phosphorescence lifetimes are thought to be critical to the complexes' efficacy as singlet oxygen sensitisers in the photodynamic therapy experiments carried out in this study.

Table 6. Emission maxima ($\lambda_{max,em}$, nm), phosphorescence lifetimes (τ, μs), and quantum yields (ϕ) of $Re^{V}O$ triarylcorroles.

Complex	$\lambda_{max,em}$	τ	ϕ (%)
Re[T*p*CF_3PC](O)	777	61	3.7
Re[T*p*CO_2CH_3PC](O)	776	66	2.8
Re[T*p*FPC](O)	775	65	2.9
Re[TPC](O)	770	61	2.8
Re[T*p*CH_3PC](O)	782	59	2.6
Re[T*p*OCH_3PC](O)	788	55	2.6
PtTPTBP	770	48	51

3.1.1 Attempts at bromination

It was of great interest to fully brominate the β-positions of the $Re^{V}O$ triarylcorroles – it was hoped that the products would exhibit enhanced phosphorescence due to the heavy atom effect. Two synthetic approaches were attempted, as outlined in Figure 57. Neither worked as hoped, with each leading to an inseparable mixture of polybrominated complexes.

Metal insertion into pre-formed β-octabromocorroles ligands,[111] an approach that has worked for Au corroles, among others, led to partial debromination in the case of $Re^{V}O$ triarylcorroles.

Direct β-octabromination with elemental bromine has been shown to work for Cu and Ir[119] corroles. In the case of $Re^{V}O$ triarylcorroles, however, even a large excess of bromine and long reaction times led to a mixture of penta-, hexa-, and hepta-brominated products.

The reason for the failure of the above two approaches may lie in the inherent instability of the $Re^{V}O$ β-octabromocorrole complexes. The strongly domed geometries of these complexes may result in prohibitive steric interactions among the three *meso*-aryl and eight β–bromo complexes. However, preliminary analyses suggest that the desired octabrominated product was obtained for Re[T*p*CH$_3$PC](O) and, with careful optimization, the product may even be isolable in reasonable yield.

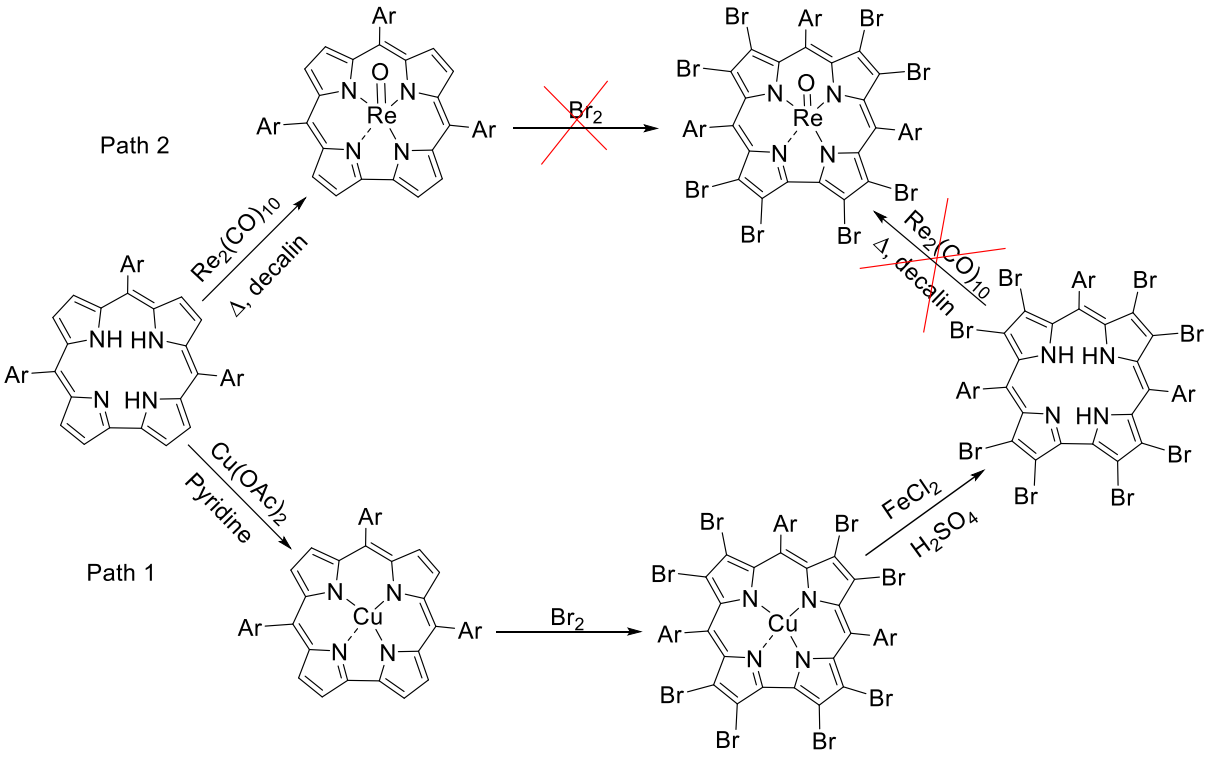

Figure 57. Two different paths toward octabromination of Re corroles.

3.1.2 Amphiphilic $Re^{V}O$ corroles

For photodynamic therapy experiments with rhenium corroles, water-soluble complexes were needed. Toward that end, the synthesis of *N*-alkylated *meso*-pyridylcorrole ligands were explored (Figure 46), following literature procedures.[143] Unfortunately, several attempts to synthesize 4-pyridyl- and 3-pyridyl- corroles led to the corresponding porphyrins instead. In particular, several variations of Grykos's water-methanol method, including different acid concentrations and longer reaction times, also failed. Accordingly, the attention was turned to

para- and *meta*-carboxylated $Re^{V}O$ triarylcorroles. For that, rhenium was inserted into the corresponding ester-appended corroles and the resulting complexes were hydrolysed with alkali in aqueous THF (Figure 58).

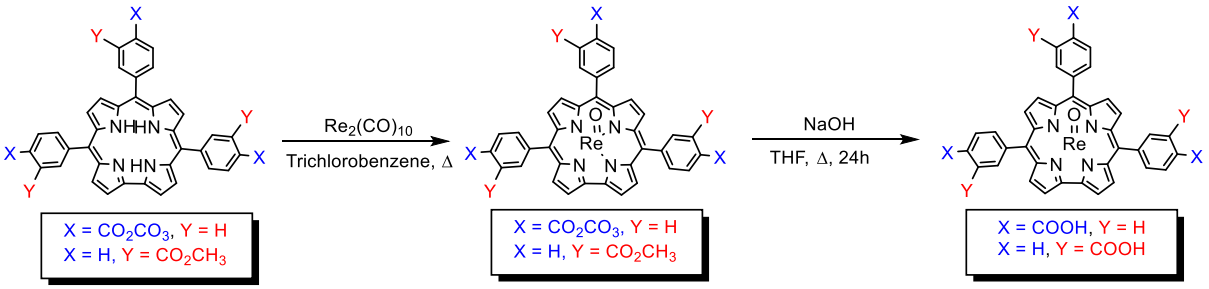

Figure 58. Synthesis of carboxylated $Re^{V}O$ corroles via ester hydrolysis.

3.2 99-TECHNETIUM(V)-OXO COMPLEXES

A key point of interest with regard to Re corroles was that they could serve as a stepping stone to technetium corroles, which were unknown prior to this work. Further, the hope was that a synthesis for ^{99}Tc corroles could lead to ^{99m}Tc corroles. The Tc insertion work was carried out (by me) in the laboratory of Prof. Roger Alberto at the University of Zurich, Switzerland, where excellent facilities are available for the necessary radiochemical operations.

For synthetic purposes, I used starting materials based on the long-lived ^{99}Tc isotope ($t_{1/2}$ = 211,000 years), including $^{99}TcCl_4$ and $(Et_4N)_2[^{99}Tc^{I}(CO)_3Cl_3]$.[144] Two different solvents were tried for the ^{99}Tc insertion – DMSO and decalin. Of the different conditions examined, only $(Et_4N)_2[Tc^{I}(CO)_3Cl_3]$ in decalin at ~170°C led to the desired $^{99}Tc^{V}O$ corrole products. As for rhenium, the yields was improved by increasing the reaction time. Although larger quantities of solvent were initially employed, the volume was subsequently reduced to only a few drops, just enough to produce a slurry.

Although rhenium insertion into free-base corroles is accompanied by a change in colour from green to red, ^{99}Tc insertion was not accompanied by an obvious colour change. Product formation was tested with TLC analysis, which also helped identify ratio of DCM/*n*-hexane as eluent for column chromatography. After column chromatographic separation, the fractions were tested with liquid scintillation counting (LSC) to determine the amount of radioactivity. The radioactive fraction was then analysed with ^{1}H NMR spectroscopy.

As for $Re^{V}O$ corroles, ^{1}H NMR spectra had to be acquired at low-temperature to distinguish between the *ortho* and *meta* protons on a given phenyl ring. Furthermore, IR analysis revealed a ν_{TcO} band at 973 ± 5 cm^{-1} for all the products, strongly suggesting the formation of the expected $^{99}Tc^{V}O$ corroles (Table 7). Single-crystal X-ray structure determinations were attempted on all the products, but a high-quality structure was only obtained for ^{99}Tc[T*p*OCH$_3$PC](O), as shown in Figure 59. Key metrical parameters for the structure, including the M-N distances (1.992 Å) and M-N$_4$ displacement (0.68 Å), were similar to those observed for $Re^{V}O$ corroles (Table 5).

Table 7. Redox potentials (V vs. SCE) and Tc-O stretching frequencies ^{99}TcO corroles.

Complex	$E_{1/2ox}$	$E_{1/2red}$	ΔE	ν_{TcO} (cm^{-1})
^{99}Tc[T*p*CF$_3$PC](O)	1.28	-0.79	2.07	977
^{99}Tc[TPC](O)	1.18	-0.91	2.09	970
^{99}Tc[T*p*CH$_3$PC](O)	1.16	-0.90	2.06	972
^{99}Tc[T*p*OCH$_3$PC](O)	1.15	-0.89	2.04	968

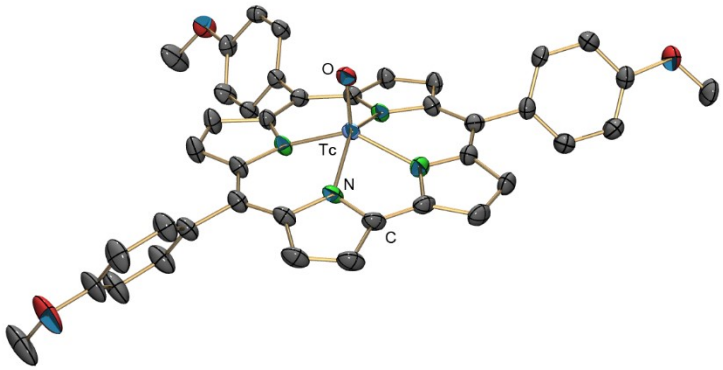

Figure 59. X-ray structure of ^{99}Tc[T*p*OCH$_3$PC](O).

As in the case of ReO corroles, the Soret maxima of the ^{99}TcO corroles did not shift with the *meso*-aryl *para*-substituent. Interestingly, however, the Soret maxima of the ReO corroles exhibited a substantial redshift of about 35 nm relative to the ^{99}TcO corroles (Table 8, Figure 62). This difference was analysed by my colleague Dr. Hugo Vazquez-Lima and ascribed to relativistic effects in the Re case, whereby the 5d orbitals are substantially destabilized relative

to the Tc 4d orbitals. This difference in turn affects metal(d)-corrole(LUMO) orbital interactions, which explained the observed spectral shift.

Table 8. UV-vis absorption maxima (λ_{max}, nm) of ^{99}Tc complexes.

Complex	λ_{max} (nm)		
	Soret	Q	Q
^{99}Tc[T*p*CF$_3$PC](O)	410	468	528
^{99}Tc[TPC](O)	410	468	584
^{99}Tc[T*p*CH$_3$PC](O)	412	463	580
^{99}Tc[TpOCF$_3$PC](O)	413	556	588

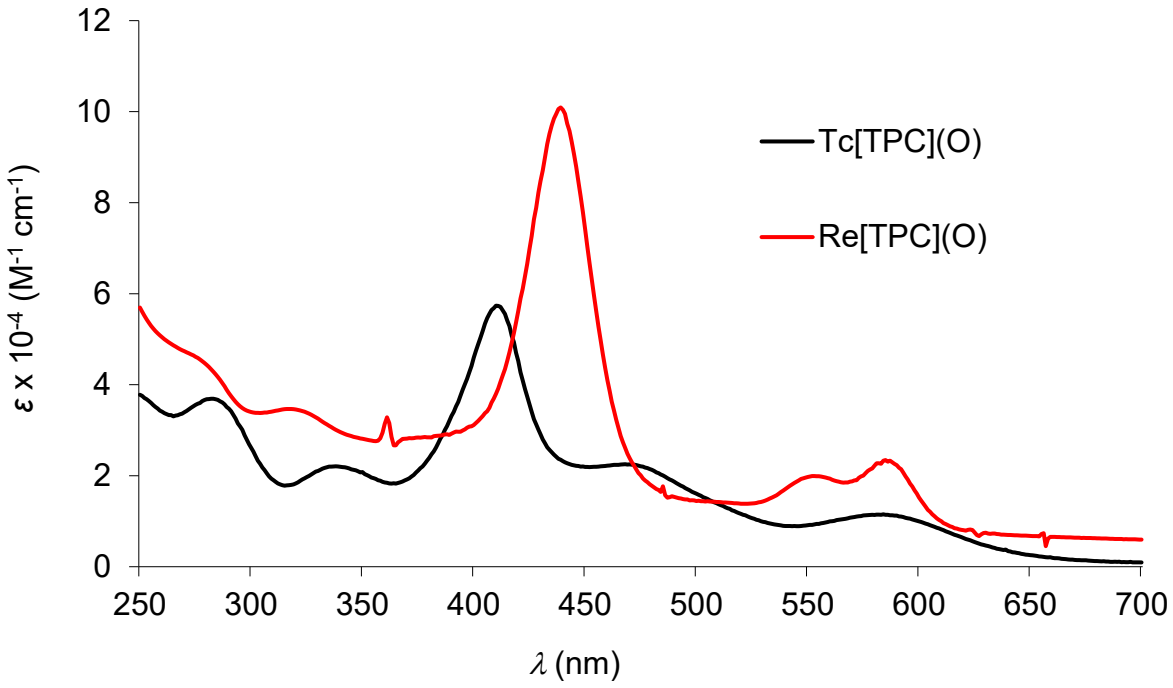

Figure 60. Electronic absorption spectra of ^{99}Tc[TPC](O) and Re[TPC](O).

In another key distinction between ReO and ^{99}TcO corroles, cyclic voltammetry measurements revealed a slightly smaller electrochemical HOMO-LUMO gap of ~2.02 eV for the ^{99}TcO corroles, which is ~0.20 eV lower than that observed for the ReO series (Table 7, Figure 59) A 2.0 eV HOMO-LUMO gap is still roughly the same as the π–π* gap of the corrole macrocycle.

However, the lower HOMO-LUMO gap in the Tc case might also signify Tc-centered reduction. My limited time in Zürich did not permit a spectroelectrochemical investigation at this point.

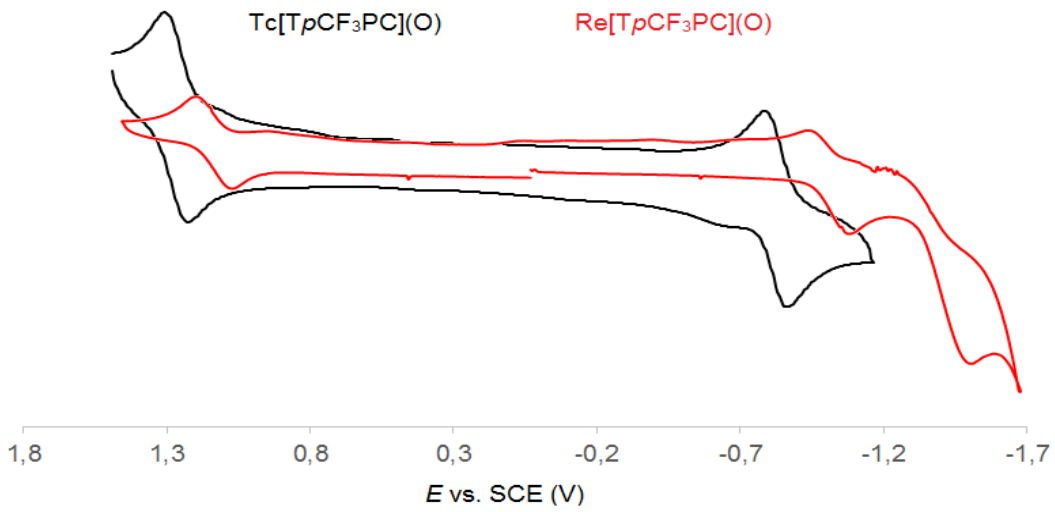

Figure 61. Cyclic voltammograms of ^{99}Tc[T*p*CF$_3$PC](O) and Re[T*p*CF$_3$PC](O).

4 RESULTS AND DISCUSSION: PHOTODYNAMIC THERAPY EXPERIMENTS

The photodynamic therapy (PDT) experiments were performed at the Department of Cancer Research and Molecular Medicine, Norwegian University of Science and Technology, Trondheim, Norway, together with co-supervisor Odrun A. Gederaas.

All experiments were performed in duplicate, including dark toxicity tests and light treatment control experiments (without photosensitizer).

4.1 CELL VIABILITY ASSAY

The MTT assay is a well-known method for measuring the number of living cells after an *in vitro* cytotoxicity experiment. The water-soluble yellow tetrazolium salt 3-(4,5-dimethylthiazol-2-yl)-2,5-diphenyltetrazolium bromide (MTT) is converted to water-insoluble purple formazan crystals only by living cells. Accordingly, the MTT assay allows one to optically visualise whether a batch of cells is alive or dead, as there will be a yellow solution for dead cells and a purple one for living cells. By using a spectrophotometer, it is possible to quantitate the proportion of living versus dead cells (described in detail in section 4.2.1).[145]

4.2 LIGHT SOURCE

In the phototoxicity measurements, cells at room temperature were illuminated from below by a LumiSource® (PCI Biotech AS, Oslo) light source. The lamp is designed to provide homogenous illumination of living cells in an *in vitro* setting across an area of 45 x 17 cm. The lamp consists of four tubes (4 x 18W Osram L 18/67) that emit light at a peak wavelength of 435 nm, resulting in 13 mW/cm^2 light intensity at the cells.[146]

4.3 CELL SURVIVAL STUDY

Two cell lines were used in this study – AY27 rat bladder cancer cells and WiDr human colon cancer cells. One day before the experiments, the cells were seeded in Petri dishes (diameter 6 cm, Nunc Denmark) at a density of 0.4 x 10^6 cells per dish. Stock solutions (1 mM) of *meta*-carboxy, and *para*-carboxy $Re^{V}O$ corrole were prepared in K_2CO_3 solution (0.15 M) prior to further dissolving in RPMI medium and preparing the growth medium (10 μM). After washing the cells with PBS, growth medium (10 μM, 24 h 37˚C) was added in the dark. The dishes were washed in PBS, again, before exposing to blue light. After irradiation in PBS, cells were grown

(for 24 hours) in regular cultivation medium before performing MTT-assay (described in section 4.2.1). Control samples, which neither contained Re nor were exposed to light, were used. Also, dishes containing only Re were used as control to "dark toxicity".

Because of my limited time at NTNU, the concentration of the Re photosensitiser was chosen on the basis of similar experiments with gold corroles,[22] as shown in Figure 62. A concentration of 10 μM was used, and cell viability were tested on both *meta* and *para* gold corroles, as described earlier, in addition to viability studies of free-base corrole. Their study showed that the *meta*-carboxy gold corrole had an LD_{50} after ~3 minutes (lethal dose with 50% cell survival) and complete cell death after ~20 minutes, while the *para*-substituted gold corrole had an LD_{50} after ~18 minutes and complete cell death after 40 minutes. The free-base corrole did not show any cell death at all.

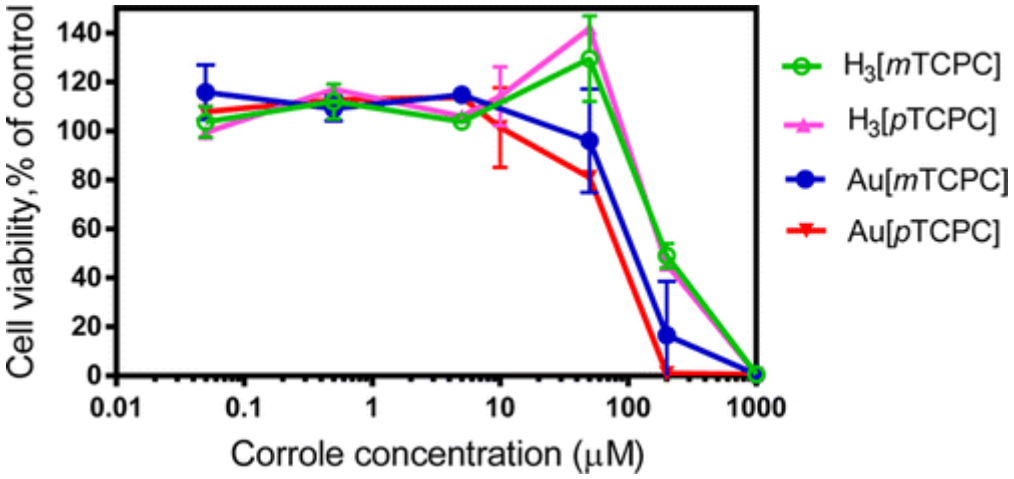

Figure 62. Cytotoxic effects of blue light illumination on AY27 cells in presence of free-base corrole (H_3[*m*TCPC] or H_3[*p*TCPC]) and corresponding gold-corroles (Au[*m*TCPC] or Au[*p*TCPC], reused from ref. 22, with permission from author.

4.4 METHOD

4.4.1 Day 1

The cells were washed with PBS, harvested from the cultivation flasks, and loosened by the enzyme trypsin (3 mL, 2%). After 3-5 min, growth medium (10 mL) was added and the cell suspension was transferred to a 50 mL tube and centrifuged (5 min, 1500 rpm, 4˚C), followed by removal of dead cells. The cell pellet was carefully resuspended in growth medium (0.5 mL), prior to further dilution with growth medium to a total volume of 10 mL. Subsequently, the cell suspension (20 µL) was added to a Bürker chamber. The cell number in four 1-mm^2 squares were manually counted, which provided the cell concentration in the stock solution. After dilution with growth medium, the cells were seeded in Petri dishes (diameter 60 mm) containing 3 mL of cell suspension ($0.25 – 0.35 \cdot 10^6$ cells/dish). The dishes were incubated for ~24 h at 37˚C, with each experiment including 20 - 30 dishes.

4.4.2 Day 2

Growth medium was removed and new medium was added (3 mL, 37˚C) to control dishes (without photosensitiser). For PDT experiments, growth medium was removed and photosensitiser-containing medium (3 mL, 37˚C) was added to the remaining dishes in the dark. All dishes were covered with aluminium foil and incubated for 24 h (37˚C, 5% CO_2).

4.4.3 Day 3

The control dishes (which did not undergo light treatment) were washed twice with PBS (3 mL, 37˚C) and growth medium (3 mL, 37˚C) was added, before they were placed in an incubator (37˚C, 5% CO_2). Additional PBS was added (3 mL, 37˚C) to all the remaining dishes before illumination with monochromatic blue light, as previously described. After illumination over different time intervals, the PBS was removed and growth medium was added (3 mL, 37˚C). All dishes were then placed under further incubation (24 h, 37˚C).

4.4.4 Day 4

The MTT assay was performed 24 h after PDT treatment measuring the indirect activity of living cells. MTT working solution (0.5 mg/mL) were freshly made using 1:9 MTT stock solution (5 mg/mL, 37˚C) and growth medium (37˚C). All dishes were carefully washed with PBS (2mL) before adding the MTT working solution (2 mL, 1 h, 37˚C). After incubation, the MTT working solution was removed and isopropanol (2 mL, RT) was added before placing on an orbital shaker (30 min, 70 rpm). The shaken suspension was transferred to 15-mL tubes and centrifuged (5 min, 1500 rpm, 4˚C). The supernatant was transferred into cuvettes and diluted

10-fold with isopropanol. Absorbance were measured on a double-beam UV-vis spectrophotometer (UV-1700 Shimadzu, Japan), using isopropanol as reference at λ_{ex} = 595 nm.

4.5 Results and discussion

The PDT experiments were conducted in duplicates. The influence of different doses of light on the viability of both AY27 and WiDr is displayed in Figure 63, where red curves refer to WiDr cells, the blue curves refer to AY27 cells, and the black curve refer to cell death exclusively by light. Dotted lines refer to *para*-carboxy complex while the continuous lines refer to the *meta*-carboxy complex.

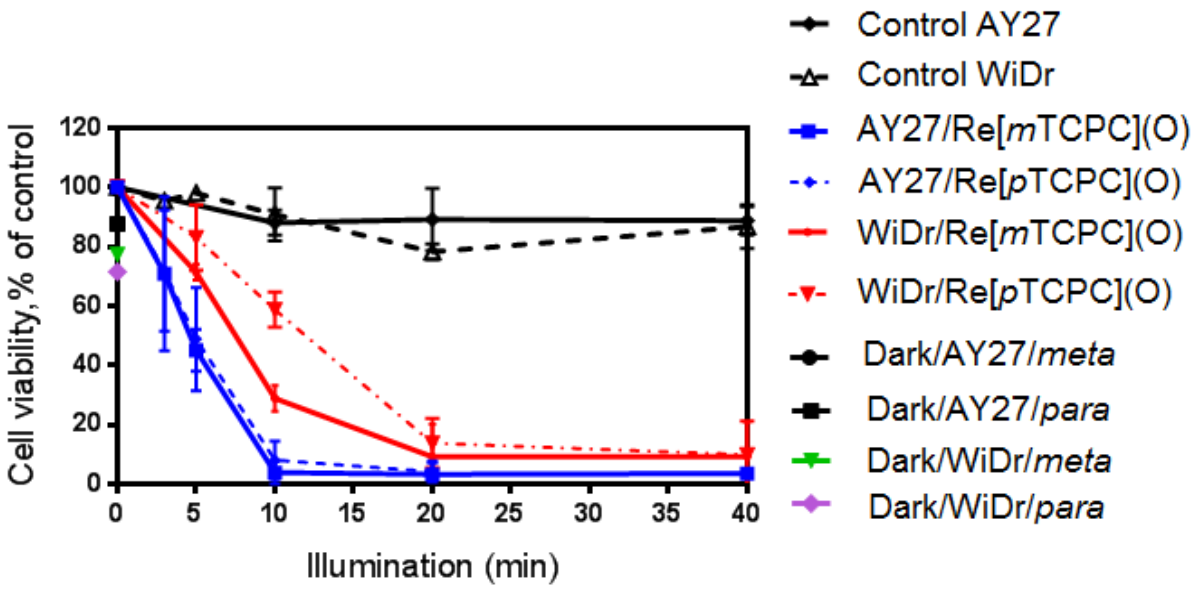

Figure 63. Viability study of AY27 and WiDr cells as a function of light exposure (0-40 min). The black curves represents cells exposed only to light, while the red and blue curves correspond to WiDr and AY27, respectively. A continuous line represents the *meta*-carboxy complex, while a dotted line corresponds to the *para*-carboxy complex. Error bars are ± SD of two parallels. Dots in black, green or pink colours along the y-axis correspond to dark toxicity (0 min light).

As illustrated in Figure 63, there is a slight dark toxicity for both compounds for both cells lines. Dark toxicity is most prevalent for the WiDr where cell viability is ~80% for the *meta* and ~70% for the *para*. For the AY27 cells, cell viability under dark toxicity measurements was found to be around ~90% for both the *meta* and *para* isomers. For the AY27 cells, the *meta* and

para isomers were found to be almost equally effective, as shown by LD_{50} at ~5 min and nearly complete cell death after 10-20 minutes of illumination, thus rivalling the Au corroles.

For WiDr, the *meta* isomer resulted in faster cell death than the *para*. However, both reached complete cell death after < 20 minutes of illumination, with LD_{50} after ~10 and ~15 minutes illumination respectively.

5 CONCLUSION AND FURTHER WORK

The main accomplishments of this thesis are threefold:

(1) I have developed a general synthesis for rhenium insertion into corroles using $Re_2(CO)_{10}$ as rhenium source. Prior to this work, the only Re corrole known was one obtained accidentally via the ring contraction of a porphyrin.

(2) The success with the synthesis of ReO corroles prompted an exploration of the corresponding technetium analogues, a venture that paid off nicely. Through a collaborative project with Professor Roger Alberto at the University of Zürich, I developed the first synthesis of ^{99}Tc corroles using $(Et_4N)_2[^{99}Tc(CO)_3Cl_3]$ as the ^{99}Tc source.

(3) Two amphiphilic $Re^{V}O$ corroles with pendant carboxyl groups were found to act as highly effective photosensitisers in photodynamic therapy against rat bladder cancer cells and human colon cancer cells under blue light illumination.

Overall, a total of 13 new 4d and 5d metallocorroles were synthesized, of which 6 were also characterized by single-crystal X-ray structure determination. These results were published in two papers in *Chemistry – A European Journal* (see Appendices I and II). The photodynamic therapy work is currently being written up for publication.

There are clear plans for extending the above work in the future. Thus, I plan to synthesize a wide range of amphiphilic 5d metallocorroles for application in photodynamic therapy and also attempt to gain deeper insight into the mechanism of action of the PDT sensitisers.

A second major goal is to synthesize ^{99m}Tc corroles and other ^{99m}Tc tetrapyrroles for radioimaging and combined radioimaging and photodynamic therapy, i.e., theranostics.

6 EXPERIMENTAL

6.1 GENERAL PROCEDURE OF MAKING FREE-BASE CORROLE

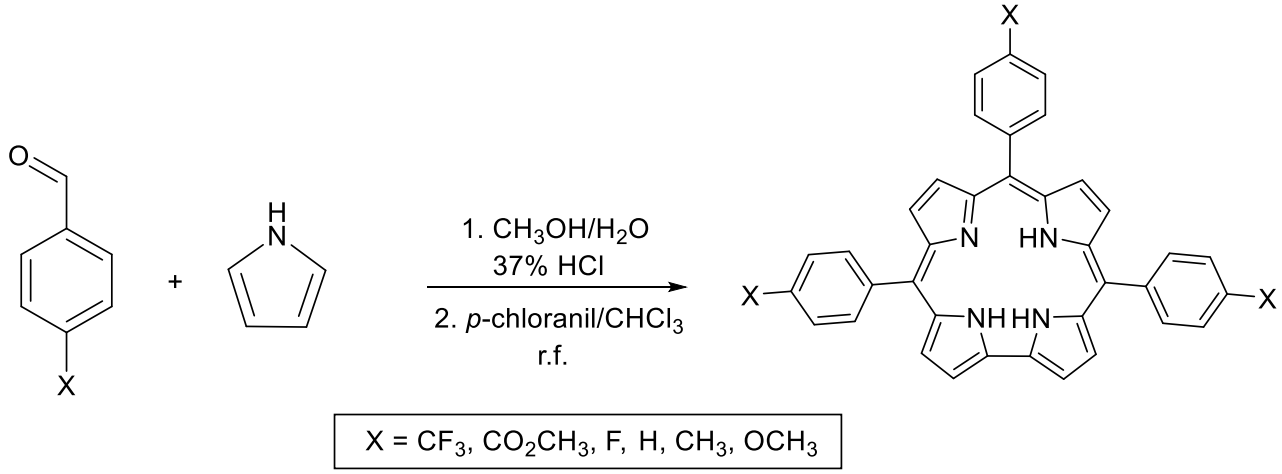

Figure 64. Syntheses of *meso*-aryl free-base corroles.

Free-base *meso*-triarylcorroles were synthesized using the so-called water-methanol method developed by Gryko *et al.,* shown in Figure 64.[75] The first step of this two-step procedure consist of dissolving pyrrole and an aromatic aldehyde in 1:1 methanol/water acidified with HCl. This step makes the required bilane after about 3 hours of stirring at room temperature. The yields are not particularly affected by longer reaction times, which makes for convenient overnight reactions. The bilane is then extracted with chloroform ($CHCl_3$), the organic layer is collected and washed twice with water, dried over sodium sulphate and filtered. The second step involves oxidation with a mild oxidizing agent. The organic phase is diluted to with $CHCl_3$ and, to the resulting mixture, *p*-chloranil (1.23 g, 5 mmol) is added. The mixture is then heated to reflux and left to stir for 1 hour. This step results in oxidative cyclization of the bilane to a corrole, which is isolated after removal of the solvent via rotary evaporation. The crude product is dissolved in DCM and chromatographed on a silica gel column with different eluents for the different compounds. For X = CH_3, H, and F, n-hexane and CH_2Cl_2 was used in 5:1 ratio. For X = CF_3, the polarity was increased through 3:1 n-hexane/CH_2Cl_2, 3:2 nhexane/CH_2Cl_2 and 1:1 n-hexane/CH_2Cl_2. For X = OCH_3, 1:1 n-hexane/CH_2Cl_2 was used as eluent. For the corrole-esters, two silica gel columns were run, first with 95:5 toluene/ethyl acetate, and the next with 99:1 toluene/ethyl acetate. Generally, yields of 12-40% were obtained.

6.2 RHENIUM(V)-OXO CORROLES: GENERAL PROCEDURE AND SYNTHESIS

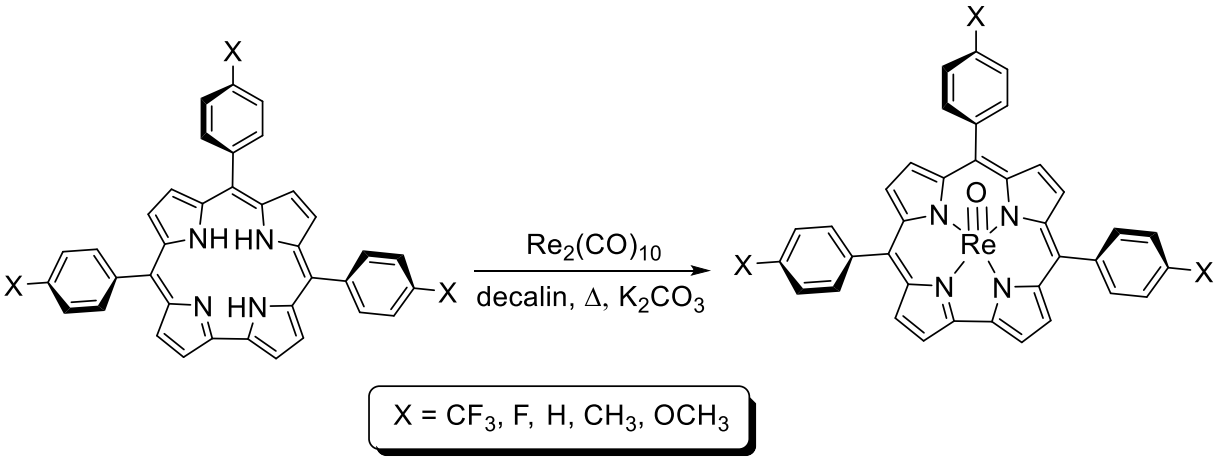

Figure 65. Synthesis of $Re^{V}O$ corroles.

To a 50-mL three-necked round-bottom flask fitted with a reflux condenser and containing decalin (15 mL) and a magnetic stir bar, a free-base corrole, H_3[T*p*XPC] (0.094 mmol), $Re_2(CO)_{10}$ (0.188 mmol), and potassium carbonate (100 mg) were added. The contents were deoxygenated with a flow of argon and then refluxed overnight with constant stirring under argon. Completion of the reaction was indicated by the disappearance of the Soret band of the of the free-base corrole and appearance of a new Soret band at approximately 440 nm. Upon cooling, the reaction mixture was loaded directly on to silica gel column. The decalin was first removed by eluting with pure hexane. Subsequently, different solvent mixtures were used to elute the various ReO corroles: 3:1 *n*-hexane/dichloromethane for X = CF_3, H, CH_3 and F; 1:3 *n*-hexane/dichloromethane for X = OCH_3. All fractions with λ_{max} ~440 nm were collected and dried. The products were further purified with a second column chromatography and finally with preparative thin-layer chromatography, all with the same solvent as in the first round.

Re[T*p*CF_3PC](O). Yield 55 mg (62.9 %). UV-vis (CH_2Cl_2) λ_{max} [nm, ε x 10^{-4} ($M^{-1}cm^{-1}$)]: 438 (10.74), 552 (1.63), 585 (1.99). ^{1}H NMR (400 MHz, –20°C): δ 9.76 (d, 2H, $^3J_{HH}$ = 4 Hz, β-H); 9.38 (d, 2H, $^3J_{HH}$ = 4 Hz, β-H); 9.36 (d, 2H, $^3J_{HH}$ = 4 Hz, β-H); 9.16 (d, 2H, $^3J_{HH}$ = 4 Hz, β-H); 8.77 (d, 2H, $^3J_{HH}$ = 8 Hz, 5,15-*o*1-Ph); 8.69 (d, 1H, $^3J_{HH}$ = 8 Hz, 10-*o*1-Ph); 8.26 (d, 2H, $^3J_{HH}$ = 8 Hz, 5,15-*o*2-Ph); 8.22 (d, 2H, $^3J_{HH}$ = 8 Hz, 5,15-*m*1-Ph); 8.19 (d, 1H, $^3J_{HH}$ = 8 Hz, 10-*m*1-Ph); 8.10 (d, 3H, $^3J_{HH}$ = 8 Hz, 5,15-*m*2-Ph & 10-*o*2-Ph overlapping); 8.05 (d, 1H, $^3J_{HH}$ = 8 Hz,

10-*m*2-Ph). Elemental analysis: Found: C 51.40, H 2.31, N 6.40; calcd: C 51.67, H 2.17, N 6.03. MS (ESI): M^+ = 930.10 (expt), 929.81 (calcd for $C_{40}H_{20}N_4F_9ORe$). IR ν_{ReO}: 990 cm^{-1}.

Re[T*p*FPC](O). Yield 52 mg (70.26 %). UV-vis (CH_2Cl_2): λ_{max} (nm), [ε x 10^{-4} ($M^{-1}cm^{-1}$)]: 438 (10.16), 553 (1.53), 585 (1.93). ^{1}H NMR (400 MHz, –20°C): δ 9.71 (d, 2H, $^3J_{HH}$ = 4 Hz, *β*-H); 9.37 (d, 2H, $^3J_{HH}$ = 4 Hz, *β*-H); 9.36 (d, 2H, $^3J_{HH}$ = 4 Hz, *β*-H); 9.16 (d, 2H, $^3J_{HH}$ = 4 Hz, *β*-H); 8.59 (d, 2H, $^3J_{HH}$ = 8 Hz, 5,15-*o*1-Ph); 8.51 (d, 1H, $^3J_{HH}$ = 8 Hz, 10-*o*1-Ph); 8.08 (d, 2H, $^3J_{HH}$ = 8 Hz, 5,15-*o*2-Ph); 7.91 (d, 1H, $^3J_{HH}$ = 8 Hz, 10-*o*2-Ph); 7.66 (d, 2H, $^3J_{HH}$ = 8 Hz, 5,15-*m*1-Ph); 7.60 (d, 1H, $^3J_{HH}$ = 8 Hz, 10-*m*1-Ph); 7.54 (d, 2H, $^3J_{HH}$ = 8 Hz, 5,15-*m*2-Ph); 7.48 (d, 1H, $^3J_{HH}$ = 8 Hz, 10-*m*2-Ph); 4. Elemental analysis: Found: C 56.34, H 2.90, N 6.68; calcd: C 56.99, H 2.59, N 7.18. MS (ESI): M^+ = 780.11 (expt), 779.84 (calcd for $C_{37}H_{20}F_3N_4ORe$) IR ν_{ReO}: 992 cm^{-1}.

Re[TPC](O). Yield 58 mg (84.19 %). UV-vis (CH_2Cl_2): λ_{max} (nm), [ε x 10^{-4} ($M^{-1}cm^{-1}$)]: 439 (10.09), 552 (1.99), 585 (2.34). ^{1}H NMR (400 MHz, –20°C): δ 9.70 (d, 2H, $^3J_{HH}$ = 4 Hz, *β*-H); 9.39 (d, 2H, $^3J_{HH}$ = 4 Hz, *β*-H); 9.8 (d, 2H, $^3J_{HH}$ = 4 Hz, *β*-H); 9.17 (d, 2H, $^3J_{HH}$ = 4 Hz, *β*-H); 8.61 (d, 2H, $^3J_{HH}$ = 8 Hz, 5,15-*o*1-Ph); 8.54 (d, 1H, $^3J_{HH}$ = 8 Hz, 10-*o*1-Ph); 8.13 (d, 2H, $^3J_{HH}$ = 8 Hz, 5,15-*o*2-Ph); 7.94 (m, 4H, $^3J_{HH}$ = 8 Hz, 5,15-*m*1-Ph; 10-*p*-Ph & 10-*o*2-Ph overlapping); 7.90 (m, 1H, 10-*m*1-Ph); 7.83 (m, 4H, 5,15-*m*2-Ph & 5,15-*p*-Ph overlapping); 7.76 (d, 1H, $^3J_{HH}$ = 8 Hz, 10-*m*2-Ph). Elemental analysis: Found: C 60.58, H 3.34, N 7.25; calcd: C 61.23, H 3.81, N 7.72. MS (ESI): M^+ = 726.14 (expt), 725.81 (calcd for $C_{37}H_{23}N_4ORe$). IR ν_{ReO}: 992 cm^{-1}.

Re[T*p*CH$_3$PC](O). Yield 50.2 mg (68.9 %) UV-vis (CH_2Cl_2): λ_{max} (nm), [ε x 10^{-4} ($M^{-1}cm^{-1}$)]: 440 (11.18), 555 (1.86), 587 (2.37). ^{1}H NMR (400 MHz, –20°C): δ 9.67 (d, 2H, $^3J_{HH}$ = 4 Hz, *β*-H); 9.33 (d, 2H, $^3J_{HH}$ = 4 Hz, *β*-H); 9.14 (broad s, 2H, $^3J_{HH}$ = 4 Hz, *β*-H); 9.02 (broad s, 2H, $^3J_{HH}$ = 4 Hz, *β*-H); 8.44 (d, 2H, $^3J_{HH}$ = 8 Hz, 5,15-*o*1-Ph); 8.36 (d, 1H, $^3J_{HH}$ = 8 Hz, 10-*o*1-Ph); 7.97 (d, 2H, $^3J_{HH}$ = 8 Hz, 5,15-*o*2-Ph); 7.79 (d, 2H, $^3J_{HH}$ = 8 Hz, 5,15-*m*1-Ph); 7.73 (d, 1H, $^3J_{HH}$ = 8 Hz, 10-*m*1-Ph); 7.66 (d, 2H, $^3J_{HH}$ = 8 Hz, 5,15-*m*2-Ph); 7.59 (d, 1H, $^3J_{HH}$ = 8 Hz, 10-*m*2-Ph); 2.76 (s, 6H, 5,15-*p*-CH_3); 2.74 (s, 3H, 10-*p*-CH_3). Elemental analysis: Found: C 61.81, H 3.85, N 6.96; calcd: C 62.56, H 3.81, N 7.30. MS (ESI): M^+ = 768.18 (expt), 767.89 (calcd for $C_{40}H_{29}N_4ORe$). IR ν_{ReO}: 984 cm^{-1}.

Re[T*p*OMePC](O). Yield 47 mg (61.28 %). UV-vis (CH_2Cl_2): λ_{max} (nm), [ε x 10^{-4} ($M^{-1}cm^{-1}$)]: 441 (10.84), 556 (1.79), 592 (2.29). ^{1}H NMR (400 MHz, –20°C): δ 9.70 (d, 2H, $^3J_{HH}$ = 4 Hz, *β*-H); 9.36 (d, 2H, $^3J_{HH}$ = 4 Hz, *β*-H); 9.15 (d, 2H, $^3J_{HH}$ = 4 Hz, *β*-H); 9.02 (d, 2H, $^3J_{HH}$ = 4 Hz, *β*-H); 8.46 (d, 2H, $^3J_{HH}$ = 8 Hz, 5,15-*o*1-Ph); 8.36 (d, 1H, $^3J_{HH}$ = 8 Hz, 10-*o*1-Ph); 7.99 (d, 2H, $^3J_{HH}$ = 8 Hz, 5,15-*o*2-Ph); 7.80 (d, 1H, $^3J_{HH}$ = 8 Hz, 10-*o*2-Ph); 7.49 (d, 2H, $^3J_{HH}$ = 8 Hz, 5,15-*m*1-Ph); 7.46 (d, 1H, $^3J_{HH}$ = 8 Hz, 10-*m*1-Ph); 7.38 (d, 2H, $^3J_{HH}$ = 8 Hz, 5,15-*m*2-Ph); 7.31 (d, 1H, $^3J_{HH}$ = 8 Hz, 10-*m*2-Ph); 4.11 (s, 6H, 5,15-*p*-OCH_3); 4.09 (s, 3H, 10-*p*-OCH_3). Elemental analysis: Found: C 59.14, H 3.82, N 6.58; calcd: C 58.88, H 3.58, N 6.87. MS (ESI): M^+ = 816.17 (expt), 815.89 (calcd for $C_{40}H_{294}N_4O_4Re$). IR ν_{ReO}: 990 cm^{-1}.

6.3 AMPHIPHILIC RE^VO COMPLEXES

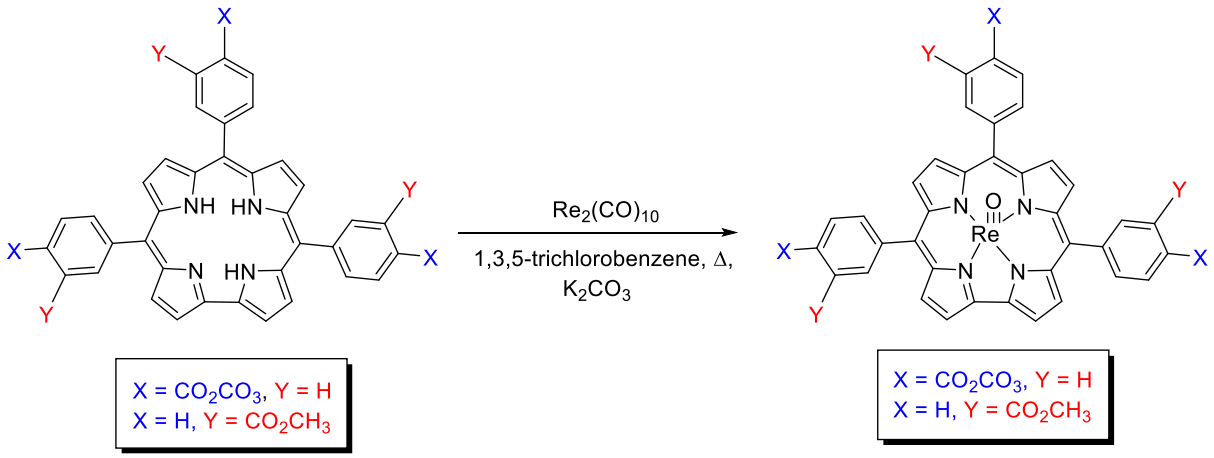

Figure 66. Reaction scheme for synthesis of Re^VO tris(*p/m*-carbomethoxyphenyl)corrole.

To a 50 mL round bottomed flask equipped with a magnetic stirrer and reflux condenser free-base corrole, H_3[T*p*CO_2CH_3PC](O) or H_3[T*m*CO_2CH_3PC](O) (0.142 mmol, 1 eq.), $Re_2(CO)_{10}$ (0.444 mmol, 3 eq.), and potassium carbonate (100mg) were added and dissolved in 1,3,5-thrichlorobenzene. The content were deoxygenated with a flow of argon and then refluxed overnight with constant stirring under Ar. Upon cooling, the reaction mixture was loaded directly on to silica gel column with *n*-hexane as the mobile phase. The 1,3,5-trichlorobenzene was first removed by eluting with pure hexane, followed by dichloromethane as eluent. The products were further purified with preparative thin-layer chromatography, with dichloromethane.

Re[T*p*CO_2CH_3PC](O). Yield 68 mg (53.17 %). UV-vis (CH_2Cl_2): λ_{max} (nm), [ε x 10^{-4} ($M^{-1}cm^{-1}$)]: 441 (11.17), 555 (1.61), 587 (2.05). ^{1}H NMR (400 MHz, –20°C): δ 9.67 (d, 2H, $^3J_{HH}$ = 4.40 Hz, *β*-H); 9.32 (d, 4H, $^3J_{HH}$ = 4.48 Hz, *β*-H); 9.12 (d, 2H, $^3J_{HH}$ = 5.20 Hz, *β*-H); 8.66 (d, 2H, $^3J_{HH}$ = 7.52 Hz, 5,15-*o*1-Ph); 8.58 (d, 1H, $^3J_{HH}$ = 7.96 Hz, 10-*o*1-Ph); 8.52 (d, 2H, $^3J_{HH}$ = 8.20 Hz, 5,15-*o*2-Ph); 8.49 (d, 1H, $^3J_{HH}$ = 7.88 Hz, 10-*o*2-Ph); 8.41 (d, 2H, $^3J_{HH}$ = 7.84 Hz, 5,15-*m*2-Ph); 8.35 (d, 1H, $^3J_{HH}$ = 7.94 Hz, 10-*m*2-Ph); 8.16 (d, 2H, $^3J_{HH}$ = 7.60 Hz, 5,15-*m*1-Ph); 7.99 (d, 1H, $^3J_{HH}$ = 7.96 Hz, 10-*m*1-Ph); 4.03 (s, 6H, 5,15-*p*-CH_3); 4.01 (s, 3H, 10-*p*-CH_3). MS (ESI): M^+ = 900.16 (expt), 900.15 (calcd for $C_{43}H_{29}N_4O_7Re$). IR ν_{ReO}: 989 cm^{-1}.

Re[T*m*CO_2CH_3PC](O). Yield 49 mg (39.27 %). UV-vis (CH_2Cl_2): λ_{max} (nm), [ε x 10^{-4} ($M^{-1}cm^{-1}$)]: 439 (8.37), 553 (1.20), 586 (1.57). ^{1}H NMR (400 MHz, –20°C): δ 9.72 (d, 2H, $^3J_{HH}$ = 4.04 Hz, *β*-H); 9.34 (d overlapping, 4H, $^3J_{HH}$ = 4.28 Hz, *β*-H); 9.25 (s, 1H, 5,15-o1m-Ph); 9.17 (s, 0.5H, 10-*o*1m-Ph); 9.13 (d, 2H, $^3J_{HH}$ = 4.68 Hz, *β*-H); 8.82 (d, 1H, $^3J_{HH}$ = 7.60 Hz, 5,15-*o*1-Ph); 8.74 (1.5H, 5,15-*o*2m-Ph overlapping with 10-o1-Ph); 8.58 (s, 0.5H, 10-*o*2m-Ph); 8.48 (overlapping d, 3H, $^3J_{HH}$ = 6.88 Hz, 5,10,15-*p*-Ph); 8.32 (d, 1H, $^3J_{HH}$ = 7.20 Hz, 5,15-*o*2-Ph); 8.16 (d, 0.5H, $^3J_{HH}$ = 7.92 Hz, 10-*o*2-Ph); 8.04 (t, 1H, $^3J_{HH}$ = 7.72 Hz 5,15-*m*1-Ph); 7.99 (t, 0.5H, $^3J_{HH}$ = 7.56 Hz 10-*m*1-Ph); 7.92 (t, 1H, $^3J_{HH}$ = 8.00 Hz 5,15-*m*2-Ph); 7.86 (t, 0.5H, $^3J_{HH}$ = 7.72 Hz, 10-*m*2-Ph); 4.01 (s, 3H, 5,15-*m1*-CO_2CH_3); 3.98 (s, 1.5H, 10-*m1*-CO_2CH_3); 3.92 (s, 3H, 5,15-*m2*-CO_2CH_3); 3.88 (s, 1.5H, 10-*m2*-CO_2CH_3). MS (ESI): M^+ = 900.16 (expt), 900.16 (calcd for $C_{43}H_{29}N_4O_7Re$). IR ν_{ReO}: 985 cm^{-1}.

6.3.1 Hydrolysis of $Re^{V}O$ tris(*p/m*-carbomethoxyphenyl)corrole

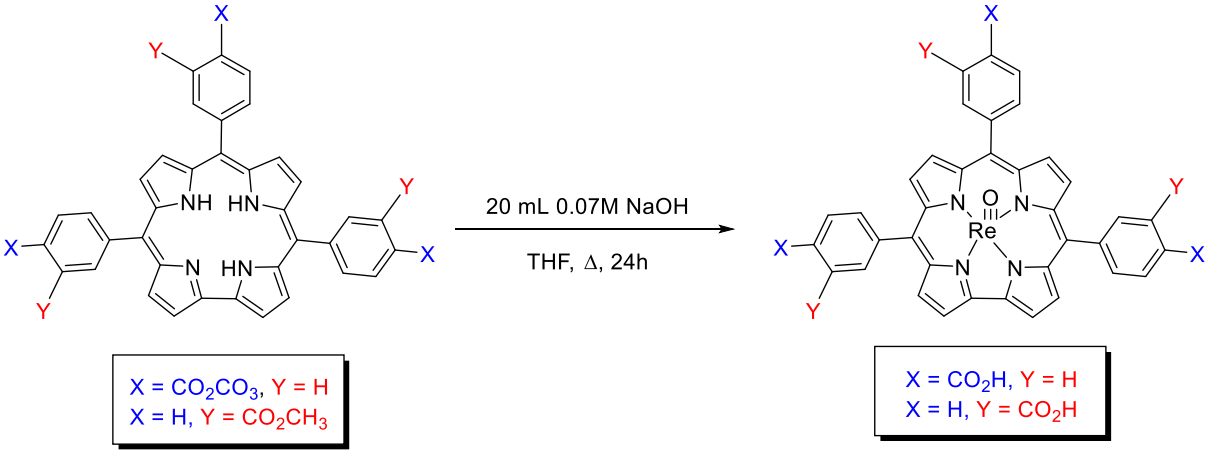

Figure 67. Alkaline hydrolysis of $Re^{V}O$ tris(*p/m*-carbomethoxyphenyl)corrole.

To a 250 mL round bottomed flask equipped with a magnetic stirrer and reflux condenser, Re[T-*p/m*-CO_2CH_3PC](O) was dissolved in 50 mL THF followed by addition of 0.07 M sodium hydroxide solution (20 mL) and the mixture was heated to reflux (~100˚C) for 24 hours. The mixture was cooled to room temperature, transferred to a separation funnel containing 150 mL ethyl acetate and washed with acidified water. The organic phase was collected and washed with water 3 times, dried over sodium sulphate and rotary evaporated, filtrated and washed with dichloromethane affording pure carboxycorroles.

Re[T*p*CO_2HPC](O). Yield 19.7 mg (64.5 %). UV-vis (THF): λ_{max} (nm), [ε x 10^{-4} ($M^{-1}cm^{-1}$)]: 439 (11.06), 553 (1.34), 585 (1.87). MS (ESI): M^+ = 858.11 (expt), 858.11 (calcd for $C_{40}H_{23}N_4O_7Re$). IR ν_{ReO}: 990 cm^{-1}.

Re[T*m*CO_2HPC](O). Yield 17.3 mg (56.6 %). UV-vis (THF): λ_{max} (nm), [ε x 10^{-4} ($M^{-1}cm^{-1}$)]: 438 (10.03), 553 (1.37), 586 (1.81). MS (ESI): M^+ = 858.11 (expt), 857.10 (calcd for $C_{40}H_{23}N_4O_7Re$). IR ν_{ReO}: 992 cm^{-1}.

6.3.2 ^{99}Technetium(V)-oxo corroles: general procedure and synthesis

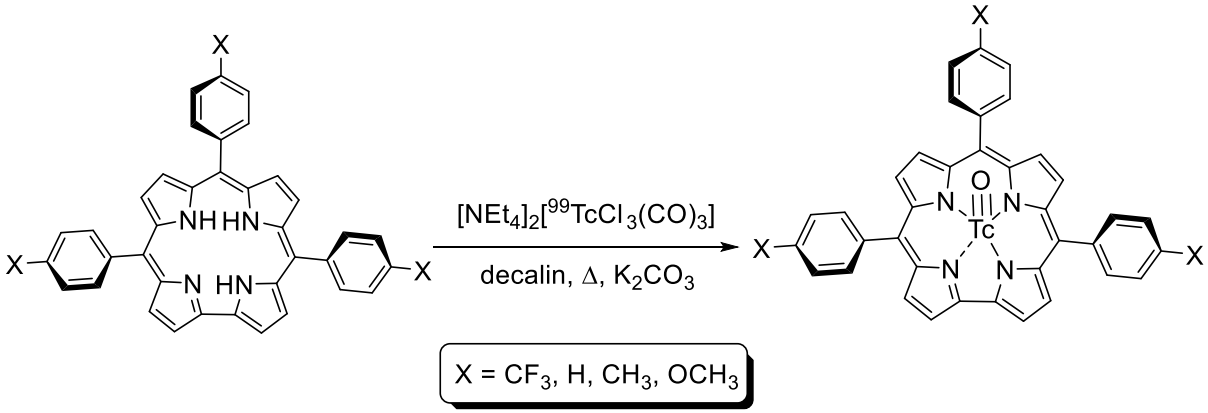

Figure 68. Reaction scheme for synthesis of $^{99}Tc^{V}O$ corroles.

Insertion of technetium in to corroles proved to be very similar to the insertion of rhenium. To a 2.5-mL microwave vial equipped with a magnetic stirring bar, a free-base corrole, H_3[T*p*XPC] (0.025 mmol), [NEt4]2[^{99}TcCl3(CO)3] (0.05 mmol), potassium carbonate (25 mg) and ~5 drops decalin were added.. The vial was sealed with a rubber septa and the content were deoxygenated with a flow of nitrogen and then heated for 8h with constant stirring at 170°C. Upon cooling, the reaction mixture was loaded directly on to silica gel column with *n*-hexane as the mobile phase. The decalin was first removed by eluting with pure hexane. Different solvent mixtures were then used to elute the various TcO corroles: 6:1 *n*-hexane/dichloromethane for X = CF_3, H and CH_3; 1:1 *n*-hexane/dichloromethane for X = OCH_3. For X = CF_3, H and CH_3 the product came as the second band with a dark green to almost brown colour. For X = OCH_3 the product came in the first band. The fraction were tested on TLC-plate for purity. All analyses were done on this fraction and no further purification were done.

^{99}Tc[T*p*CF$_3$PC](O). Yield 3.3 mg (15.67 %). UV-vis (CH_2Cl_2) λ_{max} [nm, ε x 10^{-4} ($M^{-1}cm^{-1}$)]: 410 (6.45), 468 (2.18), 528 (1.27). ^{1}H NMR (500 MHz, –50°C): δ 9.68 (d, 2H, $^3J_{HH}$ = 4.35 Hz, β-H); 9.34 (d, 2H, $^3J_{HH}$ = 4.15 Hz, β-H); 9.32 (d, 2H, $^3J_{HH}$ = 3.05 Hz, β-H); 9.12 (d, 2H, $^3J_{HH}$ = 4.8 Hz, β-H); 8.74 (d, 2H, $^3J_{HH}$ = 7.8 Hz, 5,15-*o*1-Ph); 8.66 (d, 1H, $^3J_{HH}$ = 8.05 Hz, 10-*o*1-Ph); 8.27 (d, 2H, $^3J_{HH}$ = 7.8 Hz, 5,15-*o*2-Ph); 8.22 (d, 2H, $^3J_{HH}$ = 7.8 Hz, 5,15-*m*1-Ph); 8.19 (d, 1H, $^3J_{HH}$ = 8.45 Hz, 10-*m*1-Ph); 8.10 (d, 2H, $^3J_{HH}$ = 8.45 Hz, 5,15-*m*2-Ph); 8.07 (d, 1H, $^3J_{HH}$ = 8.07 Hz, 10-*o*2-Ph); 8.05 (d, 1H, $^3J_{HH}$ = 8.1 Hz, 10-*m*2-Ph). IR ν_{TcO}: 977 cm^{-1}.

^{99}Tc[TPC](O). Yield 8.2 mg (51.2 %). UV-vis (CH_2Cl_2): λ_{max} (nm), [ε x 10^{-4} ($M^{-1}cm^{-1}$)]: 410 (5.73), 468 (2.25), 584 (1.15). ^{1}H NMR (500 MHz, –50°C): δ 9.61 (d, 2H, $^3J_{HH}$ = 4.35 Hz, *β*-H); 9.36 (d, 2H, $^3J_{HH}$ = 3.95 Hz, *β*-H); 9.34 (d, 2H, $^3J_{HH}$ = 4.4 Hz, *β*-H); 9.13 (d, 2H, $^3J_{HH}$ = 5.1 Hz, *β*-H); 8.61 (d, 2H, $^3J_{HH}$ = 7.45 Hz, 5,15-*o*1-Ph); 8.52 (d, 1H, $^3J_{HH}$ = 7.6 Hz, 10-*o*1-Ph); 8.16 (d, 2H, $^3J_{HH}$ = 6.35 Hz, 5,15-*o*2-Ph); 7.95 (m, 3H, $^3J_{HH}$ = 16 Hz, 5,15-*m*1-Ph; 10-*m1*-Ph overlapping); 7.91 (d, 1H, $^3J_{HH}$ = 8.2 Hz 10-*o*2-Ph); 7.83 (m, 5H, 5,15-*m*2-Ph & 5, 10,15-*p*-Ph overlapping); 7.75 (t, 1H, $^3J_{HH}$ = 7.65 Hz, 10-*m*2-Ph). IR ν_{TcO}: 970 cm^{-1}.

^{99}Tc[T*p*MePC](O). Yield 3.6 mg (21.3 %) UV-vis (CH_2Cl_2): λ_{max} (nm), [ε x 10^{-4} ($M^{-1}cm^{-1}$)]: 412 (4.13), 463 (1.36), 580 (0.83). ^{1}H NMR (500 MHz, –50°C): δ 9.59 (d, 2H, $^3J_{HH}$ = 4.3 Hz, *β*-H); 9.34 (4H, *β*-H, broad singlet, overlapping); 9.14 (d, 2H, $^3J_{HH}$ = 4.9 Hz, *β*-H); 8.49 (d, 2H, $^3J_{HH}$ = 7.6 Hz, 5,15-*o*1-Ph); 8.40 (d, 1H, $^3J_{HH}$ = 7.7 Hz, 10-*o*1-Ph); 8.05 (d, 2H, $^3J_{HH}$ = 7.65 Hz, 5,15-*o*2-Ph); 7.84 (d, 1H, $^3J_{HH}$ = 7.4 Hz, 10-*o*2-Ph); 7.75 (d, 2H, $^3J_{HH}$ = 7.65 Hz, 5,15-*m*1-Ph); 7.70 (d, 1H, $^3J_{HH}$ = 7.85 Hz, 10-*m*1-Ph); 7.64 (d, 2H, $^3J_{HH}$ = 7.65 Hz, 5,15-*m*2-Ph); 7.56 (d, 1H, $^3J_{HH}$ = 7.65 Hz, 10-*m*2-Ph); 2.72 (s, 9H, 5,10,15-*p*-CH_3); IR ν_{TcO}: 972 cm^{-1}.

^{99}Tc[T*p*OMePC](O). Yield 3.8 mg (19.66 %). UV-vis (CH_2Cl_2): λ_{max} (nm), [ε x 10^{-4} ($M^{-1}cm^{-1}$)]: 413 (4.32), 556 (1.79), 588 (0.83). ^{1}H NMR (500 MHz, –50°C): δ 9.58 (d, 2H, $^3J_{HH}$ = 4.35 Hz, *β*-H); 9.34 (d, 2H, $^3J_{HH}$ = 4.8 Hz, *β*-H); 9.32 (d, 2H, $^3J_{HH}$ = 4.6 Hz, *β*-H); 9.13 (d, 2H, $^3J_{HH}$ = 5.1 Hz, *β*-H) 8.51 (d, 2H, $^3J_{HH}$ = 8.5 Hz, 5,15-*o*1-Ph); 8.42 (d, 1H, $^3J_{HH}$ = 8.3 Hz, 10-*o*1-Ph); 8.08 (d, 2H, $^3J_{HH}$ = 8.15 Hz, 5,15-*o*2-Ph); 7.87 (d, 1H, $^3J_{HH}$ = 8.2 Hz, 10-*o*2-Ph); 7.47 (d, 2H, $^3J_{HH}$ = 8.6 Hz, 5,15-*m*1-Ph); 7.41 (d, 1H, $^3J_{HH}$ = 7.75 Hz, 10-*m*1-Ph); 7.35 (d, 2H, $^3J_{HH}$ = 8.75 Hz, 5,15-*m*2-Ph); 7.27 (d, 1H, 10-*m*2-Ph); 4.13 (s, 6H, 5,15-*p*-OCH_3); 4.11 (s, 3H, 10-*p*-OCH_3). IR ν_{TcO}: 968 cm^{-1}.

7 REFERENCES

1. American Cancer Society, *The Histrody of Cancer,* https://www.cancer.org/cancer/cancer-basics/history-of-cancer/what-is-cancer.html. (accesed 12.11.17)
2. Kreftregisteret, *Kreftstatistikk*. https://www.kreftregisteret.no/Registrene/Kreftstatistikk/.
3. Larsen, I. K.; Møller, B.; Johannesen, T. B.; Larønningen, S.; Robsahm, T. E.; Grimsrud, T. K.; Ursin, G. Cancer in Norway 2015. Cancer Registry of Norway: **2016**.
4. El-Bayoumy, K.; Sinha, R.; Pinto, J.; Rivlin, R. Cancer chemoprevention by garlic and garlic-containing sulfur and selenium compounds1-3. *J. Nutr.* **2006,** *136*, 864S-869S.
5. Teo, R. D.; Hwang, J. Y.; Termini, J.; Gross, Z.; Gray, H. B. Fighting cancer with corroles. *Chem. Rev.* **2017**, *117*, 2711-2729.
6. Lloyd, N. C.; Morgan, H. W.; Nicholson, B. K.; Ronimus, R. S. The composition of Ehrlich's salvarsan: resolution of a century-old debate. *Angew. Chem. Int. Ed.*. **2005,** *44*, 941-944.
7. Ehrlich, P.; Bertheim, A., Über das salzsaure3.3'-Diamino-4.4'-dioxy-arsenobenzol und seine nächsten Verwandten. *Ber. Dtsch. Chem. Ges.* **1912**, *45*, 756-766.
8. Alderden, R.; Hall, M.; Hambley, T. The discovery and development of cisplatin. *J. Chem. Educ.* **2006,** *83*, 728-734.
9. Dennis, E. J. G. J. D.; Dai, F.; Rakesh, K. J. Photodynamic therapy for cancer. *Nat. Rev. Cancer* **2003,** *3*, 380-387.
10. Ethirajan, M.; Chen, Y.; Joshi, P.; Pandey, R. K. The role of porphyrin chemistry in tumor imaging and photodynamic therapy. *Chem. Rev.* **2010,** *40*, 340-362.
11. Sessler, J.; Miller, R. Texaphyrins - New drugs with diverse clinical applications in radiation and photodynamic therapy. *Biochem. Pharmacol.* **2000,** *59*, 733-739.
12. Johnstone, E. V.; Yates, M. A.; Poineau, F.; Sattelberger, A. P.; Czerwinski, K. R. Technetium: The first radioelement on the periodic table. *J. Chem. Educ.* **2017,** *94*, 320-326.
13. Hackney, J. C. Technetium - Element 43. *J. Chem. Educ.* **1951**, 186-190.
14. Liepe, K.; Kropp, J.; Runge, R.; Kotzerke, J. Therapeutic efficiency of rhenium-188-HEDP in human prostate cancer skeletal metastases. *Brit. J. Cancer* **2003,** *89*, 625-629.
15. Roelandts, R. The history of phototherapy: Something new under the sun? *J. Am. Acad. Dermatol.* **2002,** *46*, 926-930.
16. Josefsen, L.; Boyle, R.; Josefsen, L. Photodynamic therapy and the development of metal-based photosensitisers. *Metal-Based Drugs* **2008,** *2008*, 276109-276133.
17. Hönigsmann, H. History of phototherapy in dermatology. *Photochem. Photobiol. Sci.* **2012,** *12*, 16-21.
18. Berg, K.; Selbo, P. K.; Prasmickaite, L.; Tjelle, T. E.; Sandvig, K.; Moan, J.; Gaudernack, G.; Fodstad, O.; Kjølsrud, S.; Anholt, H.; Rodal, G. H.; Rodal, S. K.; Høgset, A. Photochemical internalization: A novel technology for delivery of macromolecules into cytosol. *Cancer res.* **1999,** *59*, 1180-1183.
19. Hoegset, A.; Prasmickaite, L.; Tjelle, T.; Berg, K.; Hoegset, A. Photochemical transfection: A new technology for light-induced, site-directed gene delivery. *Hum. Gene Ther.* **2000,** *11*, 869-880.
20. Anslyn, E. V.; Dougherty, D. A. *Modern physical organic chemistry*. University Science Books: Sausalito, **2006**, cap.16, 935-999
21. Rodriguez-Serrano, A.; Rai-Constapel, V.; Daza, M. C.; Doerr, M.; Marian, C. M. Internal heavy atom effects in phenothiazinium dyes: Enhancement of intersystem crossing via vibronic spinorbit coupling. *Phys. Chem. Chem. Phys.* **2015,** *17*, 11350-11358.

22. Alemayehu, A. B.; Day, N. U.; Mani, T.; Rudine, A. B.; Thomas, K. E.; Gederaas, O. A.; Vinogradov, S. A.; Wamser, C. C.; Ghosh, A. Gold tris(carboxyphenyl)corroles as multifunctional materials: Room temperature near-IR phosphorescence and applications to photodynamic therapy and dye-sensitized solar cells. *ACS Appl. Mater. Interfaces* **2016,** *8*, 18935-18942.
23. Dysart, J. S.; Patterson, M. S., Characterization of photofrin photobleaching for singlet oxygen dose estimation during photodynamic therapy of mll cells in vitro. *Phys. Med. Bio.* **2005,** *50*, 2597-2616.
24. Kadish, K. M.; Smith, K. M.; Guilard, R. The Porphyrin handbook : Vol. 1 : Synthesis and organic chemistry. *Academic Press: San Diego*, **2000**, Vol. 1.
25. Milgrom, L. R. The colours of life: An introduction to the chemistry of porphyrins and related compounds. *Oxford University Press: Oxford*, **1997**.
26. Zhao, J.; Wu, W.; Sun, J.; Guo, S. Triplet photosensitisers: From molecular design to applications. *Chem. Soc. Rev.* **2013,** *42*, 5323-5351.
27. Barata, J. F. B.; Neves, M. G. P. M. S.; Faustino, M. A. F.; Tomé, A. C.; Cavaleiro, J. A. S. Strategies for corrole functionalization. *Chem. Rev.* **2017**, *117*, 3192-3253.
28. Zhang, W.; Lai, W.; Cao, R. Energy-related small molecule activation reactions: Oxygen reduction and hydrogen and oxygen evolution reactions catalyzed by porphyrin- and corrole-based systems. *Chem. Rev.* **2017**, *117*, 3717-3797.
29. Karkas, M. D.; Verho, O.; Johnston, E.; Akermark, B., Artificial photosynthesis: Molecular systems for catalytic water oxidation. *Chem. Rev.* **2014**, 114, 11863-12001.
30. Mironov, A. F. Lanthanide porphyrin complexes. **2013**, *82*, 333-351.
31a. Gouterman, M. Spectra of porphyrins, *J. Mol. Spectros.* **1961,** *6,* 138-163.
31b. Rimington, C. Spectral-absorption coefficients of some porphyrins in the soret-band region. *Biochem. J.* **1960,** *75*, 620-623.
32. Knyukshto, V. N.; Ngo, T. H.; Dehaen, W.; Maes, W.; Kruk, M. M. Phosphorescence of free base corroles. *RSC Adv.* **2016,** *6*, 43911-43915.
33. Palmer, J. H.; Durrell, A. C.; Gross, Z.; Winkler, J. R.; Gray, H. B. Near-IR phosphorescence of iridium(III) corroles at ambient temperature. *J. Am. Chem. Soc.* **2010,** *132*, 9230-9231.
34. Sommer, Jr.; Shelton, A.; Parthasarathy, A.; Ghiviriga, I.; Reynolds, Jr.; Schanze, K. S. Photophysical properties of near-infrared phosphorescent π-extended platinum porphyrins. *Chem. Mat.* **2011,** *23*, 5296-5304.
35. Rothemund, P. Formation of porphyrins from pyrrole and aldehydes [4]. *J. Am. Chem. Soc.* **1935,** *57*, 2010-2011.
36. Adler, A. D.; Longo, F. R.; Finarelli, J. D.; Goldmacher, J.; Assour, J.; Korsakoff, L. A simplified synthesis for meso-tetraphenylporphine. *J. Org. Chem.* **1967,** *32*, 476-476.
37. Lindsey, J. S.; Schreiman, I. C.; Hsu, H. C.; Kearney, P. C.; Marguerettaz, A. M., Rothemund and Adler-Longo reactions revisited: Synthesis of tetraphenylporphyrins under equilibrium conditions. *J. Org. Chem.* **1987,** *52*, 827-836.
38. Arsenault, G. P.; Bullock, E.; MacDonald, S. F. Pyrromethanes and porphyrins therefrom. *J. Am. Chem. Soc.* **1960,** *82*, 4384-4389.
39. Woodward, R. B.; Ayer, W. A.; Beaton, J. M.; Bickelhaupt, F.; Bonnett, R.; Buchschacher, P.; Closs, G. L.; Dutler, H.; Hannah, J.; Hauck, F. P.; It, S. ô.; Langemann, A.; Le Goff, E.; Leimgruber, W.; Lwowski, W.; Sauer, J.; Valenta, Z.; Volz, H. The total synthesis of chlorophyll. *J. Am. Chem. Soc.* **1960,** *82*, 3800-3802.
40. Kitaoka, S.; Nobuoka, K.; Ishikawa, Y. Ionic liquids for tetraarylporphyrin preparation. *Tetrahedron* **2005,** *61*, 7678-7685.
41. Babu, M.; Amaravathi, M.; Giribabu, L.; Chandramouli, G. Synthesis of *meso*-substituted porphyrins in room temparature ionic liquid. *J. Chem. Res.* **2008,** 666-668.

42. Kobayashi, N.; Takeuchi, Y.; Matsuda, A., *Meso*-aryl subporphyrins. *Angew. Chem. Int. Ed.* **2007,** *46*, 758-760.
43. Xue, Z.; Shen, Z.; Mack, J.; Kuzuhara, D.; Yamada, H.; Okujima, T.; Ono, N.; You, X.; Kobayashi, N. A Facile one-pot synthesis of *meso*-aryl-substituted [14]triphyrin(2.1.1). *J. Am. Chem. Soc.* **2008,** *130*, 16478-16479
44. Xue, Z. L.; Mack, J.; Lu, H.; Zhang, L.; You, X. Z.; Kuzuhara, D.; Stillman, M.; Yamada, H.; Yamauchi, S.; Kobayashi, N.; Shen, Z., The synthesis and properties of free-base [14]triphyrin(2.1.1) compounds and the formation of subporphyrinoid metal complexes. *Chem. Eur. J.*, **2011,** *17*, 4396-4407.
45. Kuzuhara, D.; Yamada, H.; Xue, Z.; Okujima, T.; Mori, S.; Shen, Z.; Uno, H. New synthesis of meso -free-[14]triphyrin(2.1.1) by McMurry coupling and its derivatization to Mn(I) and Re(I) complexes. *Chem. Commun.* **2010,** *47*, 722-724.
46. Xue, Z.; Kuzuhara, D.; Ikeda, S.; Okujima, T.; Mori, S.; Uno, H.; Yamada, H. Synthesis and characterization of new platinum(II) and platinum(IV) triphyrin complexes. *Inorg. Chem.* **2013,** *52*, 1688-1690.
47. Furuta, H.; Asano, T.; Ogawa, T. *N*-confused porphyrins – A new isomer of tetraphenylporphyrin. *J. Am. Chem. Soc.* **1994,** *116*, 767-768.
48. Lash, T. D.; Richter, D. T.; Shiner, C. M. Conjugated macrocycles related to the porphyrins. Part 16. Synthesis of hexa- and heptaalkyl-substituted inverted or *N*-confused porphyrins by the '3 + 1' methodology. *J. Org. Chem.* **1999,** *64*, 7973-7982.
49. Furuta, H.; Maeda, H.; Osuka, A. Oxyindolophyrin: A novel fluoride receptor derived from *N*-confused corrole isomer. *J. Am. Chem. Soc.* **2001,** *123*, 6435-6436.
50. Maeda, H.; Furuta, H. A dozen years of *N*-confusion: From synthesis to supramolecular chemistry. *Pure Appl. Chem.* **2006,** *78*, 29-44.
51. Mori, S.; Osuka, A. Aromatic and antiaromatic gold(III) hexaphyrins with multiple gold-carbon bonds. *J. Am. Chem. Soc.* **2005,** *127*, 8030-8031.
52. Shin, J. Y.; Furuta, H.; Yoza, K.; Igarashi, S.; Osuka, A. *Meso*-aryl-substituted expanded porphyrins [16]. *J. Am. Chem. Soc.* **2001,** *123*, 7190-7191.
53. Woodward, R. B. The total synthesis of vitamin B_{12}. *Pure Appl. Chem.* **1973,** *33*, 145-178.
54. Bauer, V. J.; Clive, D. L. J.; Dolphin, D.; Paine, J. B.; Harris, F. L.; King, M. M.; Loder, J.; Wang, S. W. C.; Woodward, R. B. Sapphyrins: Novel aromatic pentapyrrolic macrocycles. *J. Am. Chem. Soc.* **1983,** *105*, 6429-6436.
55. Richter, D. T.; Lash, T. D. Synthesis of sapphyrins, heterosapphyrins, and carbasapphyrins by a "4 + 1" approach. *J. Org. Chem.* **2004,** *69*, 8842-8850.
56. Shamov, G. A. Oxidative nucleophilic substitution of hydrogen in the sapphyrin dioxouranium(VI) complex: A relativistic DFT study. *J. Am. Chem. Soc.* **2011,** *133*, 4316-4329.
57. Linstead, R. P.; Lowe, A. R. 214. Phthalocyanines. Part III. Preliminary experiments on the preparation of phthalocyanines from phthalonitrile. *J. Chem. Soc.* **1934**, 1022-1027.
58. Kadish, K. M.; Smith, K. M.; Guilard, R., *The porphyrin handbook: Applications of phthalocyanines*. Academic Press: San Diego, **2003**, Vol. 19.
59. Nemykin, V.; Lukyanets, E. Synthesis of substituted phthalocyanines. *Arkivoc* **2010**, 136-208.
60. Matano, Y. Synthesis of aza-, oxa-, and thiaporphyrins and related compounds. *Chem. Rev.* **2017,** *117*, 3138.
61. Fitzgerald, J. P.; Haggerty, B. S.; Rheingold, A. L.; May, L.; Brewer, G. A. Iron octaethyltetraazaporphyrins: Synthesis, characterization, coordination chemistry, and comparisons to related iron porphyrins and phthalocyanines. *Inorg. Chem.* **1992,** *31*, 2006-2013.

62. Ramdhanie, B.; Stern, C. L.; Goldberg, D. P. Synthesis of the first corrolazine: A new member of the porphyrinoid family [3]. *J. Am. Chem. Soc.* **2001,** *123*, 9447-9448.
63. Fujiki, M.; Tabei, H.; Isa, K., New tetrapyrrolic macrocycle: Alpha, beta, gamma.-triazatetrabenzcorrole. *J. Am. Chem. Soc.* **1986,** *108*, 1532-1536.
64. Goldberg, D. Corrolazines: New frontiers in high-valent metalloporphyrinoid stability and reactivity. *Accounts Chem. Res.*, **2007**, *40*, 626-634.
65. Scheer, H. An overview of chlorophylls and bacteriochlorophylls: Biochemistry, functions and applications. *In:* Chlorophylls and bacteriochlorophylls: Biochemistry, functions and applications. Grimm, B.; Porra, R. J.; Rüdiger, W.; Scheer, H. (EDS). Springer: Dordrecht, **2006,** 1-25.
66. Battersby, A. R.; Dutton, C. J.; Fookes, C. J. R.; Turner, S. P. D. Synthetic studies relevant to biosynthetic research on vitamin B_{12}. Part 6. Synthesis of chlorins by a photochemical approach. *J. Chem. Soc., Perkin Transactions 1* **1988**, 1557.
67. Montforts, F. P., A Directed Synthesis of the Chlorin System. *Angew. Chem. Int. Ed.* **1981,** *20*, 778-779.
68. Lindsey, J. S. De novo synthesis of gem-dialkyl chlorophyll analogues for probing and emulating our green world. *Chem. Rev.* **2015,** *115*, 6534-6620.
68b. Taniguchi, M.; Lindsey, J. S. Synthetic chlorins, possible surrogated for chrolophyll, prepared by derivatization of phorphyrins. *Chem. Rev.* **2017,** *117*, 344-535.
69. Yu, Z.; Ptaszek, M. Multifunctional bacteriochlorins from selective palladium-coupling reactions. *Org. Lett.* **2012,** *14*, 3708-3711.
70. Yu, Z.; Pancholi, C.; Bhagavathy, G. V.; Kang, H. S.; Nguyen, J. K.; Ptaszek, M. Strongly conjugated hydroporphyrin dyads: Extensive modification of hydroporphyrins' properties by expanding the conjugated system. *J.Org. Chem.* **2014,** *79*, 7910-7925.
71. Johnson, A. W.; Kay, I. T. 306. Corroles. Part I. Synthesis. *J. Am. Chem. Soc.* **1965**, 1620-1629.
72. Gross, Z.; Galili, N.; Saltsman, I. The first direct synthesis of corroles from pyrrole. *Angew. Chem. Int. Ed.* **1999,** *38*, 1427-1429.
73. Paolesse, R.; Jaquinod, L.; Nurco, D.; Mini, S.; Sagone, F.; Boschi, T.; Smith, K. 5,10,15-triphenylcorrole: A product from a modified Rothemund reaction. *Chem. Commun.* **1999,** 1307-1308.
74. Wasbotten, I.; Wondimagegn, T.; Ghosh, A. Electronic absorption, resonance raman, and electrochemical studies of planar and saddled copper(III) meso-triarylcorroles. Highly substituent-sensitive soret bands as a distinctive feature of high-valent transition metal corroles. *J. Am. Chem. Soc.* **2002,** *124*, 8104-8116.
75. Koszarna, B.; Gryko, D. T. Efficient synthesis of *meso*-substituted corroles in a H_2O-MeOH mixture. *J. Org. Chem.* **2006,** *71*, 3707-3717.
76. Rohand, T.; Dolusic, E.; Ngo, T. H.; Maes, W.; Dehaen, W. Efficient synthesis of aryldipyrromethanes in water and their application in the synthesis of corroles and dipyrromethenes. *Arkivoc* **2007**, 307-324.
77. Ricchelli, F., Photophysical properties of porphyrins in biological membranes. *J. Photochem. Photobiol.* **1995,** *29*, 109-118.
78. Buckley, H. L.; Chomitz, W. A.; Koszarna, B.; Tasior, M.; Gryko, D. T.; Brothers, P. J.; Arnold, J. Synthesis of lithium corrole and its use as a reagent for the preparation of cyclopentadienyl zirconium and titanium corrole complexes. *Chem. Commun.* **2012,** *48*, 10766-10768.
79. Buckley, H. L.; Arnold, J. Recent developments in out-of-plane metallocorrole chemistry across the periodic table. *Dalton Trans.* **2014,** *44*, 30-36.
80. Simkhovich, L.; Mahammed, A.; Goldberg, I.; Gross, Z. Synthesis and characterization of germanium, tin, phosphorus, iron, and rhodium complexes of

tris(pentafluorophenyl)corrole, and the utilization of the iron and rhodium corroles as cyclopropanation catalysts. *Chem. Eur. J.* **2001,** *7*, 1041-1055.
81. Yun, L.; Vazquez-Lima, H.; Fang, H.; Yao, Z.; Geisberger, G.; Dietl, C.; Ghosh, A.; Brothers, P. J.; Fu, X. Synthesis and reactivity studies of a tin(II) corrole complex. *Inorg. Chem.* **2014,** *53*, 7047-7054.
82. Schöfberger, W.; Lengwin, F.; Reith, L. M.; List, M.; Knör, G. Lead corrole complexes in solution: powerful multielectron transfer reagents for redox catalysis. *Inorg. Chem. Commun.* **2010,** *13*, 1187-1190.
83. Liang, X.; Mack, J.; Zheng, L.-M.; Shen, Z.; Kobayashi, N. Phosphorus(V)-corrole: synthesis, spectroscopic properties, theoretical calculations, and potential utility for in vivo applications in living cells. *Inorg. Chem.* **2014,** *53*, 2797-2802.
84. Ghosh, A.; Ravikanth, M., Synthesis, structure, spectroscopic, and electrochemical properties of highly fluorescent phosphorus(V)– *meso*-triarylcorroles. *Chem. Eur. J.* **2012,** *18*, 6386-6396.
85. Kadish, K. M.; Erben, C.; Ou, Z.; Adamian, V. A.; Will, S.; Vogel, E. Corroles with group 15 metal ions. Synthesis and characterization of octaethylcorroles containing As, Sb, and Bi ions in +3, +4, and +5 oxidation states. *Inorg. Chem.* **2000,** *39*, 3312-3319.
86. Reith, L. M.; Stiftinger, M.; Monkowius, U.; Knör, G.; Schoefberger, W. Synthesis and characterization of a stable bismuth(III) A_3-corrole. *Inorg. Chem.* **2011,** *50*, 6788-6797.
87. Brothers, P. J., Boron complexes of porphyrins and related polypyrrole ligands: Unexpected chemistry for both boron and the porphyrin. *Chem. Commun.* **2008,** *18*, 2090-2102.
88. Albrett, A. M.; Boyd, P. D. W.; Clark, G. R.; Brothers, P. J.; Gonzalez, E.; Ghosh, A. Reductive coupling and protonation leading to diboron corroles with a B-H-B bridge. *Dalton Trans.* **2010,** *39*, 4032-4034.
89. Mahammed, A.; Gross, Z. Aluminum corrolin, a novel chlorophyll analogue. *J. Inorg. Biochem.* **2002,** *88*, 305-309.
90. Blumenfeld, C. M.; Grubbs, R. H.; Moats, R. A.; Gray, H. B.; Sorasaenee, K. Decorating metal oxide surfaces with fluorescent chlorosulfonated corroles. *Inorg. Chem.* **2013,** *52*, 4774-4776.
91. Aviv, I.; Gross, Z. Corrole-based applications. *Chem. Commun.* **2007,** *20*, 1987-1999.
92. Murakami, Y.; Matsuda, Y.; Yamada, S. Transition-metal complexes of pyrrole pigments. Part 20. Redox behaviour of chromium complexes with macrocyclic tetrapyrroles. *Dalton Trans.* **1981,** *3*, 855-861.
93. Meier-Callahan, A. E.; Gray, H. B.; Gross, Z. Stabilization of high-valent metals by corroles: Oxo[tris(pentafluorophenyl)corrolato]chromium(V). *Inorg. Chem.* **2000,** *39*, 3605-3607.
94. Boschi, T.; Licoccia, S.; Paolesse, R.; Tagliatesta, P.; Tehran, M. A. Synthesis and characterization of novel metal(III) complexes of corrole – crystal and molecular-structure of (2,3,7,8,12,13,17,18-octamethylcorrolat)(triphenylarsine)rhodium(III). *Dalton Trans.* **1990,** *2*, 463-468.
95. Kadish, K. M.; Adamian, V. A.; Van Caemelbecke, E.; Gueletii, E.; Will, S.; Erben, C.; Vogel, E. Electrogeneration of oxidized corrole dimers. Electrochemistry of (OEC)M where M = Mn, Co, Ni, or Cu and OEC is the trianion of 2,3,7,8,12,13,17,18-octaethylcorrole. *J. Am. Chem. Soc.* **1998,** *120*, 11986-11993.
96. Gross, Z.; Golubkov, G.; Simkhovich, L. Epoxidation catalysis by a manganese corrole and isolation of an oxo-manganese(V) corrole. *Angew. Chem. Int. Ed.* **2000,** *39*, 4045-4047.

97. Singh, P.; Dutta, G.; Goldberg, I.; Mahammed, A.; Gross, Z. Expected and unexpected transformations of manganese(III) tris(4-nitrophenyl)corrole. *Inorg. Chem.* **2013,** *52*, 9349-9355.
98. Liu, H. Y.; Lai, T. S.; Yeung, L. L.; Chang, C. K. First synthesis of perfluorinated corrole and its Mn=O complex. *Org. Lett.* **2003,** *5*, 617-620.
99. Gershman, Z.; Goldberg, I.; Gross, Z. DNA binding and catalytic properties of positively charged corroles. *Angew. Chem. Int. Ed.* **2007,** *46*, 4320-4324.
100. Liu, H.; Mahmood, M.; Qiu, S.; Chang, C. Recent developments in manganese corrole chemistry. *Coord. Chem. Rev.* **2013**, *257*, 1306-1333.
101. Bougher, C. J.; Liu, S.; Hicks, S. D.; Abu-Omar, M. M. Valence tautomerization of high-valent manganese(V)-oxo corrole induced by protonation of the oxo ligand. *J. Am. Chem. Soc.* **2015,** *137*, 14481-14487.
102. Han, Y.; Lee, Y.-m.; Mariappan, M.; Fukuzumi, S.; Nam, W. Manganese(V)–oxo corroles in hydride-transfer reactions. *Chem. Commun.* **2009,** *46*, 8160-8162.
103. Simkhovich, L.; Galili, N.; Saltsman, I.; Gross, Z.; Goldberg, I. Coordination chemistry of the novel 5,10,15-tris(pentafluorophenyl)corrole: Synthesis, spectroscopy, and structural characterization of its cobalt(III), rhodium(III), and iron(IV) complexes. *Inorg. Chem.* **2000,** *39*, 2704-2705.
104. Vazquez-Lima, H.; Norheim, H. K.; Einrem, R. F.; Ghosh, A. Cryptic noninnocence: FeNO corroles in a new light. *Dalton Trans.* **2015,** *44*, 10146-10151.
105. Norheim, H. K.; Capar, J.; Einrem, R. F.; Gagnon, K. J.; Beavers, C. M.; Vazquez-Lima, H.; Ghosh, A. Ligand noninnocence in FeNO corroles: Insights from beta-octabromocorrole complexes. *Dalton Trans.* **2016,** *45*, 681-689.
106. Ganguly, S.; Vazquez-Lima, H.; Ghosh, A. Wolves in sheep's clothing: μ-oxo-diiron corroles revisited. *Chem. Eur. J.* **2016,** *22*, 10336-10340.
106b. Ghosh, A. Electronic structure of corrole derivativer: Insights from molecular structures, spectroscopy, electrochemistry, and quantum chemical calculations. *Chem. Rev.* **2017**, *117*, 3798-3881.
107. Steene, E.; Wondimagegn, T.; Ghosh, A. Electrochemical and electronic absorption spectroscopic studies of substituent effects in iron(IV) and manganese(IV) corroles. Do the compounds feature high-valent metal centers or noninnocent corrole ligands? Implications for peroxidase compound I and II intermediates. *J. Phys. Chem. B* **2001,** *105*, 11406-11413.
108. Conlon, M.; Johnson, A. W.; Overend, W. R.; Rajapaksa, D.; Elson, C. M. Structure and reactions of cobalt corroles. *Perkin Trans. 1.* **1973**, 2281-2288.
109. Meier-Callahan, A. E.; Di Bilio, A.; Simkhovich, L.; Mahammed, A.; Goldberg, I.; Gray, H.; Gross, Z. Chromium corroles in four oxidation states. *Inorg. Chem.* **2001,** *40*, 6788-6793.
110. Will, S.; Lex, J.; Vogel, E.; Schmickler, H.; Gisselbrecht, J.-P.; Haubtmann, C.; Bernard, M.; Gross, M. Nickel and copper corroles: Well-known complexes in a new light. *Angew. Chem. Int. Ed.* **1997,** *36*, 357-361.
111. Capar, C.; Thomas, K. E.; Ghosh, A. Reductive demetallation of copper corroles: First simple route to free-base octabromocorroles. *J. Porphyrins Phthalocyanines,.* **2008,** *12*, 964-967.
112. Luobeznova, I.; Raizman, M.; Goldberg, I.; Gross, Z. Synthesis and full characterization of molybdenum and antimony corroles and utilization of the latter complexes as very efficient catalysts for highly selective aerobic oxygenation reactions. *Inorg. Chem.* **2006,** *45*, 386-394.
113. Jérôme, F.; Billier, B.; Barbe, J. M.; Espinosa, E.; Dahaoui, S.; Lecomte, C.; Guilard, R. Evidence for the formation of a Ru(III)−Ru(III) bond in a ruthenium corrole homodimer. *Angew. Chem. Int. Ed.* **2000,** *39*, 4051-4053.

114. Simkhovich, L.; Luobeznova, I.; Goldberg, I.; Gross, Z. Mono- and binuclear ruthenium corroles: Synthesis, spectroscopy, electrochemistry, and structural characterization. *Chem. Eur. J.* **2003,** *9*, 201-208.
114b. Alemayehu. A. B.; Vazques-Lima, H.; Gagnon, J. K.; Ghosh, A. Stepwise deoxygenation of nitrite as a route to two families of ruthenium corroles: Group 8 periodic trends and relativistic effects, *Inorg. Chem.* **2017,** *56*, 5285-5294.
115. Kadish, K. M.; Koh, W.; Tagliatesta, P.; Sazou, D.; Paolesse, R.; Licoccia, S.; Boschi, T. Electrochemistry of rhodium and cobalt corroles. Characterization of (OMC)Rh(PPh_3) and (OMC)Co(PPh_3) where OMC is the trianion of 2,3,7,8,12,13,17,18-octamethylcorrole. *Inorg. Chem.* **1992,** *31*, 2305-2313.
116. Brückner, C.; Barta, C. A.; Briñas, R. P.; Bauer, J. A. K. Synthesis and structure of [*meso*-triarylcorrolato]silver(III). *Inorg. Chem.* **2003,** *42*, 1673-1680.
117. Tse, M.; Zhang, Z.; Mak, T.; Chan, K. S. Synthesis of an oxorhenium(V) corrolate from porphyrin with detrifluoromethylation and ring contraction. *Chem. Commun.* **1998,** *11*, 1199-1200.
118. Palmer, J. H.; Lancaster, K. M., Molecular redox: Revisiting the electronic structures of the group 9 metallocorroles. *Inorg. Chem.* **2012,** *51*, 12473-12482.
119. Palmer, J. H.; Day, M. W.; Wilson, A. D.; Henling, L. M.; Gross, Z.; Gray, H. B. Iridium corroles. *J. Am. Chem. Soc.* **2008,** *130*, 7786-7787.
120. Palmer, J. H.; Mahammed, A.; Lancaster, K. M.; Gross, Z.; Gray, H. B. Structures and reactivity patterns of group 9 metallocorroles. *Inorg. Chem.* **2009,** *48*, 9308-9315.
121. Thomas, K. E.; Alemayehu, A. B.; Conradie, J.; Beavers, C.; Ghosh, A. Synthesis and molecular structure of gold triarylcorroles. *Inorg. Chem.* **2011,** *50*, 12844-12851.
122. Rabinovich, E.; Goldberg, I.; Gross, Z. Gold(I) and gold(III) corroles. *Chem. Eur. J.* **2011,** *17*, 12294-12301.
123. Alemayehu, A. B.; Vazquez-Lima, H.; Beavers, C. M.; Gagnon, K. J.; Bendix, J.; Ghosh, A. Platinum corroles. *Chem. Commun.* **2014,** *50*, 11093-11096.
124. Alemayehu, A. B.; Gagnon, K. J.; Terner, J.; Ghosh, A. Oxidative metalation as a route to size-mismatched macrocyclic complexes: Osmium corroles. *Angew. Chem. Int. Ed.* **2014,** *53*, 14411-14414.
125. Padilla, R.; Buckley, H. L.; Ward, A. L.; Arnold, J. Synthesis, structure and reactivity of group 4 corrole complexes. *Chem. Commun.* **2014,** *50*, 2922-2924.
126. Ziegler, J. A.; Buckley, H. L.; Arnold, J. Synthesis and reactivity of tantalum corrole complexes. *Dalton Trans.* **2017,** *46*, 780-785.
127. Padilla, R., Preparation and characterization of a tungsten(V) corrole dichloride complex. *J. Porphyrins Phthalocyanines.* **2015,** *150*.
128. Alemayehu, A. B.; Vazquez-Lima, H.; Gagnon, K. J.; Ghosh, A. Tungsten biscorroles: New chiral sandwich compounds. *Chem. Eur. J.* **2016,** *22*, 6914-6920.
129. Buckley, H. L.; Anstey, M. R.; Gryko, D. T.; Arnold, J. Lanthanide corroles: A new class of macrocyclic lanthanide complexes. *Chem. Commun.* **2013,** *49*, 3104-3106.
130. Lu, G.; Li, J.; Jiang, X.; Ou, Z.; Kadish, K. M. Europium triple-decker complexes containing phthalocyanine and nitrophenyl-corrole macrocycles. *Inorg. Chem.* **2015,** *54*, 9211-9222.
131. Lu, G.; Li, J.; Yan, S.; He, C.; Shi, M.; Zhu, W.; Ou, Z.; Kadish, K. M. Self-assembled organic nanostructures and nonlinear optical properties of heteroleptic corrole–phthalocyanine europium triple-decker complexes. *Dyes and Pigments* **2015,** *121*, 38-45.
132. Lu, G.; Yan, S.; Shi, M.; Yu, W.; Li, J.; Zhu, W.; Ou, Z.; Kadish, K. M. A new class of rare earth tetrapyrrole sandwich complexes containing corrole and phthalocyanine macrocycles: Synthesis, physicochemical characterization and X-ray analysis. *Chem. Commun.* **2015,** *51*, 2411-2413.

133. Ward, A. L.; Buckley, H. L.; Lukens, W. W.; Arnold, J. Synthesis and characterization of thorium(IV) and uranium(IV) corrole complexes. *J. Am. Chem. Soc.* **2013,** *135*, 13965-13971.
134. Aviezer, D.; Cotton, S.; David, M.; Segev, A.; Khaselev, N.; Galili, N.; Gross, Z.; Yayon, A. Porphyrin analogues as novel antagonists of fibroblast growth factor and vascular endothelial growth factor receptor binding that inhibit endothelial cell proliferation, tumor progression, and metastasis. *Cancer Res.* **2000,** *60,* 2973.
135. Naik, A.; Rubbiani, R.; Gasser, G.; Spingler, B. Visible-light-induced annihilation of tumor cells with platinum–porphyrin conjugates. *Angew. Chem. Int. Ed.* **2014,** *53*, 6938-6941.
136. Fu, B.; Huang, J.; Ren, L.; Weng, X.; Zhou, Y.; Du, Y.; Wu, X.; Zhou, X.; Yang, G. Cationic corrole derivatives: A new family of G-quadruplex inducing and stabilizing ligands. *Chem. Commun.* **2007,** 3264-3266.
137. Paolesse, R.; Nardis, S.; Sagone, F.; Khoury, R. G. Synthesis and functionalization of *meso*-aryl-substituted corroles. *J. Org. Chem.* **2001,** *66*, 550-556.
138. Mahammed, A.; Gross, Z.; Goldberg, I. Highly selective chlorosulfonation of tris(pentafluorophenyl)corrole as a synthetic tool for the preparation of amphiphilic corroles and metal complexes of planar chirality. *Org. Lett.* **2001,** *3*, 3443-3446.
139. Hasmik, A.; Jun, M.; Altan, R.; Vinod, V.; Jae Youn, H.; Atif, M.; Daniel, L. F.; Harry, B. G.; Zeev, G.; Lali, K. M.-K. Tumor detection and elimination by a targeted gallium corrole. *Proc. Natl. Acad. Sci. US.* **2009,** *106*, 6105-6110.
140. Ghosh, A.; Steene, E. High-valent transition metal centers and noninnocent ligands in metalloporphyrins and related molecules: a broad overview based on quantum chemical calculations. *J. Biol. Inorg. Chem.* **2001,** *6*, 739-752.
141. Alemayehu, A.; Conradie, J.; Ghosh, A. A first TDDFT study of metallocorrole electronic spectra: Copper *meso*-triarylcorroles exhibit hyper spectra. *Eur. J. Inorg. Chem.* **2011,** 1857-1864.
142. Pyykkö, P.; Riedel, S.; Patzschke, M., Triple-Bond Covalent Radii. *Chem. Eur. J.* **2005,** *11*, 3511-3520.
143. Zhang, Z.; Wen, J. Y.; Lv, B. B.; Li, X.; Ying, X.; Wang, Y. J.; Zhang, H. T.; Wang, H.; Liu, H. Y.; Chang, C. K. Photocytotoxicity and G-quadruplex DNA interaction of water-soluble gallium(III) tris(N-methyl-4-pyridyl)corrole complex. *Appl. Organomet. Chem.* **2016,** *30*, 132-139.
144. Alberto, R.; Schibli, R.; Egli, A.; Abram, U.; Abram, S.; Kaden, T. A.; August Schubiger, P. Steps towards $[(C_5Me_5)TcO_3]$: Novel synthesis of $[(C_5Me_5)Tc(CO)_3]$ from $[\{Tc(\mu\text{-}3\text{-}OH)(CO)_3\}_4]$ and oxidation of $[(C_5Me_5)M(CO)_3]$ (M = Tc, Re) with Br_2. *Polyhedron* **1998,** *17*, 1133-1140.
145. Carmichael, J.; Degraff, W. G.; Gazdar, A. F.; Minna, J. D.; Mitchell, J. B. Evaluation of a tetrazolium-based semiautomated colorimetric assay: assessment of chemosensitivity testing. *Cancer Res.* **1987,** *47*, 936-942.
146. Bogoeva, V.; Siksjø, M.; Sæterbø, K. G.; Melø, T. B.; Bjørkøy, A.; Lindgren, M.; Gederaas, O. A. Ruthenium porphyrin-induced photodamage in bladder cancer cells. *Photodiagn. Photodyn.* **2016,** *14*, 9-17.

8 SUPPORTING INFORMATION

8.1 MATERIALS

8.1.1 ReO

All chemicals were obtained from Sigma-Aldrich and used as purchased, except for dichloromethane used for cyclic voltammetry analyses, which was dried using 4 Å molecular sieves. CHROMASOLV® for HPLC grade *n*-hexane, dichloromethane, ethyl acetate, and toluene were used for column chromatography. Silica gel 60 (0.04–0.063 mm particle size; 230–400 mesh, Sigma) was used for chromatography and the columns used were generally ~3 cm wide and ~12 cm in height. ^{1}H NMR spectra were recorded on Bruker Avance III HD 400 MHz spectrometer. UV/Vis spectra were recorded on an HP 8454 spectrophotometer at room temperature. Cyclic voltammetry analyses were carried out in dried dichloromethane containing 0.1 M TBAP as supporting electrolyte. An EG&G 263A potentiostat having a standard three-electrode set-up, consisting of a glassy carbon working electrode (3 mm i.d.), a platinum wire counter electrode, and saturated calomel reference electrode (SCE). X-ray data were collected on beamline 11.3.1 at the Advanced Light Source of Lawrence Berkeley National Laboratory. Electrospray Ionization (ESI) mass spectrum were recorded on an LTQ Orbitrap XL spectrometer.

8.1.2 ^{99}TcO

All commercially available chemicals were reagent grade and used without further purification. FTIR spectra were measured as KBr pellets on PerkinElmer Spectrum Two spectrophotometer. ^{1}H NMR spectra were recorded on Bruker DRX500 500 MHz spectrometer. UV/Vis spectra in dichloromethane were recorded on Cary 50 spectrometer using 1 cm quartz cuvette. Cyclic voltammetry analysis were carried out in acetonitrile containing 0.1 M TBAP as supporting electrolyte with a Metrohm 757 VA Computrace electrochemical analyser equipped with a standard three-electrode set-up, consisting of a glassy carbon working electrode (3 mm i.d.), a platinum auxiliary electrode and Ag/AgCl reference electrode. Crystallographic data was collected at 183K with Mo Ka radiation (λ=0.7108 Å) with graphite on an Oxford Diffraction Xcalibur system with a Ruby detector.

8.1.3 Cell viability study

RPMI-1640 medium, L-glutamine, foetal bovine serum (FBS), sodium pyruvate, nonessential amino acids, trypsin and phosphate buffered saline (PBS) were obtained from Gibco BRL, Life Technologies (Inchinnan, Scotland). Gentamicin sulphate was purchased from Schering Corp (Kenilworth, NJ) and absolute ethanol from Arcus A/S (Oslo, Norway). MTT solution was obtained from Sigma-Aldrich (St. Louis, MO). All other chemicals were of the highest quality that is commercially available.

8.2 RHENIUM COMPLEXES

8.2.1 Analysis of Re[T*p*CF$_3$PC](O)

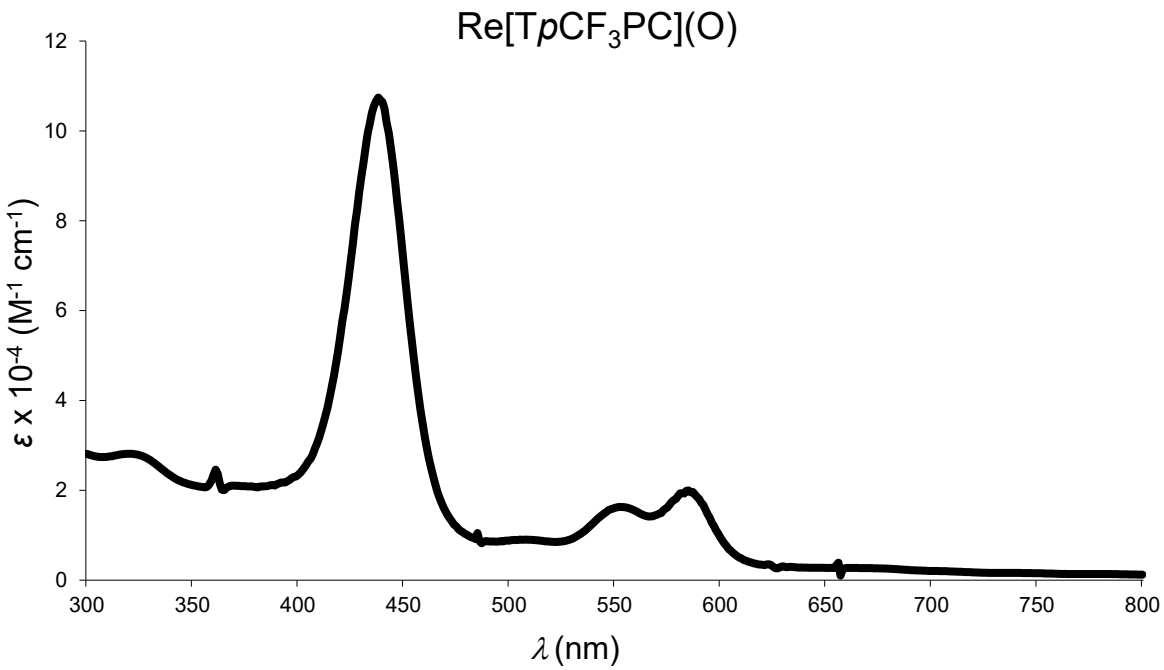

Figure 69. UV-vis spectrum in DCM.

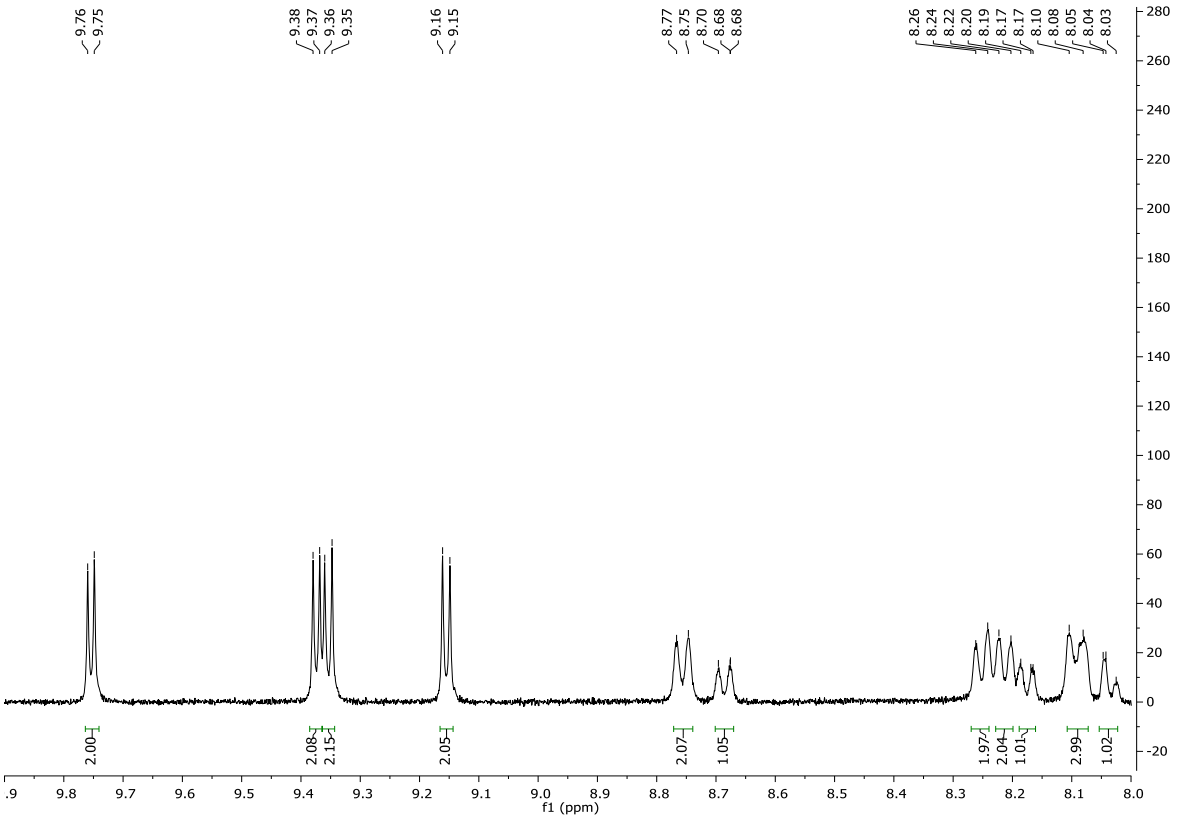

Figure 70. ^{1}H NMR spectrum.

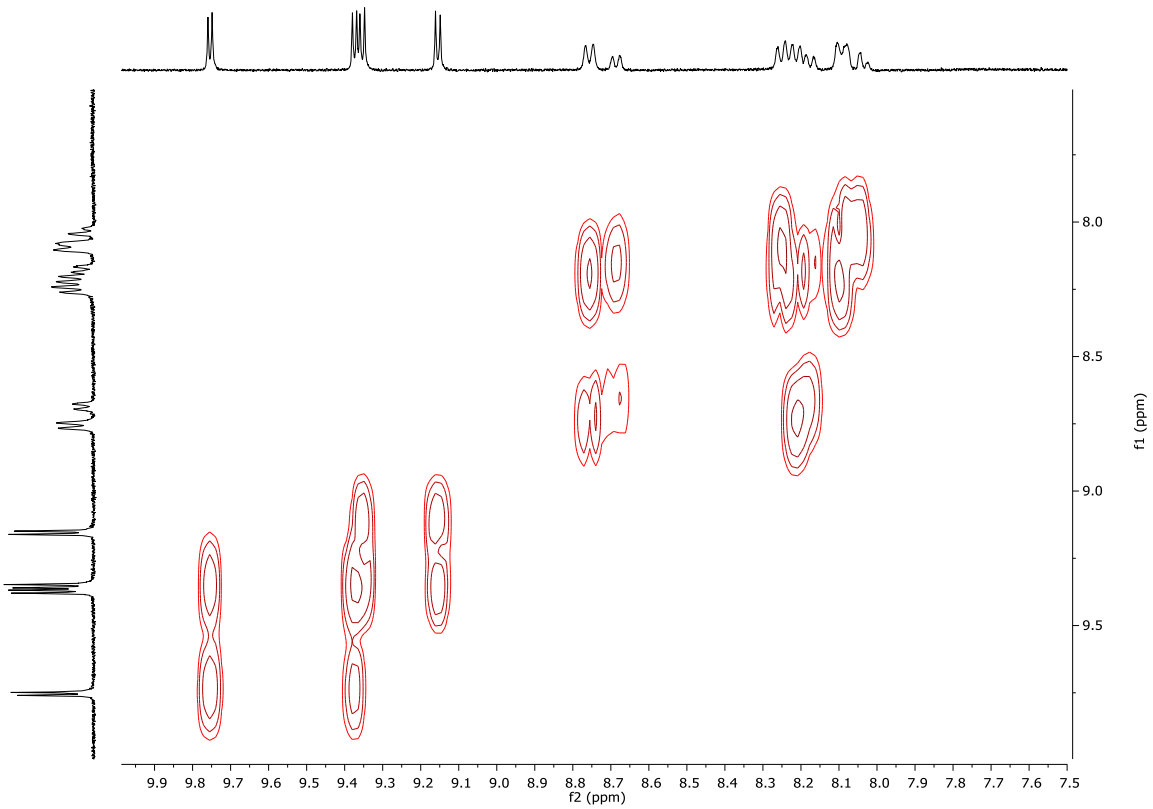

Figure 71. ^{1}H - ^{1}H COSY.

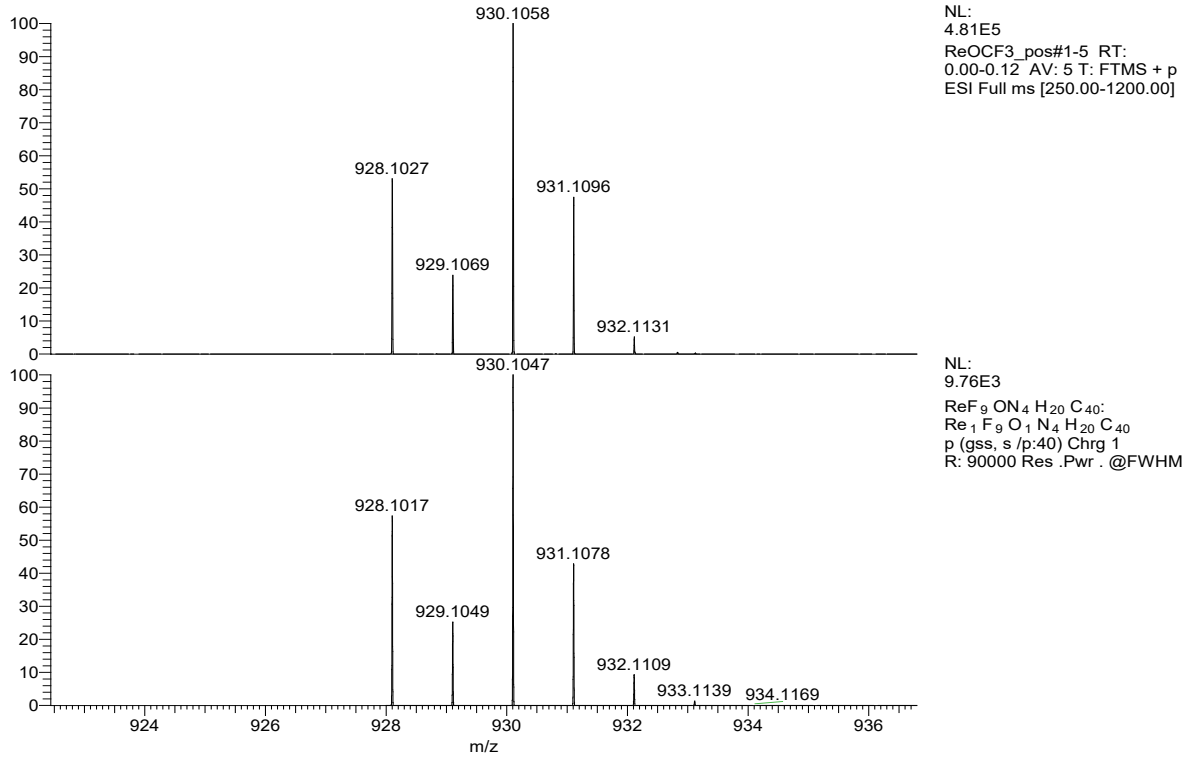

Figure 72. ESI-MS spectrum: measured (top) and calculated (bottom).

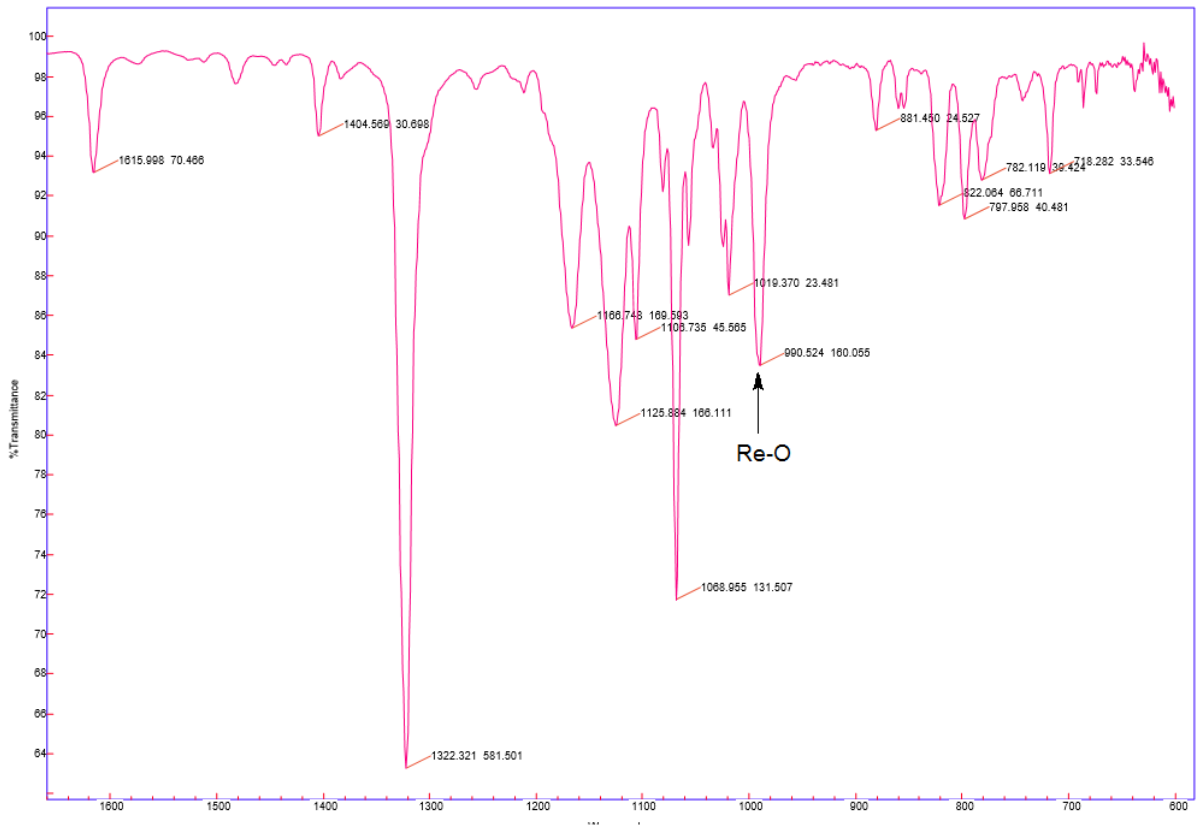

Figure 73. IR spectrum.

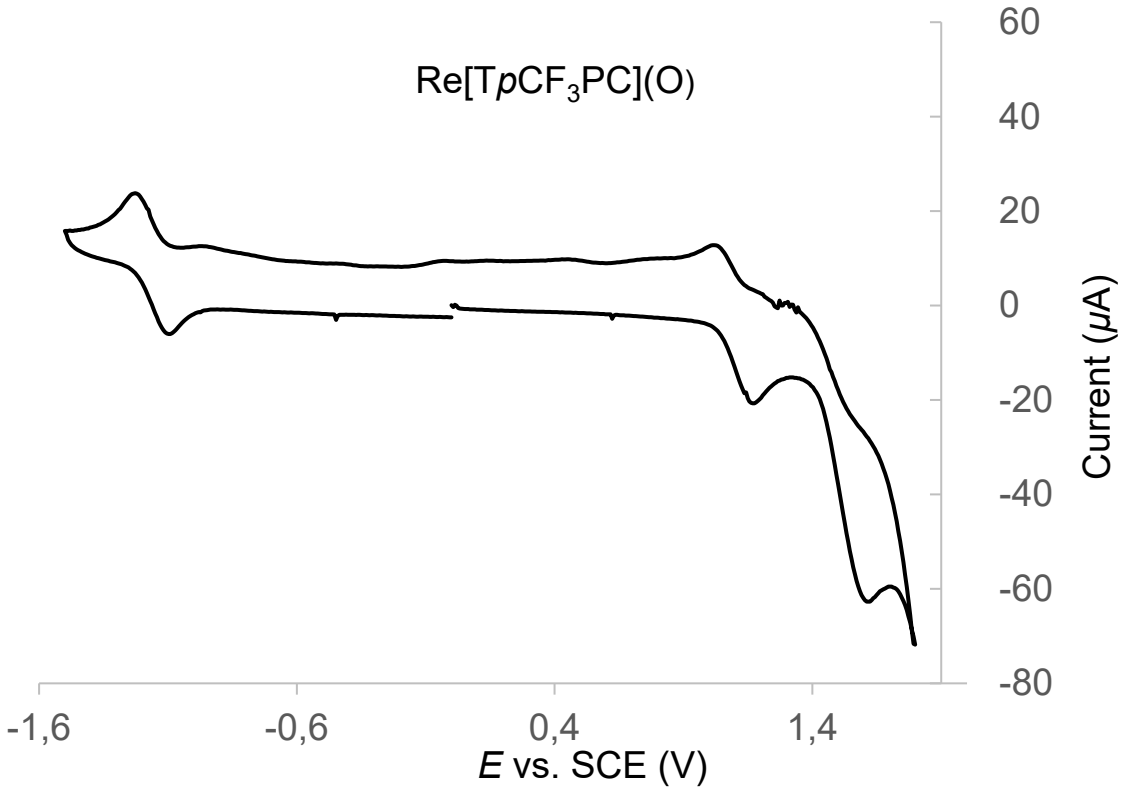

Figure 74. Cyclic voltammogram in DCM containing 0.1 M TBAP.

Table 9. Single crystal X-ray data collection and structure calculations.

Sample	Re[T*p*CF$_3$PC](O)
Chemical formula	$C_{40.25}H_{20.50}Cl_{0.50}F_9N_4ORe$
Formula mass	951.03
Crystal system	Monoclinic
Space group	$P\,2_1/c$
λ (Å)	0.7749
a (Å)	16.4309(6)
b (Å)	14.2677(5)
c (Å)	14.1303(5)
α (deg)	90
β (deg)	93.141(2)
γ (deg)	90
Z	4
V (Å^3)	3307.6(2)
Temperature (K)	100(2)
Density (g/cm^3)	1.910
Measured reflections	57324
Unique reflections	10091
Parameters	581
Restraints	403
R_{int}	0.0501
θ range (deg)	2.062 – 33.606
R_1, wR_2 all data	0.0272, 0.0526
S (GooF) all data	1.023
Max/min res. Dens. (e/Å^3)	1.082/-1.078

8.2.2 Analysis of Re[T*p*CO$_2$CH$_3$PC](O)

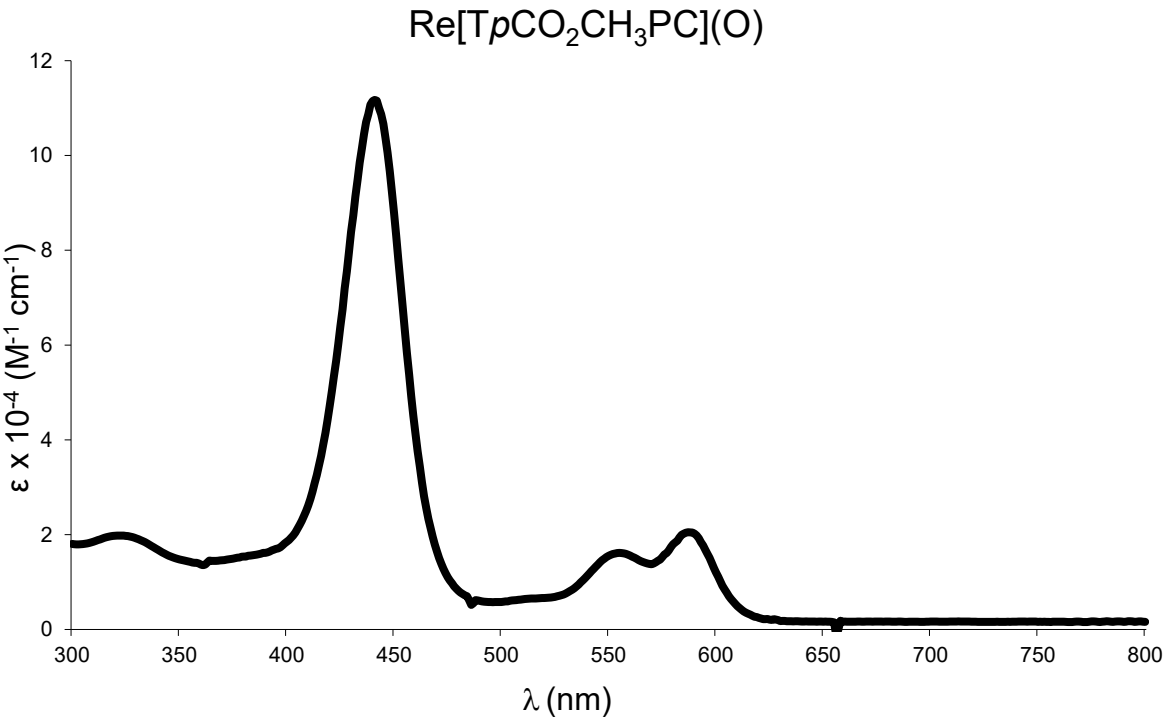

Figure 75. UV-vis spectrum in DCM.

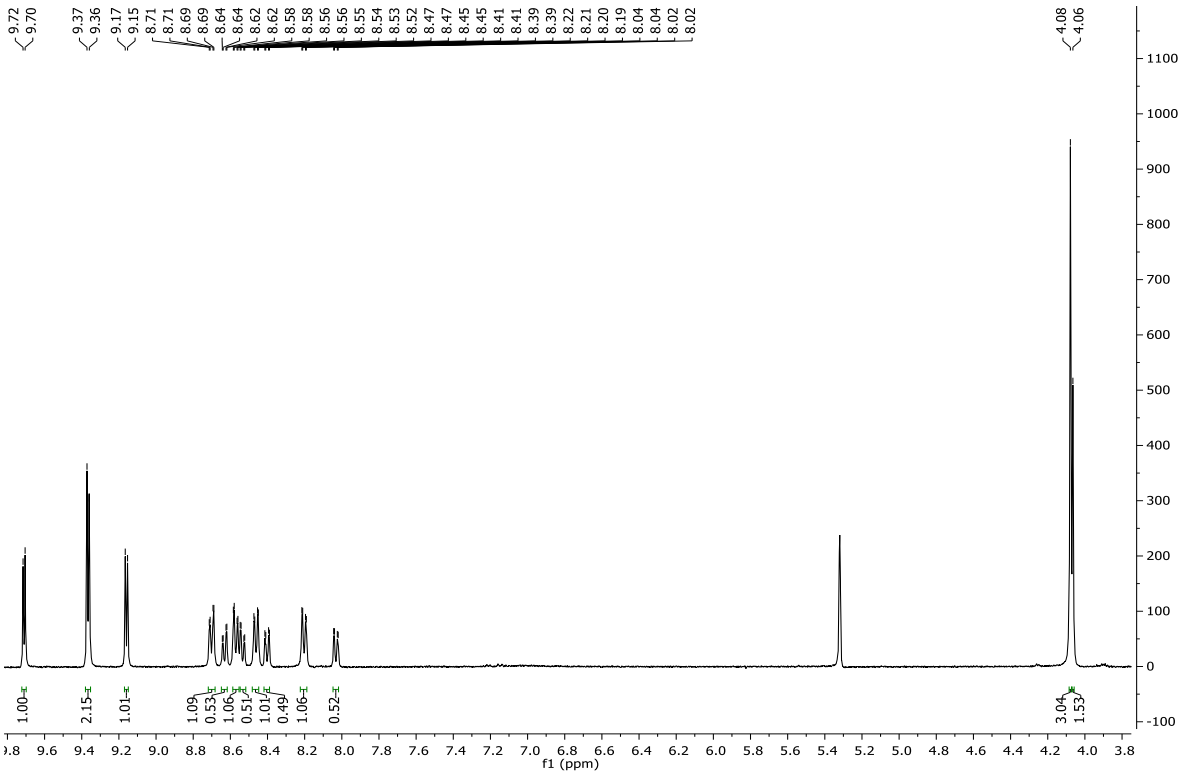

Figure 76. ^{1}H NMR spectrum.

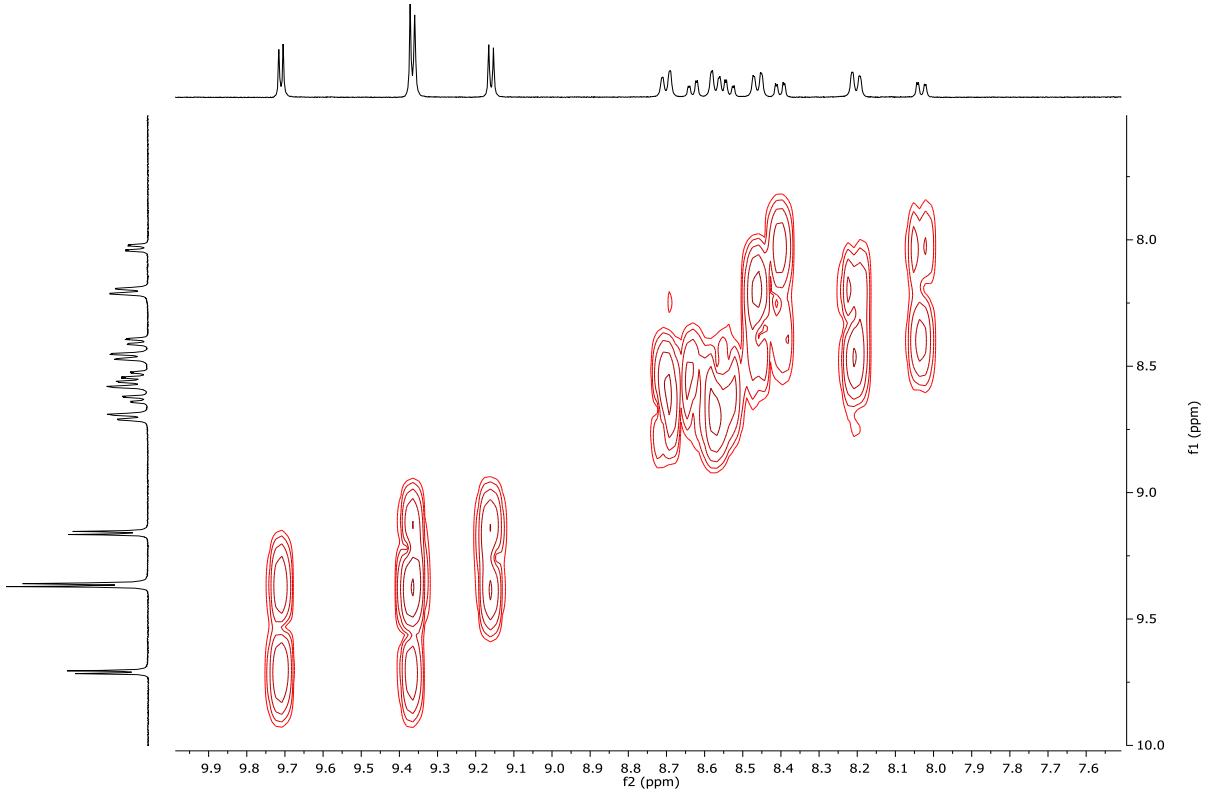

Figure 77. ^{1}H - ^{1}H COSY.

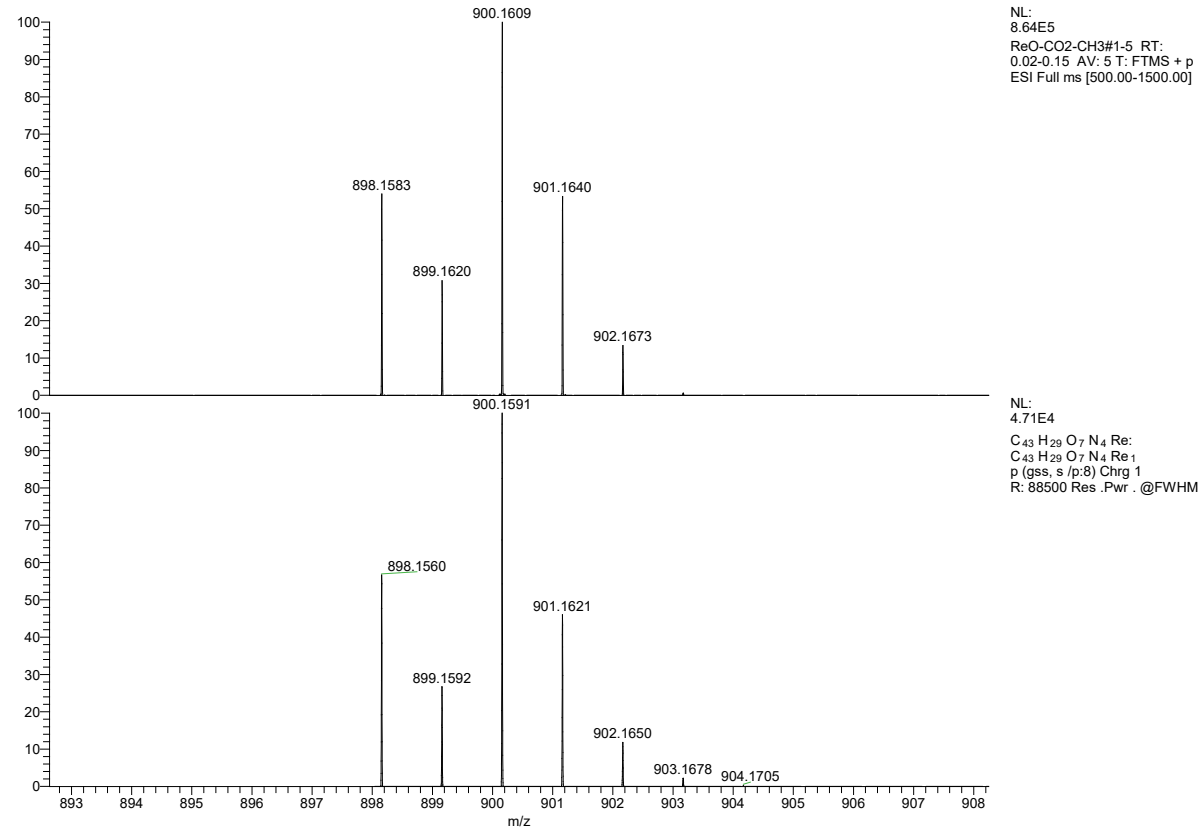

Figure 78. ESI-MS spectrum: measured (top) and calculated (bottom).

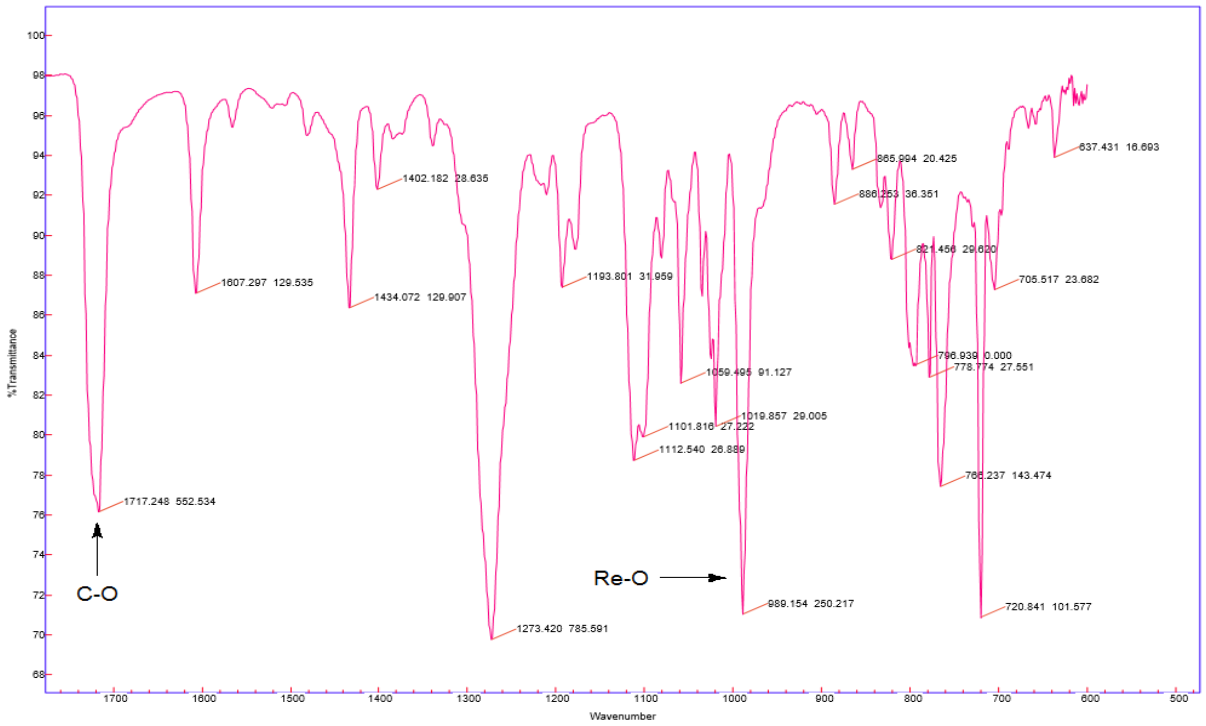

Figure 79. IR spectrum.

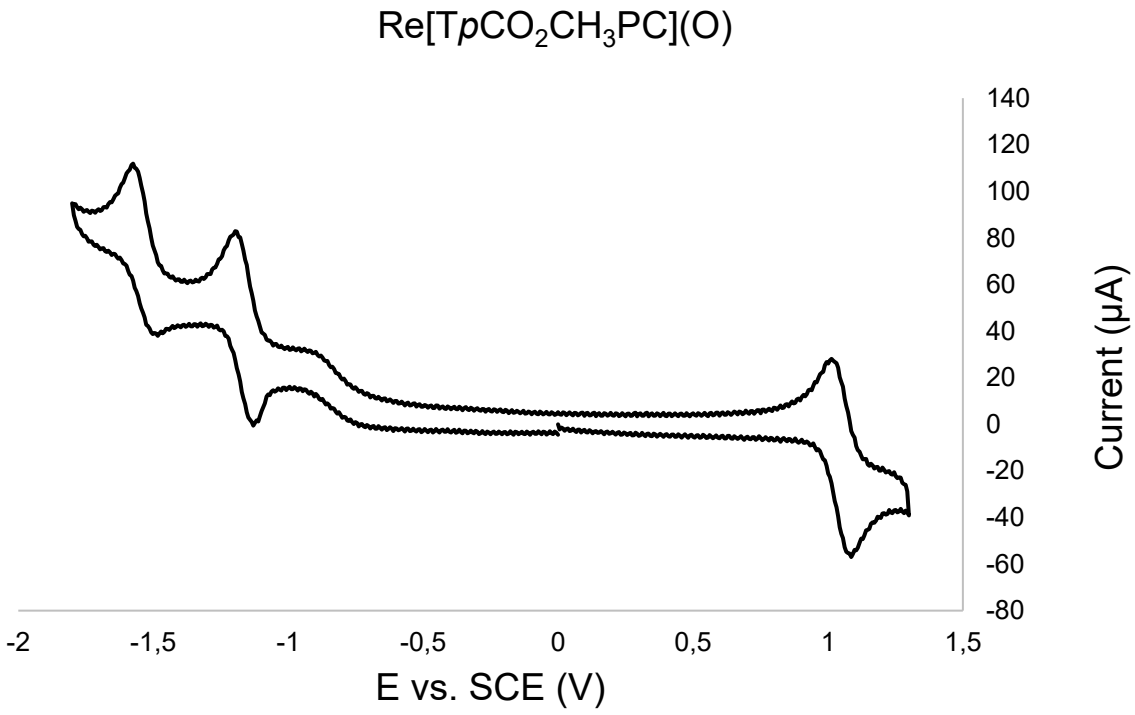

Figure 80. Cyclic voltammogram in DCM containing 0.1 M TBAP.

8.2.3 Analysis of Re[T*p*CO$_2$HPC](O)

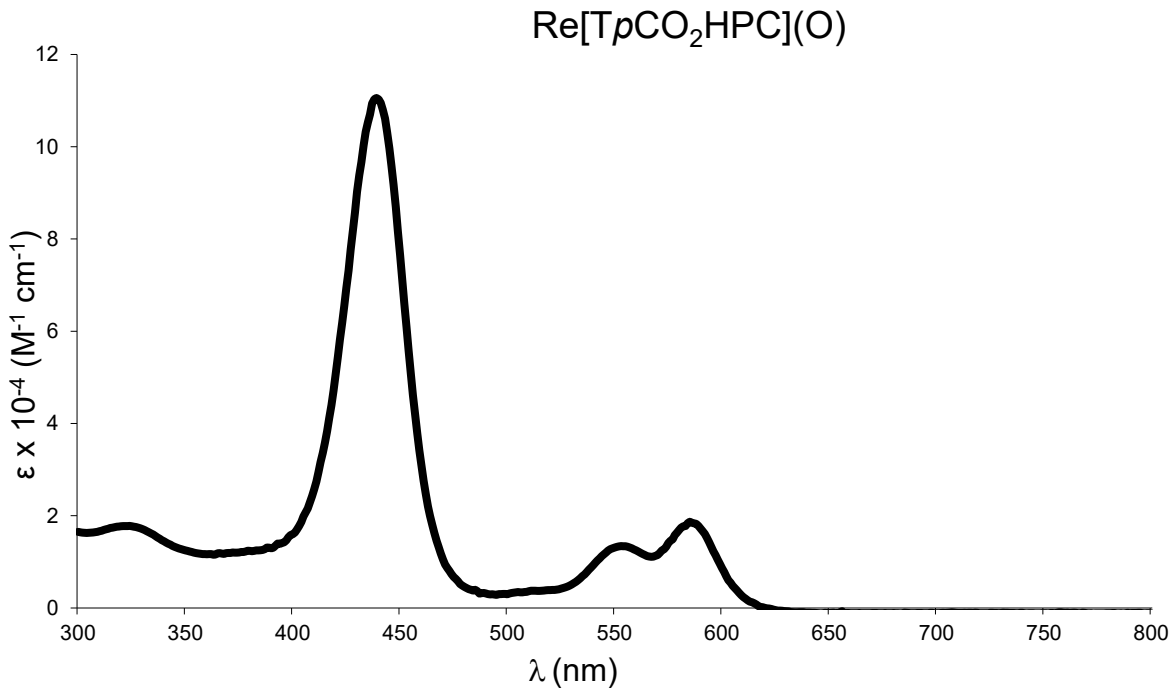

Figure 81. UV-vis spectrum in THF.

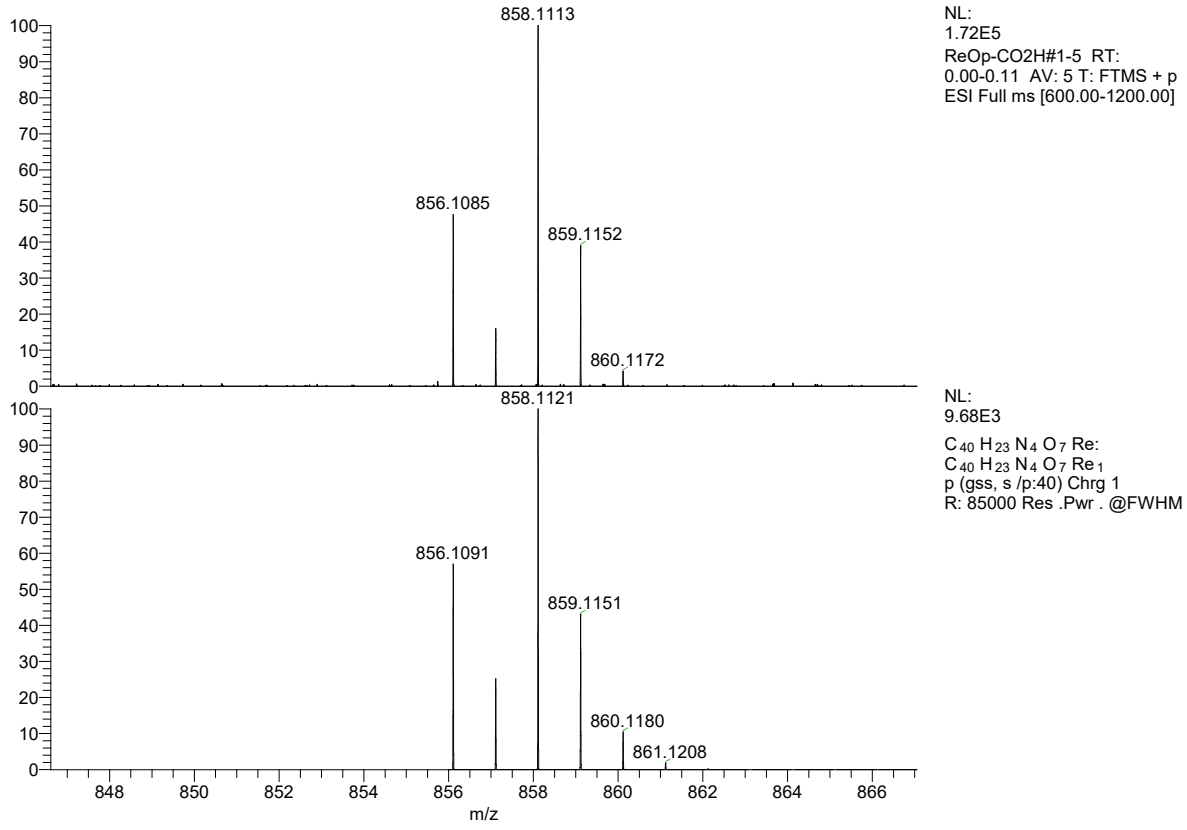

Figure 82. ESI-MS spectrum: measured (top) and calculated (bottom).

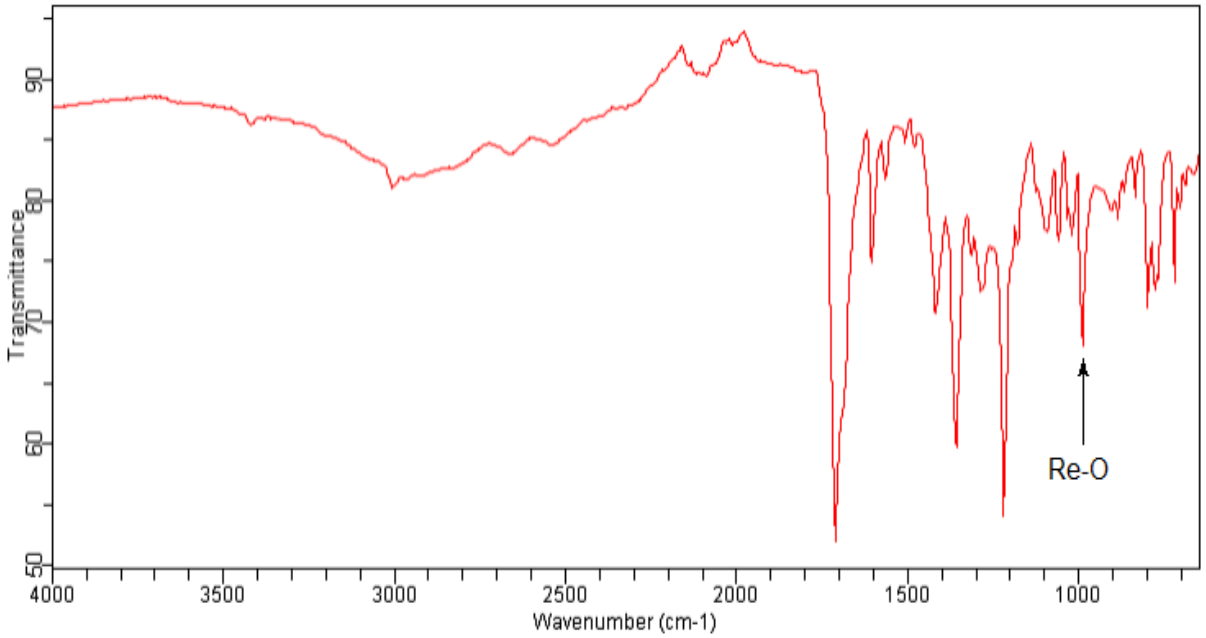

Figure 83. IR spectrum.

8.2.4 Analysis of Re[T*m*CO_2CH_3PC](O)

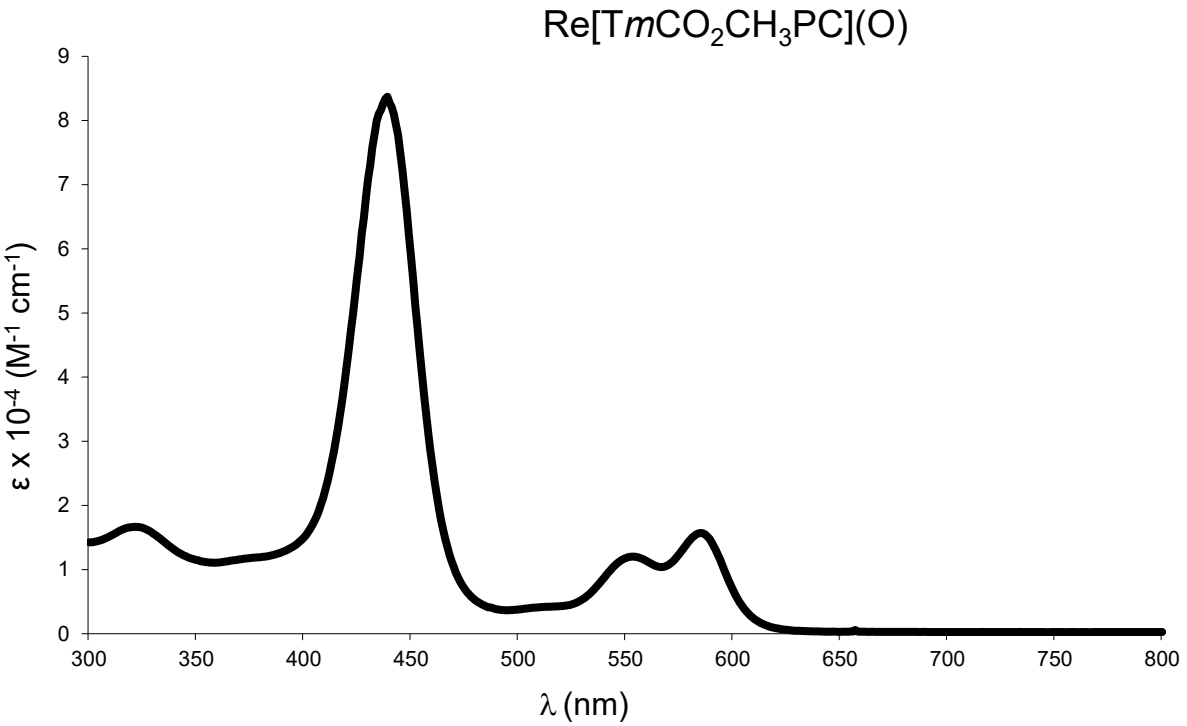

Figure 84. UV-vis spectrum in DCM.

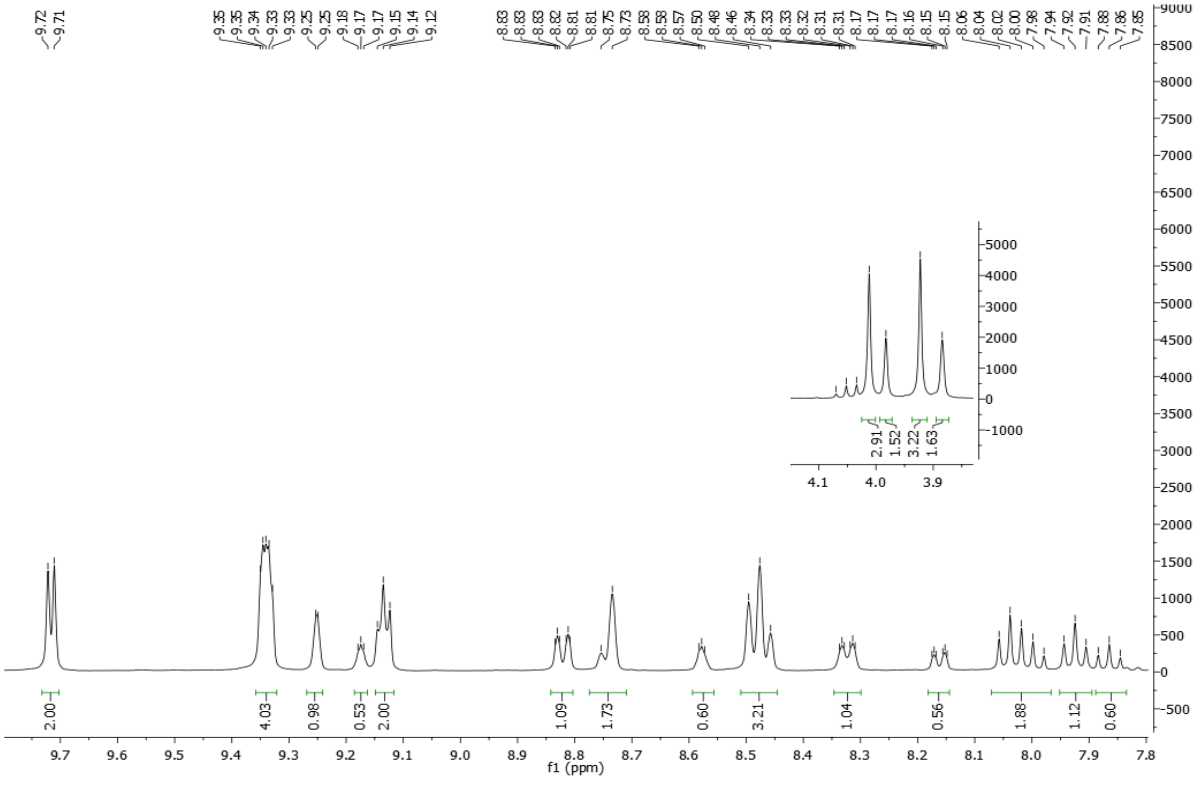

Figure 85. ^{1}H NMR spectrum.

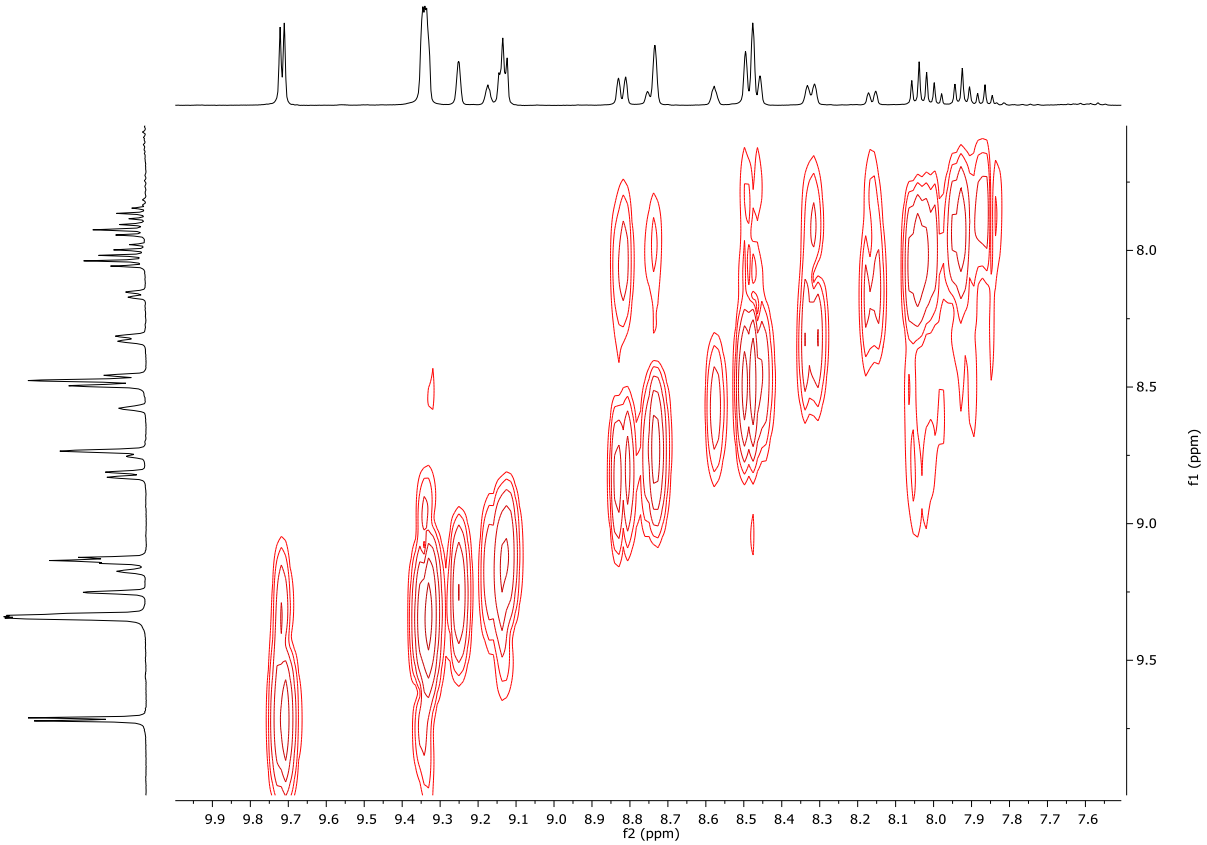

Figure 86. ^{1}H - ^{1}H COSY.

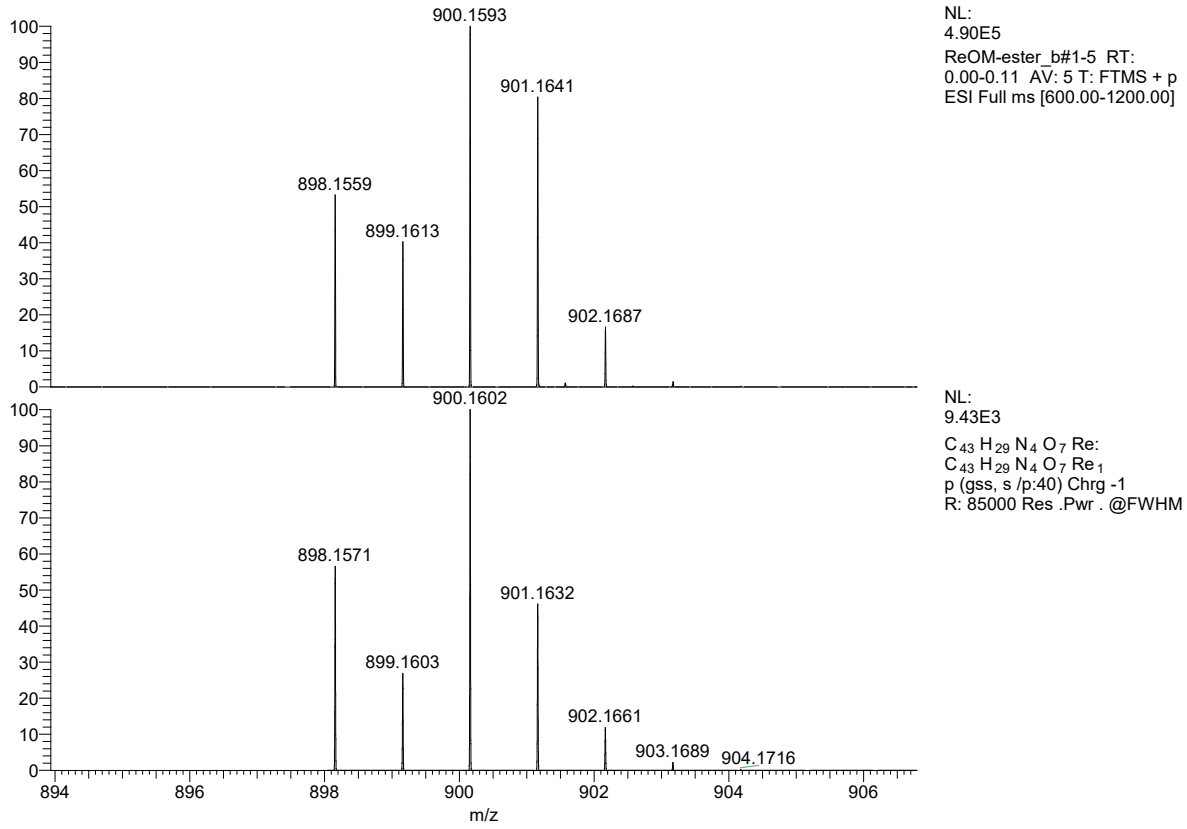

Figure 87. ESI-MS spectrum: measured (top) and calculated (bottom).

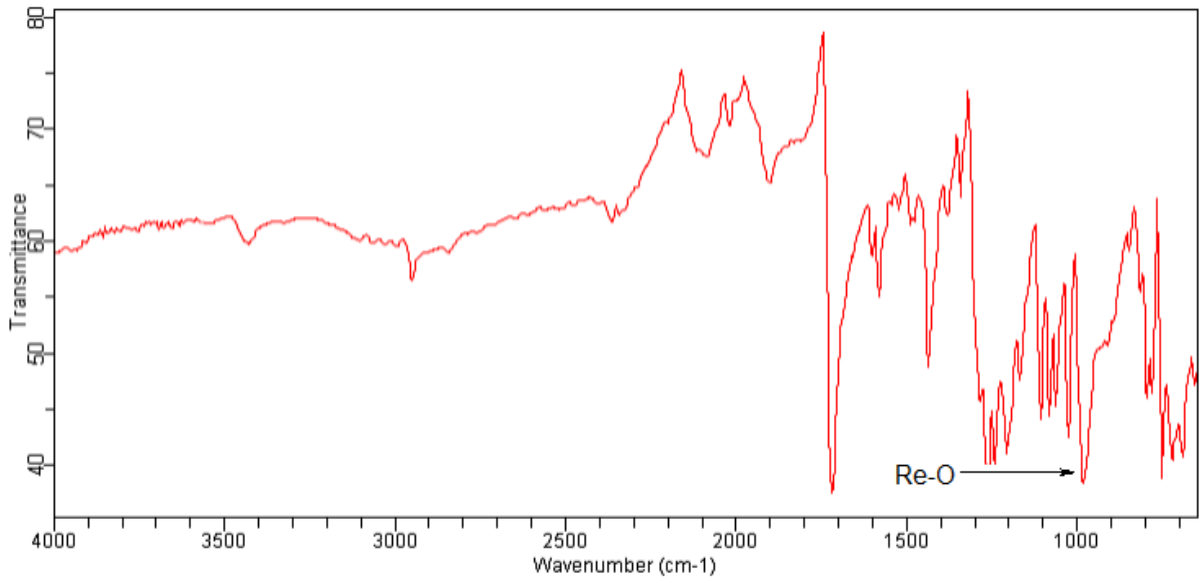

Figure 88. IR spectrum.

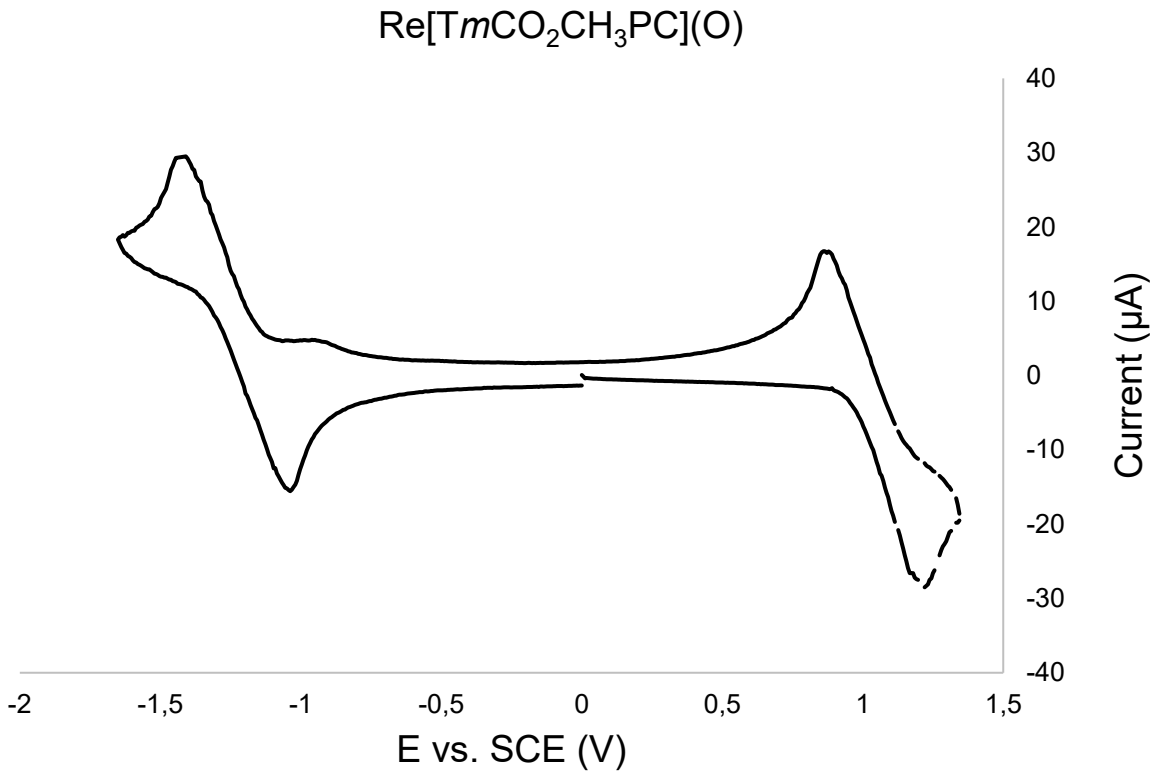

Figure 89. Cyclic voltammogram in DCM containing 0.1 M TBAP.

8.2.5 Analysis of Re[T*m*CO_2HPC](O)

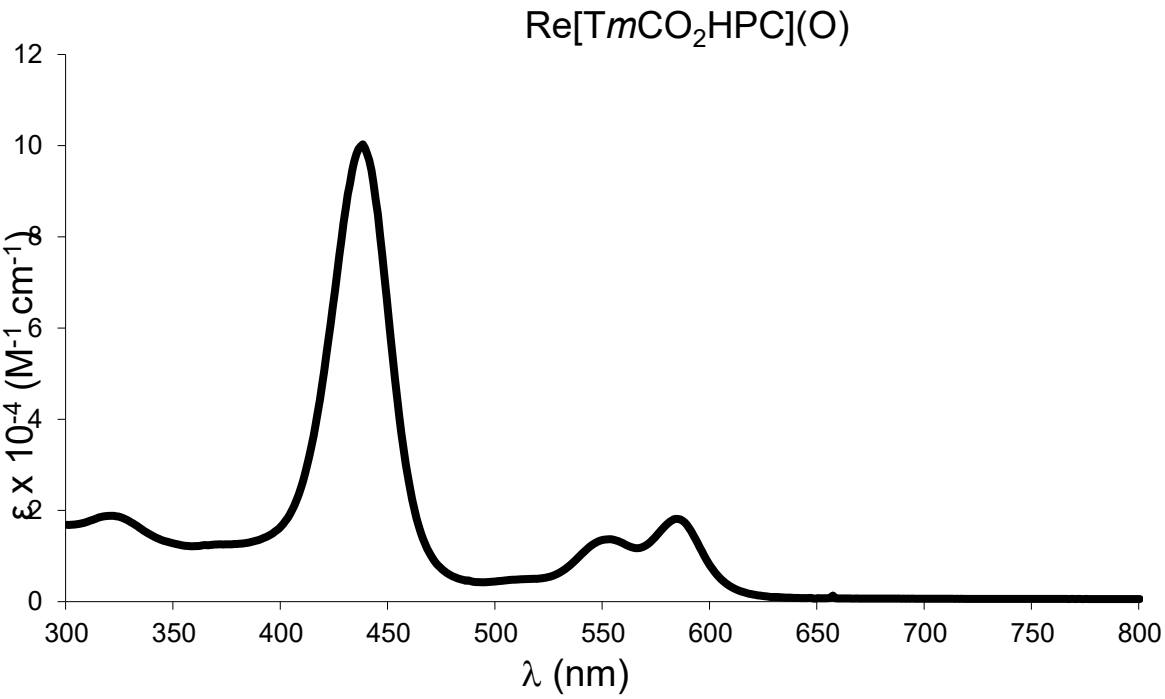

Figure 90. UV-vis spectrum in THF.

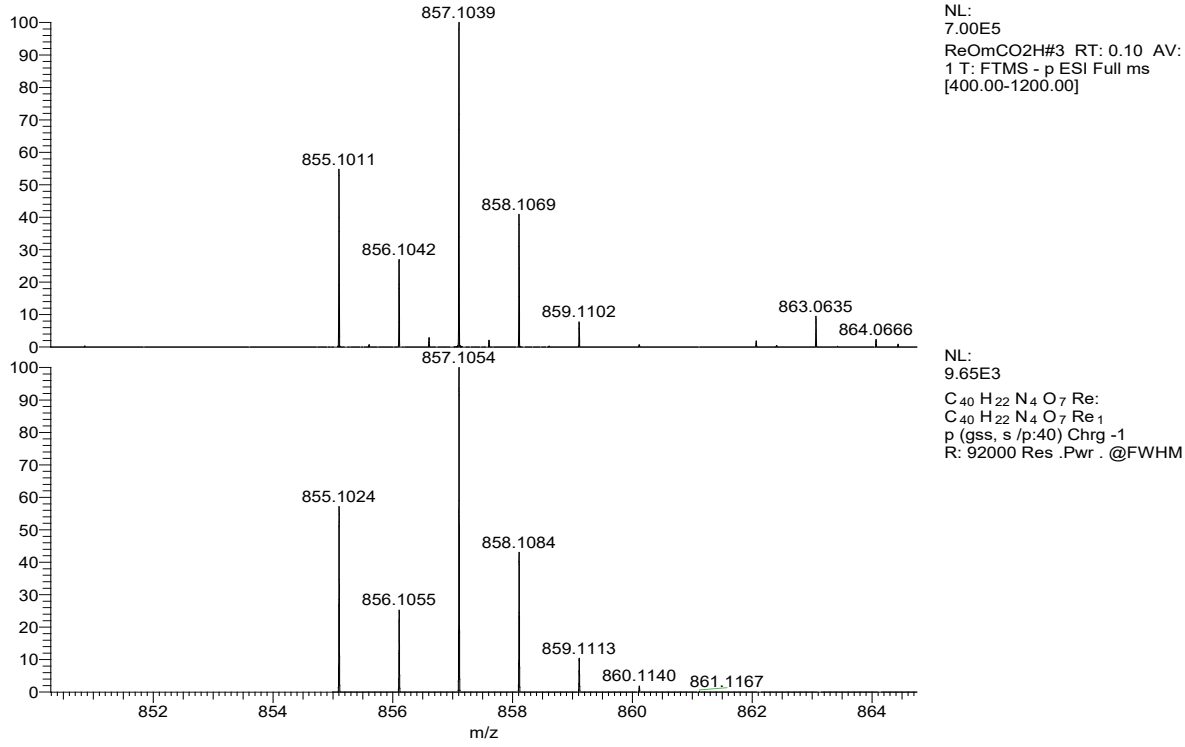

Figure 91. ESI-MS spectrum: measured (top) and calculated (bottom).

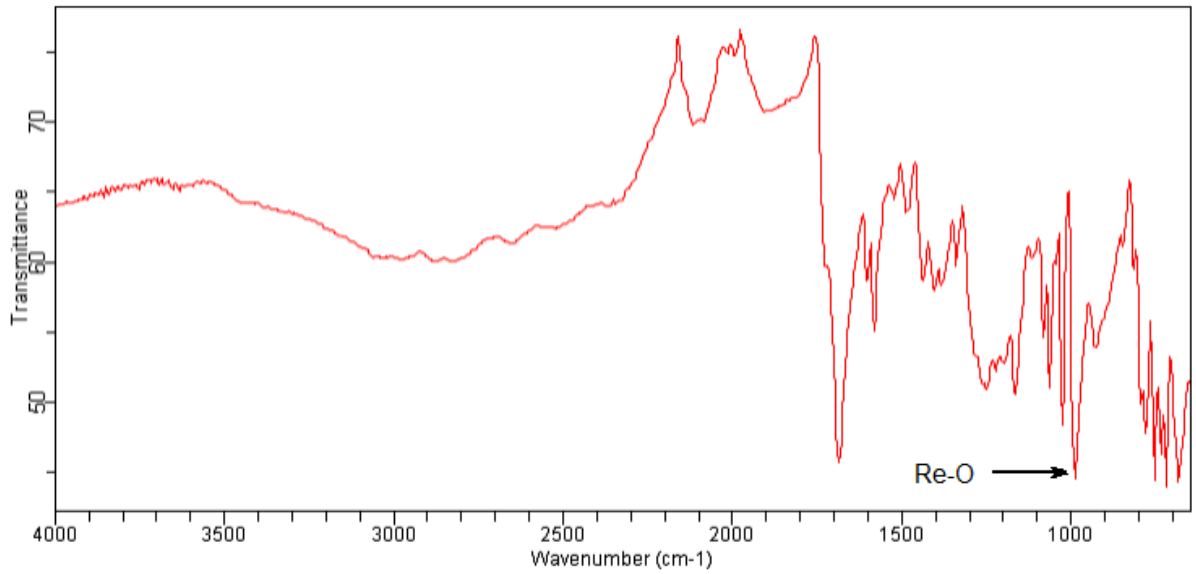

Figure 92. IR spectrum.

8.2.6 Analysis of Re[T*p*FPC](O)

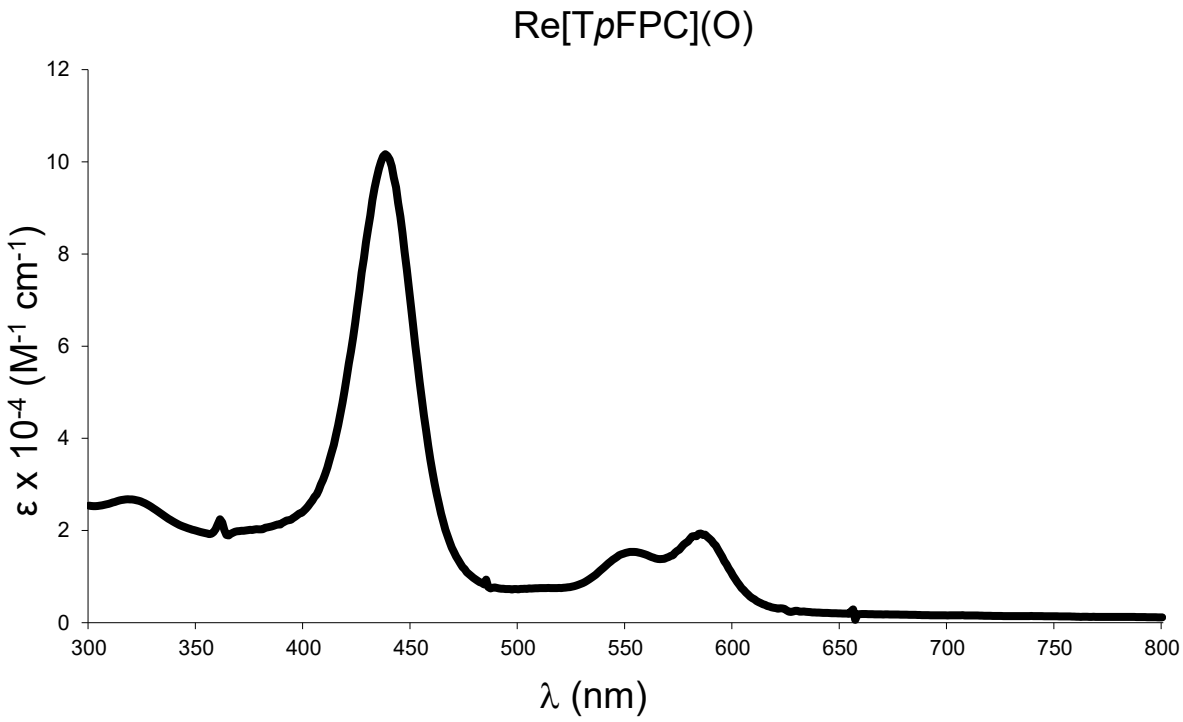

Figure 93. UV-vis spectrum in DCM.

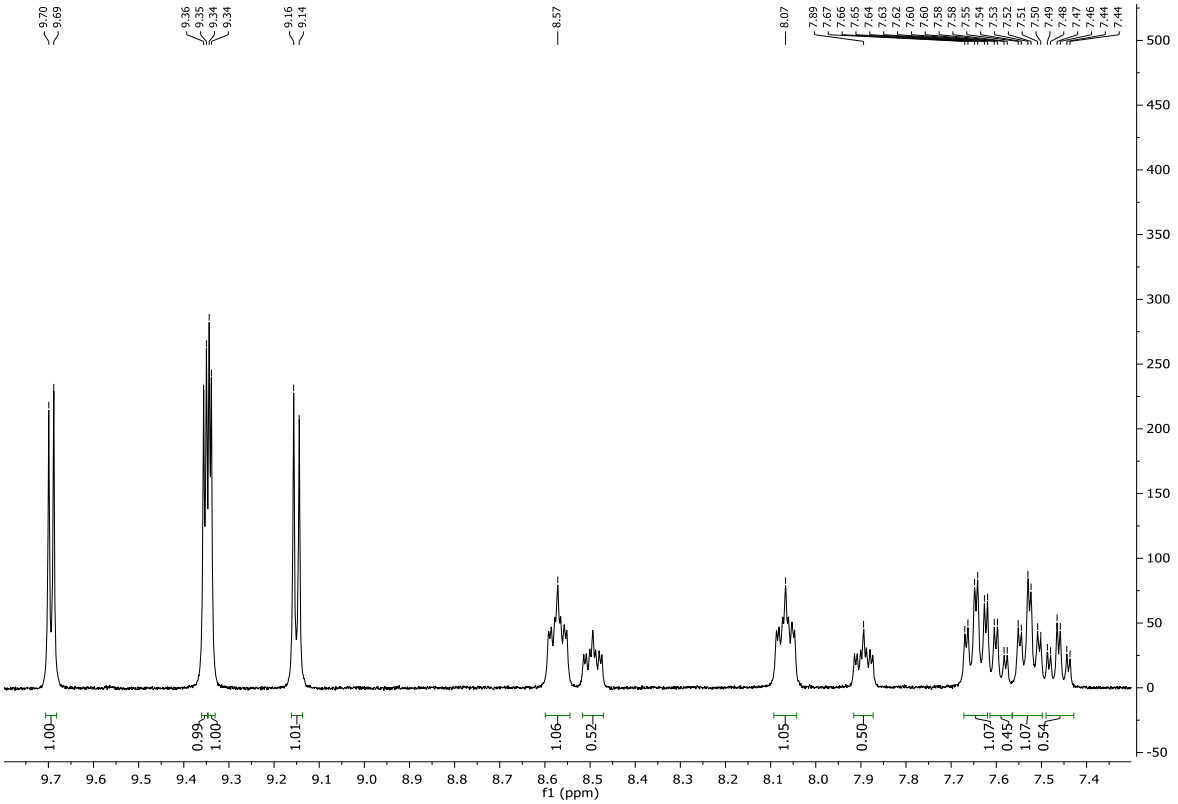

Figure 94. ^{1}H NMR.

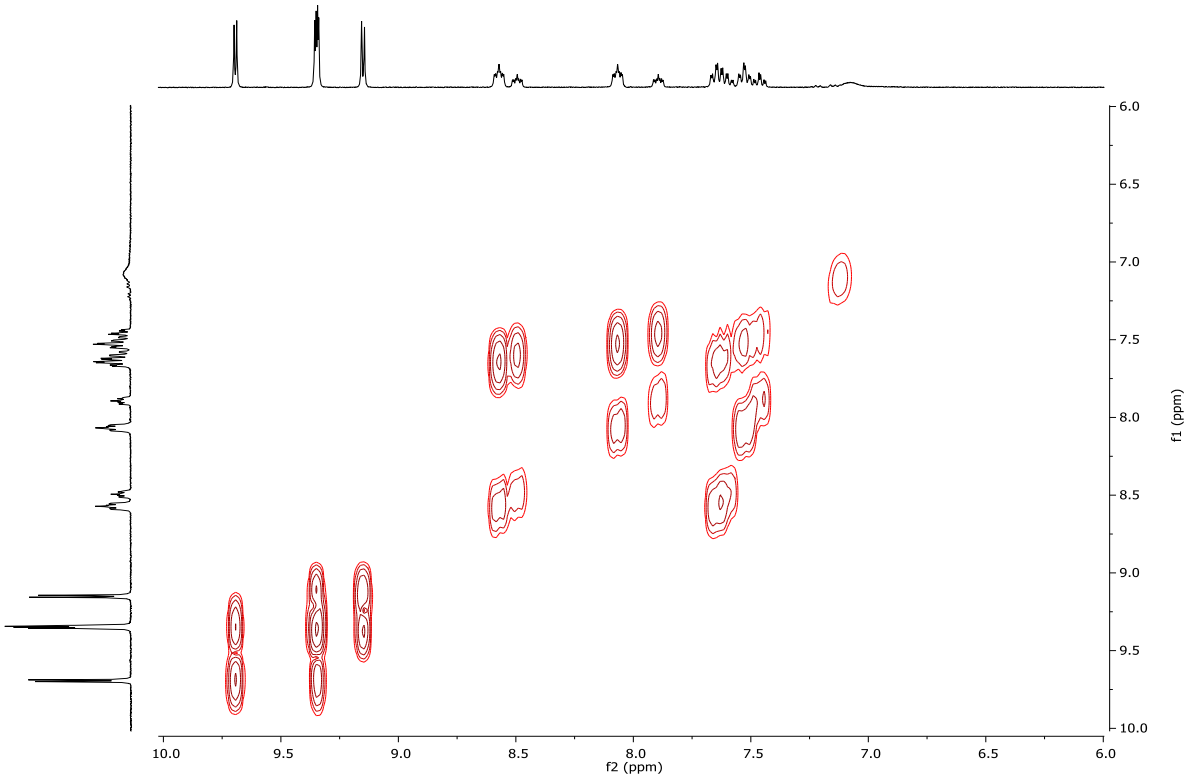

Figure 95. ^{1}H - ^{1}H COSY.

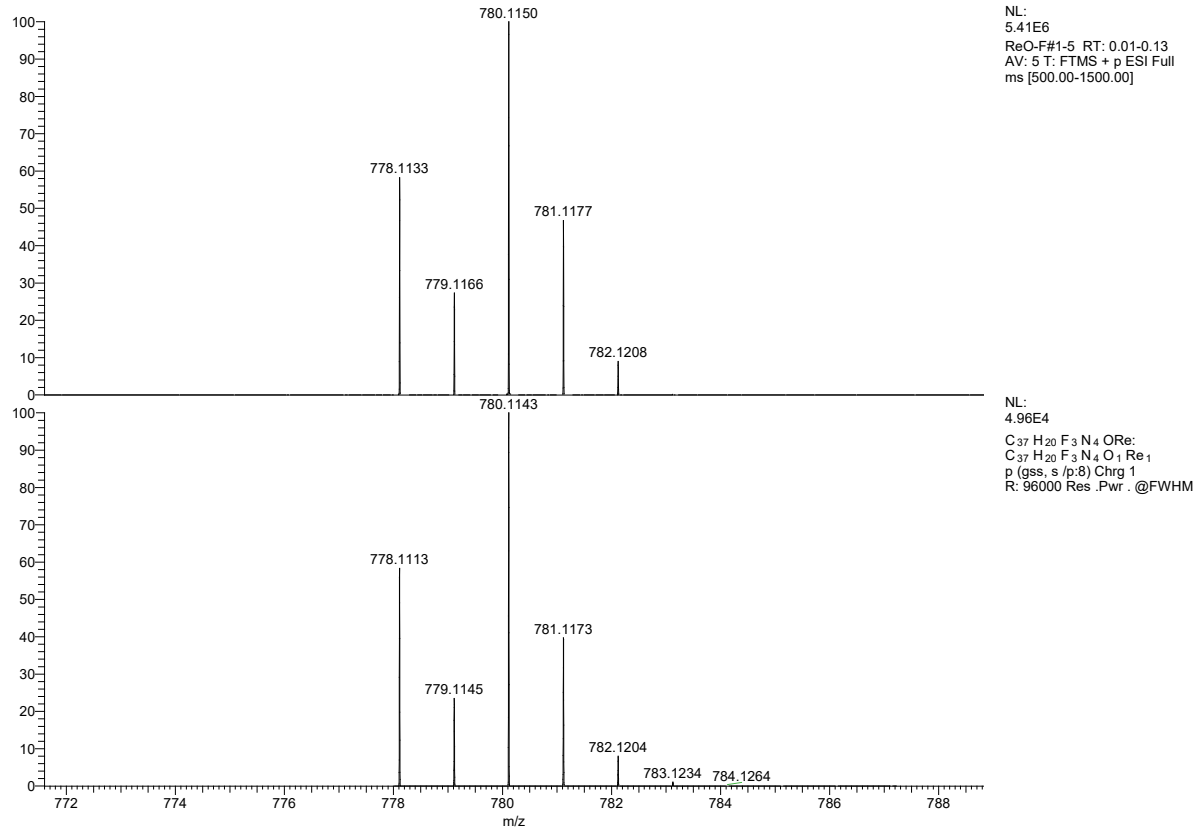

Figure 96. ESI-MS spectrum: measured (top) and calculated (bottom).

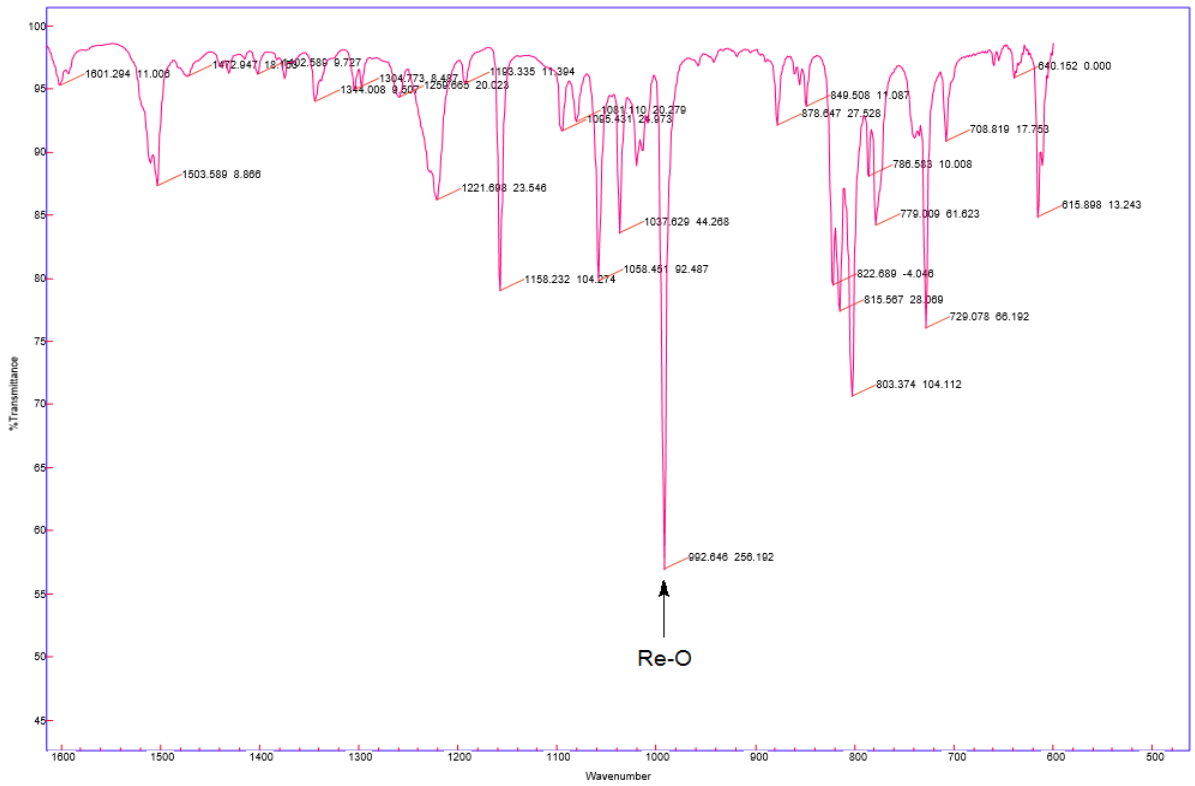

Figure 97. IR spectrum.

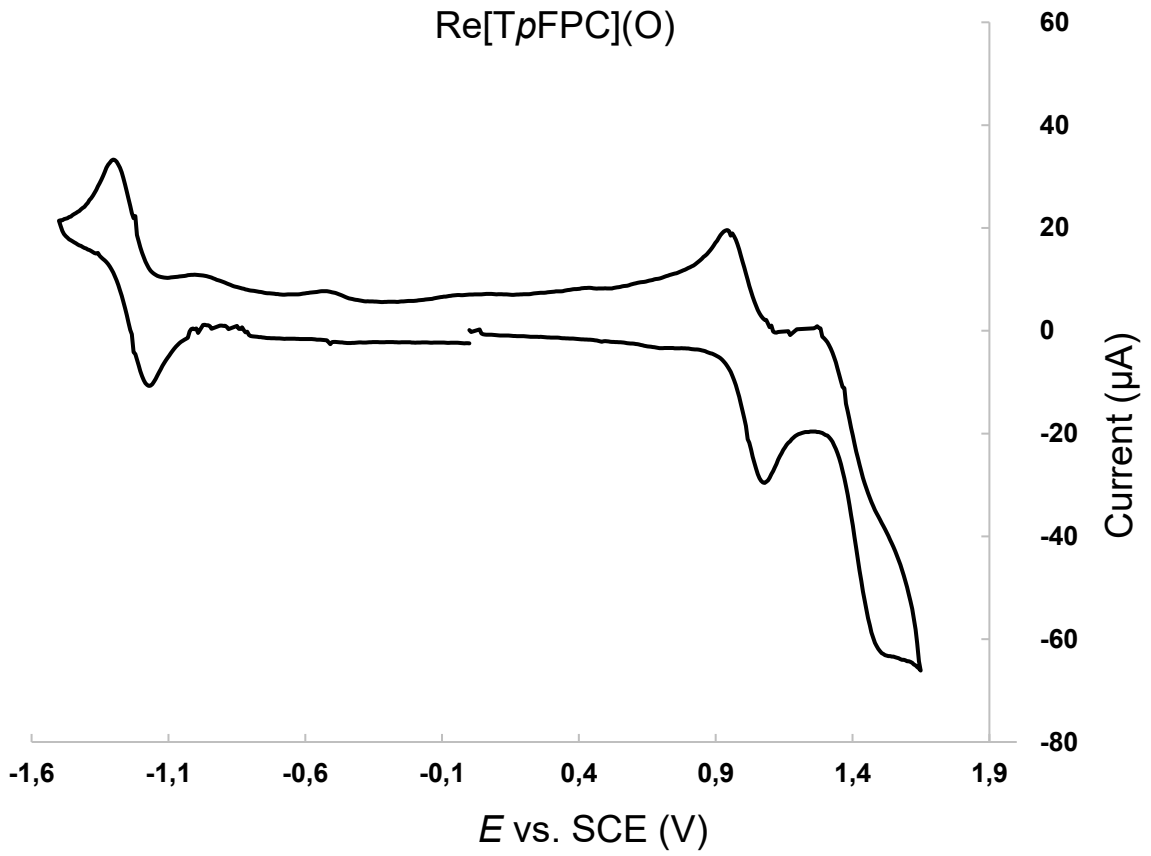

Figure 98. Cyclic voltammogram in DCM containing 0.1 M TBAP.

Table 10. Single crystal X-ray data collection and structure calculations.

Sample	Re[TpFPC](O)
Chemical formula	$C_{37.35}H_{20.69}Cl_{0.69}F_3N_4ORe$
Formula mass	809.28
Crystal system	Monoclinic
Space group	$P\,2_1/c$
λ (Å)	0.7749
a (Å)	12.2806(4)
b (Å)	22.2084(7)
c (Å)	10.7507(4)
α (deg)	90
β (deg)	102.546(2)
γ (deg)	90
Z	4
V (Å^3)	2862.05(17)
Temperature (K)	100(2)
Density (g/cm^3)	1.878
Measured reflections	27807
Unique reflections	5236
Parameters	441
Restraints	18
R_{int}	0.0787
θ range (deg)	2.105 – 27.867
R_1, wR_2 all data	0.0377, 0.0660
S (GooF) all data	1.039
Max/min res. Dens. (e/Å^3)	0.793/-1.102

8.2.7 Analysis of Re[TPC](O)

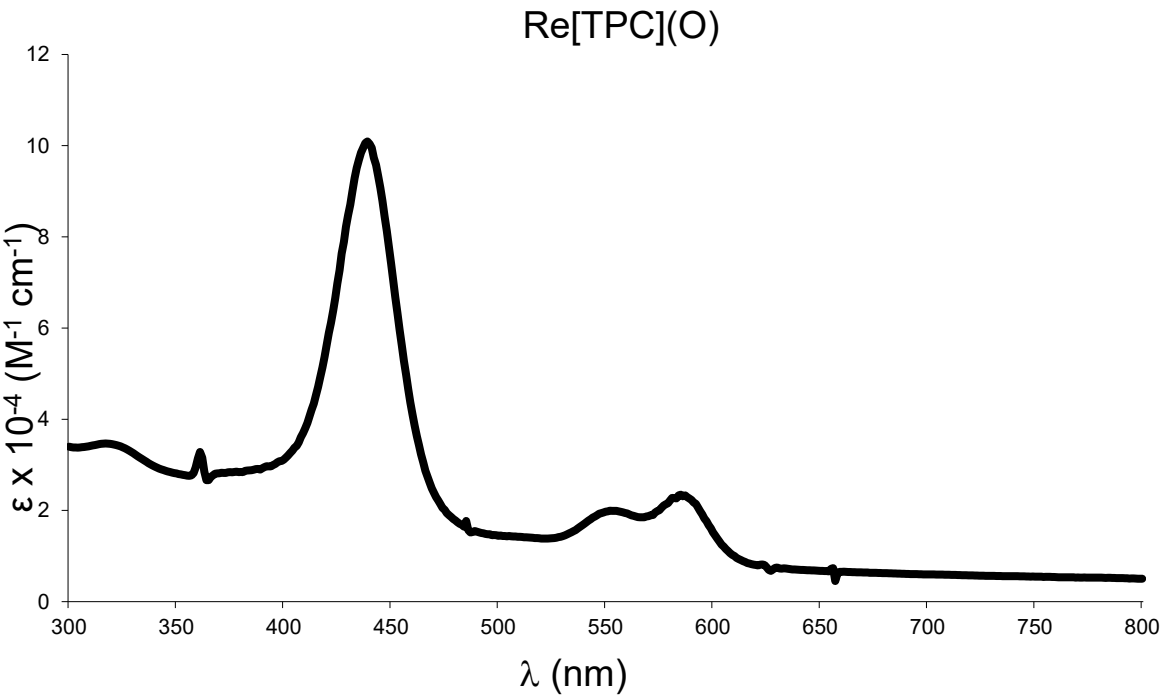

Figure 99. UV-vis spectrum in DCM.

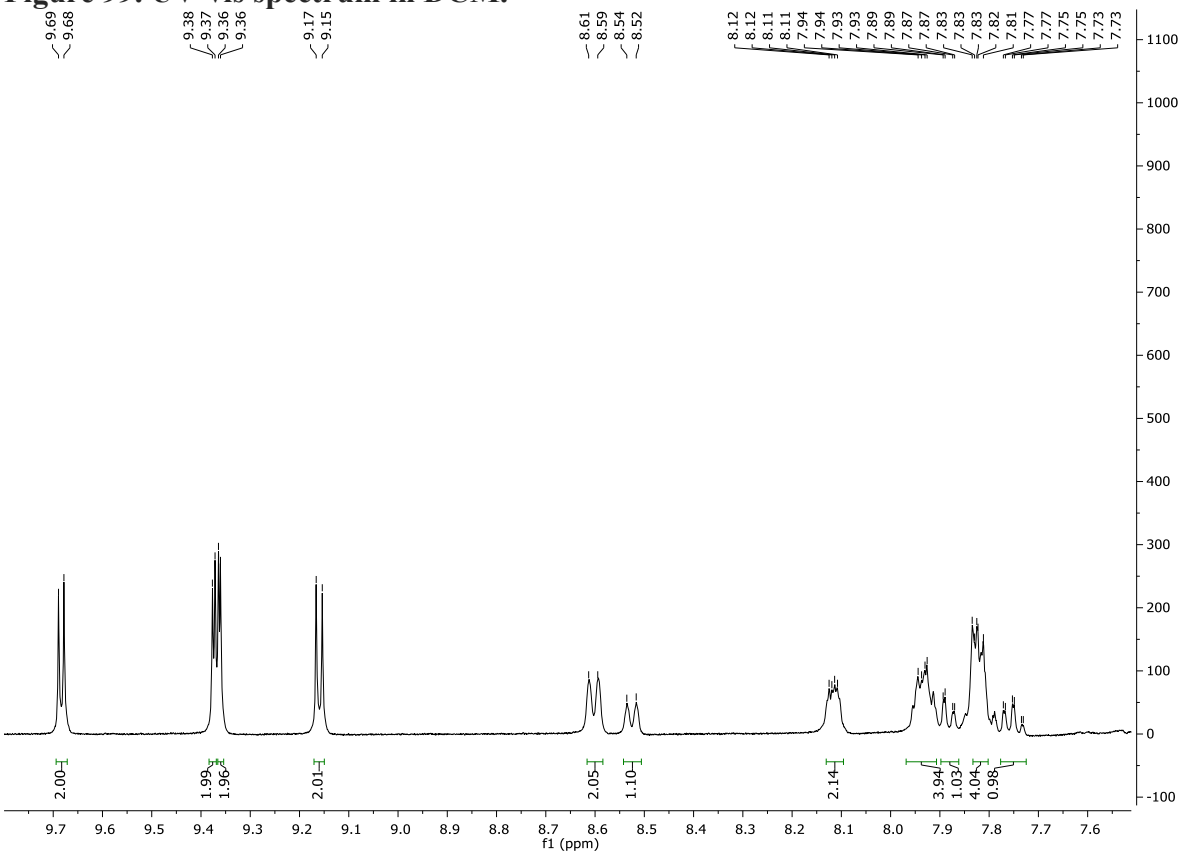

Figure 100. ^{1}H NMR.

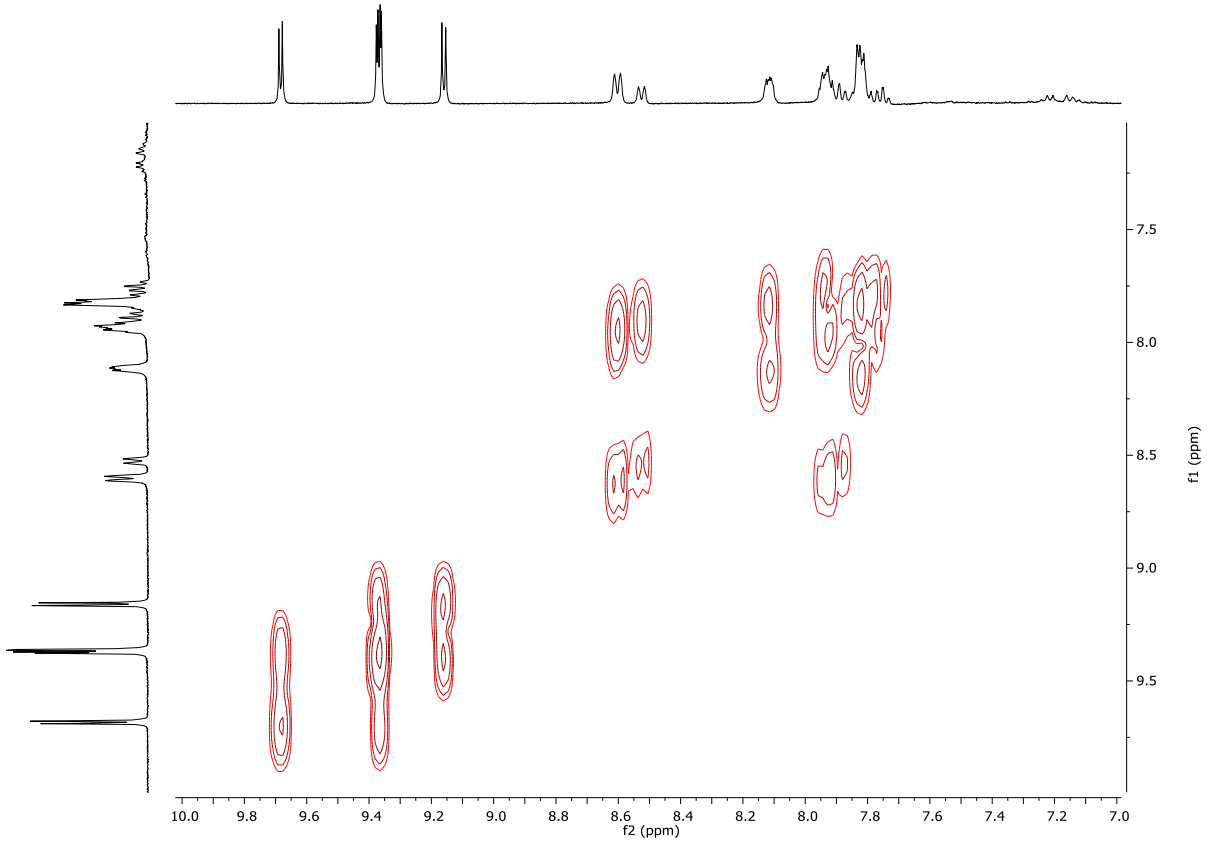

Figure 101. ^{1}H - ^{1}H COSY.

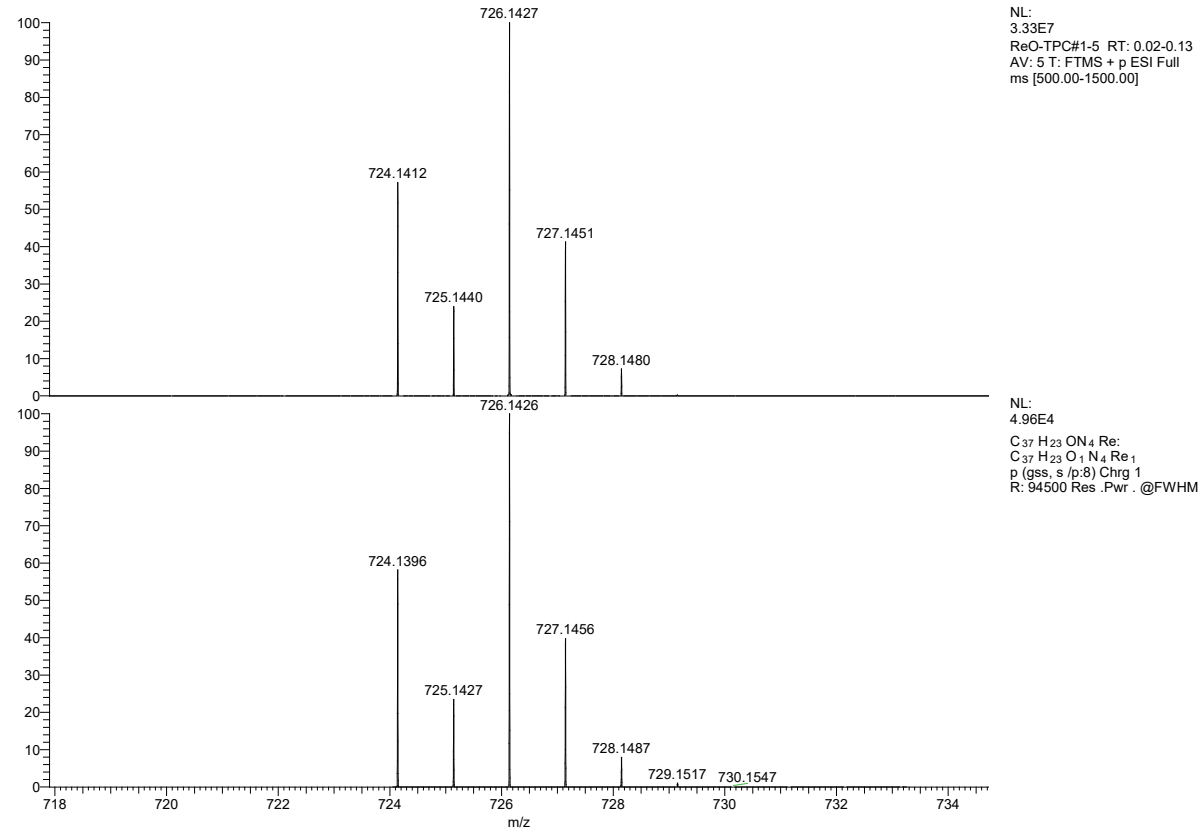

Figure 102. ESI-MS spectrum: measured (top) and calculated (bottom).

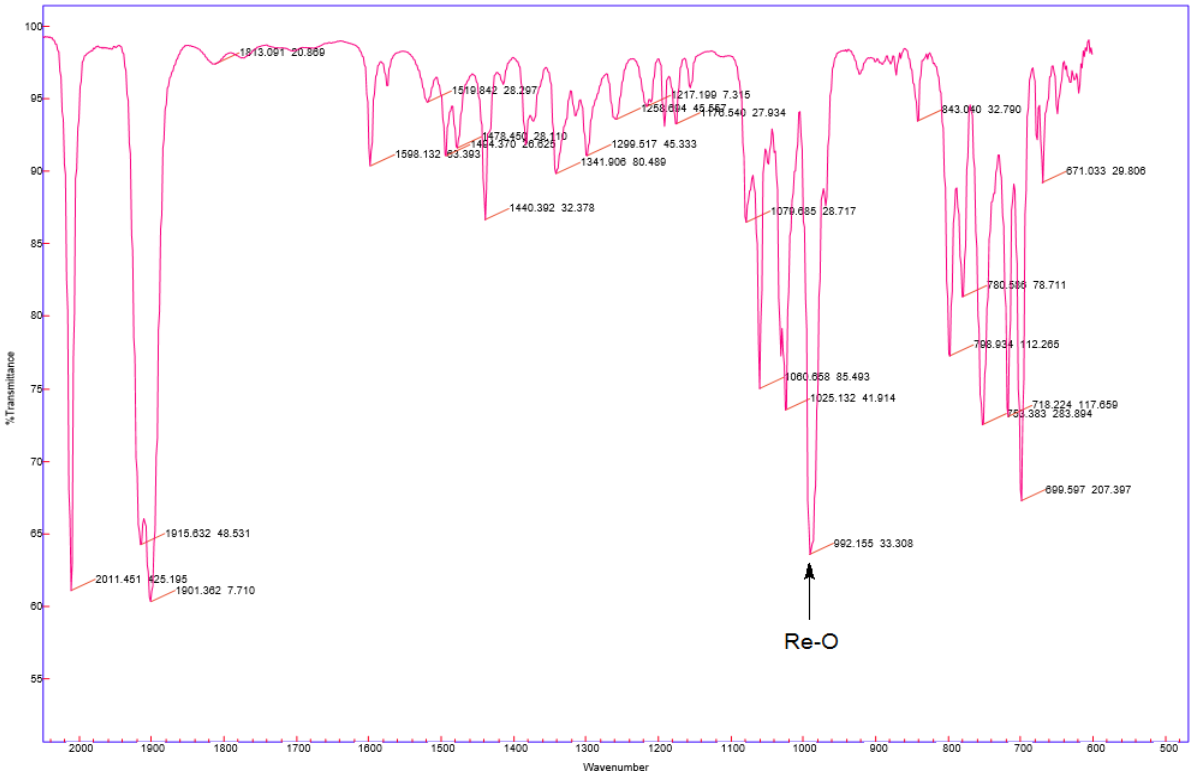

Figure 103. IR spectrum.

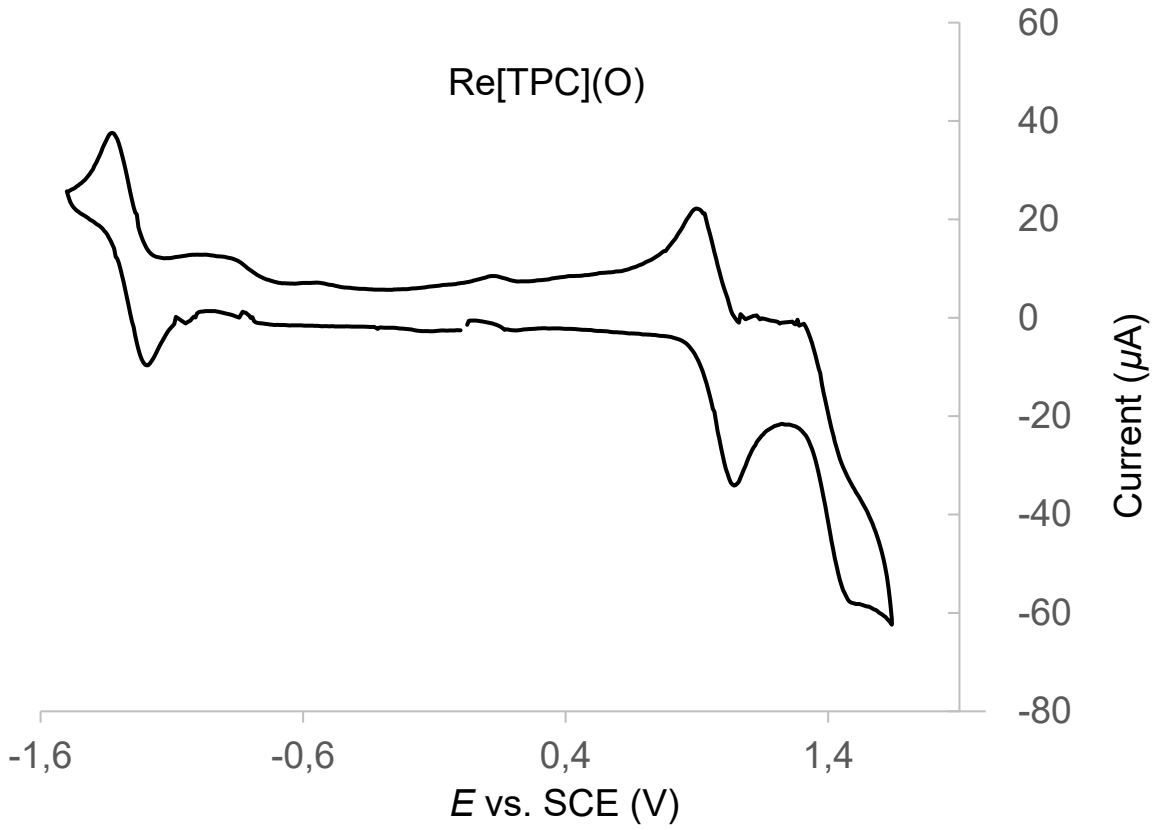

Figure 104. Cyclic voltammogram in DCM containing 0.1 M TBAP.

Table 11. Single crystal X-ray data collection and structure calculations.

Sample	Re[TPC](O)
Chemical formula	$C_{37}H_{23}N_4ORe$
Formula mass	725.79
Crystal system	Monoclinic
Space group	$P\,2_1/c$
λ (Å)	0.7749
a (Å)	10.3452(4)
b (Å)	8.0511(3)
c (Å)	32.4589(12)
α (deg)	90
β (deg)	97.055(2)
γ (deg)	90
Z	4
V (Å^3)	2683.04(18)
Temperature (K)	100(2)
Density (g/cm^3)	1.797
Measured reflections	73342
Unique reflections	8931
Parameters	388
Restraints	0
R_{int}	0.0693
θ range (deg)	2.163 – 34.735
R_1, wR_2 all data	0.0346, 0.0556
S (GooF) all data	1.032
Max/min res. Dens. (e/Å^3)	1.174/-2.522

8.2.8 Analysis of Re[T*p*CH$_3$PC](O)

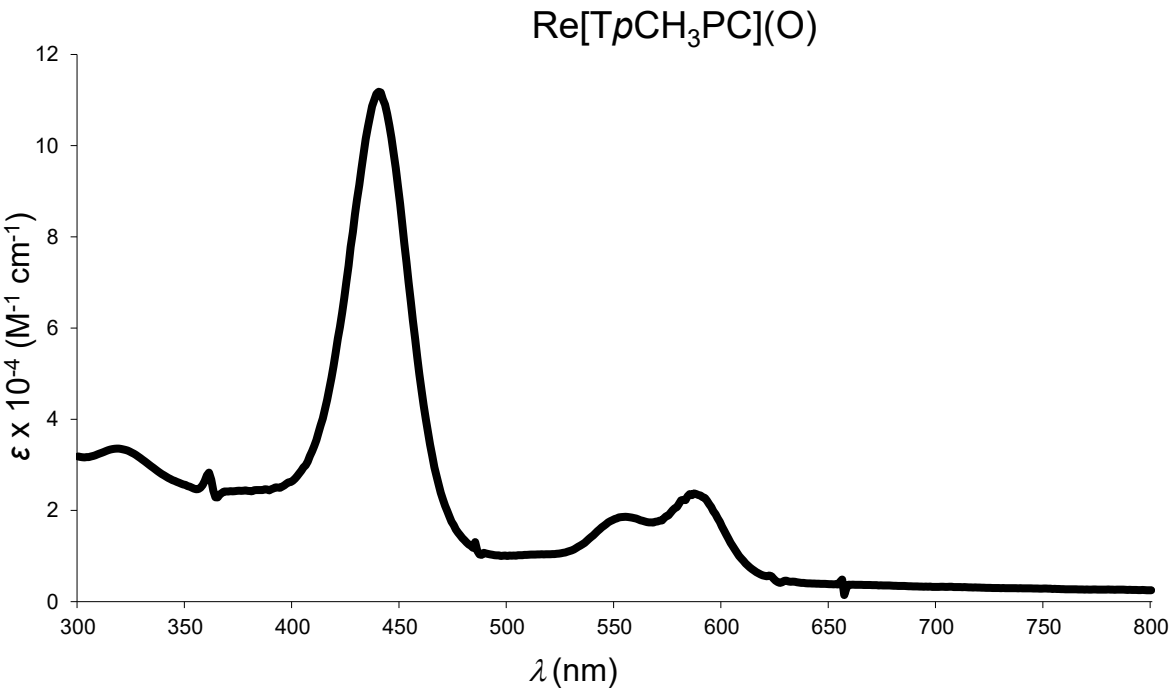

Figure 105. UV-vis spectrum in DCM.

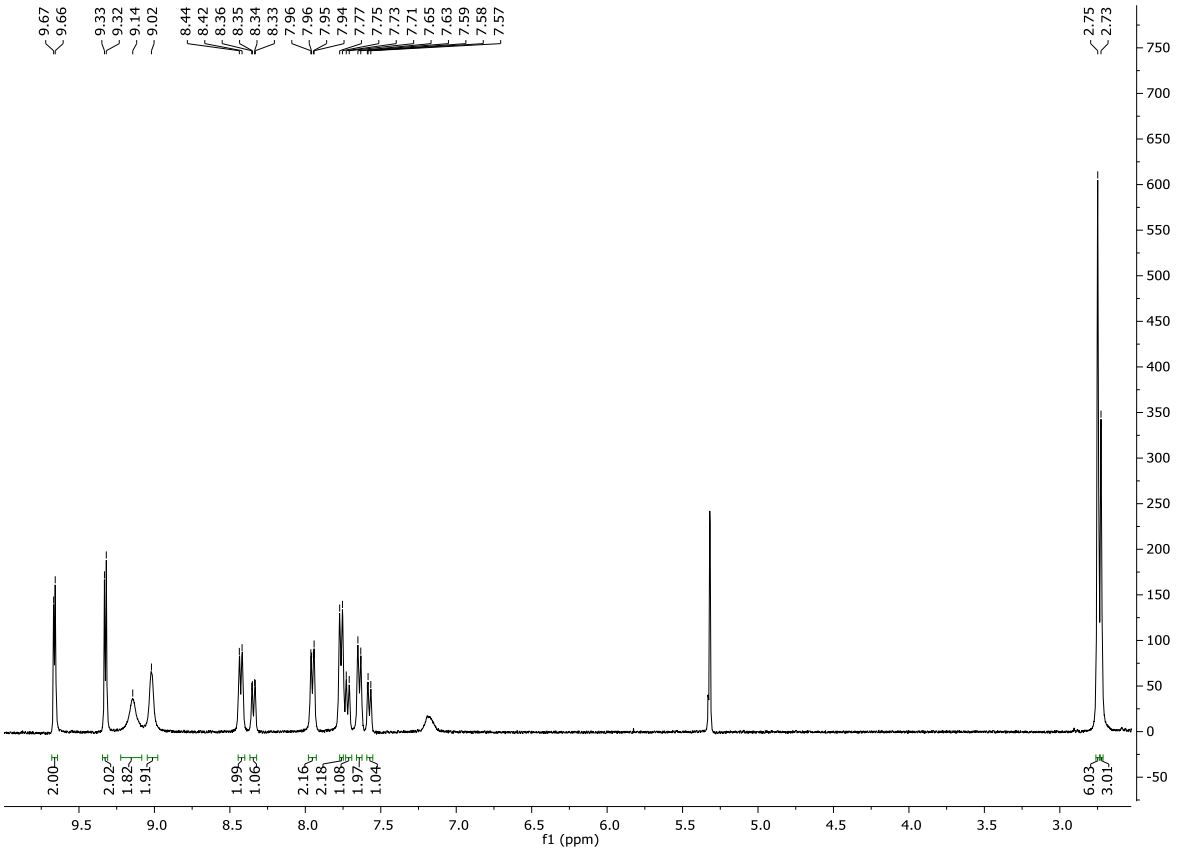

Figure 106. ^{1}H NMR.

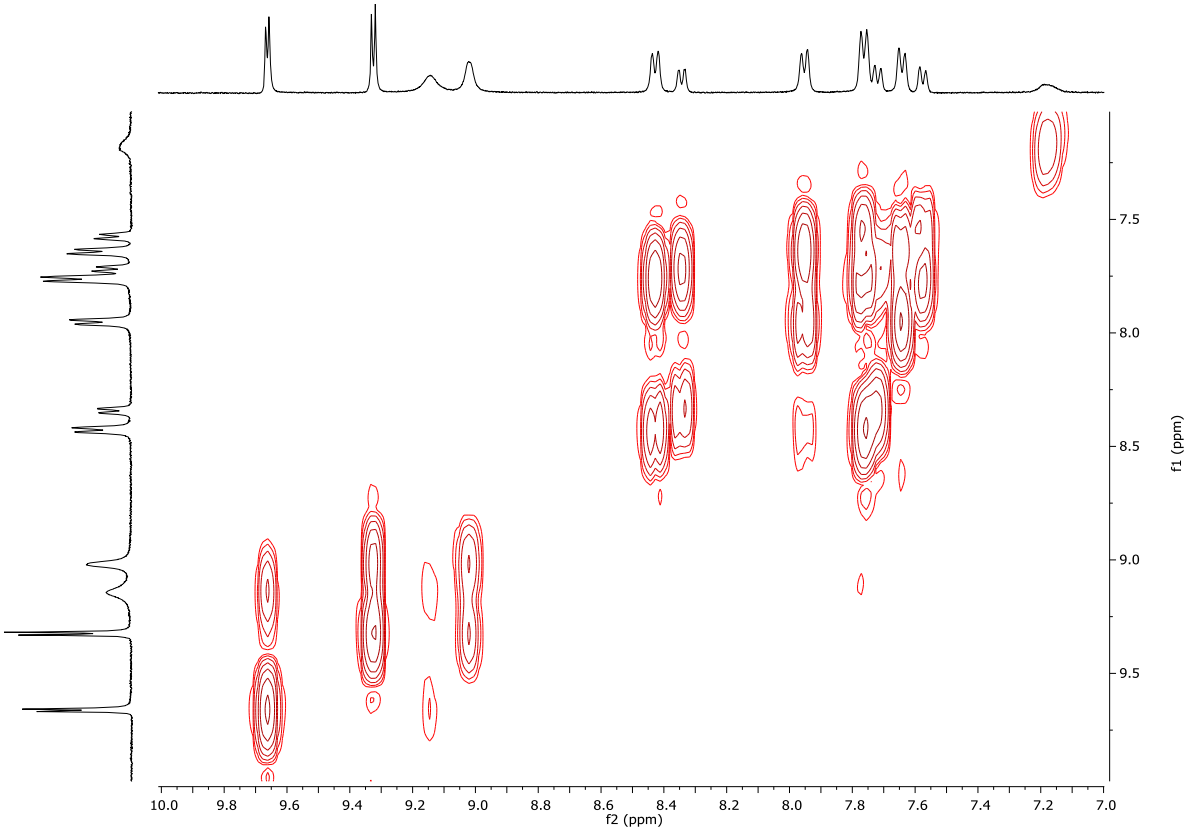

Figure 107. ^{1}H - ^{1}H COSY.

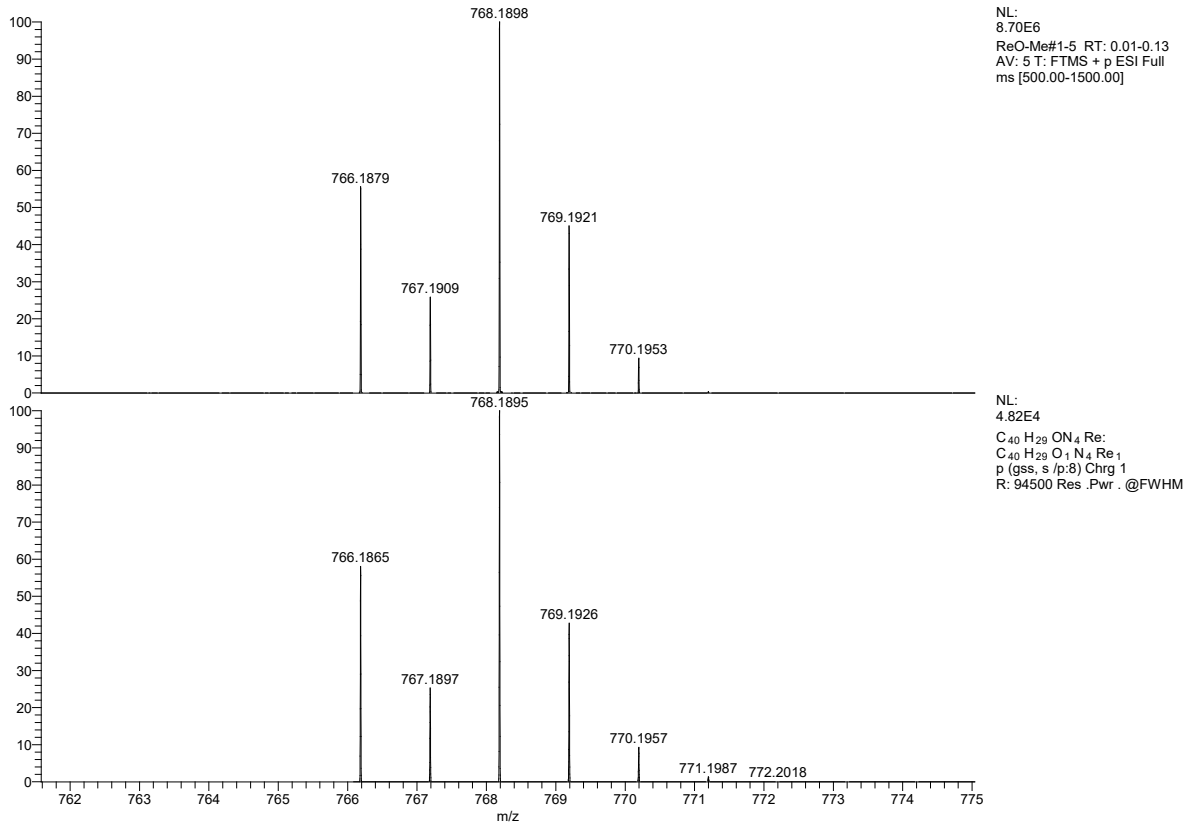

Figure 108. ESI-MS spectrum: measured (top) and calculated (bottom).

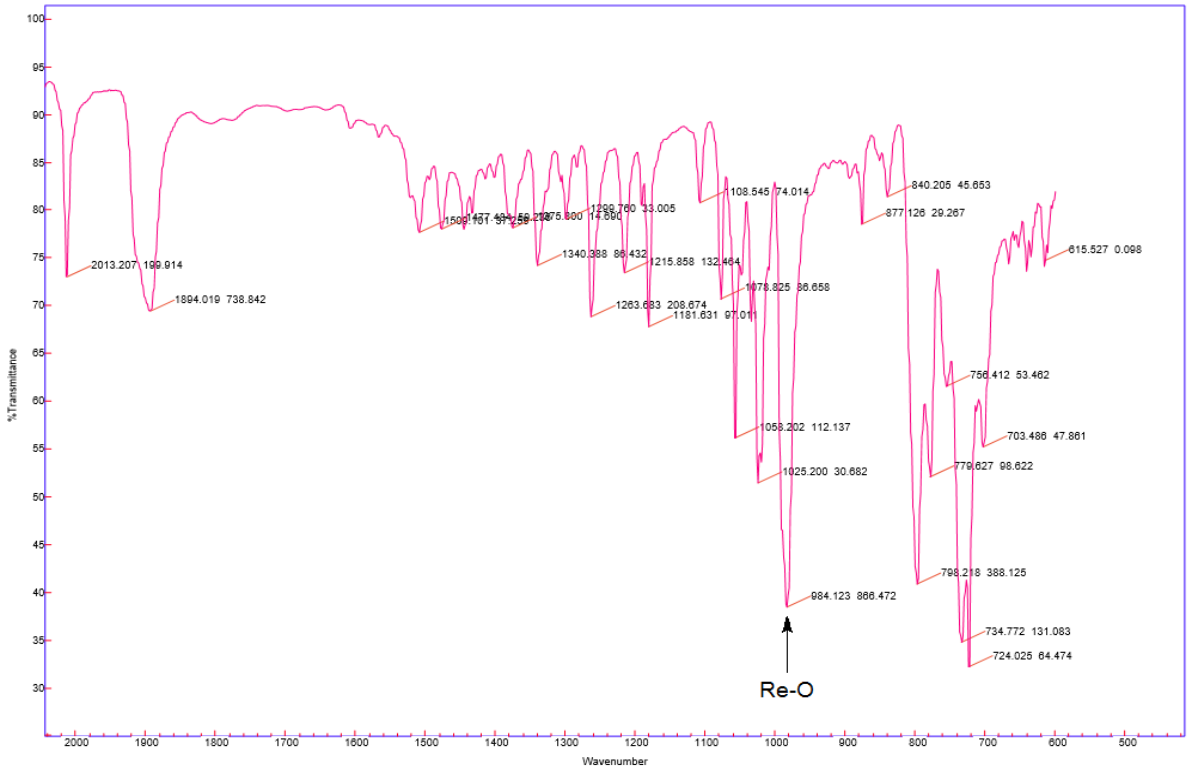

Figure 109. IR spectrum.

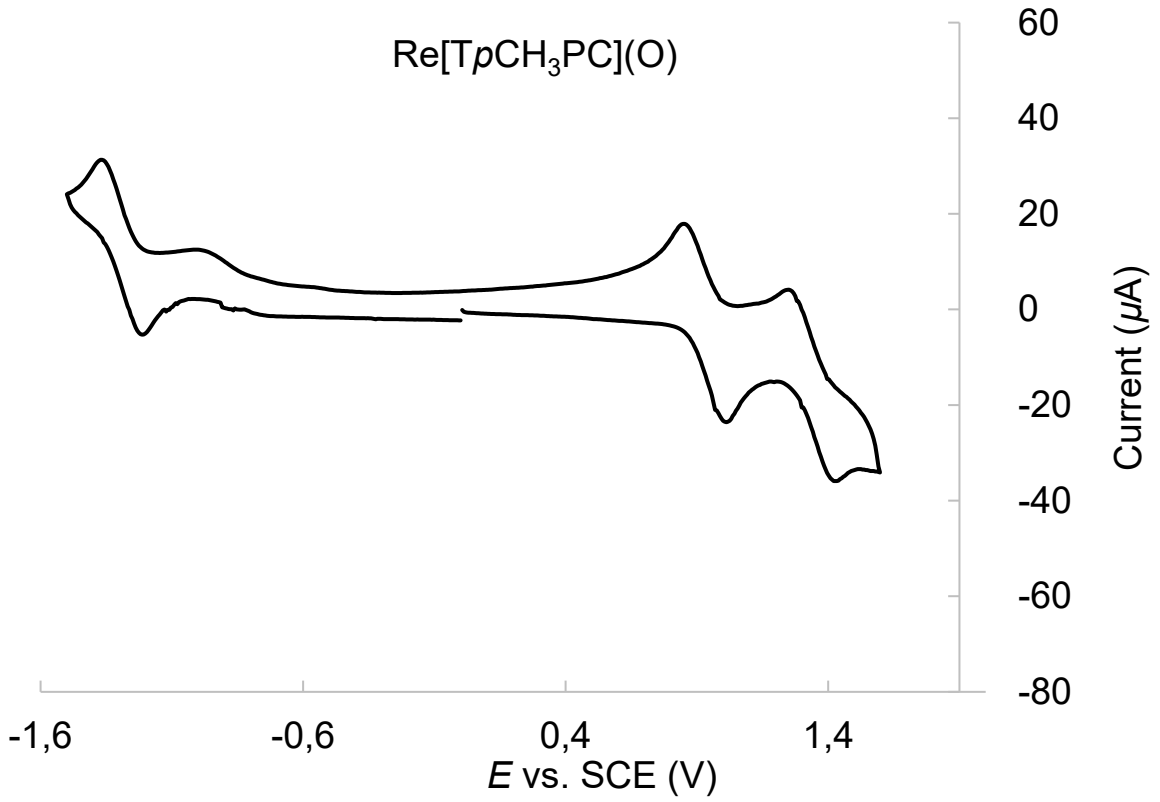

Figure 110. Cyclic voltammogram in DCM containing 0.1 M TBAP.

Table 12. Single crystal X-ray data collection and structure calculations.

Sample	Re[T*p*CH$_3$PC](O)
Chemical formula	$C_{40}H_{29}N_4ORe$
Formula mass	767.87
Crystal system	Triclinic
Space group	*P* -1
λ (Å)	0.7749
a (Å)	7.2799(4)
b (Å)	15.3860(7)
c (Å)	16.2273(7)
α (deg)	95.414(3)
β (deg)	102.719(3)
γ (deg)	91.141(3)
Z	2
V (Å^3)	1763.54(15)
Temperature (K)	100(2)
Density (g/cm^3)	1.446
Measured reflections	25719
Unique reflections	11826
Parameters	419
Restraints	0
R_{int}	0.0671
θ range (deg)	2.123 – 36.695
R_1, wR_2 all data	0.0505, 0.0915
S (GooF) all data	1.026
Max/min res. Dens. (e/Å^3)	2.104/-1.896

8.2.9 Analysis of Re[T*p*OCH$_3$PC](O)

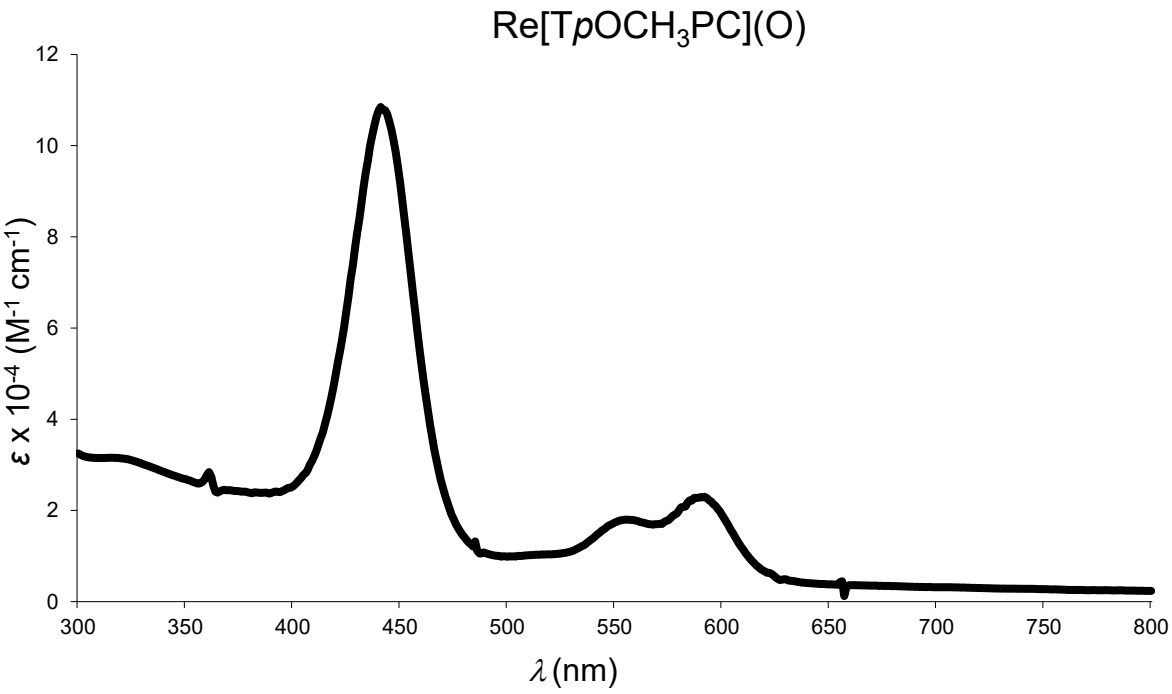

Figure 111. UV-vis spectrum in DCM.

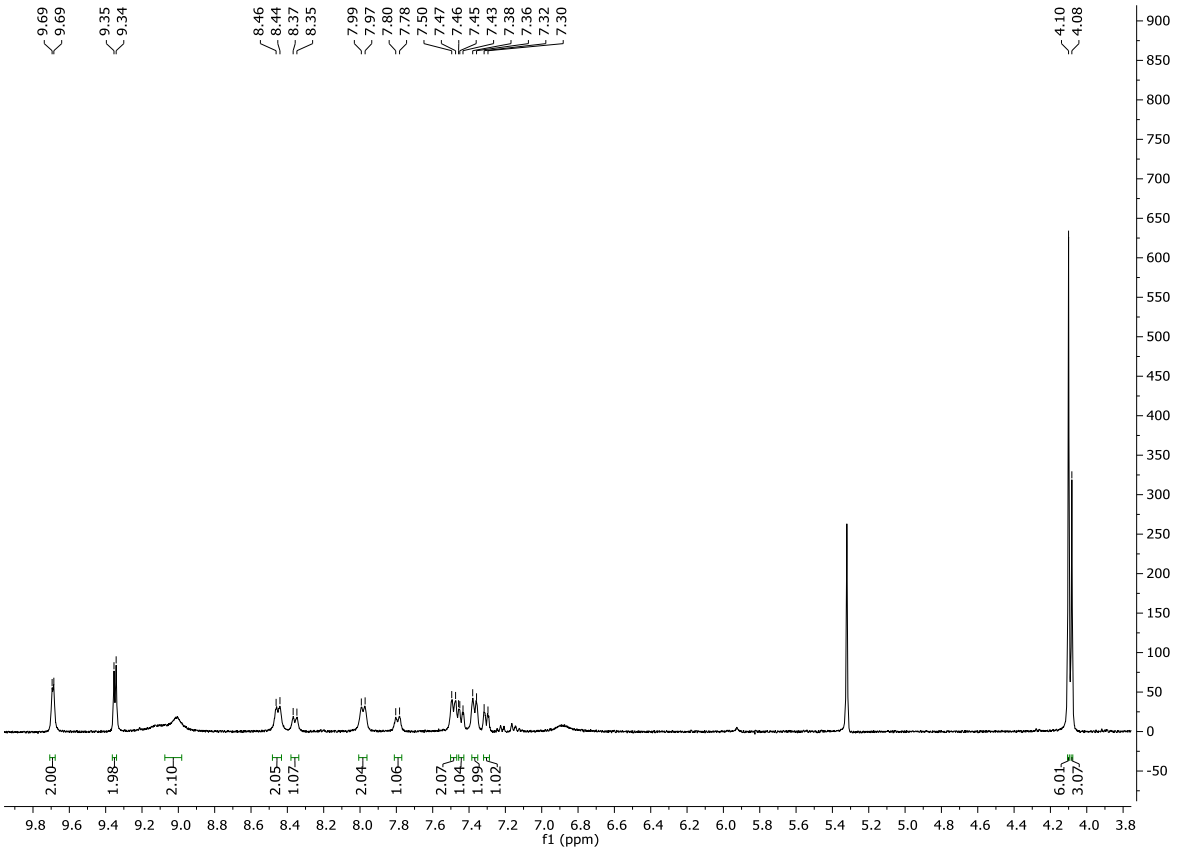

Figure 112. ^{1}H NMR.

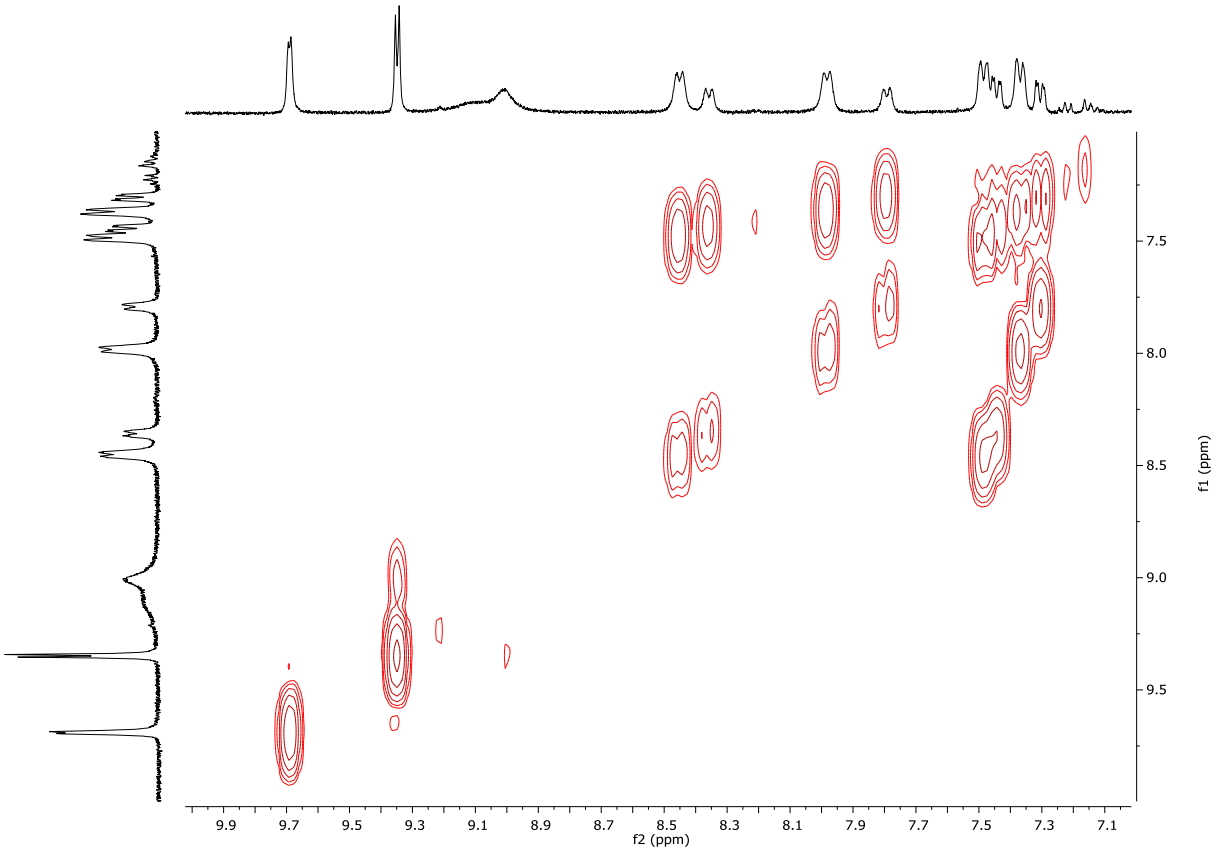

Figure 113. ^{1}H - ^{1}H COSY.

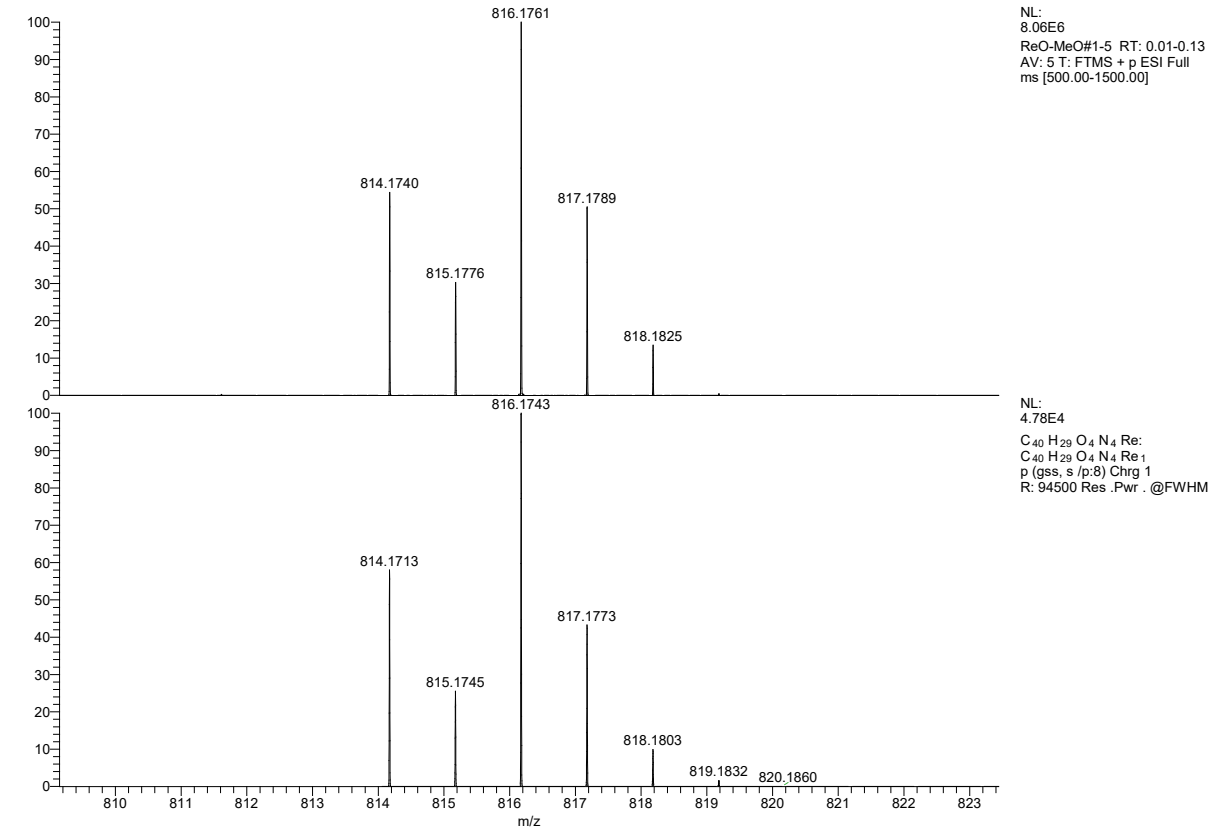

Figure 114. ESI-MS spectum: measured (top) and calculated (bottom).

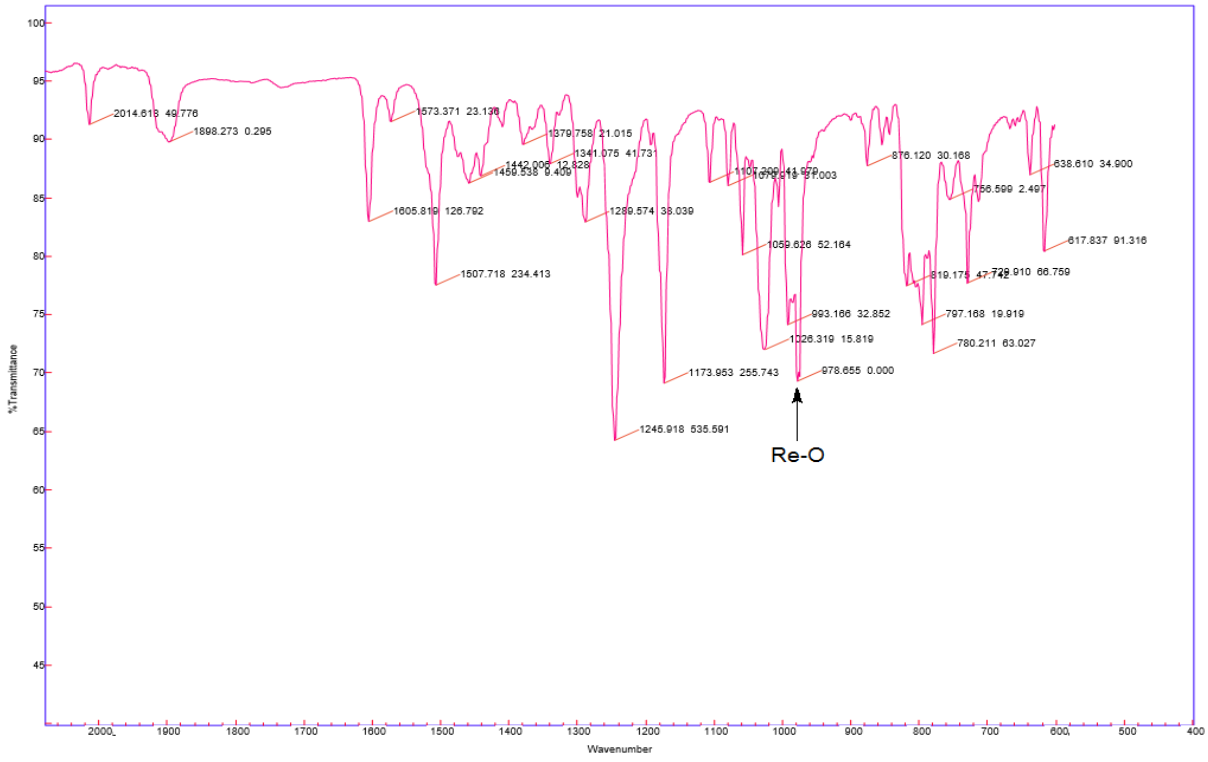

Figure 115. IR spectrum.

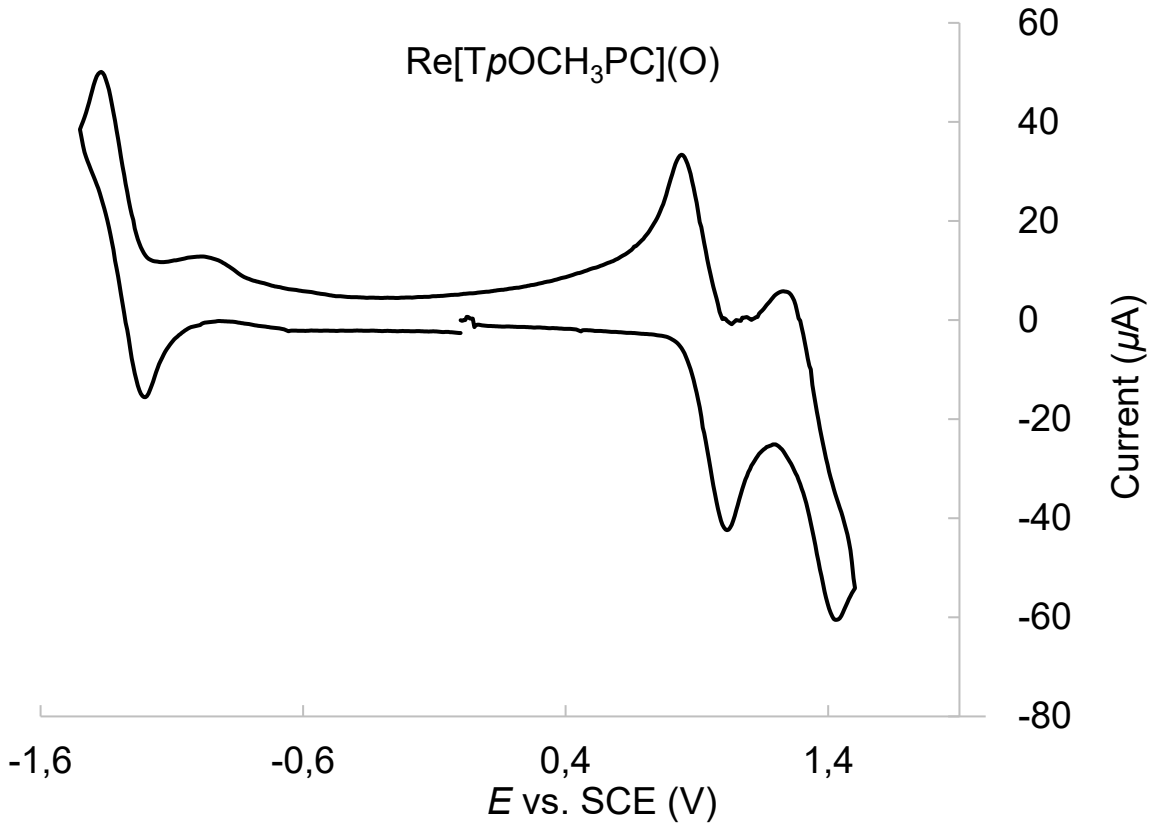

Figure 116. Cyclic voltammogram in DCM containing 0.1 M TBAP.

Table 13. Single crystal X-ray data collection and structure calculations.

Sample	Re[T*p*OCH$_3$PC](O)
Chemical formula	$C_{40}H_{29}N_4O_4Re$
Formula mass	815.87
Crystal system	Monoclinic
Space group	$P\ 2_1/c$
λ (Å)	0.7293
a (Å)	13.3584(7)
b (Å)	8.0963(4)
c (Å)	30.2638(17)
α (deg)	90
β (deg)	101.898(2)
γ (deg)	90
Z	4
V (Å^3)	3202.8(3)
Temperature (K)	100(2)
Density (g/cm^3)	1.692
Measured reflections	97288
Unique reflections	22512
Parameters	445
Restraints	0
R_{int}	0.0293
θ range (deg)	2.341 – 43.551
R_1, wR_2 all data	0.0376, 0.0774
S (GooF) all data	1.312
Max/min res. Dens. (e/Å^3)	4.696/-5.881

8.3 ^{99}TECHNETIUM COMPLEXES

8.3.1 Analysis of ^{99}Tc[T*p*CF$_3$PC](O)

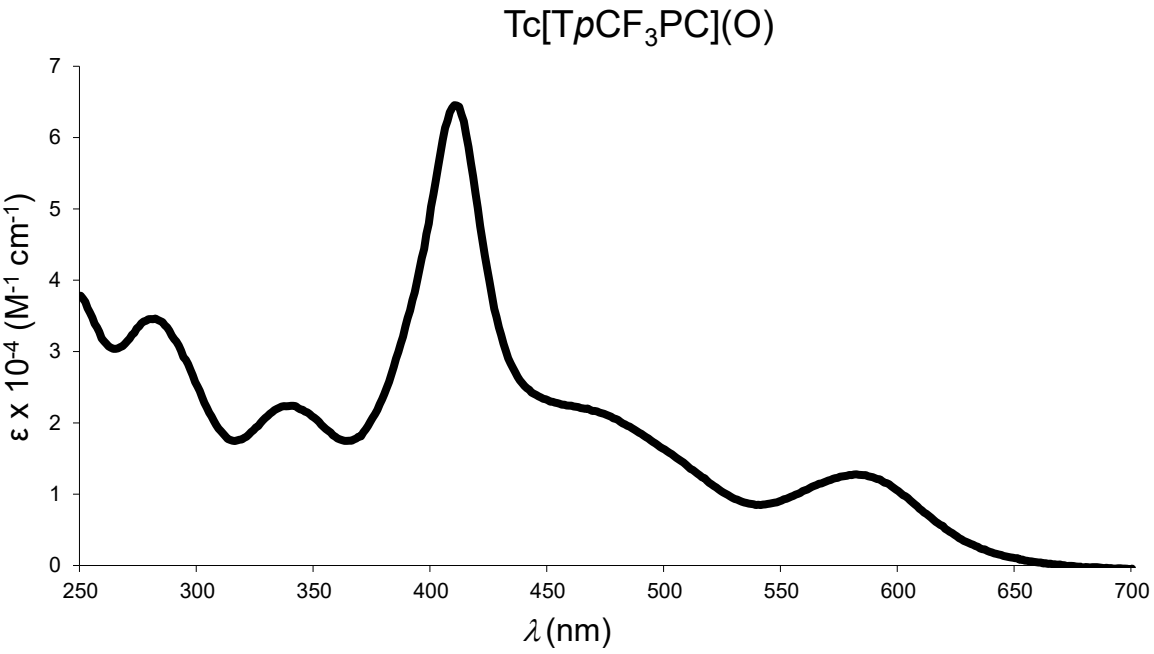

Figure 117. UV-vis spectrum in DCM.

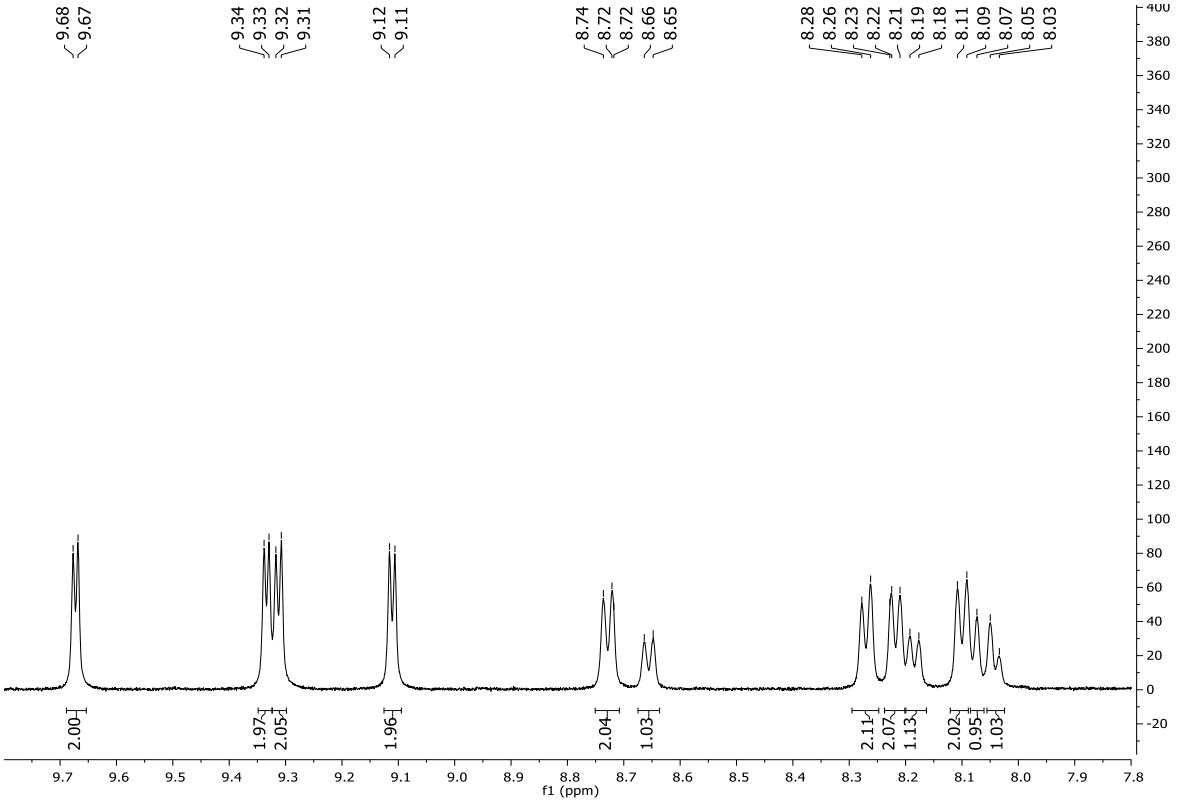

Figure 118. ^{1}H NMR.

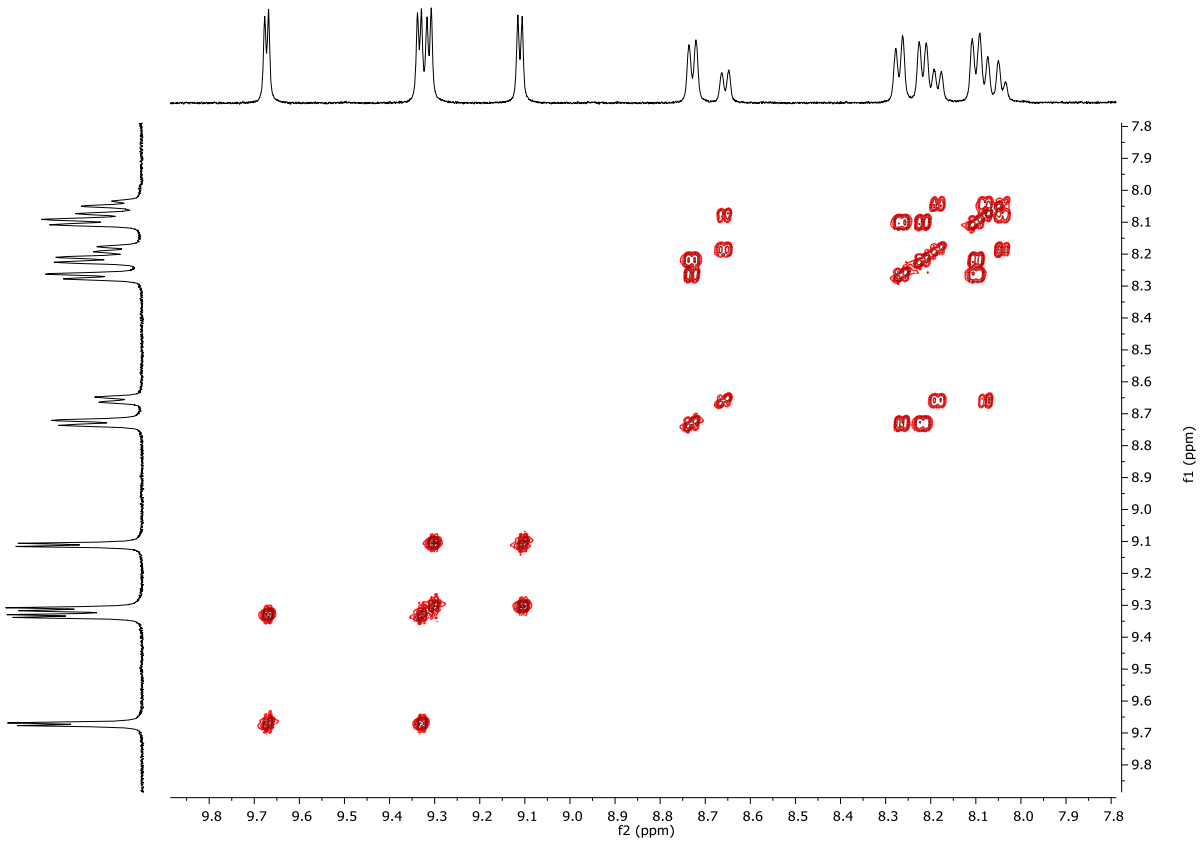

Figure 119. ^{1}H - ^{1}H COSY.

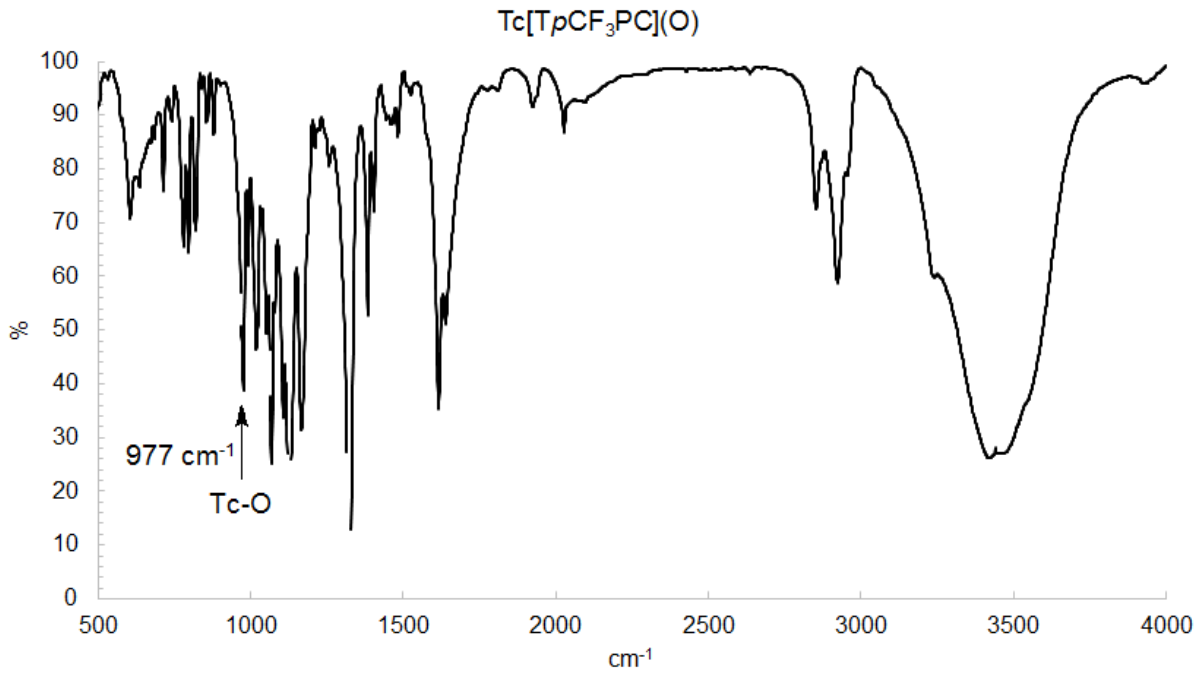

Figure 120. IR spectrum.

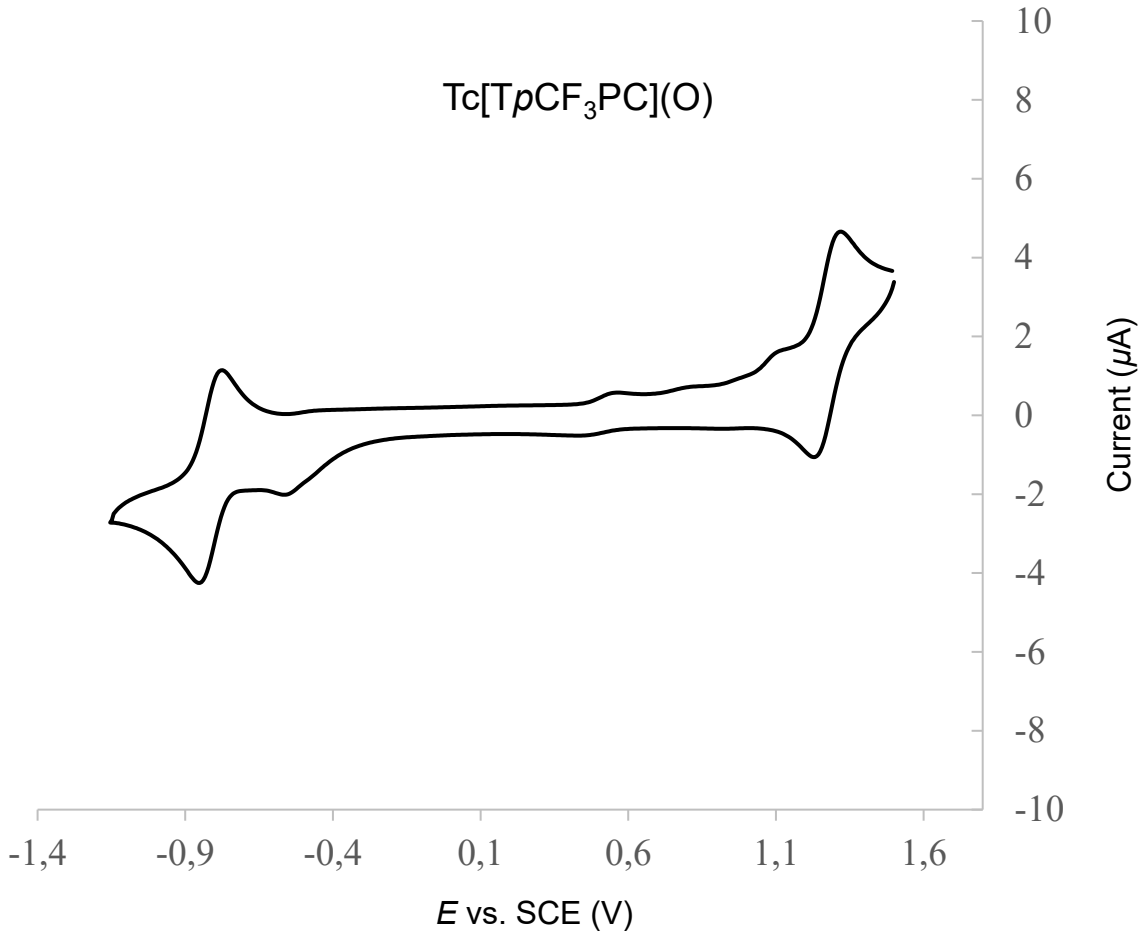

Figure 121. Cyclic voltammogram in acetonitrile containing 0.1 M TBAP.

8.3.2 Analysis of ^{99}Tc[TPC](O)

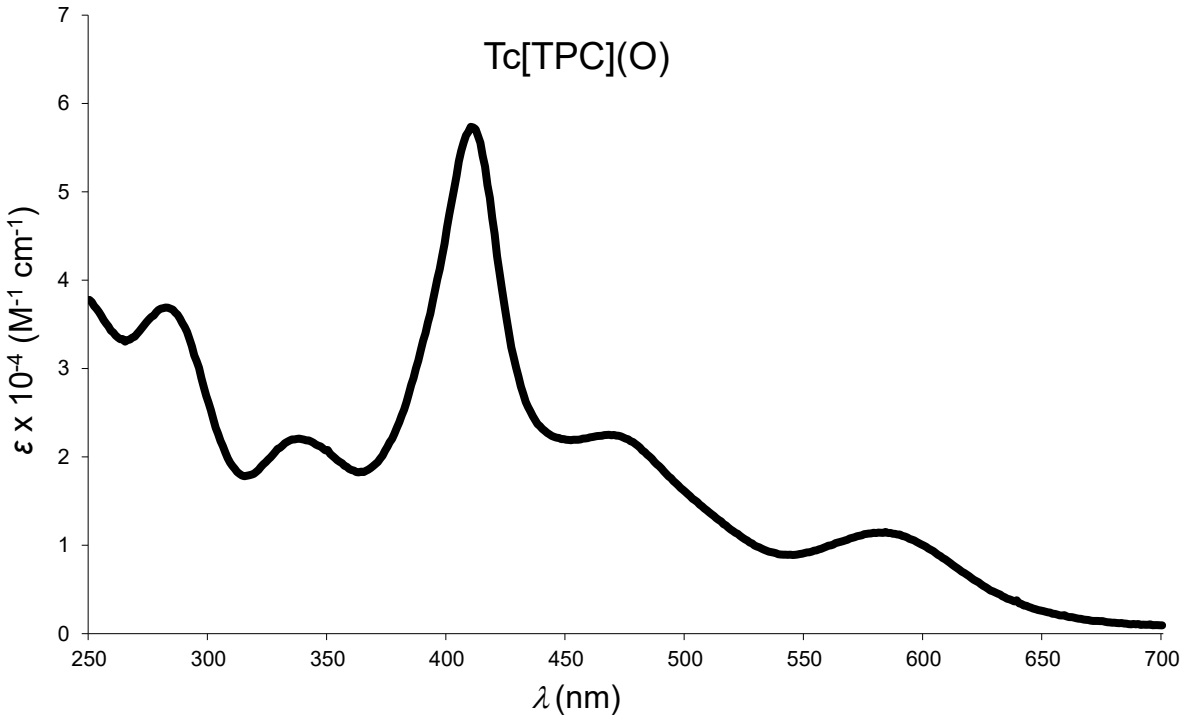

Figure 122. UV-vis spectrum in DCM.

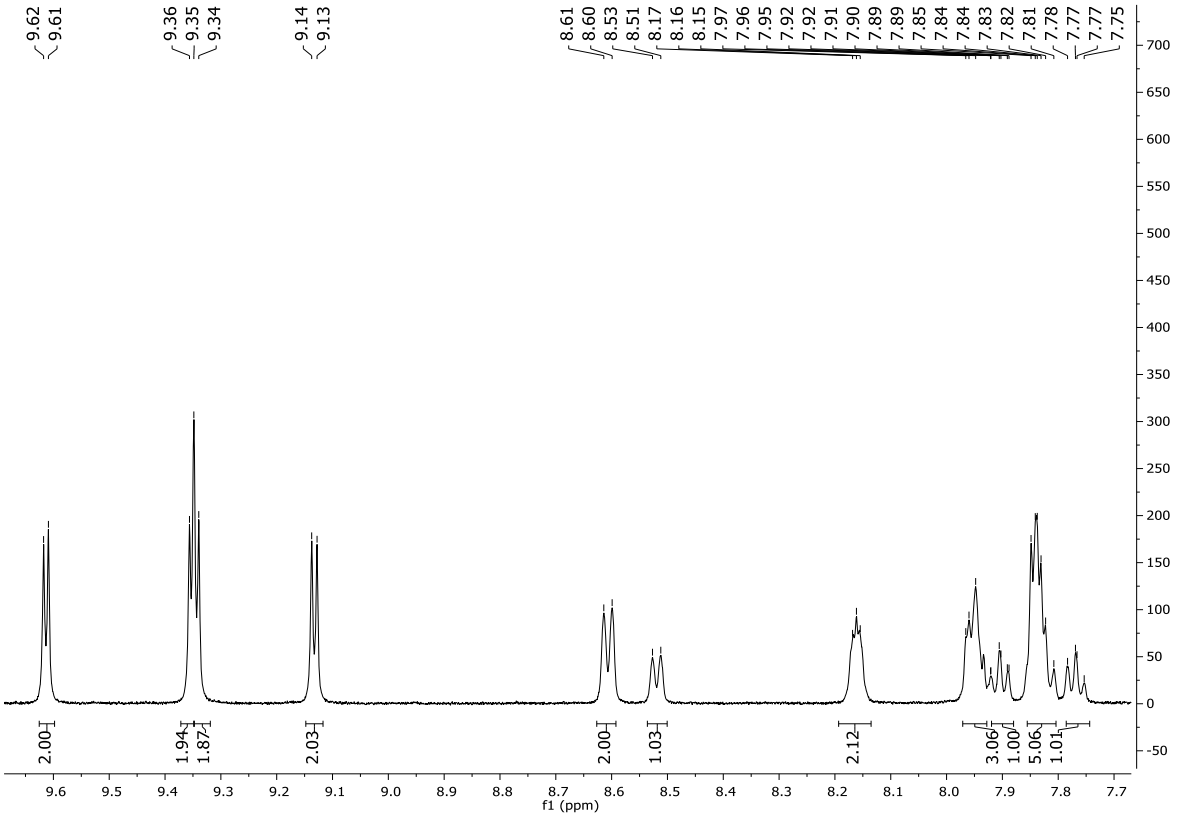

Figure 123. ^{1}H NMR.

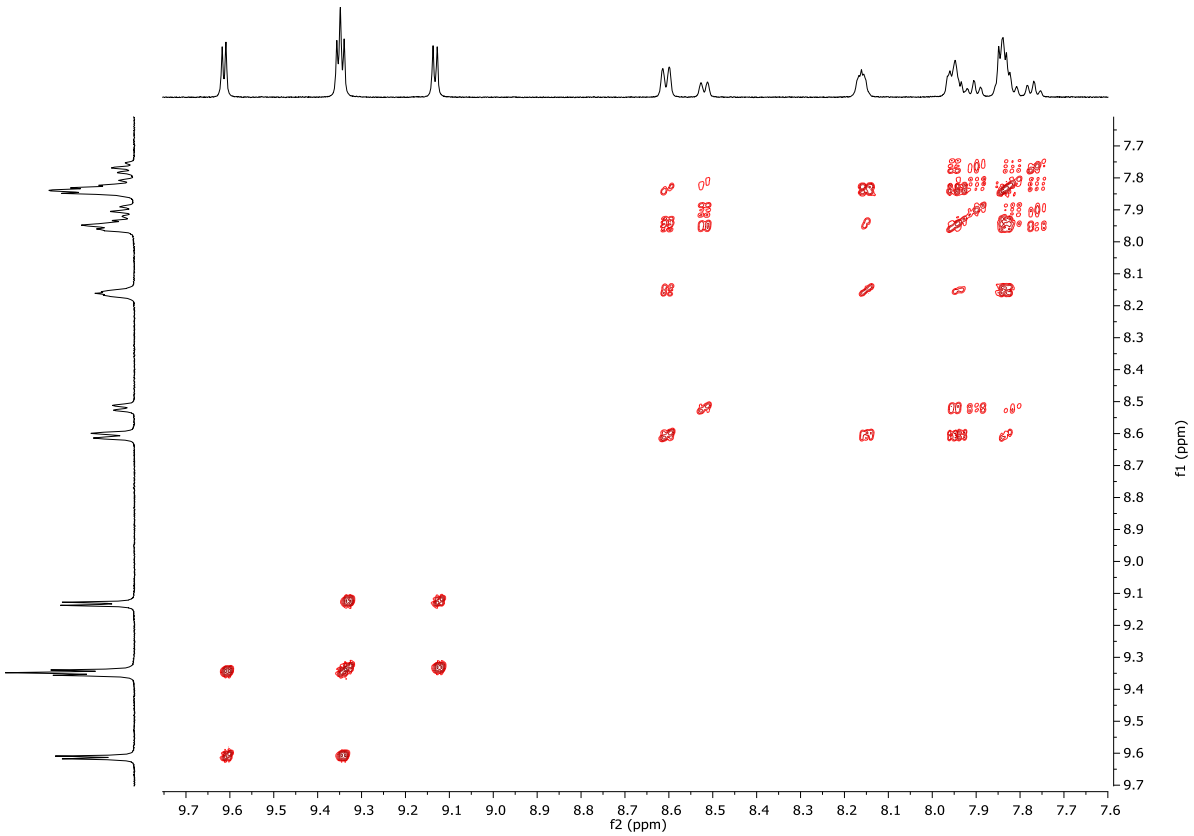

Figure 124. ^{1}H - ^{1}H COSY.

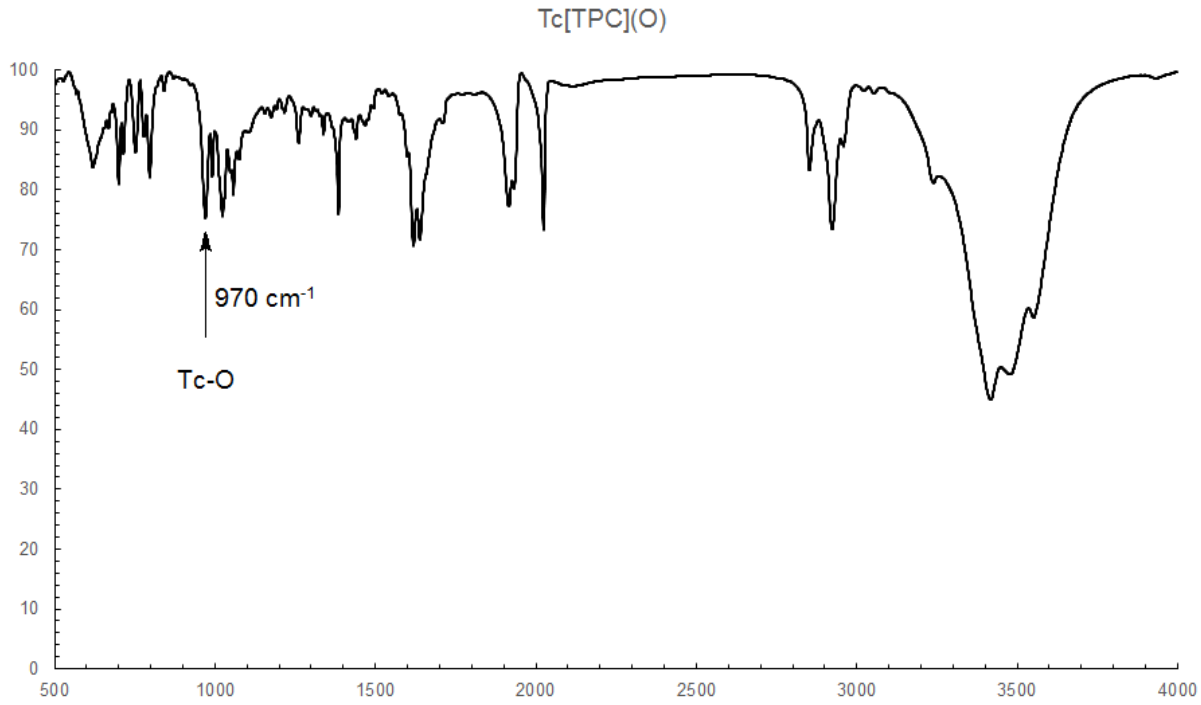

Figure 125. IR spectrum.

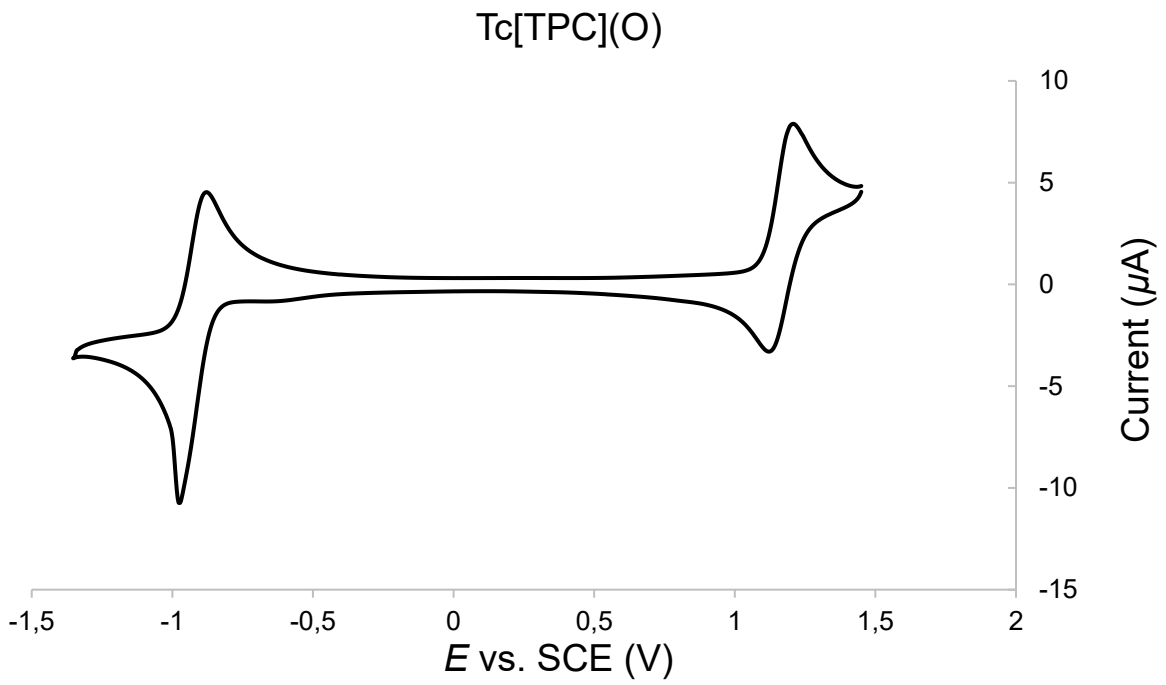

Figure 126. Cyclic voltammogram in acetonitrile containing 0.1 M TBAP.

8.3.3 Analysis of ^{99}Tc[T*p*CH$_3$PC](O)

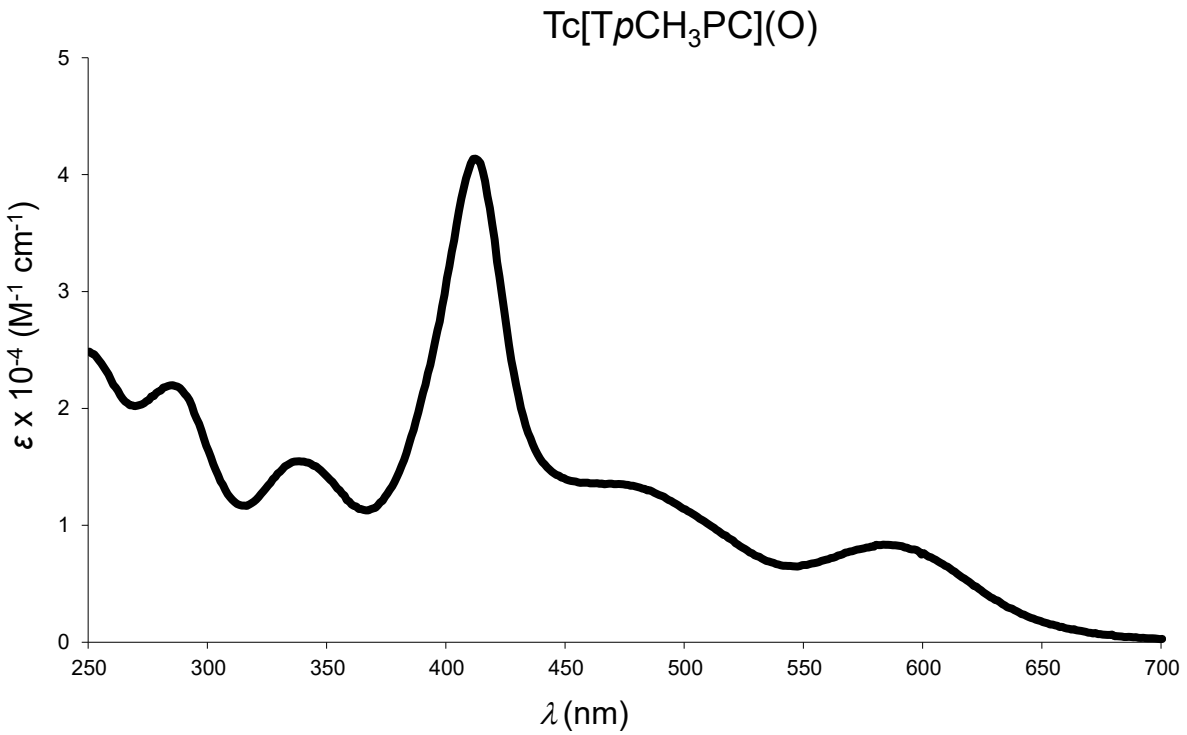

Figure 127. UV-vis spectrum in DCM.

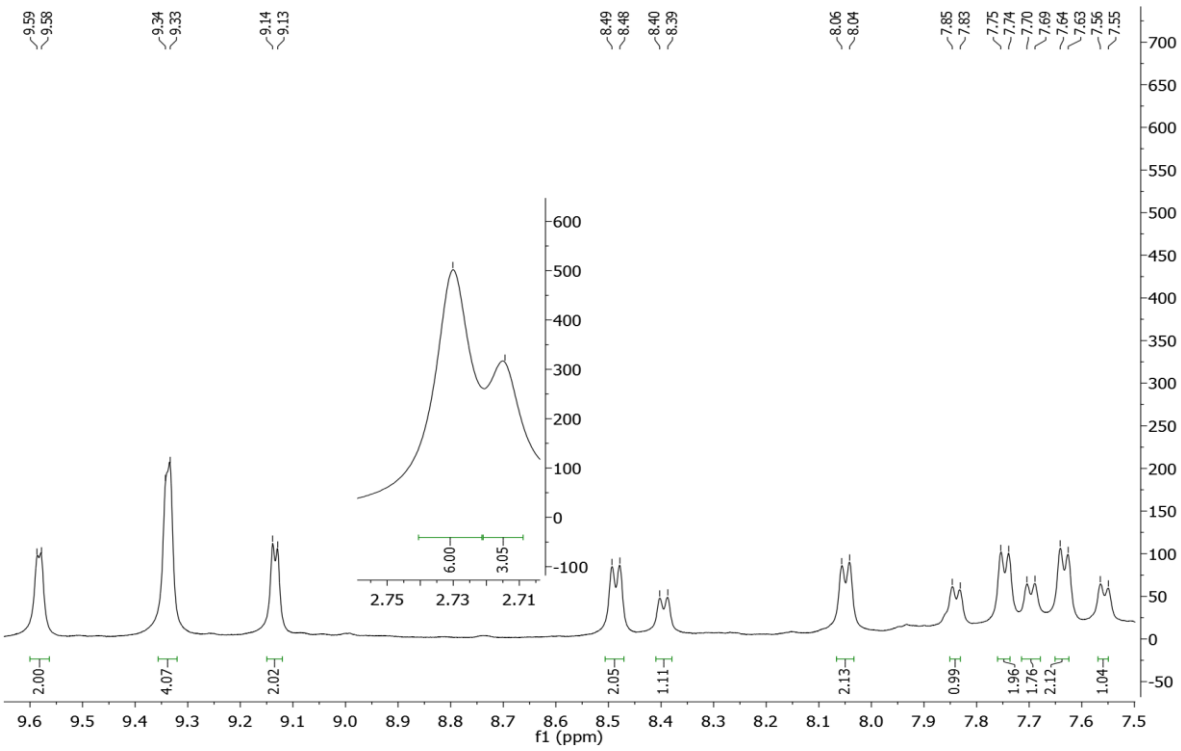

Figure 128. ^{1}H NMR.

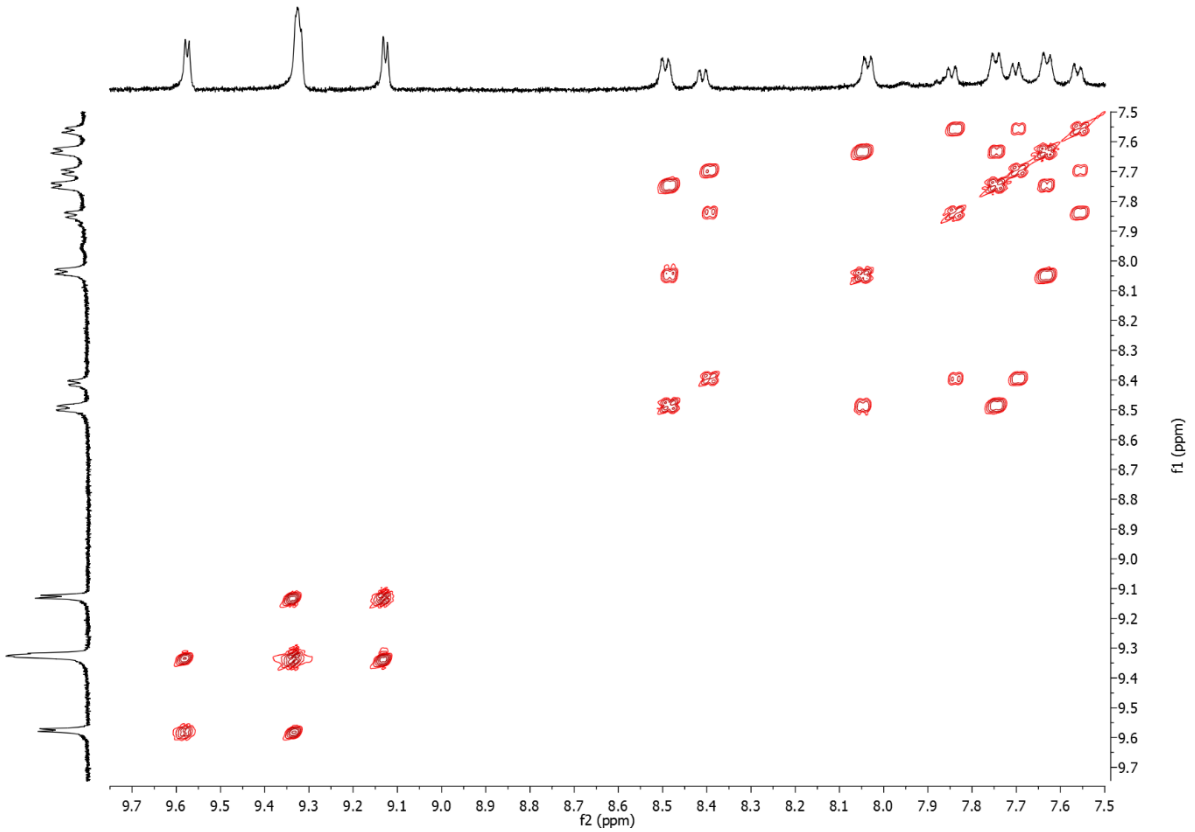

Figure 129. ^{1}H - ^{1}H COSY.

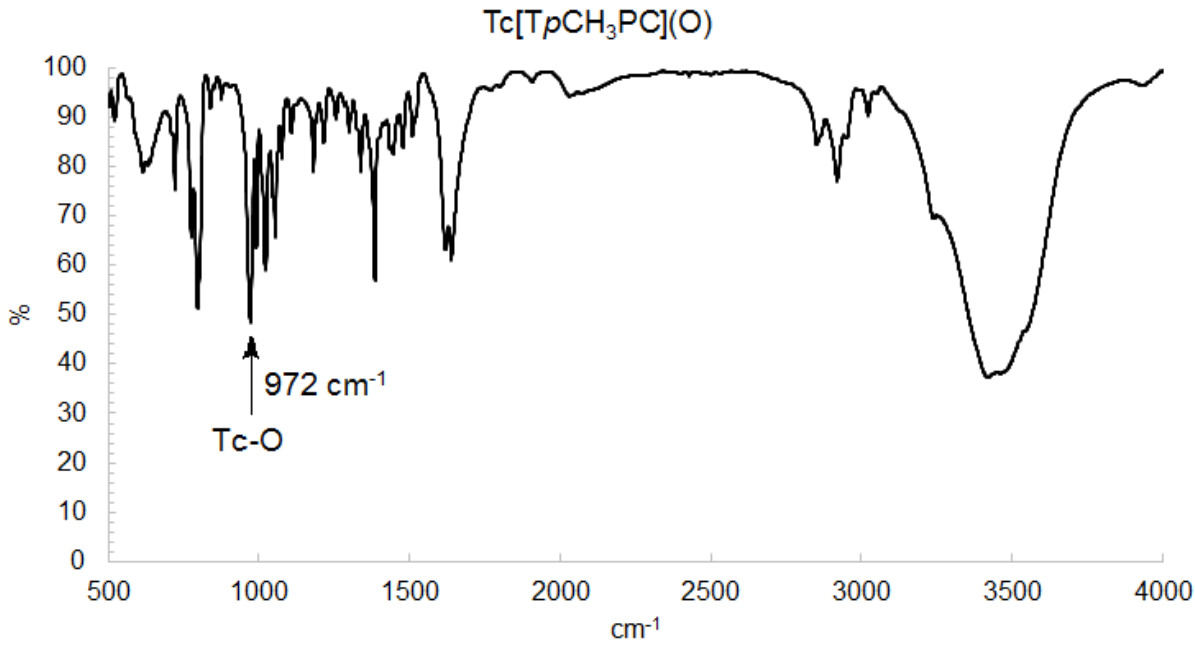

Figure 130. IR spectrum.

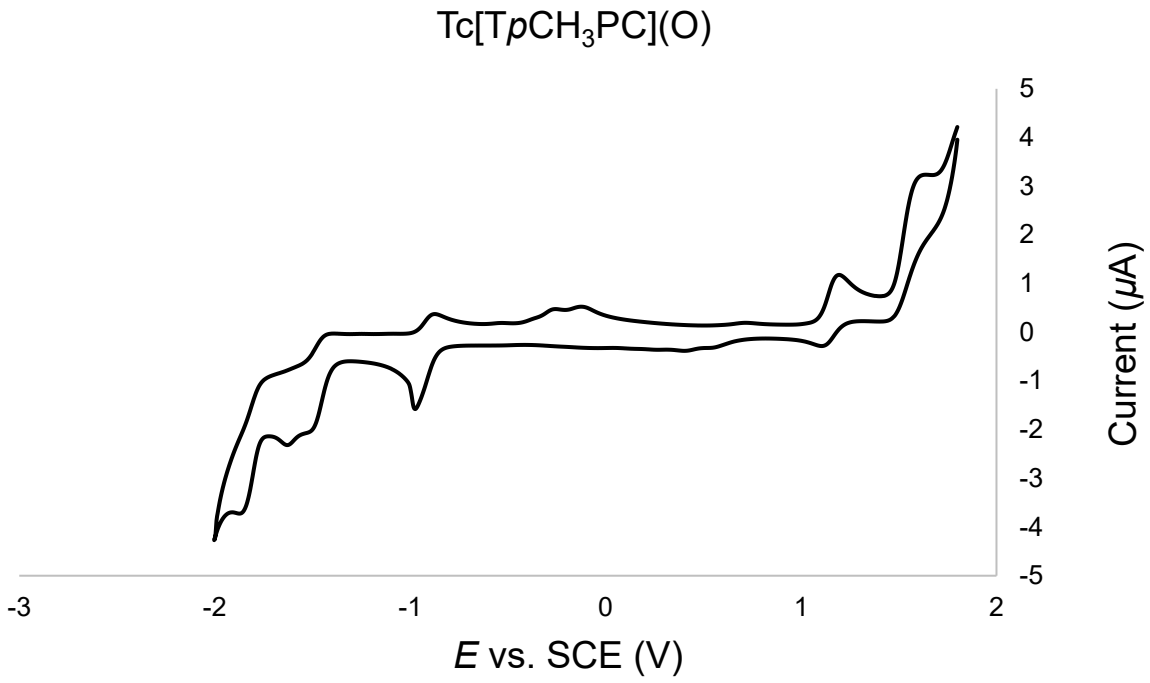

Figure 131. Cyclic voltammogram in acetonitrile containing 0.1 M TBAP.

8.3.4 Analysis of ^{99}Tc[T*p*OCH$_3$PC](O)

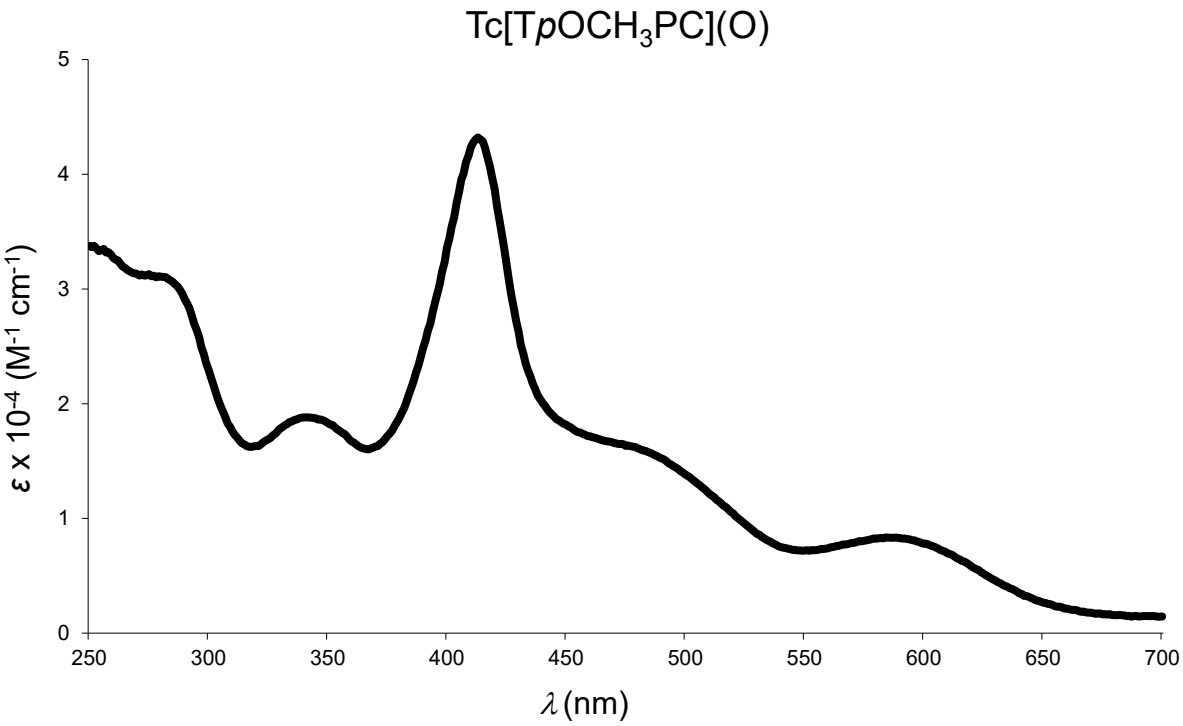

Figure 132. UV-vis spectrum in DCM.

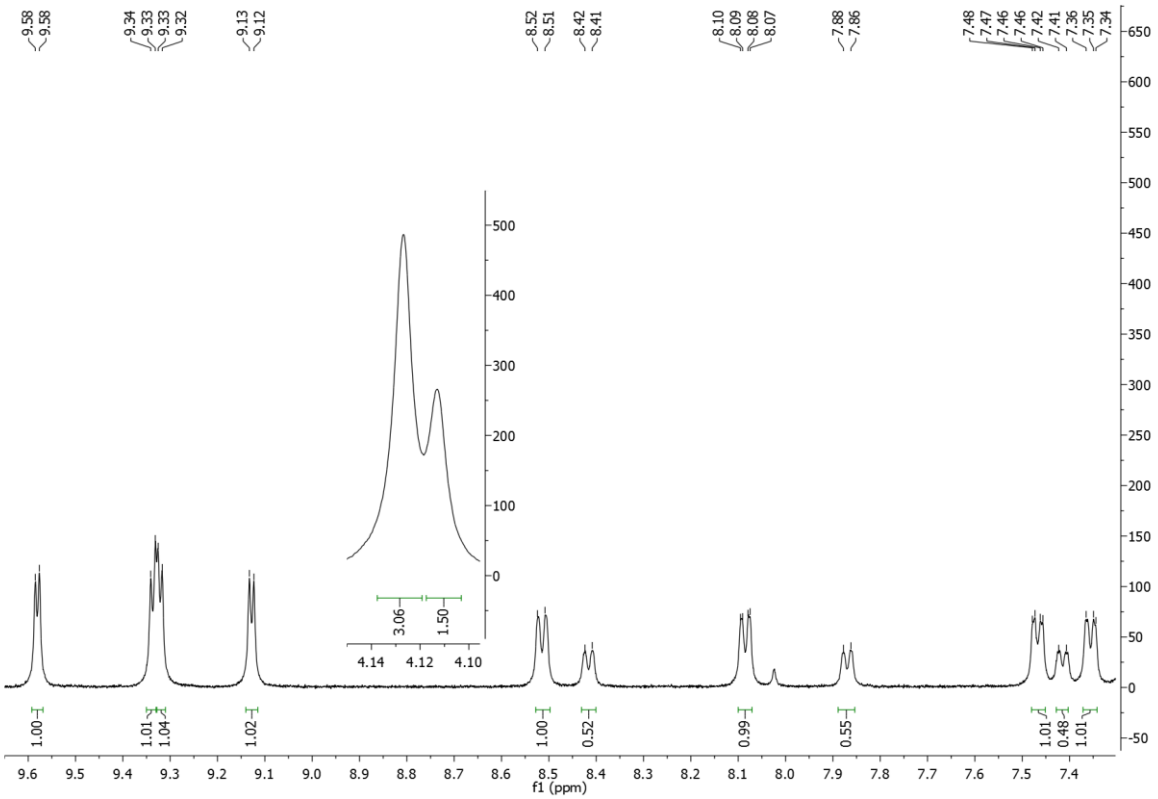

Figure 133. ^{1}H NMR.

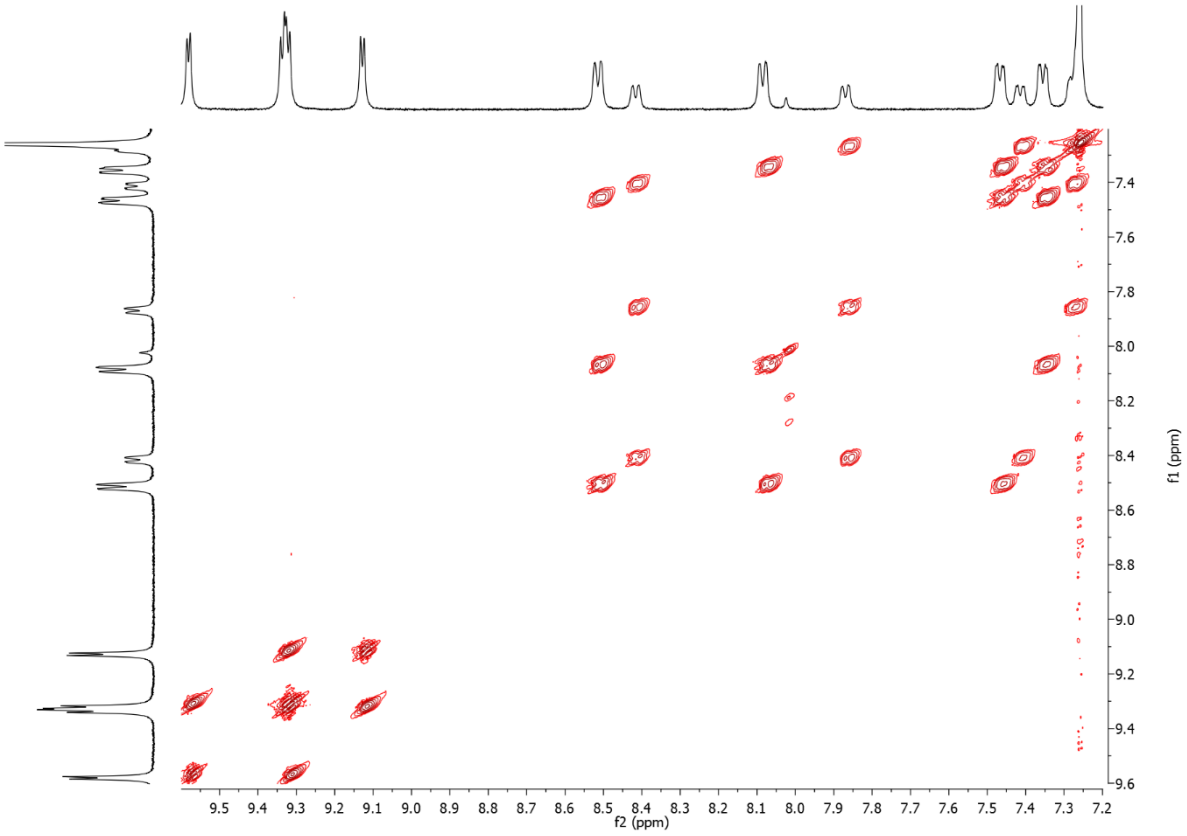

Figure 134. ^{1}H - ^{1}H COSY.

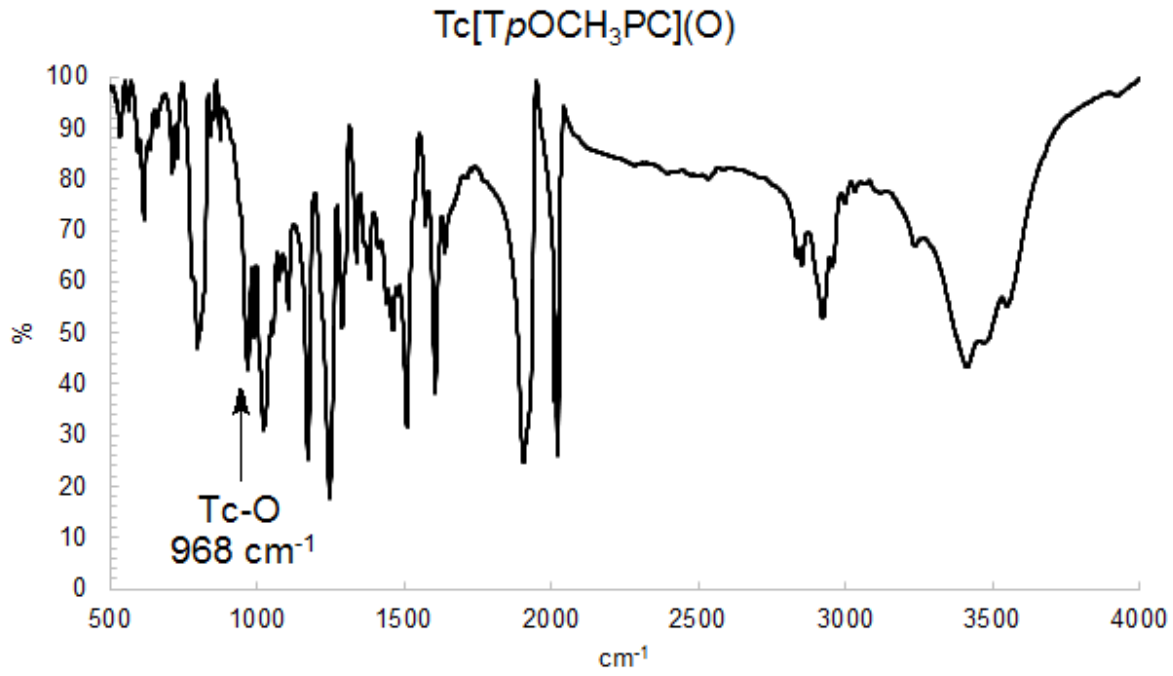

Figure 135. IR spectrum.

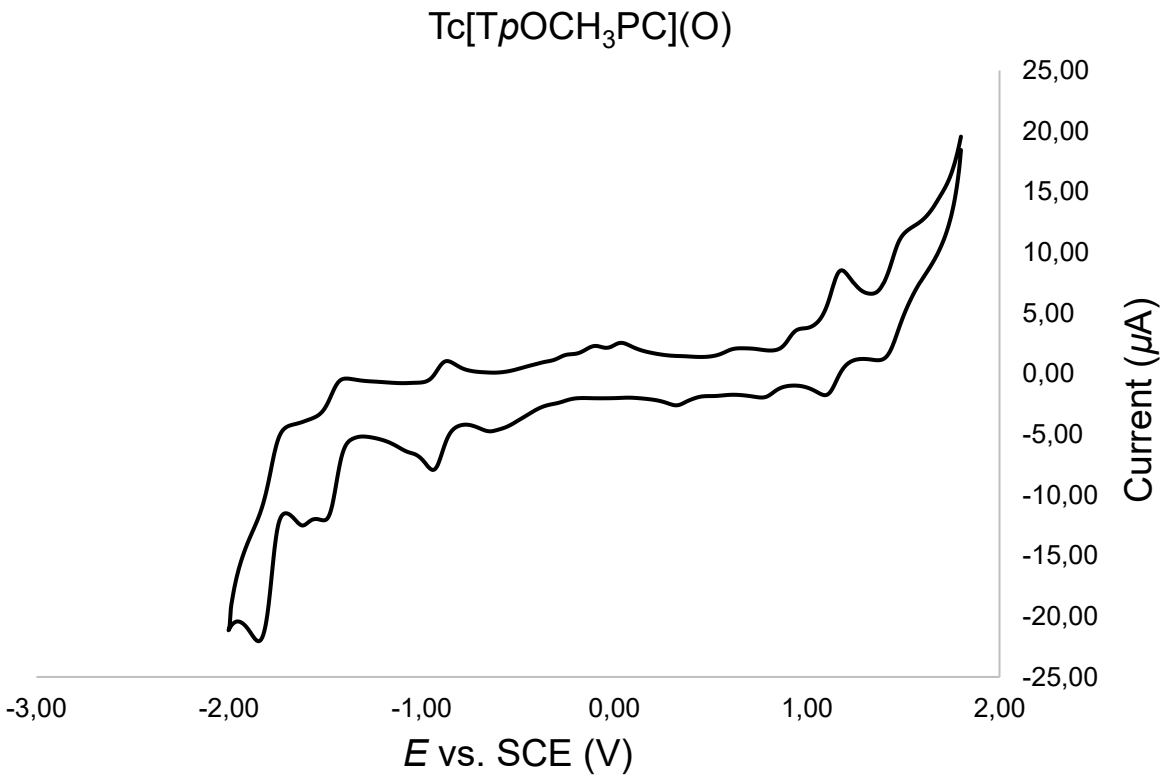

Figure 136. Cyclic voltammogram in acetonitrile containing 0.1 M TBAP.

Table 14. Single crystal X-ray data collection and structure calculations.

	^{99}Tc[T*p*OCH$_3$PC](O)
Formula	$C_{40}H_{29}N_4O_4Tc$
M_w / g mol^{-1}	728.69
Space group	$P2_1/c$
Temperature / K	183
a / Å	13.3606 (4)
b / Å	8.0885 (3)
c / Å	30.4262 (9)
α / °	90
β / °	101.142 (3)
γ / °	90
μ / mm^{-1}	0.50
Z	4
V / Å^3	3226.11 (16)
ρ_{calc} / g cm^{-3}	1.498
Crystal description	Green prism
Θ range [°]	2.7 to 32.7
Index ranges	-17<=h<=17, -10<=k<=8, -40<=l<=40
Refl collected	27266
Indep refl	7947
Refl obs I > 2σ(I)	6851
Compl to theta	99.3 to 28.28
Max. and min. transm	0.805 and 0.948
Restraints / param	0 / 445
Goodness-of-fit on F^2	1.23
Final diff ρ_{max} (e$^-$/ Å^3)	0.76 and -0.70
R1[a, c]	0.054
wR2[b, c]	0.114

APPENDIX

Appendix I: Metal-Ligand Misfits: Facile Access to Rhenium-Oxo Corroles by Oxidative Metalation

Appendix II: Synthesis and Molecular Structure of ^{99}Tc Corroles

APPENDIX I

ChemPubSoc Europe

DOI: 10.1002/chem.201504307

CHEMISTRY
A European Journal
Communication

Metallocorroles |*Hot Paper*|

Metal–Ligand Misfits: Facile Access to Rhenium–Oxo Corroles by Oxidative Metalation

Rune F. Einrem,[a] Kevin J. Gagnon,[b] Abraham B. Alemayehu,*[a] and Abhik Ghosh*[a]

Abstract: With the exception of a single accidental synthesis, rhenium corroles are unknown, but of great interest as catalysts and potential radiopharmaceuticals. Oxidative metalation of *meso*-triarylcorroles with $[Re_2(CO)_{10}]$ in refluxing decalin has provided a facile and relatively high-yielding route to rhenium(V)–oxo corroles. The complexes synthesized could all be fully characterized by single-crystal X-ray structure analyses.

The 5d metallocorroles are fascinating synthetic targets, combining a large coordinated ion with the tight N_4 cavity of a sterically constrained macrocyclic ligand.[1] Recent efforts by a handful of groups, including ours, have led to the synthesis of several such complexes, including Hf,[2] W,[3] Os,[4] Ir,[5] Pt,[6] and Au[7] corroles. Unsurprisingly, some of the syntheses are difficult and low-yielding. For example, the most effective reported synthesis of Au corroles, using Au^{III} acetate as the gold source, proceeded with yields of only up to approximately 25%.[7c] Syntheses of platinum corroles are even more challenging, a serendipitous synthesis leading to only 5–6% yields of a mixture of regioisomeric products.[6] By contrast, Ir and Os corroles are comparatively easily obtained and also in reasonably good yields.[4,5] There are good reasons for seeking improved synthetic routes to the 5d metallocorroles. For example, gold corroles have found applications in organic solar cells and the photodynamic therapy of cancer.[8]

Curiously, with the exception of an accidental synthesis involving an unexpected ring contraction of a porphyrin, there have been no reports of rhenium corroles.[9] This is a significant gap in our knowledge because rhenium–oxo corroles are not only potentially important as catalysts,[10] they may also find applications in radioimaging and -therapy.[11] Furthermore, an efficient route to rhenium corroles may pave the way to an analogous route to technetium corroles.[12] We were delighted to discover that an oxidative metalation protocol, akin to the one used for Os corroles,[4] also works well for rhenium insertion. Thus, five different $Re^{V}O$ *meso*-tris(*p*-X-phenyl)corrole complexes [Re(T*p*XPC)(O)] (X = CF_3, F, H, CH_3, and OCH_3) could be synthesized from the corresponding free-base corroles, H_3[T*p*XPC], and $[Re_2(CO)_{10}]$ in refluxing decalin in a few hours and in yields of 62–84% (Scheme 1).

All five complexes proved amenable to single-crystal X-ray structure determination (Figure 1 and Tables 1 and 2). The Re–O distances varied over a narrow range of 1.668(4)–1.6859(15) Å, in good agreement with the sum of covalent radii reported by Pyykkö and co-workers for triple-bonded Re (1.10 Å) and triple-bonded O (0.53 Å).[13] The Re–N distances of 1.995 ± 0.019 Å are distinctly shorter than those in other N-coordinated Re complexes, reflecting the sterically constrained nature of the complexes. Furthermore, for all five complexes, the corrole macrocycle is significantly domed, with the Re displaced some 0.7 Å from the corrole N_4 plane.

The key physicochemical properties of the complexes were found to be as follows. First, the ^{1}H NMR spectra, which could be fully assigned with COSY and NOESY analyses, showed that the compounds are diamagnetic, consistent with the expected d_{xy^2} electronic configuration of the $Re^{V}O$ center. Second, the Soret maxima of the complexes (Table 3 and Figure S1 in the Supporting Information) are not sensitive to the *para* substituent X, and are redshifted by only 3 nm from X = CF_3 to X = OCH_3. Third, the electrochemical HOMO–LUMO gaps are large (approximately 2.24 ± 0.02 eV; Table 3 and Figure S2 in the Supporting Information), which is essentially equal to the π–π* gap of a typical porphyrin or corrole macrocycle.[4,7c,14] Over a lengthy series of studies, we have established that the last two characteristics are typical of an innocent $[corrole]^{3-}$ ligand, such as that found in Au and Os–N corroles, as opposed to a noninnocent $[corrole]^{\cdot 2-}$ ligand, for which copper[15] and iron[16,17] corroles provide some of the best studied examples.

Consistent with literature reports,[9,10] the Re–O stretching mode ($\tilde{\nu}_{Re-O}$) of the complexes is readily discernible in the IR spectra, with little interference from other skeletal modes. The $\tilde{\nu}_{Re-O}$ value varies significantly with the *meso para* substituent (Table 3), being upshifted with increasing electron-withdrawing character of the substituent. Between *para*-OMe ($\tilde{\nu}_{Re-O}$ = 978 cm^{-1}) and the more electron-deficient complexes ($\tilde{\nu}_{Re-O}$ = 990–992 cm^{-1}), $\tilde{\nu}_{Re-O}$ is upshifted by 12–14 cm^{-1}. These frequency shifts may be rationalized in terms of elementary bonding considerations: a more electron-deficient corrole should result in stronger π-donation by the axial oxo ligand and thus to an overall stronger Re–O bond.

[a] *R. F. Einrem, Dr. A. B. Alemayehu, Prof. Dr. A. Ghosh*
Department of Chemistry, UiT - The Arctic University of Norway
9037 Tromsø (Norway)
E-mail: abraham.alemayehu@uit.no
abhik.ghosh@uit.no

[b] *Dr. K. J. Gagnon*
Advanced Light Source, Lawrence Berkeley National Laboratory
Berkeley, CA 94720-8229 (USA)

Supporting information for this article, including spectroscopic data and crystallographic information files, is available on the WWW under http://dx.doi.org/10.1002/chem.201504307.

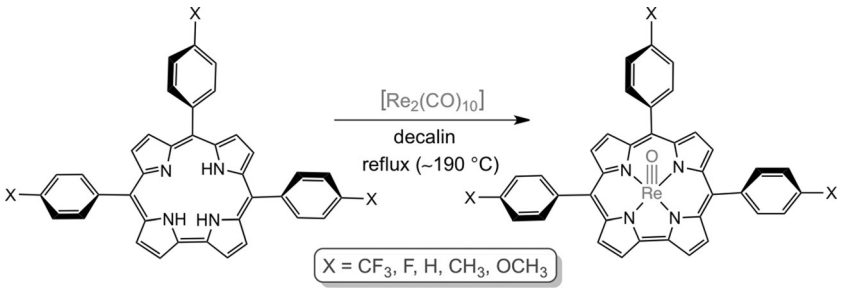

Scheme 1. A general synthetic route for $Re^{V}O$ triarylcorroles.

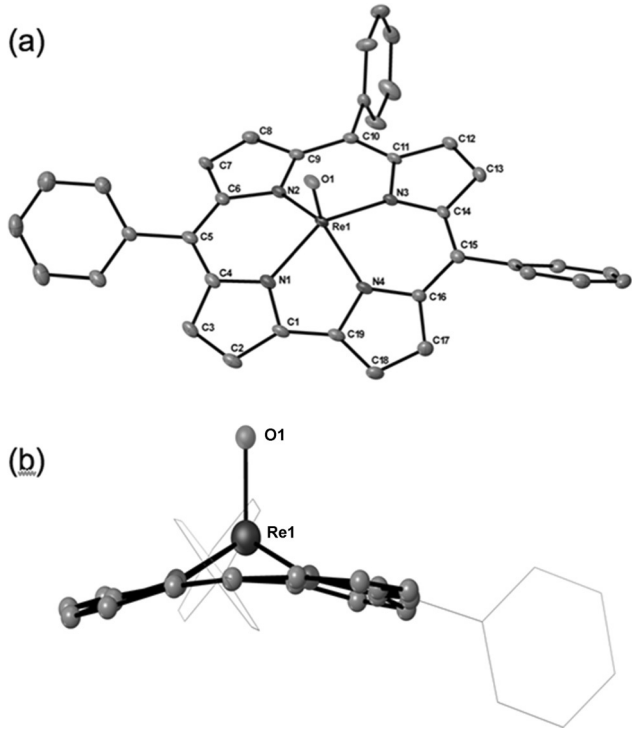

Figure 1. Two views of [Re(TPC)(O)] (TPC = triphenylcorrole): a) Single-crystal X-ray structure with nonhydrogen atom numbering and thermal ellipsoids set at 50% probability; b) side-on view showing the displacement of the Re atom above the macrocycle.

Several points are worth making by way of conclusion. First, the general and facile synthesis of ReO triarylcorroles presented herein contrasts sharply with the capricious, low-yielding protocols reported for Au and Pt corroles.[6,7] We believe that the ease of the present syntheses is closely related to our use of a metal carbonyl starting material, which decarbonylates on thermolysis and releases reactive, coordinatively unsaturated $[Re(CO)_n]$ ($n<5$) fragments, that readily latch onto a corrole ligand. Second, a variety of applications may be envisioned for ReO corroles, including oxygen atom transfer catalysis, photocatalytic water splitting, phosphorescence and oxygen sensing, photodynamic therapy, and even cancer chemotherapy. Finally, the present syntheses may pave the way for the synthesis of the heretofore unknown technetium corroles. In particular, facile access to ^{99m}Tc corroles is of great interest as a route to a new class of potential radiopharmaceuticals.

Experimental Section

General procedure for the synthesis of [Re(T*p*XPC)(O)]. To a 50 mL three-necked round-bottom flask fitted with a reflux condenser and containing decalin (15 mL) and a magnetic stirring bar was added a free-base corrole, H_3[T*p*XPC] (0.094 mmol), $[Re_2(CO)_{10}]$ (0.188 mmol), and potassium carbonate (100 mg). The contents were deoxygenated with a flow of argon and then heated at reflux overnight with constant stirring under Ar. Completion of the reaction was indicated by the disappearance of the Soret absorption of the free-base corrole and appearance of a new Soret maximum at approximately $\lambda_{max}=440$ nm. Upon cooling, the reaction mixture was loaded directly onto a silica gel column with *n*-hexane as the mobile phase. The decalin was first removed by eluting with pure hexane. Different solvent mixtures were then used to elute the various ReO corroles: 3:1 v/v *n*-hexane/dichloromethane for X = CF_3, H, CH_3 and F; 1:3 v/v *n*-hexane/dichloromethane for X = OCH_3. All fractions with $\lambda_{max}\approx440$ nm were collected and dried. The products were further purified by a second round of column chromatography and finally by preparative thin-layer chromatography, with the same solvents as in the first round. Yields and analytical details for the different complexes are as follows.

[Re(T*p*CF_3PC)(O)]: Yield = 55 mg (62.9%). ^{1}H NMR (400 MHz, −20 °C, CD_2Cl_2): $\delta=9.76$ (d, 2H, ^3J(H,H) = 4 Hz, β-H); 9.38 (d, 2H, ^3J(H,H) = 4 Hz, β-H); 9.36 (d, 2H, ^3J(H,H) = 4 Hz, β-H); 9.16 (d, 2H, ^3J(H,H) = 4 Hz, β-H); 8.77 (d, 2H, ^3J(H,H) = 8 Hz, 5,15-*o*1-Ph); 8.69 (d, 1H, ^3J(H,H) = 8 Hz, 10-*o*1-Ph); 8.26 (d, 2H, ^3J(H,H) = 8 Hz, 5,15-*o*2-Ph); 8.22 (d, 2H, ^3J(H,H) = 8 Hz, 5,15-*m*1-Ph); 8.19 (d, 1H, ^3J(H,H) = 8 Hz, 10-*m*1-Ph); 8.10 (d, 3H, ^3J(H,H) = 8 Hz, 5,15-*m*2-Ph and 10-*o*2-Ph overlapping); 8.05 ppm (d, 2H, ^3J(H,H) = 8 Hz, 10-*m*2-Ph); IR (ATR, diamond): $\tilde{\nu}_{Re-O}=990$ cm^{-1}; UV/Vis (CH_2Cl_2): λ_{max} (ε) = 438 (10.74), 552 (1.63), 585 nm (1.99×10^4 mol^{-1} dm^3 cm^{-1}); MS (ESI): *m/z* calcd for $C_{40}H_{20}ON_4F_9Re$: 929.81 [M^+]; found: 930.10; elemental analysis calcd for $C_{40}H_{20}ON_4F_9Re$: C 51.67, H 2.17, N 6.03; found: C 51.40, H 2.31, N 6.40.

[Re(T*p*FPC)(O)]: Yield = 52 mg (70.26%). ^{1}H NMR (400 MHz, −20 °C, CD_2Cl_2): $\delta=9.71$ (d, 2H, ^3J(H,H) = 4 Hz, β-H); 9.37 (d, 2H, ^3J(H,H) = 4 Hz, β-H); 9.36 (d, 2H, ^3J(H,H) = 4 Hz, β-H); 9.16 (d, 2H, ^3J(H,H) = 4 Hz, β-H); 8.59 (d, 2H, ^3J(H,H) = 8 Hz, 5,15-*o*1-Ph); 8.51 (d, 1H, ^3J(H,H) = 8 Hz, 10-*o*1-Ph); 8.08 (d, 2H, ^3J(H,H) = 8 Hz, 5,15-*o*2-Ph); 7.91 (d, 1H, ^3J(H,H) = 8 Hz, 10-*o*2-Ph); 7.66 (d, 2H, ^3J(H,H) = 8 Hz, 5,15-*m*1-Ph); 7.60 (d, 1H, ^3J(H,H) = 8 Hz, 10-*m*1-Ph); 7.54 (d, 2H, ^3J(H,H) = 8 Hz, 5,15-*m*2-Ph); 7.48 ppm (d, 1H, ^3J(H,H) = 8 Hz, 10-*m*2-Ph); 4; IR (ATR diamond): $\tilde{\nu}_{Re-O}=992$ cm^{-1}; UV/Vis (CH_2Cl_2): λ_{max} (ε) = 438 (10.16), 553 (1.53), 585 nm (1.93×10^4 mol^{-1} dm^3 cm^{-1}); MS

Table 1. Crystallographic data for the complexes analyzed.

Sample	[Re(T*p*CF$_3$PC)(O)]	[Re(T*p*FPC)(O)]	[Re(TPC)(O)]	[Re(T*p*CH$_3$PC)(O)]	[Re(T*p*OCH$_3$PC)(O)]
chemical formula	$C_{40.25}H_{20.50}Cl_{0.50}F_9N_4ORe$	$C_{37.35}H_{20.69}Cl_{0.69}F_3N_4ORe$	$C_{37}H_{23}N_4ORe$	$C_{40}H_{29}N_4ORe$	$C_{40}H_{29}N_4O_4Re$
formula mass	951.03	809.28	725.79	767.87	815.87
crystal system	monoclinic	monoclinic	monoclinic	triclinic	monoclinic
space group	$P2_1/c$	$P2_1/c$	$P2_1/c$	$P\bar{1}$	$P2_1/c$
λ [Å]	0.7749	0.7749	0.7749	0.7749	0.7293
a [Å]	16.4309(6)	12.2806(4)	10.3452(4)	7.2799(4)	13.3584(7)
b [Å]	14.2677(5)	22.2084(7)	8.0511(3)	15.3860(7)	8.0963(4)
c [Å]	14.1303(5)	10.7507(4)	32.4589(12)	16.2273(7)	30.2638(17)
α [°]	90	90	90	95.414(3)	90
β [°]	93.141(2)	102.546(2)	97.055(2)	102.719(3)	101.898(2)
γ [°]	90	90	90	91.141(3)	90
Z	4	4	4	2	4
V [Å^3]	3307.6(2)	2862.05(17)	2683.04(18)	1763.54(15)	3202.8(3)
temperature [K]	100(2)	100(2)	100(2)	100(2)	100(2)
density [g cm^{-3}]	1.910	1.878	1.797	1.446	1.692
measured reflections	57324	27807	73342	25719	97288
unique reflections	10091	5236	8931	11826	22512
parameters	581	441	388	419	445
restraints	403	18	0	0	0
R_{int}	0.0501	0.0787	0.0693	0.0671	0.0293
θ range [°]	2.062–33.606	2.105–27.867	2.163–34.735	2.123–36.695	2.341–43.551
R_1, wR_2 all data	0.0272, 0.0526	0.0377, 0.0660	0.0346, 0.0556	0.0505, 0.0915	0.0376, 0.0774
S (GoF) all data	1.023	1.039	1.032	1.026	1.312
max/min res. dens. [e Å^{-3}]	1.082/−1.078	0.793/−1.102	1.174/−2.522	2.104/−1.896	4.696/−5.881

Table 2. Crystallographic metal–ligand distances.

Distance [Å]	[Re(T*p*CF$_3$PC)(O)]	[Re(T*p*FPC)(O)]	[Re(TPC)(O)]	[Re(T*p*CH$_3$PC)(O)]	[Re(T*p*OCH$_3$PC)(O)]
Re1–N1	1.986(2)	1.987(5)	1.986(3)	1.977(4)	1.9894(17)
Re1–N2	2.000(2)	2.012(5)	2.005(2)	2.006(3)	2.0077(16)
Re1–N3	2.014(2)	2.006(4)	2.004(3)	2.004(4)	2.0070(16)
Re1–N4	1.988(2)	1.995(4)	1.990(2)	1.981(4)	1.9854(16)
Re1–O	1.6772(18)	1.668(4)	1.677(2)	1.681(3)	1.6859(15)
ΔRe1–N$_4$	0.6949(11)	0.704(2)	0.7045(13)	0.6949(17)	0.6891(9)

Table 3. Spectroscopic and electrochemical properties: Soret λ_{max} (nm), IR $\tilde{\nu}_{Re-O}$ (cm^{-1}), and $E_{1/2}$ values (V).

Complex	λ_{max}	$E_{1/2(ox)}$	$E_{1/2(red)}$	ΔE	$\tilde{\nu}_{Re-O}$
[Re(T*p*CF$_3$PC)(O)]	438	1.10	−1.16	2.26	990
[Re(T*p*FPC)(O)]	438	1.01	−1.23	2.24	992
[Re(TPC)(O)]	439	0.98	−1.26	2.24	992
[Re(T*p*CH$_3$PC)(O)]	440	0.94	−1.29	2.23	984
[Re(T*p*OCH$_3$PC)(O)]	441	0.93	−1.29	2.22	978

(ESI): *m/z* calcd for $C_{37}H_{20}OF_3N_4Re$: 779.84 [M^+]; found: 780.11; elemental analysis calcd for $C_{37}H_{20}OF_3N_4Re$: C 56.99, H 2.59, N 7.18; found: C 56.34, H 2.90, N 6.68.

[Re(TPC)(O)]: Yield = 58 mg (84.19%). ^{1}H NMR (400 MHz, −20 °C, CD_2Cl_2): δ = 9.70 (d, 2H, ^3J(H,H) = 4 Hz, β-H); 9.39 (d, 2H, ^3J(H,H) = 4 Hz, β-H); 9.8 (d, 2H, ^3J(H,H) = 4 Hz, β-H); 9.17 (d, 2H, ^3J(H,H) = 4 Hz, β-H); 8.61 (d, 2H, ^3J(H,H) = 8 Hz, 5,15-*o*1-Ph); 8.54 (d, 1H, ^3J(H,H) = 8 Hz, 10-*o*1-Ph); 8.13 (d, 2H, ^3J(H,H) = 8 Hz, 5,15-*o*2-Ph); 7.94 (m, 4H, ^3J(H,H) = 8 Hz, 5,15-*m*1-Ph; 10-*p*-Ph and 10-*o*2-Ph overlapping); 7.90 (m, 1H, 10-*m*1-Ph); 7.83 (m, 4H, 5,15-*m*2-Ph and 5,15-*p*-Ph overlapping); 7.76 ppm (d, 1H, ^3J(H,H) = 8 Hz, 10-*m*2-Ph); IR (ATR, diamond): $\tilde{\nu}_{Re-O}$ = 992 cm^{-1}; UV/Vis (CH_2Cl_2): λ_{max} (ε) = 439 (10.09), 552 (1.99), 585 nm (2.34 × 10^4 mol^{-1} dm^3 cm^{-1}); MS (ESI): *m/z* calcd for $C_{37}H_{23}N_4ORe$: 725.81 [M^+]; found: 726.14; elemental analysis calcd for $C_{37}H_{23}N_4ORe$: C 61.23, H 3.81, N 7.72; found: C 60.58, H 3.34, N 7.25.

[Re(T*p*CH$_3$PC)(O)]: Yield = 50.2 mg (68.9%) ^{1}H NMR (400 MHz, −20 °C, CD_2Cl_2): δ = 9.68 (d, 2H, ^3J(H,H) = 4 Hz, β-H); 9.34 (d, 2H, ^3J(H,H) = 4 Hz, β-H); 9.16 (d, 2H, ^3J(H,H) = 4 Hz, β-H); 9.03 (d, 2H, ^3J(H,H) = 4 Hz, β-H); 8.44 (d, 2H, ^3J(H,H) = 8 Hz, 5,15-*o*1-Ph); 8.36 (d, 1H, ^3J(H,H) = 8 Hz, 10-*o*1-Ph); 7.97 (d, 2H, ^3J(H,H) = 8 Hz, 5,15-*o*2-Ph); 7.79 (d, 2H, ^3J(H,H) = 8 Hz, 5,15-*m*1-Ph); 7.73 (d, 1H, ^3J(H,H) = 8 Hz, 10-*m*1-Ph); 7.66 (d, 2H, ^3J(H,H) = 8 Hz, 5,15-*m*2-Ph); 7.59 (d, 1H, ^3J(H,H) = 8 Hz, 10-*m*2-Ph); 2.76 (s, 6H, 5,15-*p*-CH$_3$); 2.74 ppm (s, 3H, 10-*p*-CH$_3$); IR (ATR, diamond): $\tilde{\nu}_{Re-O}$ = 984 cm^{-1}; UV/Vis (CH_2Cl_2): λ_{max} (ε) = 440 (11.18), 555 (1.86), 587 nm (2.37 × 10^4 mol^{-1} dm^3 cm^{-1}); MS (ESI): *m/z* calcd for $C_{40}H_{29}N_4ORe$: 767.89 [M^+]; found: 768.18; elemental analysis calcd for $C_{40}H_{29}N_4ORe$: C 62.56, H 3.81, N 7.30; found: C 61.81, H 3.85, N 6.96.

[Re(T*p*OCH$_3$PC)(O)]: Yield = 47 mg (61.28%). ^{1}H NMR (400 MHz, −20 °C, CD_2Cl_2): δ = 9.70 (d, 2H, ^3J(H,H) = 4 Hz, β-H); 9.36 (d, 2H, ^3J(H,H) = 4 Hz, β-H); 9.15 (d, 2H, ^3J(H,H) = 4 Hz, β-H); 9.02 (d, 2H, ^3J(H,H) = 4 Hz, β-H); 8.46 (d, 2H, ^3J(H,H) = 8 Hz, 5,15-*o*1-Ph); 8.36 (d, 1H, ^3J(H,H) = 8 Hz, 10-*o*1-Ph); 7.99 (d, 2H, ^3J(H,H) = 8 Hz, 5,15-*o*2-

Ph); 7.80 (d, 1H, ^3J(H,H) = 8 Hz, 10-*o*2-Ph); 7.49 (d, 2H, ^3J(H,H) = 8 Hz, 5,15-*m*1-Ph); 7.46 (d, 1H, ^3J(H,H) = 8 Hz, 10-*m*1-Ph); 7.38 (d, 2H, ^3J(H,H) = 8 Hz, 5,15-*m*2-Ph); 7.31 (d, 1H, ^3J(H,H) = 8 Hz, 10-*m*2-Ph); 4.11 (s, 6H, 5,15-*p*-OCH_3); 4.09 ppm (s, 3H, 10-*p*-OCH_3); IR (ATR diamond): $\tilde{\nu}_{Re-O}$ = 990 cm^{-1}; UV/Vis (CH_2Cl_2): λ_{max} (ε) = 441 (10.84), 556 (1.79), 592 nm (2.29×10^4 $mol^{-1}\,dm^3\,cm^{-1}$); MS (ESI): *m/z* calcd for $C_{40}H_{29}O_4N_4Re$: 815.89 [M^+]; found: 816.17; elemental analysis calcd for $C_{40}H_{29}O_4N_4Re$: C 58.88, H 3.58, N 6.87; found: C 59.14, H 3.82, N 6.58.

Crystallization and crystallography: Approximately 5–10 mg of each ReO corrole was dissolved in a minimum quantity of dichloromethane in a vial and carefully layered with *n*-hexane. The vial was covered with aluminum foil and left to stand for two weeks, during which X-ray-quality crystals formed for all five ReO corroles. X-ray data were collected on beamline 11.3.1 at the Advanced Light Source of Lawrence Berkeley National Laboratory, Berkeley, California. The samples were mounted on MiTeGen kapton loops and placed in a 100(2) K nitrogen cold stream provided by an Oxford Cryostream 800 Plus low-temperature apparatus on the goniometer head of a Bruker D8 diffractometer equipped with a PHOTON100 CMOS detector operating in shutterless mode. Diffraction data were collected by using synchrotron radiation monochromated with silicon(111) to a wavelength of 0.7749(1) Å. An approximate full sphere of data was collected by using a combination of phi and omega scans with scan speeds of 1 second per 4 degrees for the phi scans, and 1 second per degree for the omega scans at $2\theta = 0$ and -45. The structures were solved by intrinsic phasing (SHELXT) and refined by full-matrix least squares on F^2 (SHELXL-2014). All non-hydrogen atoms were refined anisotropically. Hydrogen atoms were geometrically calculated and refined as riding atoms.

Acknowledgements

This work was supported by the Research Council of Norway and the Advanced Light Source at Berkeley, California. The Advanced Light Source is supported by the Director, Office of Science, Office of Basic Energy Sciences, of the U.S. Department of Energy under Contract No. DE-AC02-05CH11231.

Keywords: corroles · oxidation · metalation · rhenium · size mismatch

[1] For reviews on metallocorroles, see: a) I. Aviv-Harel, Z. Gross, *Coord. Chem. Rev.* **2011**, *255*, 717–736; b) K. E. Thomas, A. Alemayehu, J. Conradie, C. M. Beavers, A. Ghosh, *Acc. Chem. Res.* **2012**, *45*, 1203–1214; c) J. H. Palmer, *Struct. Bonding (Berlin)* **2011**, *142*, 49–90; d) H. L. Buckley, J. Arnold, *Dalton Trans.* **2015**, *44*, 30–36.

[2] R. Padilla, H. L. Buckley, A. L. Ward, J. Arnold, *Chem. Commun.* **2014**, *50*, 2922–2924.

[3] I. Nigel-Etinger, I. Goldberg, Z. Gross, *Inorg. Chem.* **2012**, *51*, 1983–1985.

[4] A. B. Alemayehu, K. J. Gagnon, J. Terner, A. Ghosh, *Angew. Chem. Int. Ed.* **2014**, *53*, 14411–14414; *Angew. Chem.* **2014**, *126*, 14639–14642.

[5] J. H. Palmer, A. C. Durrell, Z. Gross, J. R. Winkler, H. B. Gray, *J. Am. Chem. Soc.* **2010**, *132*, 9230–9231.

[6] A. B. Alemayehu, H. Vazquez-Lima, C. M. Beavers, K. J. Gagnon, J. Bendix, A. Ghosh, *Chem. Commun.* **2014**, *50*, 11093–11096.

[7] a) A. B. Alemayehu, A. Ghosh, *J. Porphyrins Phthalocyanines* **2011**, *15*, 106–110; b) E. Rabinovich, I. Goldberg, Z. Gross, *Chem. Eur. J.* **2011**, *17*, 12294–12301; c) K. E. Thomas, A. B. Alemayehu, J. B. Conradie, C. M. Beavers, A. Ghosh, *Inorg. Chem.* **2011**, *50*, 12844–12851; d) K. E. Thomas, C. M. Beavers, A. Ghosh, *Mol. Phys.* **2012**, *110*, 2439–2444.

[8] a) S.-L. Lai, L. Wang, C. Yang, M.-Y. Chan, X. Guan, C.-C. Kwok, C.-M. Che, *Adv. Funct. Mater.* **2014**, *24*, 4655–4665; b) R. D. Teo, H. B. Gray, P. Lim, J. Termini, E. Domeshek, Z. Gross, *Chem. Commun.* **2014**, *50*, 13789–13792.

[9] M. K. Tse, Z. Y. Zhang, T. C. W. Mak, K. Chan, *Chem. Commun.* **1998**, 1199–1200.

[10] C. C. Romão, F. E. Kühn, W. A. Herrmann, *Chem. Rev.* **1997**, *97*, 3197–3246.

[11] Reviews: a) R. Alberto, H. Braband in *Comprehensive Inorganic Chemistry II: From Elements to Applications* (Eds.: R. Alberto, H. Braband), Elsevier, Amsterdam, **2013**, pp. 785–817; b) S. Jürgens, W. A. Hermann, F. E. Kühn, *J. Organomet. Chem.* **2014**, *751*, 83–89.

[12] For a recent report on ^{99m}Tc imaging agents, see: M. Benz, B. Spingler, R. Alberto, H. Braband, *J. Am. Chem. Soc.* **2013**, *135*, 17566–17572.

[13] a) P. Pyykkö, S. Riedel, M. Patzschke, *Chem. Eur. J.* **2005**, *11*, 3511–3520; b) P. Pyykkö, M. Atsumi, *Chem. Eur. J.* **2009**, *15*, 186–197; c) P. Pyykkö, M. Atsumi, *Chem. Eur. J.* **2009**, *15*, 12770–12779.

[14] For electrochemical HOMO–LUMO gaps of closed-shell corrole derivatives, see: L. Simkhovich, A. Mahammed, I. Goldberg, Z. Gross, *Chem. Eur. J.* **2001**, *7*, 1041–1055.

[15] Key references on Cu corroles: a) I. H. Wasbotten, T. Wondimagegn, A. Ghosh, *J. Am. Chem. Soc.* **2002**, *124*, 8104–8116; b) C. Brückner, R. P. Briñas, J. A. K. Bauer, *Inorg. Chem.* **2003**, *42*, 4495–4497; c) M. Bröring, F. Brégier, E. C. Tejero, C. Hell, M. C. Holthausen, *Angew. Chem. Int. Ed.* **2007**, *46*, 445–448; *Angew. Chem.* **2007**, *119*, 449–452; d) A. B. Alemayehu, E. Gonzalez, L.-K. Hansen, A. Ghosh, *Inorg. Chem.* **2009**, *48*, 7794–7799; e) A. B. Alemayehu, L.-K. Hansen, A. Ghosh, *Inorg. Chem.* **2010**, *49*, 7608–7610; f) A. B. Alemayehu, J. Conradie, A. Ghosh, *Eur. J. Inorg. Chem.* **2011**, *2011*, 1857–1864; g) S. Berg, K. E. Thomas, C. M. Beavers, A. Ghosh, *Inorg. Chem.* **2012**, *51*, 9911–9916; h) K. E. Thomas, H. Vazquez-Lima, Y. Fang, Y. Song, K. J. Gagnon, C. M. Beavers, K. M. Kadish, A. Ghosh, *Chem. Eur. J.* **2015**, *21*, 16839–16847.

[16] a) E. Steene, T. Wondimagegn, A. Ghosh, *J. Phys. Chem. B* **2001**, *105*, 11406–11413; addition/correction: E. Steene, T. Wondimagegn, A. Ghosh, *J. Phys. Chem. B* **2002**, *106*, 5312–5312; b) I. Wasbotten, A. Ghosh, *Inorg. Chem.* **2006**, *45*, 4910–4913; c) B. O. Roos, V. Veryazov, J. Conradie, P. R. Taylor, A. Ghosh, *J. Phys. Chem. A* **2008**, *112*, 14099–14102; d) H. Vazquez-Lima, H.-K. Norheim, A. Ghosh, *Dalton Trans.* **2015**, *44*, 10146–10151.

[17] a) O. Zakharieva, V. Schünemann, M. Gerdan, S. Licoccia, S. Cai, F. A. Walker, A. X. Trautwein, *J. Am. Chem. Soc.* **2002**, *124*, 6636–6648; b) R. K. Hocking, S. D. George, Z. Gross, F. A. Walker, K. O. Hodgson, B. Hedman, E. I. Solomon, *Inorg. Chem.* **2009**, *48*, 1678–1688; c) For a review, see: F. A. Walker, S. Licoccia, R. Paolesse, *J. Inorg. Biochem.* **2006**, *100*, 810–837.

Received: October 27, 2015
Published online on December 7, 2015

APPENTIX II

ChemPubSoc Europe

DOI: 10.1002/chem.201605015

CHEMISTRY
A European Journal
Communication

Technetium Complexes

Synthesis and Molecular Structure of ^{99}Tc Corroles

Rune F. Einrem,[a] Henrik Braband,[b] Thomas Fox,[b] Hugo Vazquez-Lima,[a] Roger Alberto,*[b] and Abhik Ghosh*[a]

Abstract: The first ^{99}Tc corroles have been synthesized and fully characterized. A single-crystal X-ray structure of a ^{99}TcO triarylcorrole revealed nearly identical geometry parameters as the corresponding ReO structure. A significant spectral shift between the Soret maxima of TcO (410–413 nm) and ReO (438–441 nm) corroles was observed and, based on two-component spin–orbit ZORA TDDFT calculations, ascribed to relativistic effects in the Re case. The syntheses reported herein potentially pave the way toward ^{99m}Tc-porphyrinoid-based radiopharmaceuticals.

Although of great interest as a potentially new class of radiopharmaceuticals for a combined imaging–therapy[1] strategy in photodynamic therapy,[2] $^{99(m)}$Tc porphyrinoids remain essentially unknown to this date.[3] The only previous report of a $^{99(m)}$Tc porphyrinoid is that of a mesoporphyrin IX dimethyl ester complexed to one or two $\{^{99}Tc(CO)_3\}^+$ fragments, with each fragment facially coordinated by three porphyrin nitrogen atoms.[4,5] In a recent report on a general route to rhenium(V)–oxo corroles,[6] we expressed the hope that the synthetic approach would provide a stepping stone to $^{99(m)}$Tc^{V}O corroles. A significant step toward fulfilment of that promise is reported herein, with the synthesis of a series of complexes with the general formula ^{99}Tc[T*p*XPC](O), where T*p*XPC refers to a *meso*-tris(*para*-X-phenyl)corrole and X = CF_3, H, Me, and OMe.[7] Besides standard characterization by means of UV/Vis, IR, ^{1}H and ^{13}C NMR spectroscopy, and electrochemistry, one of the complexes, ^{99}Tc[T*p*OMePC](O), was also structurally characterized by means of single-crystal X-ray diffraction analysis. The results allow for detailed comparisons with ReO corroles, including potential insights into relativistic effects on the properties of 4d versus 5d metallocorroles.

The insertion of large 4d[8] and 5d[9–14] elements into the constrained N_4 cavity of corroles is often capricious, requiring careful, element-specific optimization of the reaction conditions. Once synthesized, however, the majority of 5d metallocorroles are stable and hence of unusual interest as optical sensors, near-IR dyes, phosphors, and light-emitting diodes.[12,16,17] A promising approach to these size-mismatched metal–ligand assemblies involves oxidative metalation, that is, the interaction of a free-base corrole with a metal carbonyl precursor in a high-boiling solvent such as decalin, whereby the carbonyl ligands are lost in the course of reaction and the product is a relatively high oxidation-state metallocorrole. Recent successes of this approach include relatively high-yielding syntheses of Re^{V}O[6] and Os^{VI}N[11] corroles and of tungsten biscorroles.[10] Given the relative inaccessibility of $^{99}Tc_2(CO)_{10}$, we chose to examine the much more readily accessible ^{99}Tc(I) compound $(NEt_4)_2[fac\text{-}^{99}TcCl_3(CO)_3]$[18] as the ^{99}Tc source and found it to afford the highly stable ^{99}Tc^{V}O corroles in reasonably good yields (15–51%, Figure 1).

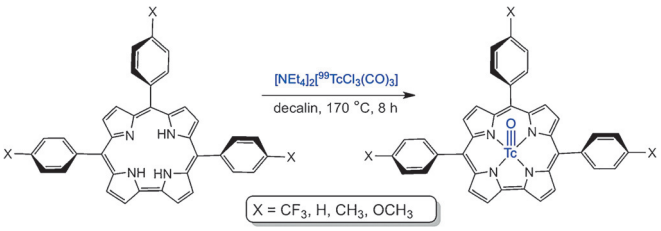

Figure 1. A general synthetic route for ^{99}Tc^{V}O triarylcorroles.

Of the four complexes synthesized, a single-crystal X-ray structure could be determined for ^{99}Tc[T*p*OMePC](O), revealing a coordination geometry very similar to that observed for the analogous Re^{V}O complex (Figure 2).[6] The ^{99}Tc–O distance of 1.660(2) Å is very slightly longer than the sum of Pyykkö's covalent radii for triple-bonded Tc (1.10 Å) and triple-bonded O (0.53 Å).[19] As in the case of Re^{V}O corroles, the corrole macrocycle in the present structure is significantly domed, with the ^{99}Tc displaced some 0.681 Å from the corrole N_4 plane, essentially the same displacement as that in the analogous Re^{V}O structure. The average ^{99}Tc–N bond distances (1.992 Å) are also essentially identical to the average Re–N distances (1.998 Å) found for Re[T*p*OMePC](O).[6]

Key physicochemical properties of the complexes were found to be as follows: First, the ^{1}H NMR spectra, which could be fully assigned with COSY and NOESY analyses, showed that the compounds are diamagnetic, consistent with the expected d_{xy}^2 electronic configuration of the ^{99}Tc^{V}O center. Second, the Soret maxima of the complexes (Table 1 and Figure 3) are in-

[a] *R. F. Einrem, Dr. H. Vazquez-Lima, Prof. Dr. A. Ghosh*
Department of Chemistry, UiT-The Arctic University of Norway
9037 Tromsø (Norway)
E-mail: abhik.ghosh@uit.no

[b] *Dr. H. Braband, Dr. T. Fox, Prof. Dr. R. Alberto*
Department of Chemistry, University of Zurich
Winterthurerstrasse 190, 8057 Zürich (Switzerland)
E-mail: ariel@chem.uzh.ch

Supporting information (including additional experimental details and a crystallographic information file) and the ORCID identification number(s) for the author(s) of this article can be found under: http://dx.doi.org/10.1002/chem.201605015.

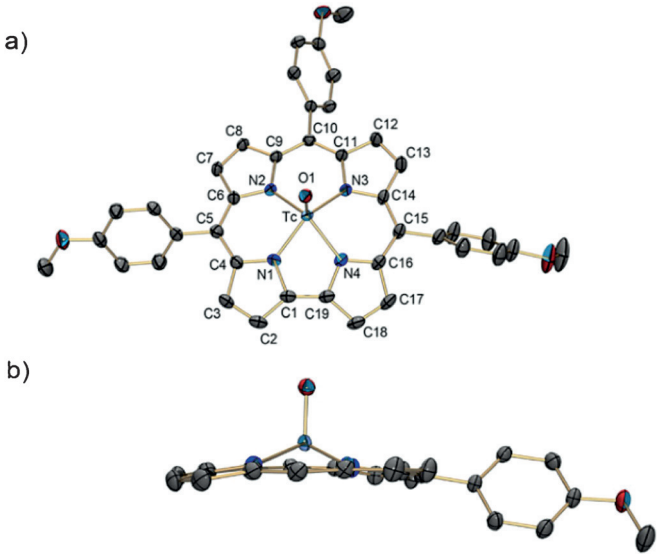

Figure 2. Two views of ^{99}Tc[T*p*OMePC](O):[15] a) ORTEP with nonhydrogen atom numbering (ellipsoids set at 20% probability; b) side-on view (20%) showing the displacement of the ^{99}Tc atom above the macrocycle.

Table 1. Spectroscopic and electrochemical properties: Soret λ_{max}, $E_{1/2}$, and ν_{TcO} IR values.

Complex	λ_{max} [nm]	$E_{1/2\,ox}$ [V]	$E_{1/2\,red}$ [V]	ΔE [V]	ν_{TcO} [cm^{-1}]
Tc[T*p*CF$_3$PC](O)	410	1.28	−0.79	2.07	977
Tc[TPC](O)	410	1.18	−0.91	2.09	970
Tc[T*p*CH$_3$PC](O)	412	1.16	−0.90	2.06	972
Tc[T*p*OCH$_3$PC](O)	413	1.15	−0.89	2.04	968

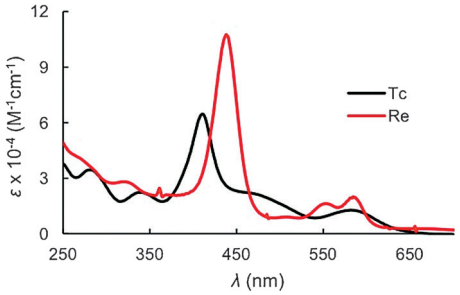

Figure 3. Comparison of the electronic absorption spectra of Tc[T*p*CF$_3$PC](O) and Re[T*p*CF$_3$PC](O) in dichloromethane.

sensitive to the *para*-substituent X, redshifting by only 3 nm from X = CF$_3$ to X = OCH$_3$. Third, the electrochemical HOMO–LUMO gaps are large, approximately 2.04–2.09 V (Table 1), which is essentially the π–π* gap of a typical porphyrin or corrole macrocycle.[20] Over several recent studies, we have shown that the last two characteristics are typical of an innocent corrole^{3-} ligand, such as that found in Au, OsN, and ReO corroles, as opposed to a non-innocent corrole$^{\bullet 2-}$ ligand, for which copper[20] and iron[21,22] corroles provide some of the best studied examples. Finally, the ^{99}Tc^{V}O stretching mode (ν_{TcO}) of the complexes was readily discernible in the IR spectra, with little interference from other skeletal modes. As shown in Table 1, the ν_{TcO} varies slightly with the *meso para*-substituent, upshifting with increasing electron-withdrawing character of the substituent. Between *para*-OMe (968 cm^{-1}) and the more electron-deficient complexes (977 cm^{-1}), the ν_{TcO} upshifts by 9 cm^{-1}.

A notable difference between ^{99}Tc^{V}O and Re^{V}O triarylcorroles is that the Soret maximum of the latter (438–441 nm) are redshifted by some 28 nm relative to those of the former (410–413 nm; Figure 4). TDDFT calculations, with nonrelativistic, scalar relativistic, and a ZORA two-component spin–orbit relativistic Hamiltonian, all with all-electron ZORA STO-TZP basis sets showed that whereas relativity has a near-negligible effect on the Soret maximum of ^{99}Tc[TPC](O), there is a strong relativistic redshift for Re[TPC](O). According to scalar relativistic results on ^{99}Tc[TPC](O), several of the LUMOs (LUMO through LUMO + 2) are not classic Gouterman LUMOs, but antibonding combinations of Tc 4d orbitals and various corrole π MOs. Analogous 5d–π interactions are not observed in the Re case: all four frontier MOs of Re[TPC](O), HOMO − 1 through LUMO + 1, correspond to the classic Gouterman four-orbital set. Because of relativistic destabilization, the Re 5d orbitals are far too high in energy to effectively interact with the lowest unoccupied corrole MOs. Thus, whereas the Soret band of Re[TPC](O) has classic Gouterman four-orbital character, the two key transitions under the Soret envelope of the ^{99}Tc complex happen to be primarily HOMO → LUMO + 3 and HOMO − 1 → LUMO + 3 in character. Scalar relativistic calculations thus provide a satisfactory MO rationale for the observed spectral shift between ^{99}TcO and ReO corroles. It is worth noting that the spectra predicted by scalar relativistic calculations are essentially identical to those obtained with the more advanced, two-component spin–orbit method.

Given the major role of porphyrinoids in photodynamic therapy, we find it surprising that fully coordinated $^{99(m)}$Tc porphyrinoids have not been reported until now. Combined radioimaging with ^{99m}Tc and singlet oxygen formation via a single compound should potentially afford new methodology for molecular theranostics. The present synthesis of ^{99}Tc corroles, along with full structural characterization of one complex, may be viewed as an important step in that direction. We remain optimistic that medically relevant ^{99m}Tc porphyrinoid reagents will emerge within the not too distant future.

Experimental Section

Caution! ^{99}Tc is a weak β$^-$ emitter. All experiments were carried out in laboratories approved for working with low-level radioactive materials.

All commercially available chemicals, including $NH_4{}^{99}TcO_4$ (Oak Ridge) were reagent grade and used without further purification. FTIR spectra were measured as KBr pellets on a PerkinElmer Spectrum Two spectrophotometer. ^{1}H and ^{13}C NMR spectra were recorded on a Bruker DRX500 500 MHz spectrometer. All of the ^{13}C NMR spectra recorded were proton-decoupled. UV/Vis spectra in dichloromethane were recorded on a Cary 50 spectrometer using 1 cm quartz cells.

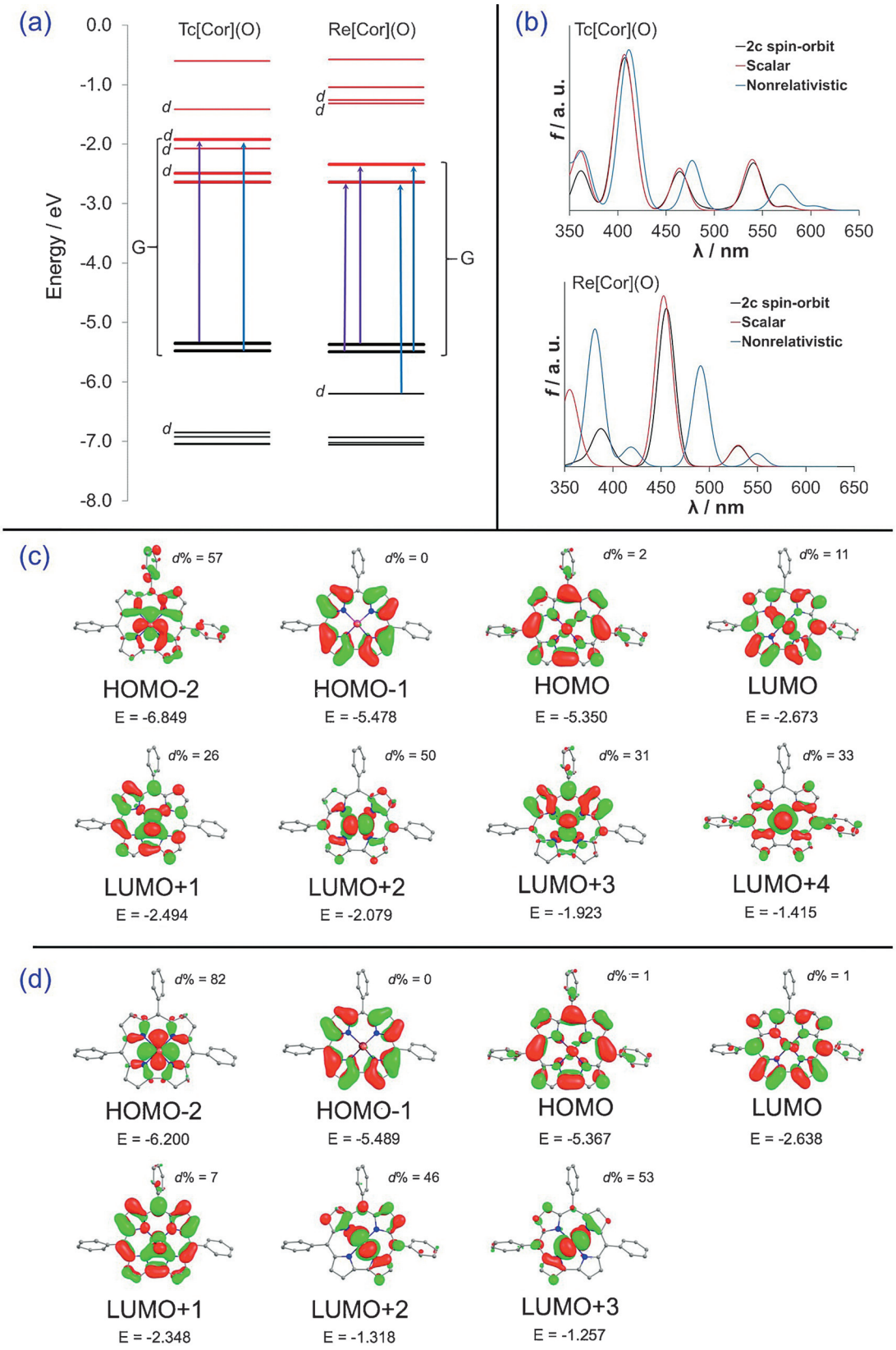

Figure 4. Selected DFT and TDDFT results on M[TPC](O) (M = Tc, Re). a) Main contributions to the two Soret transitions of the two complexes. b) Nonrelativistic, scalar relativistic, and ZORA two-component spin-orbit TDDFT simulations of the electronic absorption spectra M[Cor](O), where Cor = unsubstituted corrole. c) Selected frontier MOs of Tc[TPC](O). d) Selected frontier MOs of Re[TPC](O). In (a), the label d indicates MOs with more than 25% metal *d* character. The energy range marked G is that spanned by the Goutermann-type frontier MOs.

General procedure for the synthesis of ^{99}TcO[T*p*XPC]: Free-base corrole, H_3[T*p*XPC] (0.025 mmol), $[NEt_4]_2[^{99}TcCl_3(CO)_3]$ (0.05 mmol), and potassium carbonate (25 mg) were added to a 2.5 mL microwave vial containing decalin (0.5 mL) and a magnetic stirring bar. The vial was sealed with a rubber septa and the contents were deoxygenated with a flow of nitrogen and then heated for 8 h with constant stirring at 170 °C. Upon cooling, the reaction mixture was loaded directly on to silica gel column with *n*-hexane as the mobile phase. The decalin was first removed by eluting with pure hexane. Different solvent mixtures were then used to elute the various ^{99}TcO corroles: 6:1 *n*-hexane/dichloromethane for X = CF_3, H and CH_3 and 1:1 *n*-hexane/dichloromethane for X = OCH_3. For X = CF_3, H, and CH_3 the product emerged as the second band, dark green to almost brown color. For X = OCH_3 the product appeared in the first band. For each of these bands, the purity of the product was confirmed by TLC. Yields and analytical details for the different complexes are as follows.

Tc[T*p*CF$_3$PC](O): Yield 3.3 mg (15.7%). UV/Vis (CH_2Cl_2) λ_{max} [nm] ($\varepsilon \times 10^{-4}$ [L mol^{-1} cm^{-1}]): 410 (6.45), 468 (2.18), 528 (1.27). ^{1}H NMR (500 MHz, $CDCl_3$, −50 °C): δ 9.67 (d, 2H, $^3J_{HH}$ = 4.1 Hz, β-H); 9.33 (d, 2H, $^3J_{HH}$ = 4.2 Hz, β-H); 9.31 (d, 2H, $^3J_{HH}$ = 4.9 Hz, β-H); 9.11 (d, 2H, $^3J_{HH}$ = 4.8 Hz, β-H); 8.73 (d, 2H, $^3J_{HH}$ = 8.0 Hz, 5,15-*o*1-Ph); 8.66 (d, 1H, $^3J_{HH}$ = 8.2 Hz, 10-*o*1-Ph); 8.27 (d, 2H, $^3J_{HH}$ = 7.6 Hz, 5,15-*o*2-Ph); 8.22 (d, 2H, $^3J_{HH}$ = 7.9 Hz, 5,15-*m*1-Ph); 8.18 (d, 1H, $^3J_{HH}$ = 7.9 Hz, 10-*m*1-Ph); 8.10 (d, 2H, $^3J_{HH}$ = 8.3 Hz, 5,15-*m*2-Ph); 8.08 (d, 1H, $^3J_{HH}$ = 9.0 Hz, 10-*o*2-Ph); 8.04 ppm (d, 1H, $^3J_{HH}$ = 7.8 Hz, 10-*m*2-Ph). ^{13}C NMR (125 MHz, $CDCl_3$, −50 °C): δ 144.0 (s, 1C, C_{Ph10}); 143.1 (s, 2C, $C_{Ph5,15}$); 142.1 (s, 2C, $C_{6,14}$); 141.9 (s, 2C, $C_{9,11}$); 139.8 (s, 2C, $C_{4,16}$); 135.4 (s, 2C, $C_{1,19}$); 134.3 (s, 2C, $C_{Ph5,15}$); 134.1 (s, 3C, $C_{Ph10,5,15}$); 133.9 (s, 1C, C_{Ph10}); 129.6 (q, 3C, $^1J_{CF}$ = 31 Hz, $C_{Ph10,5,15}$), 127.9 (s, 2C, $C_{7,13}$); 126.7 (s, 4C, $C_{3,17,8,12}$); 124.9 (s, 4C, $C_{Ph5,15}$); 124.6 (s, 2C, C_{Ph10}); 124.2 (q, 3C, $^1J_{CF}$ = 273 Hz, C_F); 119.3 (s, 2C, $C_{5,15}$); 118.3 (s, 2C, $C_{2,18}$); 116.5 ppm (s, 1C, C_{10}). IR ν_{TcO}: 977 cm^{-1}.

Tc[TPC](O): Yield 8.2 mg (51.2%). UV/Vis (CH_2Cl_2): λ_{max} [nm] ($\varepsilon \times 10^{-4}$ [L mol^{-1} cm^{-1}]: 410 (5.73), 468 (2.25), 584 (1.15). ^{1}H NMR (500 MHz, $CDCl_3$, −50 °C): δ 9.61 (d, 2H, $^3J_{HH}$ = 4.3 Hz, β-H); 9.35 (d, 2H, $^3J_{HH}$ = 4.0 Hz, β-H); 9.34 (d, 2H, $^3J_{HH}$ = 4.4 Hz, β-H); 9.13 (d, 2H, $^3J_{HH}$ = 4.8 Hz, β-H); 8.61 (d, 2H, $^3J_{HH}$ = 7.5 Hz, 5,15-*o*1-Ph); 8.52 (d, 1H, $^3J_{HH}$ = 7.5 Hz, 10-*o*1-Ph); 8.16 (m, 2H, 5,15-*o*2-Ph); 7.95 (m, 3H, 5,15-*m*1-Ph; 10-*m1*-Ph overlapping); 7.91 (t, 1H, $^3J_{HH}$ = 7.4 Hz 10-*m*2-Ph); 7.83 (m, 5H, 5,15-*m*2-Ph & 5, 10,15-*p*-Ph overlapping); 7.75 ppm (t, 1H, $^3J_{HH}$ = 7.4 Hz, 10-*m*2-Ph). ^{13}C NMR (125 MHz, $CDCl_3$, −50 °C): δ 142.6 (s, 2C, $C_{6,14}$); 142.2 (s, 2C, $C_{9,11}$); 140.4 (s, 1C, C_{Ph10}); 139.5 (s, 2C, $C_{Ph5,15}$); 139.5 (s, 2C, $C_{4,16}$); 135.6 (s, 2C, $C_{1,19}$); 134.3 (s, 2C, $C_{Ph5,15}$); 134.0 (s, 2C, $C_{Ph5,15}$); 133.9 (s, 1C, C_{Ph10}); 133.7 (s, 1C, C_{Ph10}); 127.9 (s, 2C, $C_{7,13}$); 127.9 (s, 4C, $C_{Ph5,15}$); 127.8 (s, 1C, C_{Ph10}); 127.7 (s, 1C, C_{Ph10}); 127.5 (s, 2C, C_{Ph10}); 126.7 (s, 2C, $C_{8,12}$); 126.5 (s, 2C, $C_{3,17}$); 120.8 (s, 2C, $C_{5,15}$); 117.7 (s, 1C, C_{10}); 117.5 ppm (s, 2C, $C_{2,18}$). IR ν_{TcO}: 970 cm^{-1}.

Tc[T*p*MePC](O): Yield 3.6 mg (21.3%) UV/Vis (CH_2Cl_2): λ_{max} [nm] ($\varepsilon \times 10^{-4}$ [L mol^{-1} cm^{-1}]: 412 (4.13), 463 (1.36), 580 (0.83). ^{1}H NMR (500 MHz, $CDCl_3$, −50 °C): δ 9.58 (d, 2H, $^3J_{HH}$ = 3.2 Hz, β-H); 9.33 (m, 4H, β-H, broad singlet, overlapping, β-H); 9.13 (d, 2H, $^3J_{HH}$ = 4.4 Hz, β-H); 8.49 (d, 2H, $^3J_{HH}$ = 7.1 Hz, 5,15-*o*1-Ph); 8.39 (d, 1H, $^3J_{HH}$ = 7.5 Hz, 10-*o*1-Ph); 8.05 (d, 2H, $^3J_{HH}$ = 7.1 Hz, 5,15-*o*2-Ph); 7.84 (d, 1H, $^3J_{HH}$ = 6.9 Hz, 10-*o*2-Ph); 7.75 (d, 2H, $^3J_{HH}$ = 7.1 Hz, 5,15-*m*1-Ph); 7.70 (d, 1H, $^3J_{HH}$ = 7.0 Hz, 10-*m*1-Ph); 7.63 (d, 2H, $^3J_{HH}$ = 7.2 Hz, 5,15-*m*2-Ph); 7.56 (d, 1H, $^3J_{HH}$ = 7.2 Hz, 10-*m*2-Ph); 2.72 ppm (s, 9H, 5,10,15-*p*-CH_3). ^{13}C NMR (125 MHz, $CDCl_3$, −50 °C): δ 143.1 (s, 2C, $C_{6,14}$); 142.7 (s, 2C, $C_{9,11}$); 139.7 (s, 2C, $C_{4,16}$); 137.7 (s, 1C, C_{Ph10}); 137.6 (s, 2C, $C_{Ph5,15}$); 137.5 (s, 1C, C_{Ph10}); 136.9 (s, 2C, $C_{Ph5,15}$); 136.0 (s, 2C, $C_{1,19}$); 134.1 (s, 2C, $C_{Ph5,15}$); 133.9 (s, 1C, C_{Ph10}); 133.8 (s, 2C, $C_{Ph5,15}$); 133.6 (s, 1C, C_{Ph10}); 128.7 (s, 2C, $C_{Ph5,15}$); 128.6 (s, 2C, $C_{Ph5,15}$); 128.3 (s, 1C, C_{Ph10}); 128.2 (s, 1C, C_{Ph10}); 127.9 (s, 2C, $C_{7,13}$); 126.6 (s, 2C, $C_{8,12}$); 126.3 (s, 2C, $C_{3,17}$); 121.0 (s, 2C, $C_{5,15}$); 117.8 (s, 1C, C_{10}); 117.1 (s, 2C, $C_{2,18}$); 21.6 ppm (s, 3C, CH_3). IR ν_{TcO}: 972 cm^{-1}.

Tc[T*p*OMePC](O): Yield 3.8 mg (19.7%). UV/Vis (CH_2Cl_2): λ_{max} [nm] ($\varepsilon \times 10^{-4}$ [L mol^{-1} cm^{-1}]: 413 (4.32), 556 (1.79), 588 (0.83). ^{1}H NMR (500 MHz, −50 °C): δ 9.58 (d, 2H, $^3J_{HH}$ = 4.2 Hz, β-H); 9.34 (d, 2H, $^3J_{HH}$ = 4.9 Hz, β-H); 9.32 (d, 2H, $^3J_{HH}$ = 4.4 Hz, β-H); 9.13 (d, 2H, $^3J_{HH}$ = 4.6 Hz, β-H) 8.51 (d, 2H, $^3J_{HH}$ = 7.0 Hz, 5,15-*o*1-Ph); 8.42 (d, 1H, $^3J_{HH}$ = 7.5 Hz, 10-*o*1-Ph); 8.09 (d, 2H, $^3J_{HH}$ = 7.4 Hz, 5,15-*o*2-Ph); 7.87 (d, 1H, $^3J_{HH}$ = 7.5 Hz, 10-*o*2-Ph); 7.47 (d, 2H, $^3J_{HH}$ = 6.1 Hz, 5,15-*m*1-Ph); 7.41 (d, 1H, $^3J_{HH}$ = 8.4 Hz, 10-*m*1-Ph); 7.36 (d, 2H, $^3J_{HH}$ = 7.9 Hz, 5,15-*m*2-Ph); 7.27 (d, 1H, 10-*m*2-Ph, overlapping with solvent peak); 4.13 (s, 6H, 5,15-*p*-OCH_3); 4.11 (s, 3H, 10-*p*-OCH_3). ^{13}C NMR (125 MHz, $CDCl_3$, −50 °C): δ 158.9 (s, 2C, $C_{Ph5,15}$); 158.7 (s, 1C, C_{Ph10}); 143.0 (s, 2C, $C_{6,14}$); 142.4 (s, 2C, $C_{9,11}$); 139.4 (s, 2C $C_{4,16}$); 135.8 (s, 2C, $C_{1,19}$); 135.3 (s, 2C, $C_{Ph5,15}$); 135.0 (s, 2C, $C_{Ph5,15}$); 134.9 (s, 1C, C_{Ph10}); 134.7 (s, 1C, C_{Ph10}); 131.9 (s, 2C, $C_{5,15}$); 127.9 (s, 2C, $C_{3,17}$); 126.5 (s, 2C, $C_{8,12}$); 126.3 (s, 2C, $C_{7,13}$); 120.5 (s, 1C, C_{10}); 117.2 (s, 2C, $C_{2,18}$); 113.2 (s, 2C, $C_{Ph5,15}$); 113.0 (s, 2C, $C_{Ph5,15}$); 112.8 (s, 1C, C_{Ph10}); 112.4 (s, 1C, C_{Ph10}); 55.6 ppm (s, 3C, CH_3). IR ν_{TcO}: 968 cm^{-1}.

Electrochemical measurements were carried out in acetonitrile containing 0.1 M [TBA][PF_6] as the supporting electrolyte. A Metrohm 757 VA Computrace electrochemical analyzer equipped with a standard three-electrode set-up, consisting of a glassy carbon working electrode (3 mm i.d.), a platinum auxiliary electrode and Ag/AgCl reference electrode, was used throughout. All potentials are referenced with Fc/Fc^+ at 450 mV.

Crystallization and crystallography: Approximately 4–8 mg of each ^{99}Tc corrole was dissolved in a minimum quantity of dichloromethane in a vial and carefully layered with n-hexane. The vial was covered with Parafilm and left to stand for two weeks, during which X-ray quality crystals formed for ^{99}Tc[TpOMePC](O). Crystallographic data were collected at 183(2) K with Mo Kα radiation (λ = 0.7107 Å) that was monochromated with help of graphite on an Oxford Diffraction Xcalibur system with a Ruby detector. Suitable crystals were covered with oil (Infineum V8512, formerly known as Paratone N), mounted on a loop, and immediately transferred to the diffractometer. The CrysAlis^{Pro} suite of programs (version 171.32, Oxford Diffraction Ltd., UK, 2007) was used for data collection, semiempirical absorption correction, and data reduction. Additional details of data collection and structure determination are given in the Supporting Information, Table S4.1 and in the crystallographic information file. Structures were solved with direct methods using SIR97[23] and were refined by full-matrix least-squares methods on F^2 with SHELXL-97. The refinements were done with anisotropic thermal parameters for all non-hydrogen atoms, while the positions of the hydrogen atoms were calculated using the riding-model option of SHELXL97.[24]

Computational details: Geometry optimizations were generally carried out with the B3LYP exchange-correlation functional, D3 dispersion corrections, relativistic effects described by the zeroth order regular approximation (ZORA)[25] to the Dirac equation and applied as a scalar correction, and ZORA STO-TZP basis sets, all as implemented in the ADF[26] 2014 program. Furthermore, TDDFT calculations on unsubstituted M[Cor](O) (M = Tc, Re) were also carried out with a nonrelativistic Hamiltonian and with the ZORA Hamiltonian with spin–orbit coupling described at the two-component level, with ZORA STO-TZP basis sets used throughout.

Acknowledgements

We acknowledge financial support from Research Council of Norway (FRINATEK grant no. 231086, A.G.) and the Swiss National Science Foundation (project no. 200021_156256, H.B., R.A.).

Keywords: corroles · imaging · radiopharmaceuticals · technetium · theranostics

[1] Y. Zhang, J. F. Lovell, *Theranostics* **2012**, *2*, 905 – 912.
[2] M. Ethirajan, Y. Chen, P. Joshi, R. K. Pandey, *Chem. Soc. Rev.* **2011**, *40*, 340 – 362.
[3] Reviews: a) R. Alberto, H. Braband in *Comprehensive Inorganic Chemistry II,: From Elements to Applications* (Eds.: R. Alberto, H. Braband), Elsevier, **2013**, pp. 785 – 817; b) S. Jürgens, W. A. Hermann, F. E. Kühn, *J. Organomet. Chem.* **2014**, *751*, 83 – 89.
[4] a) M. Tsutsui, C. P. Hrung, *J. Am. Chem. Soc.* **1973**, *95*, 5777 – 5778; b) M. Tsutsui, C. P. Hrung, *J. Coord. Chem.* **1973**, *3*, 193 – 195.
[5] For a water-soluble porphyrin with a pendant ^{99m}Tc complex, see: M. Subbarayan, S. J. Shetty, T. S. Srivastava, O. P. D. Noronha, A. M. Samuel, *J. Porphyrins Phthalocyanines* **2001**, *5*, 824 – 828.
[6] R. F. Einrem, K. J. Gagnon, A. B. Alemayehu, A. Ghosh, *Chem. Eur. J.* **2016**, *22*, 517 – 520.
[7] For reviews on metallocorroles, see: a) I. Aviv-Harel, Z. Gross, *Coord. Chem. Rev.* **2011**, *255*, 717 – 736; b) K. E. Thomas, A. Alemayehu, J. Conradie, C. M. Beavers, A. Ghosh, *Acc. Chem. Res.* **2012**, *45*, 1203 – 1214; c) J. H. Palmer, *Struct. Bonding (Berlin)* **2011**, *142*, 49 – 90; d) H. L. Buckley, J. Arnold, *Dalton Trans.* **2015**, *44*, 30 – 36.
[8] For a discussion of synthetic aspects of Ru corroles, see for example: L. Simkhovich, I. Luobeznova, I. Goldberg, Z. Gross, *Chem. Eur. J.* **2003**, *9*, 201 – 208.
[9] Hf corroles: R. Padilla, H. L. Buckley, A. L. Ward, J. Arnold, *Chem. Commun.* **2014**, *50*, 2922 – 2924.
[10] W corroles: a) I. Nigel-Etinger, I. Goldberg, Z. Gross, *Inorg. Chem.* **2012**, *51*, 1983 – 1985; b) A. B. Alemayehu, H. Vazquez-Lima, K. J. Gagnon, A. Ghosh, *Chem. Eur. J.* **2016**, *22*, 6914 – 6920.
[11] Os corroles: A. B. Alemayehu, K. J. Gagnon, J. Terner, A. Ghosh, *Angew. Chem. Int. Ed.* **2014**, *53*, 14411 – 14414; *Angew. Chem.* **2014**, *126*, 14639 – 14642.
[12] Ir corroles: J. H. Palmer, A. C. Durrell, Z. Gross, J. R. Winkler, H. B. Gray, *J. Am. Chem. Soc.* **2010**, *132*, 9230 – 9231.
[13] Pt corroles: A. B. Alemayehu, H. Vazquez-Lima, C. M. Beavers, K. J. Gagnon, J. Bendix, A. Ghosh, *Chem. Commun.* **2014**, *50*, 11093 – 11096.
[14] Au corroles: a) A. B. Alemayehu, A. Ghosh, *J. Porphyrins Phthalocyanines* **2011**, *15*, 106 – 110; b) E. Rabinovich, I. Goldberg, Z. Gross, *Chem. Eur. J.* **2011**, *17*, 12294 – 12301; c) K. E. Thomas, A. B. Alemayehu, J. B. Conradie, C. M. Beavers, A. Ghosh, *Inorg. Chem.* **2011**, *50*, 12844 – 12851; d) K. E. Thomas, C. M. Beavers, A. Ghosh, *Mol. Phys.* **2012**, *110*, 2439 – 2444.
[15] CCDC 1505907 contains the supplementary crystallographic data for this paper. These data are provided free of charge by The Cambridge Crystallographic Data Centre.
[16] S. M. Borisov, A. B. Alemayehu, A. Ghosh, *J. Mater. Chem. C* **2016**, *4*, 5822 – 5828.
[17] A. B. Alemayehu, N. U. Day, T. Mani, A. B. Rudine, K. E. Thomas, O. A. Gederaas, S. A. Vinogradov, C. C. Wamser, A. Ghosh, *ACS Appl. Mater. Interfaces* **2016**, *8*, 18935 – 18942.
[18] S. Mundwiler, H. Braband, R. Alberto, D. McGregor, R. C. Howell, L. C. Francesconi, *Inorg. Synth.* **2014**, *36*, 149 – 155.
[19] a) P. Pyykkö, S. Riedel, M. Patzschke, *Chem. Eur. J.* **2005**, *11*, 3511 – 3520; b) P. Pyykkö, M. Atsumi, *Chem. Eur. J.* **2009**, *15*, 186 – 197; c) P. Pyykkö, M. Atsumi, *Chem. Eur. J.* **2009**, *15*, 12770 – 12779.
[20] For a recent discussion of the electronic structures of coinage metal corroles, see: K. E. Thomas, H. Vazquez-Lima, Y. Fang, Y. Song, K. J. Gagnon, C. M. Beavers, K. M. Kadish, A. Ghosh, *Chem. Eur. J.* **2015**, *21*, 16839 – 16847.
[21] a) E. Steene, T. Wondimagegn, A. Ghosh, *J. Phys. Chem. B* **2001**, *105*, 11406 – 11413; addition/correction: *J. Phys. Chem. B* **2002**, *106*, 5312 – 5312; b) H. Vazquez-Lima, H.-K. Norheim, R. F. Einrem, A. Ghosh, *Dalton Trans.* **2015**, *44*, 10146 – 10151; c) S. Ganguly, H. Vazquez-Lima, A. Ghosh, *Chem. Eur. J.* **2016**, *22*, 10336 – 10340.
[22] a) O. Zakharieva, V. Schünemann, M. Gerdan, S. Licoccia, S. Cai, F. A. Walker, A. X. Trautwein, *J. Am. Chem. Soc.* **2002**, *124*, 6636 – 6648; b) For a review, see: F. A. Walker, S. Licoccia, R. Paolesse, *J. Inorg. Biochem.* **2006**, *100*, 810 – 837.
[23] A. Altomare, M. C. Burla, M. Camalli, G. L. Cascarano, C. Giacovazzo, A. Guagliardi, A. G. G. Moliterni, G. Polidori, R. Spagna, *J. Appl. Crystallogr.* **1999**, *32*, 115 – 119.
[24] G. Sheldrick, *Acta Crystallogr. Sect. A* **2008**, *64*, 112 – 122.
[25] a) E. van Lenthe, E. J. Baerends, J. G. Snijders, *J. Chem. Phys.* **1993**, *99*, 4597 – 4610; b) E. van Lenthe, E. J. Baerends, J. G. Snijders, *J. Chem. Phys.* **1994**, *101*, 9783 – 9792.
[26] a) G. te Velde, F. M. Bickelhaupt, E. J. Baerends, C. Fonseca Guerra, S. J. A. van Gisbergen, J. G. Snijders, T. Ziegler, *J. Comput. Chem.* **2001**, *22*, 931 – 967; b) C. Fonseca Guerra, J. G. Snijders, G. te Velde, E. J. Baerends, *Theor. Chem. Acc.* **1998**, *99*, 391 – 403.

Manuscript received: October 27, 2016
Accepted Article published: November 1, 2016
Final Article published: November 23, 2016